Injectable, settable polyurethane biocomposites for bone remodeling in weight-bearing and contaminated fractures

By

Andrew J. Harmata

Dissertation

Submitted to the Faculty of the

Graduate School of Vanderbilt University

in partial fulfillment of the requirements

of the degree of

DOCTOR OF PHILOSOPHY

in

Chemical Engineering

May, 2015

Nashville, Tennessee

Approved:

Scott A. Guelcher, Ph.D.

G. Kane Jennings, Ph.D.

Jamey D. Young, Ph.D.

Jeffry S. Nyman, Ph.D.

Hak-Joon Sung, Ph.D.

ACKNOWLEDGEMENTS

First, I would like to acknowledge the various funding sources that supported the work conducted in this dissertation. These sources include Orthopaedic Extremity Trauma Research Program, Oak Ridge Institute for Science and Education Fellowship funded by the U. S. Army Medical Research and Material Command, the National Science Foundation, the National Institutes of Health, the Center for Military Biomaterials Research, and the Armed Forces Institute of Regenerative Medicine.

I want to thank my research advisor Dr. Scott Guelcher. I applied to and join the Chemical & Biomolecular Engineering program solely to work under his guidance. I greatly appreciate the opportunity to conduct research in a field that I feel a personal connection to. Dr. Guelcher's support was instrumental in my success throughout my tenure at Vanderbilt and undoubtedly will be in my future endeavors as well. His laboratory challenged me to answer mechanistic engineering and science questions, while maintaining a perspective as to our overall motivation for developing technologies that hopefully one day will improve the lives of ailing patients. I am also extremely grateful for him encouraging me to pursue career-oriented passions that extend beyond the laboratory and research. This freedom gave me the opportunity to take part in programs and experiences that are extremely unique to graduate students. Additionally, I would like to thank my committee members whom were always willing to offer their time and knowledge: Dr. Jeffry Nyman, Dr. Kane Jennings, Dr. Jamey Young, and Dr. Hak-Joon Sung.

I was fortunate to work with collaborators, both at Vanderbilt University as well as at the United States Army Institute of Surgical Research (USAISR), whom taught me a great deal about concentrations outside of my immediate expertise. I want to thank the Vanderbilt Biomechanics Lab, in particular Dr. Jeffry Nyman for teaching me about the details of good biomechanics characterization and analysis, Sasidhar Uppuganti for bearing with me throughout dozens of mechanical testing experiments, and Mathilde Granke for eagerly

answering fracture toughness questions time and time again. I would also like to thank the Vanderbilt Institute of Nanoscale Science and Engineering (VINSE, Dr. Tony Hmelo, Dr. Ben Schmidt, and Dr. Dmitry Koktysh), and the Vanderbilt University Institute of Imaging Science (VUIIS, Dr. Daniel Perrien and Erick Fleming) for access to equipment and proper training. Lastly, I am very grateful to our external collaborators who introduced me to the surgical side of orthopaedics and how to maintain focus on meeting the needs of patients. Thank you Dr. Joseph Wenke (USAISR) and his ever expanding team (Doug Cortez, Dr. Catherine Ward, Dr. Carlos Sanchez, Dr. David Tennent, Alicia Lofgren and many more).

Thank you to the entire Chemical & Biomolecular Engineering Department, including the teachers who taught a once 'biomedical engineer' chemical engineering principles and the administrative staff that some how keeps Olin afloat (Mary Gilleran, Rae Uson, Mark Holmes, Julie Canada and Julie James). I would like to especially acknowledge and thank Katarzyna Zienkiewicz. Words cannot describe how vital you are to the laboratory and how much of a joy it was to work beside you these past years. I could not have completed this program without the help from former students (Dr. Edna Margarita Prieto-Ballengee and Dr. Jonathan Page), those in my incoming class, as well as the up-and-coming students in the Guelcher Lab.

I would like to acknowledge the help and support I received from my family and friends. Thank you to my parents, Mark and Pam Harmata, and my sister, Lauren Verney-Fink, for your love and support. Thank you for listening and nodding when you did not understand the science terms I was using, learning about my research, and just being there at all times. I also want to thank all my friends, both inside and outside of Vanderbilt, for distracting me and helping me take my mind off of research. It has been great experiencing everything Nashville has to offer with you. Thank you for keeping my life/work balanced.

TABLE OF CONTENTS

LIST OF TABLES

LIST OF FIGURES

Figure Page

LIST OF ABBREVIATIONS

(3-aminopropyl)triethoxysilane (APTES)

45S5 bioactive glass (BG)

alkaline phosphatase (ALP)

biocomposite made with PCL-modified BG and PUR (PCL-BG/PUR)

bone volume fraction (BV/TV)

calcium phosphate cement (CPC)

cleaned and silanized with APTES BG (Sil-BG)

cleaned and unmodified BG (U-BG)

colony forming unit (CFU)

commercially available biphasic CPCs (CaS/P)

compressive modulus (E)

compressive strength (σ)

critical stress intensity factor, crack initiation (K_{init})

D-amino acids (D-AAs)

D-methionine (Met)

D-phenylalanine (Phe)

D-proline (Pro)

D-Tryptophan (D-Trp)

D-Tryptophan hydrochloride (D-Trp HCl)

hydroxycarbonate apatite (HCA)

iron acetylacetonate (FeAA)

isocyanate (NCO)

lysine triisocyanate- (LTI)

MASTERGRAFT® Mini Granules (MG)

maximum displacement (d_m)

maximum stress applied (σ_{max})

median fatigue life (N_f)

minimum biofilm inhibitory concentration (MBIC)

number of cycles (N)

number-average molecular weight (M_n)

overall creep strain (relative to initial strain) (c_k)

poly(ε-caprolactone) (PCL)

Polyester triol of 300 Da was synthesized with a backbone comprising 70% ε-caprolactone, 20% glycolide, and 10% D,L-lactide (T7C2G1L300)

polyurethane (PUR)

radial distance from the core of the defect (R_m)

ring opening polymerization (ROP)

shear modulus (G)

shear stress (τ)

sil-BG polymerized with ε-caprolactone for 24 h BG (24 h PCL-BG)

sil-BG polymerized with ε-caprolactone for 5 h BG (5 h PCL-BG)

simulated body fluid (SBF)

single edge notched beam (SENB)

Staphylococcus aureus (*S. aureus*)

stress intensity factor (K)

tartrate-resistant acid phosphatase (TRAP)

tin (II) 2-ethylhexanoate ($Sn(Oct)_2$)

trabecular number (Tb.N)

trabecular separation (Tb.Sp)

trabecular thickness (Tb.Th)

triethylene diamine (TEDA)

CHAPTER I

INTRODUCTION

The demand for treatment of bone defects and fractures, which result in good clinical outcomes, remains high across a variety of anatomical sites and patient populations. In the United States alone, the annual incidence of general fractures exceeds 6 million [18]. Although each type of fracture provides unique challenges, metaphyseal fractures are among the most difficult to treat [21, 22]. Tibial plateau fractures account for 1% of all fractures and 8% of fractures in the elderly. In 2006, there were over 1.6 million bone-graft procedures conducted for all forms of fractures. Due to a rapidly expanding elderly population, this number is expected to double in the next 25 years. The need for improved graft materials is evident based on the fact that ~25% of fracture patients require rehospitalization due to graft failure.

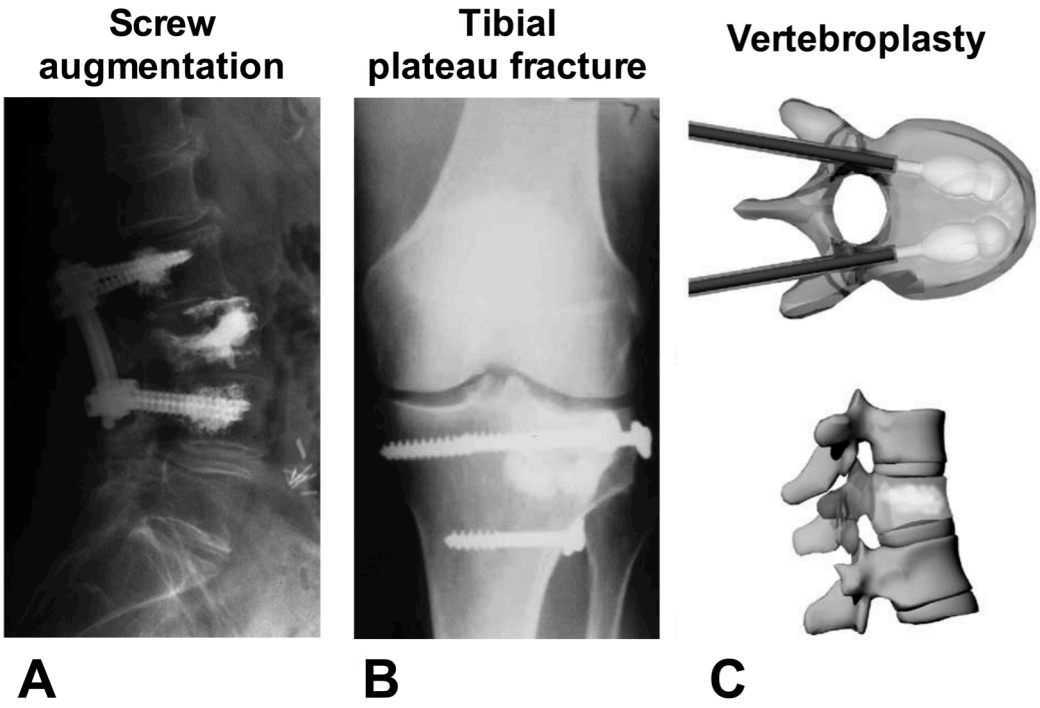

Figure 1.1. Images of orthopaedic procedures that currently utilize, or may benefit from use of, polymeric biocomposites. A) screw augmentation, B) tibial plateau fracture, and C) vertebroplasty.

When a bone fracture occurs, the normal physiological response includes a spontaneous sequence of events in order to restore function: inflammation, soft callus formation, hard callus formation, and lastly bone remodeling. If this natural process does not occur, surgical intervention is often warranted. In particular, large bone defects present a significant challenge to reconstructive surgery and often require aid through internal fixation (utilizing bone screws and metal plates) and bone grafting (from either autologous, cadaver, or synthetic sources). Orthopaedic conditions that utilize external materials, such as natural or synthetic bone grafts, to aid in fracture healing include screw augmentation [5], open tibial plateau fractures [6], and vertebroplasty [1]. Figure 1.1 displays X-ray and schematic representative images of these respective procedures. In each image, the white opaque portions of the bone are where external materials were injected into the bone fracture site.

Infection following the treatment of severe open fractures is a significant problem as bone loss occurs. Despite aggressive management tactics, infection rate is still nearly 23% [8]. The cost associated with device-related infection is estimated to be over $1 billion annually [7]. Osteomyelitis, infection of the bone and bone marrow, is a debilitating disease that is characterized by the inflammatory destruction of bone and surrounding tissues [9]. Similarly, despite surgical intervention, nearly 30% of osteomyelitis cases worsen into chronic infection [10]. Chronic osteomyelitis is associated with increased rates of non-osseous union and extremity amputation [11, 12]. In addition to being located in a weight-bearing joint, combat-related open tibial fractures that result in delayed amputation are most commonly caused by infection complications [14]. The current standard of care for contaminated bone defects includes systemic antibiotics, delivered either orally or parenterally, to stop ongoing infection and negate the need for implantation of a bone graft [15]. Additionally, systemic antibiotics can be supplemented with locally delivered antibiotics through surgically implanted poly(methyl methacrylate) (PMMA) beads [13].

Lysine-derived aliphatic polyurethanes (PUR) are tunable, injectable, biodegradable polymers that have advantageous properties for various tissue engineering applications. The cure profile and resultant cross-linking

mechanism of the polymer allows it to be administered via a minimally invasive injection method or high-bore syringe and cure *in situ,* thus conforming to any cavity shape [18-20]. The PUR reaction scheme can be leveraged to fabricate low or high porosity materials. Additionally, this polymer does not induce a prolonged inflammatory response, but does support cellular proliferation and degrades to nontoxic byproducts, when implanted *in vivo*. PUR has been used as a drug delivery vehicle for a variety of small molecules, such as growth factors [22, 23] and antibiotics. It can be tailored to promote healing in both soft[24] and hard[25] tissues, such as skin and bone, due to its tunable mechanical and degradation[26] properties. In bone applications, PUR has been combined with mineral fillers, which provide an osteoconductive substrate that also increases overall composite strength, to create high viscosity, settable, non-porous composites [27].

The goal of this dissertation was to design and characterize synthetic polyurethane-based graft composites that possess initial mechanical properties exceeding those of trabecular bone and remodel in bone defects *in vivo*. Additionally, a low porosity PUR composite vehicle was developed to deliver biofilm-dispersing D-amino acids (D-AAs) in a large animal femoral condyle plug *in vivo* model , and the biocompatibility of these D-AAs was further characterized. Mechanical testing of developed PUR composites included characterization of the following modes: quasi-static compression and torsion, dynamic compressive fatigue, and single edge notched beam (SENB) fracture toughness. *In vivo* characterization of implanted composites included micro-computed tomography (μCT), as well as histological and histomorphometry analyses.

Chapter III reportss the effect of D-AAs on bone cell differentiation *in vitro* as well as on bone healing in a large animal model. Infectious complications are a significant factor contributing to patient morbidity and limiting the success of clinical management of complex trauma. The D-isomers of amino acids (D-AAs) inhibit and disperse biofilms, that protect bacterial growth and significant contribute to chronic-relapsing infections, involving a broad range of bacterial species, such as *Staphylococcus aureus*. While local delivery of antibiotics

can achieve bactericidal concentrations, many clinically used antibiotics inhibit osteogenic differentiation *in vitro* at therapeutically relevant concentrations [21, 30, 31]. Therefor, detailed *in vitro* cell characterization on osteoblast and osteoclast differentiation cultured with varying D-AAs concentrations was evaluated by alkaline phosphatase (ALP)-positive and osteoblastic colony forming units, proliferation, and tartrate-resistant acid phosphatase (TRAP) staining, respectively. The *in vivo* remodeling capabilities of a low-viscosity D-AA augmented bone graft was evaluated as well in ovine femoral condyle defects.

In Chapter IV, the development of a high viscosity polymeric composite comprising surface modified 45S5 bioactive glass (BG) particles is described. Injectable synthetic bone grafts with strength exceeding that of trabecular bone could improve the clinical management of a number of orthopedic conditions. BG has been widely used for bone regeneration due to its bioactivity, however, incorporation of BG with a settable polymer in a composite form requires interfacial bonding between the polymer and BG phases to prevent nucleation of cracks and premature failure[32]. Surface- and material-focused characterization is presented and provides insight into the relationship between the surface modification of BG particles, by surface-initiated polymerization of poly(ε-caprolactone) (PCL), and the polyurethane polymer network formed *in situ*. The effect of surface modification on the mechanical properties of BG/PUR composites was evaluated via quasi-static compression and torsion. The *in vivo* remodeling properties of the lead-candidate BG/PUR composite was evaluated in femoral condyle defects in rats.

Relatedly, Chapter V further investigates the effects of surface modification of BG particles on the innate bioactive surface properties of BG when in physiological fluid. While grafting molecules to the surface of solid fillers has been shown to improve the overall mechanical properties of resultant polymer composites, the effect of the presence of these surface molecules on the surface bioactivity of bioactive ceramics is not well understood. Therefore, the degree to which surface grafting a silane coupling agent and PCL chains onto BG altered hydroxycarbonate apatite (HCA) formation was determined for a range of PCL chain thickness.

Modification of the BG surface was characterized by atomic force microscopy (AFM), X-ray photoelectron spectroscopy (XPS), and ellipsometry, among other techniques. HCA nucleation was determined by scanning electron microscopy (SEM), energy dispersive spectroscopy (EDS), and X-ray diffraction (XRD).

Continuing the evaluation of mechanical properties of surface-modified BG/polymer composites, Chapter VI compares the dynamic compressive fatigue properties of unmodified and surface-modified BG/polymer composites, as well as a commercially available calcium phosphate cement (CPC), when subjected to physiologically relevant stresses. Tibial plateau fractures involve a weight-bearing joint that often require subchondral grafting, which experience repetitive dynamic physiological loading from everyday activities [37-40]. The mechanical requirements of graft materials to optimize structural compatibility with the native weight-bearing bone have yet to be established. In addition to quantifying the fatigue life of grafts based on multiple individual failure parameters that correspond with mechanism of clinical failure, fatigue creep and single edge notched beam fracture toughness was characterized in order to provide additional insight related to the failure mechanisms of the grafts.

To conclude, Chapter VII summarizes the key findings of this dissertation and Chapter VIII provides suggestions for future work. Overall, this dissertation presents advancements in the development of synthetic, polyurethane-based grafts for bone fractures in weight-bearing locations and prevention of bacterial contamination.

References

1. M. Szpalski and R. Gunzburg: Applications of calcium phosphate-based cancellous bone void fillers in trauma surgery *Orthopedics.* **25**(5), S601 (2002).

2. S.S. Bajammal, M. Zlowodzki, A. Lelwica, P. Tornetta, III, T.A. Einhorn, R. Buckley, R. Leighton, T.A. Russell, S. Larsson and M. Bhandari: The use of calcium phosphate bone cement in fracture treatment *Journal of Bone and Joint Surgery-American Volume.* **90A**(6), 1186 (2008).

3. D.N. Yetkinler, R.T. McClellan, E.S. Reindel, D. Carter and R.D. Poser: Biomechanical comparison of conventional open reduction and internal fixation versus calcium phosphate cement fixation of a central depressed tibial plateau fracture *Journal of Orthopaedic Trauma.* **15**(3), 197 (2001).

4. A.J. Harmata, C.L. Ward, K. Zienkiewicz, J.C. Wenke and S.A. Guelcher: Investigating the Effects of Surface-Initiated Polymerization of ε-Caprolactone to Bioactive Glass Particles on the Mechanical Properties of Settable Polymer/Ceramic Composites *Journal of Materials Research.* **29**(20), 2398 (2014).

5. A.I. Hochbaum, I. Kolodkin-Gal, L. Foulston, R. Kolter, J. Aizenberg and R. Losick: Inhibitory Effects of D-Amino Acids on Staphylococcus aureus Biofilm Development *Journal of Bacteriology.* **193**(20), 5616 (2011).

6. I. Kolodkin-Gal, D. Romero, S. Cao, J. Clardy, R. Kolter and R. Losick: D-Amino Acids Trigger Biofilm Disassembly *Science.* **328**(5978), 627 (2010).

7. C.R. Rathbone, J.D. Cross, K.V. Brown, C.K. Murray and J.C. Wenke: Effect of Various Concentrations of Antibiotics on Osteogenic Cell Viability and Activity *Journal of Orthopaedic Research.* **29**(7), 1070 (2011).

8. C.f.D.C.a.P. (CDC): Septic arthritis following anterior cruciate ligament reconstruction using tendon allografts - Florida and Louisiana *MMWR Morb Mortal Wkly Rep.* **50**, 1081 (2001).

9. D. Simpson and J.F. Keating: Outcome of tibial plateau fractures managed with calcium phosphate cement *Injury-International Journal of the Care of the Injured.* **35**(9), 913 (2004).

10. J.J. Verlaan, F.C. Oner and W.J.A. Dhert: Anterior spinal column augmentation with injectable bone cements *Biomaterials.* **27**(3), 290 (2006).

11. A.M. Harris, P.L. Althausen, J. Kellam, M.J. Bosse and R. Castillo: Complications Following Limb-Threatening Lower Extremity Trauma *Journal of Orthopaedic Trauma.* **23**(1), 1 (2009).

12. S.R. Shah, K.F. Kurtis and A.G. Mikos: Perspectives on the prevention and treatment of infection for orthopedic tissue engineering applications *Chinese Science Bulletin.* **58**(35), 4342 (2013).

13. C.J. Sanchez, Jr., C.L. Ward, D.R. Romano, B.J. Hurtgen, S.K. Hardy, R.L. Woodbury, A.V. Trevino, C.R. Rathbone and J.C. Wenke: Staphylococcus aureus biofilms decrease osteoblast viability, inhibits osteogenic differentiation, and increases bone resorption in vitro *Bmc Musculoskeletal Disorders.* **14**, (2013).

14. L.O. Conterno and M.D. Turchi: Antibiotics for treating chronic osteomyelitis in adults *Cochrane Database of Systematic Reviews.* (9), (2013).

15. D.P. Lew and F.A. Waldvogel: Osteomyelitis *Lancet.* **364**(9431), 369 (2004).

16. J. Huh, D.J. Stinner, T.C. Burns and J.R. Hsu: Infectious Complications and Soft Tissue Injury Contribute to Late Amputation After Severe Lower Extremity Trauma *Journal of Trauma-Injury Infection and Critical Care.* **71**, S47 (2011).

17. E. Johnson, T. Burns, R. Hayda, D. Hospenthal and C. Murray: Infectious complications of open type III tibial fractures among combat casualties. *Clin Infect Dis.* **45**(4), 409 (2007).

18. E.M. Prieto, J.M. Page, A.J. Harmata and S.A. Guelcher: Injectable foams for regenerative medicine. *Nanomedicine and Nanotechnology.* **6**(2), 154 (2014).

19. J.M. Page, A.J. Harmata and S.A. Guelcher: Design and development of reactive injectable and settable polymeric biomaterials *Journal of Biomedical Materials Research Part A.* **101**(12), 3630 (2013).

20. S.A. Guelcher: Biodegradable polyurethanes: Synthesis and applications in regenerative medicine *Tissue Engineering Part B-Reviews.* **14**(1), 3 (2008).

21. A.E. Hafeman, K.J. Zienkiewicz, A.L. Zachman, H.-J. Sung, L.B. Nanney, J.M. Davidson and S.A. Guelcher: Characterization of the degradation mechanisms of lysine-derived aliphatic poly(ester urethane) scaffolds *Biomaterials.* **32**(2), 419 (2011).

22. J.M. Page, E.M. Prieto, J.E. Dumas, K.J. Zienkiewicz, J.C. Wenke, P. Brown-Baer and S.A. Guelcher: Biocompatibility and chemical reaction kinetics of injectable, settable polyurethane/allograft bone biocomposites *Acta Biomaterialia.* **8**(12), 4405 (2012).

23. J.E. Dumas, E.M. Prieto, K.J. Zienkiewicz, T. Guda, J.C. Wenke, J. Bible, G.E. Holt and S.A. Guelcher: Balancing the Rates of New Bone Formation and Polymer Degradation Enhances Healing of Weight-Bearing Allograft/Polyurethane Composites in Rabbit Femoral Defects *Tissue Engineering Part A.* **20**(1-2), 115 (2014).

24. B. Li, K.V. Brown, J.C. Wenke and S.A. Guelcher: Sustained release of vancomycin from polyurethane scaffolds inhibits infection of bone wounds in a rat femoral segmental defect model *Journal of Controlled Release.* **145**(3), 221 (2010).

25. E.J. Adolph, A.E. Hafeman, J.M. Davidson, L.B. Nanney and S.A. Guelcher: Injectable polyurethane composite scaffolds delay wound contraction and support cellular infiltration and remodeling in rat excisional wounds *Journal of Biomedical Materials Research Part A.* **100A**(2), 450 (2012).

26. J.E. Dumas, P.B. BrownBaer, E.M. Prieto, T. Guda, R.G. Hale, J.C. Wenke and S.A. Guelcher: Injectable reactive biocomposites for bone healing in critical-size rabbit calvarial defects *Biomedical Materials.* **7**(2), (2012).

27. J.E. Dumas, T. Davis, G.E. Holt, T. Yoshii, D.S. Perrien, J.S. Nyman, T. Boyce and S.A. Guelcher: Synthesis, characterization, and remodeling of weight-bearing allograft bone/polyurethane composites in the rabbit *Acta Biomaterialia.* **6**(7), 2394 (2010).

28. C. Kunze, T. Freier, E. Helwig, B. Sandner, D. Reif, A. Wutzler and H.J. Radusch: Surface modification of tricalcium phosphate for improvement of the interfacial compatibility with biodegradable polymers *Biomaterials.* **24**(6), 967 (2003).

29. M. Hashimoto, H. Takadama, M. Mizuno and T. Kokubo: Enhancement of mechanical strength of TiO2/high-density polyethylene composites for bone repair with silane-couple treatment *Materials Research Bulletin.* **41**(3), 515 (2006).

30. V.A. Koleganova, S.M. Bernier, S.J. Dixon and A.S. Rizkalla: Bioactive glass/polymer composite materials with mechanical properties matching those of cortical bone *Journal of Biomedical Materials Research Part A.* **77A**(3), 572 (2006).

31. A.J. Harmata, C.L. Ward, K. Zienkiewicz, J.C. Wenke and S.A. Guelcher: Investigating the Effects of Surface-Initiated Polymerization of ε-Caprolactone to Bioactive Glass Particles on the Mechanical Properties of Settable Polymer/Ceramic Composites *Journal of Materials Research.* **29**(20), 1 (2014).

32. C.f.D.C.a.P. (CDC): Update: allograft-associated bacterial infections - United States *MMWR Morb Mortal Wkly Rep.* **51**, 207 (2002).

33. S.F. El-Amin, Y. Khan and C. Laurencin: Bone graft substitutes *Expert Review of Medical Devices.* **3**(1), (2006).

CHAPTER II

BACKGROUND

Autologous bone graft is the gold standard for fixing many bone fractures with a defect, but it is also associated with numerous complications, including supply limitations, donor site morbidity, loss of function, and limited ability to bear mechanical loads [5]. One alternative to autograft is allograft, which is tissue obtained from a cadaver. This source also has associated complications, including risk of disease transmission [9, 10]. Attractive alternatives to autograft and allograft include various synthetic graft substitutes that attempt to mimic the physical and mechanical nature of native bone by meeting three desired criteria for bone grafts: osteo-conductivity, osteogenicity, and osteoinductivity [12]. Synthetic substitutes have been fabricated from a variety of materials, including polymers, ceramics, and combinations in the form of composites. The ideal bone graft substitute would be a material that is biocompatible, readily available, easily deliverable to the defect, structurally stable to prevent articular subsidence, and remodels to normal bone over time [15, 16].

Design of synthetic bone graft

Biomaterials are generally defined as nonviable materials used in medical devices that are intended to interact with biological systems in order to replace any tissue, organ, or function of the body [17-21]. While this classification is constantly evolving to encompass new areas of research [21], the definition of injectable biomaterials exhibits more variability depending on the specific application, reactivity of the material, and interaction with the tissue [20, 25]. Injectable biomaterials offer advantages compared to prefabricated implants due to their ability to be utilized in non-invasive surgical procedures, cure *in situ*, fill complex defects, and easily incorporate cells or therapeutics. Prefabricated biomaterials require implantation through invasive surgical procedures, which increases the risk of complications and recovery time [27, 28]. With the interest in

biomaterials for tissue engineering applications presumably rising for the foreseeable future, injectable biomaterials are anticipated to increase in clinical significance [30].

Table 2.1. Currently Marketed or Preclinical Injectable Settable Biomaterials

Clinical Application	**Crosslinker**	**Product Name(s)**
Homeostasis/wound closure	PEG acrylate	DuraSeal ®, CoSeal™
	Lysine based isocyanates	NovoSorb™, TissueGlu®
	2-octyl cyanoacrylate	Durabond™
	Transglutaminase/fibrin	Tisseel
Orthopedics	Polymethyl methacrylate	KyphX® HV-R
	Castor oil/isocyanate/calcium carbonate biocomposite	Kryptonite Bone Cement ®
Dental	Poly(lactic-co-glycolic acid) hydrogels	Fisiograft
	Urethane methacrylates	Fermit N, Evadyne,
	Amalgams	Compoglass ®, SDI alloys
Spinal disk replacement	Diisocyanate crosslinked collagen like peptides	NuCore®
Soft tissue fillers	Crosslinked hyaluronic acid	Hylaform, Restylane®, Carbylan

Settable biomaterials can be classified based on curing mechanisms. Physically settable biomaterials include environmentally responsive crosslinked (i.e. pH, temperature, micelle formation in water, etc.) and ionically crosslinked polymers [32, 33]. The lack of covalent linkages in physically settable biomaterials produces weak mechanical properties, which limits their use. Chemically settable biomaterials, which form covalent bonds *in situ*, cure by photopolymerization, thermally activated polymerization, catalyzed reactions, click-based

reactions, or enzymatically catalyzed reactions [34-38]. Table 2.1 shows a selection of chemically settable biomaterials that are currently available for clinical applications.

Challenges associated with the design of settable biomaterials

Despite the advantages of settable biomaterials, there are distinct challenges associated with the development of clinically relevant therapies and tuning its properties to those required by the specific application. Strategies for clinical translation must address sterilization procedures, handling properties, biocompatibility, and regenerative capabilities [39]. Settable biomaterials further stipulate the ability to inject low molecular weight monomers (and optionally catalysts or other additives) that subsequently react *in vivo* without damaging host tissue. The requirements of biocompatibility and biodegradability apply to both the low molecular weight precursors as well as the cured material. The following critical engineering challenges must be addressed when designing settable biomaterials for clinical use.

Despite meticulous surgical care, the incidence of bacterial infection resulting from implanted biomaterials can be as high as 5% [27, 28, 40-43]. Infection rates are highly dependent on the type, application, and location of implantation [40]. Orthopedic and cardiovascular implant infections are more serious, and as with many biomaterial infections the bacteria involved are also increasingly resistant to common antibiotics [27]. Infections associated with implants can result in tissue damage, excess surgeries, implant failure, or mortality[27,28].

Sterilization is the first line of defense against bacterial infections. Settable systems are more sensitive to sterilization procedures due to potential polymerization or loss of reactivity of the monomeric components, which would adversely affect their performance. Applications that utilize injectable systems to deliver bioactive molecules or drugs are particularly sensitive, and consequently sterilization and its effects on the

efficacy of these biologics must be analyzed. For most settable biomaterials, ethylene oxide (EtO) or gamma irradiation is the gold standard for sterilization of liquid organic components [44-46]. Radiation doses below 25 kGy have been reported to have minimal effects on the functionality of most biomedical polymers [46].

A growing amount of research has been applied to local delivery of antibiotics or other agents from an implanted material [47-55]. Local delivery of agents has the benefit of sustaining effective doses directly at the site of implantation. Although systemic delivery can provide basal levels of protection from infection, its ability to provide bacteriocidal concentrations at the implant site is limited due to ischemic conditions and the inability of the drug to diffuse to the surface of the implant [56]. Since bacterial colonization occurs on the surface of biomaterials, local delivery of antibiotics from the implant allows for a more controlled targeted therapeutic intervention. Settable biomaterials loaded with active agents during the mixing of the precursors [48, 49]. The release of the antibiotics is typically diffusion-controlled, which can be tuned based on material parameters [48, 49, 52]. While the incorporation of antibiotics for localized delivery holds much promise, concerns remain about overuse and the occurrence of resistant bacterial strains [27, 56].

Handling properties of settable biomaterials, such as storage, mixing, and delivery, must be optimized to facilitate ease of use in the clinic [25]. Storage requirements are highly dependent on the composition of the material. Water-soluble materials can be lyophilized to improve shelf life and require re-suspension or solubilization before use [57]. Stabilizers can be added to reactive organic liquids to enhance storage stability. Storage at low temperatures and/or reduced pressures in containers purged with an inert gas can further enhance stability. Regardless of the conditions under which the material is stored, care should be taken to ensure functionality is retained. Depending on the number of precursors required for a given system, the materials might need to be mixed directly prior to injection.

Rheological characterization can provide insight into the viscoelastic properties of materials *in situ*, which can directly translate into clinical performance of an injectable system. The most useful properties

obtained from rheology are shear thinning, yield stress, and cure profiles. Many biphasic injectable systems, such as injectable composites or cements, exhibit yield stresses spanning a range from 1 – 1,000 Pa [58-60]. The yield stress is directly correlated to the injectability of the system, with lower yield stresses resulting in easier injection. There are additional factors required to fully define injectability, such as diameter of the injection device and molecular interactions [61], but the yield stress and shear thinning behavior provide valuable insight on *in situ* viscoelastic properties of injectable systems that can be directly translated into clinical performance. The time between mixing and chemical gelation, also known as the working time, is a crucial parameter for characterizing settability. Working time can be calculated from the rheological cure profile measured under constant strain conditions [62, 63]. The working time is also known as the gel time, at which point the material has formed a network and can no longer flow. Working times of 5 – 15 min are preferred for clinical use [25].

In regenerative applications, biomaterials must support infiltration of cells and ingrowth of new tissue, and also degrade into non-toxic breakdown products [64]. The mechanism and rate of degradation of a biomaterial after implantation affects the release of degradation products and the healing of the surrounding tissue. Upon implantation, degradation inevitably results in loss of mechanical strength. Therefore, it is imperative to tune the degradation rate to allow proper cellular infiltration and remodeling, which will return native function and eventually mechanical properties.

Many types of biomaterials are designed to degrade by passive mechanisms (e.g., hydrolysis). Hydrolysis rates are dependent on the type of crosslinking, chemical structure of the precursors, and the anatomic site [65]. The rate of hydrolytic degradation can in many cases be adjusted to match that of remodeling. However, in the case of polyesters, a commonly utilized polymer for injectable biomaterials, hydrolysis occurs faster at low pH and the degradation products of hydrolysis are acids [66]. This can lead to auto-catalytic degradation, which can subsequently increase degradation rates at later time points *in vivo* [67]. Furthermore, the local reduction in pH can cause tissue damage which hinders healing [68].

Calcium phosphate cements

Since their initial discovery in 1982 [69], injectable calcium phosphate cements (CPCs) have been successfully introduced into the clinic for a number or orthopaedic and craniomaxillofacial applications, including repair of tibial plateau fractures and calvarial defects. CPCs have been investigated extensively as injectable bone replacement (altneratives to auto- or allo-graft) biomaterials due to their similar chemical composition to the mineral component of bone, biocompatibility [70], osteoconductivity, and fast setting times (< 5 min) [71]. These biomaterials set at a physiological pH with minimal reaction exotherm and do not release toxic monomers or solvents [72, 73]. Apatite, which has low solubility and resorbs slowly, and brushite, which has higher solubility than apatite and resorbs more rapidly, comprise the two primary classes of CPCs [74]. While CPCs set by an acid/base reaction that can reduce the pH of the paste to values as low as 3 [75], a number of *in vivo* studies have reported favorable host responses after setting [76, 77].

CPCs, such as commercially available PRO-DENSE® (Wright Medical), have recently proven mechanically superior to autografts in tibial plateau fractures. This claim is supported by a retrospective study reporting that 61% of patients treated with buttress plating and autograft experienced loss of reduction after one year, compared to 23% of patients treated with a hydroxyapatite (HA) bone cement [7]. Other CPCs include Norian® SRS® (Synthes), HydroSet (Stryker), and Beta-bsm® (ETEX). Primary limitations of first-generation single phase CPCs include brittle mechanical properties, which lead to low shear strength and fracture toughness; slow degradation and remodeling *in vivo* [78]; and the small pore size (0.1 – 10 mm), which results in slow cellular infiltration and ingrowth of new bone [70,79]. These limitation can result in prolonged recovery times, joint stiffness, and increased cost to society; consequently limiting these materials' use in weight-bearing applications [16, 80, 81]. Both low porosity as well as small pore size in CPCs contribute to slow remodeling and ingrowth of new bone, and have thus been suggested as a root cause for the failure of CPCs in periodontal bone repair [82]. Therefore, recent studies have focused on introducing macropores into CPCs and improving their

mechanical properties while preserving their favorable biocompatibility in order to improve their clinical performance.

A number of other strategies have been investigated for fabricating injectable macroporous CPCs. Biocompatible and degradable polymeric microspheres such as poly(lactic-co-glycolic acid) (PLGA) [83]), poly(trimethyl carbonate), or gelatin [84, 85] have been investigated to synthesize macroporous CPCs. While incorporation of PLGA microspheres in CPCs has been suggested to improve the initial strength of the composites, the strength decreases upon dissolution of the microspheres and does not increase until new bone starts to grow into the macropores [86]. Due to their macroporosity, injectable CPCs incorporating a porogen have significant advantages compared to monolithic CPCs. Thus, macroporous CPCs are anticipated to be considered a preferred choice for healing of bony defects after regulatory approval[78]. In an alternative approach, CaP granules suspended in aqueous solutions of hydroxy-propylmethyl-cellulose promoted faster initial ingrowth of new bone at the surface of the material, relative to macroporous CPCs [87, 88]. It has been suggested that the observed early apposition of new bone could potentially enhance the interfacial bonding between host bone and the CPC, thus reinforcing the material for weight-bearing applications[78].

Besides CPCs, there has been a recent trend towards the use of highly resorbable bone substitutes. These substitutes include β-tricalcium phosphate (β-TCP) and brushite, which are resorbed by cells and simple dissolution, respectively [81]. Caution is required when designing a bone graft substitute based on these fillers, as these material resorb rapidly than bone can often grow in, which can cause fibrous tissue to fill the defect [89].

Polymeric Biocomposites

Polymer-based tissue engineering is a promising approach for meeting the shortcomings of autografts, allografts, and CPCs, in the orthopaedic field. Various properties of polymeric materials (including mechanical

properties, degradation rate, and microstructure) can be altered over a wide range through variations in composition and structure to meet the needs of a specific application. Originally, both natural and synthetic polymers were often designed to replace heavy metal parts of endoprostheses. While this substitution did not take in the market, future polymers were designed for biodegradable applications. In general, polymer-based scaffolds and composites aim to mimic native bone properties at initial implantation as well as at later time points as the body slowly incorporates them. Additionally, the combination of ceramics with polymers in a biocomposite form has been suggested as an alternative approach to designing synthetic bone graft materials with tougher mechanical properties, improved biological behavior, and modified degradation mechanisms.

Due to their tunable degradability, biocompatibility, processibility, and versatility, polymeric biocomposites are principle materials investigated for the development of synthetic bone scaffolds, cements, and composites [90]. A polymeric biocomposite is made of two or more bulk biomaterials (at least one a polymer) of different phases intended for use in the body. Classic polymeric biocomposites for orthopaedic applications are composed of a solid synthetic ceramic phase that is osteo-conductive or -inductive [91] and a biocompatible polymer that was at one stage a liquid.

An ideal polymeric biocomposite both initially mimics the properties of the native bone tissue it is intended to replace and also remodels to form new bone. Consequently, choosing the appropriate individual components within a biocomposite and the manner in which they are combined is critical. These components must be biocompatible, biodegradable, and mechanically robust. The ideal polymeric biocomposite must be fabricated in a manner that allows it to be safely implanted into the intended defect site and subsequently promote bone remodeling or regeneration. The solid phase is typically one of the following calcium phosphate ceramics: bioactive glass (BG) [92-96], hydroxyapatite (HA) [97-104], biphasic calcium phosphate, or tricalcium phosphate (TCP) [29]. These solid phase fillers come in a variety of shapes and sizes, including macro- and nano-

rods/fibers [92, 94, 95] and particles/powders [29, 93, 96-104]. The biocompatible polymer phase is typically one (or a co-polymer mixture) of the following: polyesters, polyethers, polyanhydrides, or polyurethanes.

Table 2.2. Polymeric biocomposites that utilized surface-modification of filler

Filler Material	**Polymer Binder**
Hydroxyapatite (macro- and nano-particles) [1-4]	Glycidyl dimethacrylate, urethane dimethacrylate, and triethylene glycol Dimethacrylate [6]
	Polyethylene glycol and poly(butylene terephthalate) (PEG/PBT) block copolymer [3, 7]
	Bisphenol A glycidyl methacrylate (BisGMA) [8]
	Polyethylene [11], High-density polyethylene [13]
Bioactive Glass (fibers, particles)	Polyester urethane [14]
	Poly(ε -caprolactone)[8]
	Urethane dimethacrylate and 2-hydroxyethyl methacrylate [22]
	Poly(L-lactide) [23, 24]
Tricalcium Phosphate	Poly(L,DL -lactide) [26]
Phosphate Glass	Poly(ε-caprolactone)[4, 29]
TiO_2	High-density polyethylene [31]

Numerous polymeric biocomposites that have utilized techniques to modify the surface of the solid phase before combination with the polymer have been developed. The filler material and polymer binder combinations that fit this criterion are paired in Table 2.2. In addition to the surface modification techniques, what differentiates these biocomposites from one another are the fabrication processes used to combine the polymer and bioactive components and the polymerization of the polymer itself. A general schematic of how surface-modified polymeric biocomposites are fabricated is shown in Figure 2.1A.

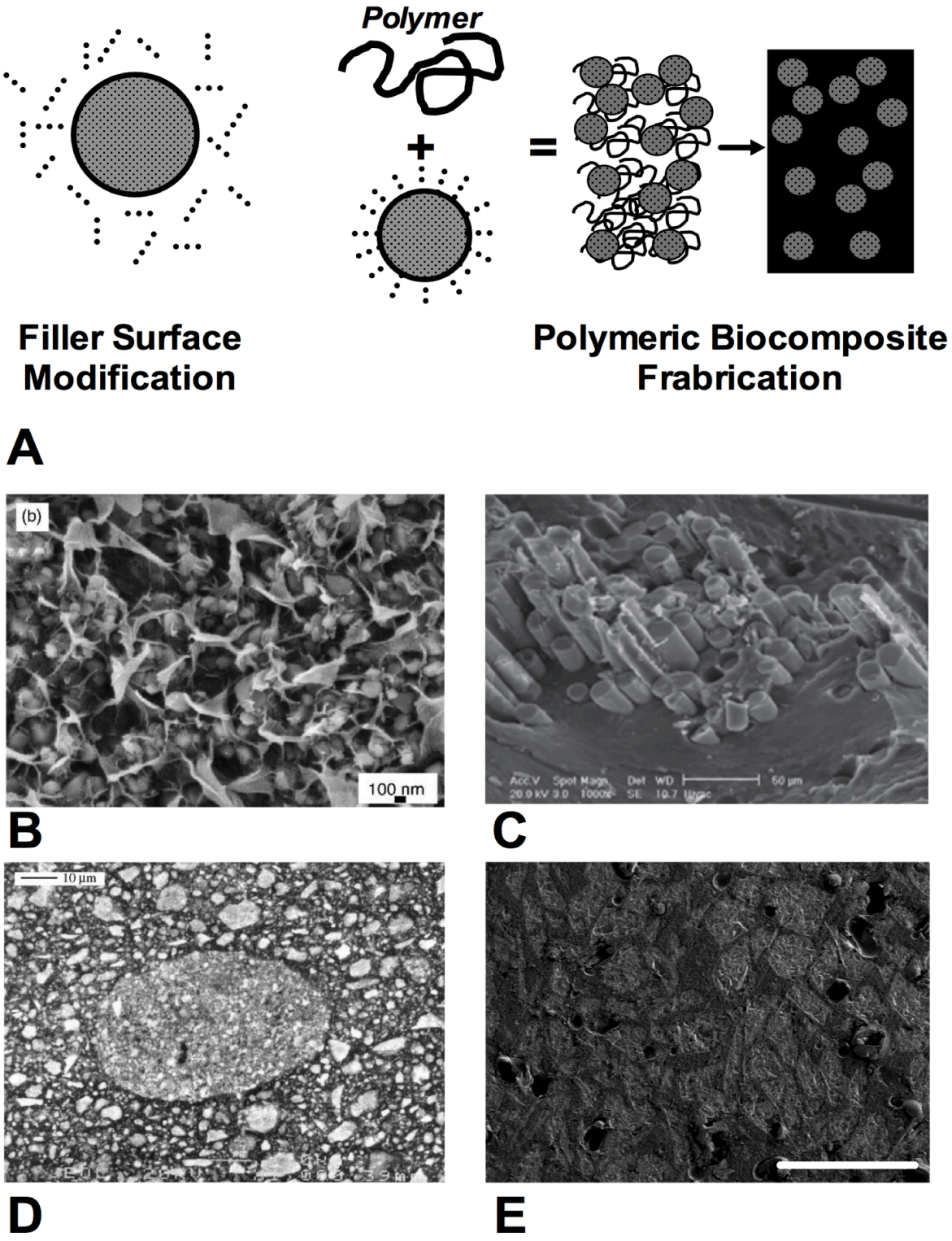

Figure 2.1. Surface modified polymeric biocomposites. A) Schematic of general fabrication of polymeric biocomposites. Cross-section SEM images of biocomposites made with silane modified fillers: B) TiO_2/HDPE, C) phosphate glass fibers/PCL, D) modified HA/BisGMA, and silane+PCL modified fillers: E) BG/PUR.

Fabrication methods utilized for surface-modified polymeric biocomposites include solvent casting, compression molding, monomer transfer molding, monomer-induced polymerization, and reactive liquid molding. All fabrication techniques other than reactive liquid molding require the polymeric biocomposite to be fabricated before *in vivo* implantation, or 'pre-fabricated.' During solvent casting, solidified polymer is dissolved in a solvent, the solid component is added to the polymer/solvent solution, the resulting slurry is transferred to the desired mold, and the solvent is evaporated [104,102]. The compression molding process involves applying heat and pressure to combine the polymer and solid phases to conform to the desired shape of an open mold cavity. The polymers used in this method can be thermosetting or plastic [92, 94, 97, 101]. Monomer transfer molding is similar to compression molding in that a predetermined shape is filled to create a pre-fabricated composite, but instead of utilizing force, monomers are polymerized within a heated mold cavity. The monomer mixture remains enclosed in a mold until it has polymerized and fully cured[94, 95]. Another method utilizing unreacted monomers is induced monomer polymerization, in which the polymer phase is formed in the presence of the solid filler to form a polymeric biocomposite. This method is often used to fabricate resin-based biocomposites. Thermosetting resins form irreversible bonds once cured, and thus the shape of the mold is critical, as the polymer phase cannot be reshaped via heating once cured [93, 99 93 98, 99]. Induced monomer polymerization can be initiated by heat and pressure [98, 99] or a photosensitizing agent activated by a light source [93]. The last polymeric biocomposite fabrication method relies on reactive liquid molding of multiple liquid components that polymerize *in situ* to fabricate the polymer phase of the biocomposite [24, 96, 105, 106]. While the previously outlined pre-fabricated methods require mold shaping, polymerization, and/or curing before *in vivo* implantation, polymeric biocomposites fabricated by this form of *in situ* polymerization can cure post-implantation *in vivo*[96] and do not require a solvent, heat, pressure, or any other form of energy to set *in vivo*, and can completely fill the cavity of a targeted defect site.

Polyurethanes

Since the 1980s, polyurethane (PUR) has been used as a biodegradable material in medical device applications [36]. PURs are a class of polymers derived from the reaction of isocyanates (hard segment) with hydroxyl-terminated oligomers (polyols, soft segment). Polyurethanes[36] comprise a diverse family of materials including cast elastomers, thermoplastic elastomers, and flexible foams. The alternating hard and soft segments in the block co-polymer provide physical strength and elasticity, respectively. PUR elastomers are widely utilized in areas ranging from medical device coatings to tissue engineering [36, 107]. Injectable and settable PURs are prepared from multi-component reactive liquid systems, which comprise polyisocyanates, polyols, water, stabilizers, and catalysts. In isocyanates-hydroxyl reaction, hydroxyl from the polyol reacts with isocyanates to form urethane bonds [36]. There are numerous types of polyols used to date, including lactide, glycolide, and caprolactone [36, 108, 109]. Common catalysts used in injectable PUR systems are amine or metal-based. Amine-based catalysts are non-toxic, but they selectivity catalyze the water-isocyanate reaction, making balanced reactions more difficult [110, 111,112], while the more cytotoxic organometallic catalysts selectively catalyze the polyol-isocyanate gelling reaction. However, the isocyanate-water reaction produces a d-substituted urea, which improves strength of the network via hydrogen bonding [113]. Furthermore, the water reaction produces carbon dioxide which acts as a blowing agent, similar to gas foaming, to form porous PUR foams *in situ* that facilitate cellular infiltration [113]. Macropores that facilitate cellular infiltration can be generated within the scaffold by the process of gas foaming [114-116] or by encapsulation of porogens[117]. Metallic catalysts selectively catalyze the polyol-isocyanate reaction, but are generally more toxic then their amine counterparts [110]. Combinations of catalysts can be utilized to produce PURs with varying porosity and mechanical properties.

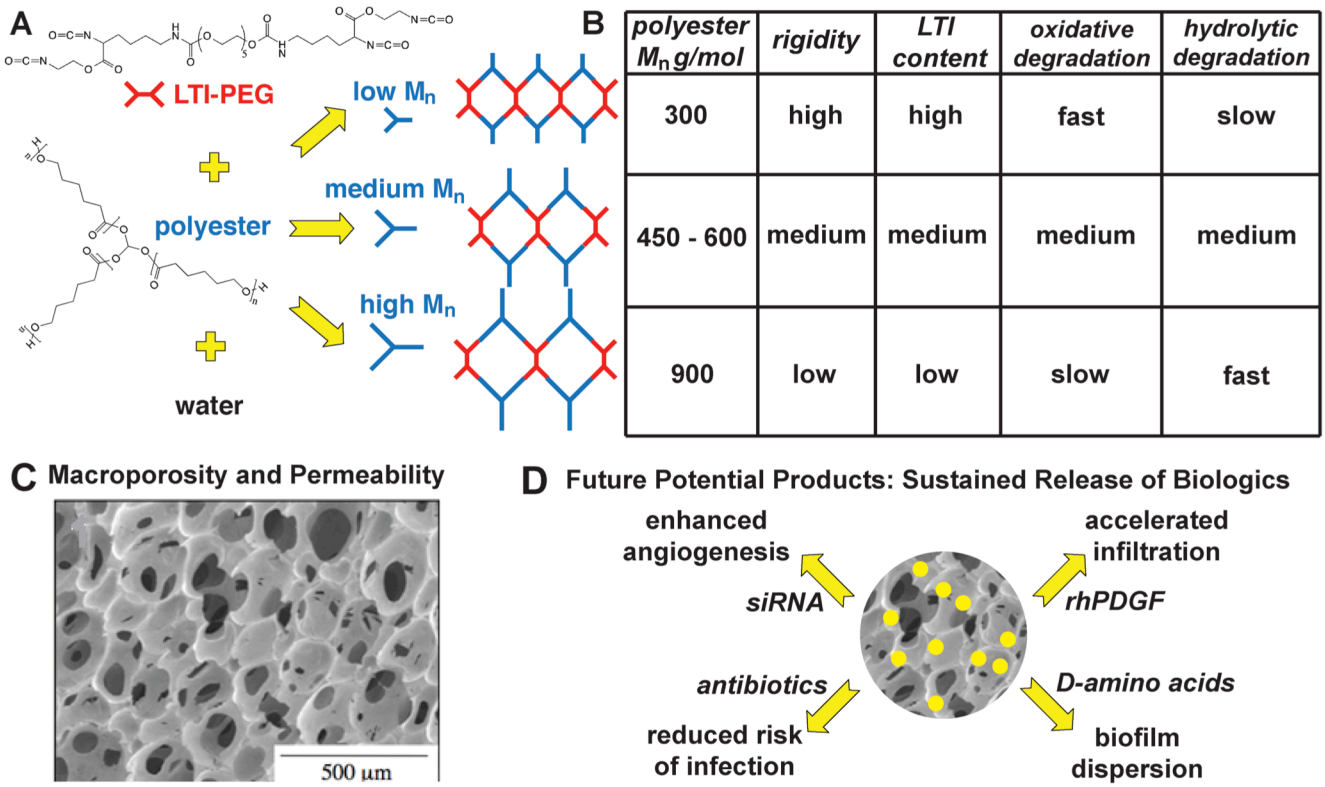

polyester M_n g/mol	rigidity	LTI content	oxidative degradation	hydrolytic degradation
300	high	high	fast	slow
450 - 600	medium	medium	medium	medium
900	low	low	slow	fast

Figure 2.2. Schematic summarizing synthesis and properties of PEUR scaffolds. (A) An LTI-PEG prepolymer (red) and polyester triol (blue) are mixed for 2 min, loaded into a syringe, and injected. (B) After 10 min, the mixture gels to form a porous polymer network. LTI content, crosslink density, rigidity, and the rate of oxidative degradation increase with decreasing molecular weight (M_n) of the hydrolytically degradable polyester. (C) Scanning electron microscopy (SEM) image of a cured PEUR scaffold shows interconnected macropores. (D) Biologics can be mixed with the reactive PEUR prior to cure, resulting in diffusion-controlled release.

The synthesis and tunability of injectable PUR foams is shown in Figure 2.2. As shown in Figure 2.2A, component 1 comprises either an isocyanate or an isocyanate-terminated prepolymers, while component 2 includes all components with active hydrogen groups that react with the isocyanate (NCO) groups. The polyol component, which comprises a hydroxyl-terminated macromer with a polyester, polyether, or polycarbonate backbone, reacts with the prepolymer to form a polymer network linked by urethane groups (the gelling reaction). The NCO groups also react with water, either added to the formulation or present in the wound

environment, to yield a disubstituted urea and gaseous carbon dioxide, which acts as a blowing agent to form interconnected macropores within the PUR network [114-116] as shown in the SEM image (Figure 2.2C).

There are numerous sources for liquid isocyanates that could be used to formulate injectable biomaterials, however, care must be taken to ensure biocompatibility. Low molecular weight, aliphatic diisocyanates such as 1,4 butane diisocyanate and 1,6 hexamethylene diisocyanate are known to have non-toxic degradation products and are widely utilized in biomedical polymers [68, 118]. However, both these diisocyanates have low vapor pressures and are highly toxic as inhalants, limiting their use as injectable precursors [119, 120]. To resolve toxicity concerns related to some of these liquid monomeric isocyanates, prepolymers of isocyanates synthesized from low molecular weight linkers can be used instead [109, 121]. Common aromatic isocyanates, such as toluene diisocyanate and methylene diphenyl diisocyanate, are highly toxic [122-124], and potentially degrade to aromatic amines, which are proven carcinogens [124-127]. While biodegradable PUR foams have been synthesized from aliphatic polyisocyanates[128], lysine-derived polyisocyanates have shown the greatest promise for injectable and settable systems[106, 112, 115, 116, 129-132]. The Guelcher Laboratory uses lysine-derived aliphatic polyisocyanates, primarily lysine triisocyanate- (LTI) based components, as an isocyanate source. Aliphatic isocyanates derived from lysine have a combination of high vapor pressure, low monomeric toxicity, non-toxic degradation products, and low melting point [109]. Lysine methyl ester diisocyanate (LDI) and lysine triisocyanate (LTI) have been utilized for injectable polyurethane applications in soft and hard tissue regeneration [106, 108, 109, 132-134]. While prepolymers of LDI were first used to synthesize porous, biodegradable scaffolds [115, 129], the technology was later adapted to fabricate a water-curable biomedical adhesive, which has been approved in the European Union [135] and has shown promising clinical data in many applications dominated by cyanoacrylates [136-138]. Generally, the isocyanate group is highly reactive toward most function groups, including not only hydroxyl but also amine [139]. PUR binders synthesized from these polyisocyanates have been shown to degrade to nontoxic compounds and support cell adhesion and proliferation *in vitro* [36, 106].

Soft tissue applications

For soft tissue applications, injectable formulations of lysine-based PUR foams have proven to produce a non-toxic reaction environment during injection, remain non-toxic until complete degradation, exhibit clinically relevant handling properties, and form a simple method for incorporating therapeutics or cells [140-142]. LDI-[115, 129] and LTI-derived[132] prepolymers have been used to synthesize injectable and settable PUR foams for regeneration of cutaneous defects in rodent models. The cured polymers degraded to biocompatible breakdown products; such as lysine, PEG, and α-hydroxy acids[143]; induced a modest and transient inflammatory response; and supported the infiltration of cells and ingrowth of granulation tissue. LTI-derived scaffolds degraded at a rate similar to that of tissue ingrowth, and the regenerated tissue exhibited reduced alignment of collagen, which highlights the potential of the scaffolds for reducing scar formation. Recently injectable biodegradable foams composed of LTI and a polyester polyol were shown to promote cellular infiltration and ingrowth in a rat excisional wound model [140]. In another study, similar LTI-based porous PUR scaffolds were loaded with pH-responsive small interfering ribonucleic acid (siRNA) nanoparticles *in vitro* [142]. The siRNA nanoparticles were uniformly loaded within the PUR precursors during mixing and remained stable while the PUR foaming reaction completed [142]. The diffusion-controlled release was hypothesized to be effective for *in vivo* gene silencing over the period of several weeks [142]. The LDI technology has been further investigated in larger animals and clinical trials as a water-curable biomedical adhesive, which is designed to react with hydroxyl and amine groups in the host tissue. LDI-derived TissuGlu® Surgical Adhesive (marketed by Cohera Medical) has been approved in the European Union[135], and has been shown to reduce the accumulation of wound exudate in large flap procedures in patients (such as abdominoplasty[144]) compared to non-degradable cyanoacrylate adhesives.

Hard tissue applications

Injectable polyurethanes derived from lysine have been utilized in the development of biocomposites intended for tissue regeneration in hard tissue sites [26, 59, 106, 145]. There are numerous advantages to using this material in bone tissue engineering applications, due to its biocompatibility[36, 107, 146], biodegradability to nontoxic products, tunable degradation properties, use as a delivery mechanism, and potential for injectability [36, 108, 109]. Injectable formulations for hard tissue applications generally include LDI- or LTI-based prepolymers, amorphous polyester polyol, water, catalyst, solid filler, and therapeutics. Mineralized matrices, such as calcium phosphates [147] or allograft bone particles [59], can be incorporated in the liquid reacting mixture to increase the mechanical properties of the PUR biocomposite. Therapeutics, such as antibiotics [52] or growth factors [148] can also be added to aid the biological properties. In order to gain an improved understanding of this complex system, a comprehensive analysis of an injectable LTI-based polyurethane composite was completed in which the reaction kinetics were ascertained [62]. The amine-based catalyst triethylene diamine (TEDA) was found to be highly selective towards the water–isocyanate reaction. When the isocyanate concentration was lowered while the catalyst concentration was increased, the reaction rate was optimally tuned to prohibit excess foaming in aqueous environments similar to an active wound bed. NMR and *in vitro* cytotoxicity testing of the leachates from the reactive PUR before and after complete cure revealed that these components were non-toxic, and evaluation in a rabbit femoral condyle defect model showed no evidence of an adverse tissue response *in vivo*.

Several previous studies have shown the ability to utilize two-component PURs as a binder within biocomposites, derived from LDI[116, 145] and LTI[59, 106, 149], as injectable bone void fillers and cements. An extracellular matrix component, such as demineralized bone matrix (DBM), calcium phosphate particles, or allograft bone particles, is blended with the reactive PUR to increase the osteoconductivity and mechanical properties of the graft and also to reduce its volumetric expansion *in situ*. Lysine-derived PUR composites are injectable, set within clinically relevant working times (e.g., 5-10 min) to form grafts with mechanical strength

approaching that of host bone, and remodel and heal to form new bone. One study showed that injectable reactive PUR/allograft biocomposites are a promising approach for healing calvarial defects and are a local delivery vehicle for recombinant human bone morphogenetic protein-2 (rhBMP-2) [150]. In a second study, porous PUR biocomposites were utilized as a delivery vehicle for an antibiotic, vancomycin. This study showed, via a contaminated critical-sized rat femoral segmental defect, that this PUR system could be a potential clinical therapy for treatment of infected bone defects [52]. In an alternative approach, injectable foams prepared from an LTI-PEG prepolymer, a poly(ε-caprolactone-co-lactide-co-glycolide) triol, allograft bone particles (180 μm), and the low-toxicity tertiary amine catalyst triethylene diamine were evaluated in femoral condyle plug defects in rats[106] and rabbits[112]. Compared to LDI prepolymers, the LTI-PEG prepolymer has reduced viscosity (20,000 cSt versus 80,000 cSt for LDI-pentaerythritol) and higher reactivity[112]. Cells infiltrated the scaffold through migration into open pores, surface degradation of the PUR to non-cytotoxic breakdown products, and osteoclast-mediated resorption of the allograft bone particles, with no signs of chronic inflammation. Lastly, another study showed that the addition of PUR to calcium phosphate cements (CaPs), specifically HA and β-TCP, enhanced these materials' mechanical properties compared to the CaPs alone, in a biocomposite modality, rendering them potentially suitable for weight-bearing applications. Additionally, when implanted into rat femoral defects, these biocomposites showed evidence of cellular infiltration and appositional remodeling [105]. These formable polymeric biocomposites offer several advantages compared to pre-set implants due to their ability to cure *in situ,* consequently fit irregularly shaped defects, which provides the potential to be utilized as a non-invasive surgical applications. While challenges including controlling expansion due to the gas blowing reaction and matching the rate of new bone formation to polymer degradation need to be addressed, the ability of PUR grafts to cure *in situ* without adversely affecting host tissue, degrade to non-cytotoxic breakdown products, and support infiltration of cells and new tissue underscores their potential as injectable biocomposite for tissue repair. These studies suggest that injectable and settable lysine-derived PURs are promising materials for both soft and hard tissue regeneration.

Drug delivery applications

Injectable lysine-derived PUR materials have also been investigated as drug delivery systems to support both diffusion-controlled release of biologics added as labile powders[52, 142, 149, 151] as well as degradation-controlled release of drugs covalently bound to the polymer[130, 131, 152-154]. In a recent study, injectable LTI-derived PUR/allograft bone composites augmented with rhBMP-2 as a labile powder enhanced new bone formation at 6 weeks in a critical-size rabbit calvarial defect model[59]. Recent studies have reported that the release kinetics of biologics can be controlled by the composition of the drug,[131] the choice of catalyst,[130] or the addition of ionic ligands[152], which offer greater tunability compared to diffusion-controlled release.

Infection

Despite diligent clinical management, which includes prophylactic antibiotics and debridement, of severe open fractures with bone loss, infection is a common occurrence. Infection is the most common cause of delayed amputation in combat-related open tibial fractures [155]. The generally accepted theory to explain the chronicity of osteomyelitis bone infection is the development of a biofilm, surface attached communities of microbial species that are protected by a self-produced extracellular polymeric matrix [156, 157]. The biofilm allows for growth of organisms to persist within immunocompetent hosts [158, 159]. Staphylococcus aureus (*S. aureus*)-based biofilms have been found in bone of patients with osteomyelitis [159, 160].

It was once hypothesized that the local delivery of antibiotics to the infected bone site could prevent or reduce the prevalence of biofilm formation. Previously, diffusion-controlled release of the antibiotic vancomycin and rhBMP-2 from a polyurethane scaffold controlled infection[52] and enhanced bone healing[161] in critical-size defects contaminated with 10^5 Colony Forming Units (CFUs) *S. aureus*. Recent research has shown that the antibiotic concentrations needed to eliminate biofilm sessile colonies can be more than 500 times those

required to kill planktonic bacteria [162]. Additionally, common antibiotics at these high concentrations negatively affect osteoblast osteogenic-activity [163].

An alternative approach to treating infection with conventional antibiotics is through the local delivery of biofilm dispersal agents. D-isomers of amino acids (D-AAs) have been shown to prevent and disperse a biofilms formed by various bacterial species, including *S. aureus* [31, 164, 165]. A previous study investigated the local delivery of various D-AAs, through augmented PUR scaffolds, to locally contaminated rat segmental defects [165]. Incorporation of D-AAs into PUR scaffolds significantly reduced bacterial contamination *in vivo*. Additionally, *in vitro* testing on clinical isolate-based biofilms of *S. aureus* demonstrated that multiple D-AAs were effective at dispersing and preventing biofilm formation. Lastly, the D-AAs tested were not cytotoxic to host mammalian cells.

Silicate bioactive glass

A bioactive material has been defined as a material that undergoes specific surface reactions when implanted into the body, leading to the nucleation of a hydroxyapatite- (HA)- like layer [166, 167]. The surface reactions involve dissolution of soluble Si, Ca, P, and Na ions that alter the local environment and have been connected to intra and extracellular responses that are critical for bone regeneration (osteogenesis) [168]. Additionally, this layer partly attributes to the materials ability to bind to native hard and soft tissues [167, 169]. Though it is not completely understood, the initial biological mechanisms of bonding to bone are thought to involve attachment of growth factors, followed by the attachment, proliferation and differentiation of osteoprogenitor cells [170]. *In vitro*, a material's bioactivity is evaluated by its ability to form a HA-like layer when immersed in simulated body fluid (SBF), a solution that has ion concentrations nearly identical to that of

physiological solution. It has been suggested that this *in vitro* bioactivity is an indication of the *in vivo* bioactivity potential of a material [171].

The most common method for fabricating bioactive glass is to form melt-derived glass produced using conventional glass processing techniques at high temperatures. A secondary fabrication method is based on chemical precursors and sol-gel processing followed by ambient atmosphere drying and thermal stabilization [168]. The sol-gel technique has many potential advantages, including the capability to produce a more homogenous mesoporous material with increased specific surface area by two orders of magnitude and porosity (two critical factors that affect bioactivity) compared to glass made from the melt-derived technique and the versatility to fabricate materials in a variety of forms [172, 173].

Since the 1970s, the mostly widely researched bioactive glass for biomedical applications has been the bioactive glass, designated 45S5 (due to its 45 wt% composition of SiO_2), because of its osteo-productive and conductive properties [174-176]. Subsequently, 45S5 bioactive glass (BG) has been used in several medical devices approved by the U.S. Food and Drug Administration [173]. This material's compositional features (composed of SiO_2, Na_2O, CaO and P_2O_5) are responsible for its Class A level of bioactivity, particularly due to its low SiO_2 content, high Na_2O and CaO content, and high CaO/ P_2O_5 ratio [177].

Reported shortcomings of BG remove it from consideration as a material that alone can be used for weight bearing bone replacement applications. Some discrepancies have risen related to the biocompatibility of BG, particularly exposed particles utilized for bone regeneration purposes [178]. In these cases, alkanilisation occurs on the surface as a result of the release of silic acid, which is attributed to some degree of inflammatory response [179, 180]. Mechanically, melt-derived BG has high compressive strength (500 MPa) but is naturally brittle, and therefore lacks the toughness desired for weight-bearing applications [177, 181, 182].

Bioactive glass has been included in numerous composites made with various degradable polymer binders, including poly(3-hydroxybutyrate), poly hydroxybutyratevaalerate, and polyurethane [181, 183, 184]. Injectable melt-derived BG/dextran composites have been reported to remodel and form new bone in rabbit femoral condyle plug defects [185]. Similarly, a BG/glycerin and polyethylene glycol (denoted NovaBone) composite showed to increase the formation of bone versus BG alone, as well as an empty defect, in vertebral body defect model in sheep [186]. Despite these composite binders being non-setting polymers with low mechanical strength and fast degradation kinetics, BG particles were reported to be present in both defect areas through 12 weeks. These results highlight the relatively slow dissolution rate of melt-derived BG and the potential for it to contribute the mechanical stability of a composite for an extended time period.

Interfacial bonding between phases within composite materials

Often the goal in the development of a composite for any application is to combine the bulk properties of various components or phases into a cohesive, uniform structure. It is not surprising then that the interface between two phases within the composite, frequently a liquid and a solid, is a vital relationship that has numerous downstream effects. The surfaces of the individual components can be altered and tailored in numerous ways, before combining them in a composite form, in order to achieve desired properties of the individual components within the composite or the resultant composite structure as a whole. The term surface modification refers to the physical attachment of molecules, predominantly silanes and/or polymers, to the surface of a solid phase material. Polymeric biocomposites are a class of biomaterials that comprise a biocompatible bulk polymer and a particulated solid phase, often referred to as a binder and filler, respectively.

While the high compressive strength and bioactive properties of bioactive glass make it an ideal material for synthetic bone, the high elastic modulus (35 GPa for BG [182]) make it necessary to be combined with a less

stiff material in the form of a composite [187]. The interface between the constituent organic and inorganic phases within a composite is often the weakest link for nucleation of cracks, which can lead to overall premature failure; consequently the bond strength of the biomaterial interfaces in composite materials is critical [187]. Interfacial bond strength is a function of both chemical and mechanical considerations. Surface parameters related to the chemistry, topography and thermodynamics are thus of great consequence. In order to improve the mechanical strength of the composite, the adhesion and bond strength of these interfaces must be understood and ideally maximized. The adhesion between the solid organic and liquid inorganic phases is directly dependent on wettability and surface energy [187]. Physical bonding is common at polymer/ceramic interfaces and frequently ceramic grafting is use to enhance adhesion in hybrid composites [187].

Silane surface modification of solid fillers

One of the most prominent surface modification techniques applied to particulated materials (typically with an inorganic composition) within polymer biocomposites is the attachment of organofunctional silanes, which are silicon-based chemicals that contain both organic and inorganic reactivity in the same molecule. Monomeric silicon chemicals (silanes) that contain at least one silicon-carbon bond (Si-C) structure are known as an organosilanes [92]. The general structure of an organosilane, $R_nSiX_{(4-n)}$, has two classes of functionality, where X is a hydrolysable group, such as halogen or amine, and R is a nonhydrolysable organic radical that typically possesses the functionality with the exposed desired characteristics [188]. Commonly utilized silanes have one organic substituent.

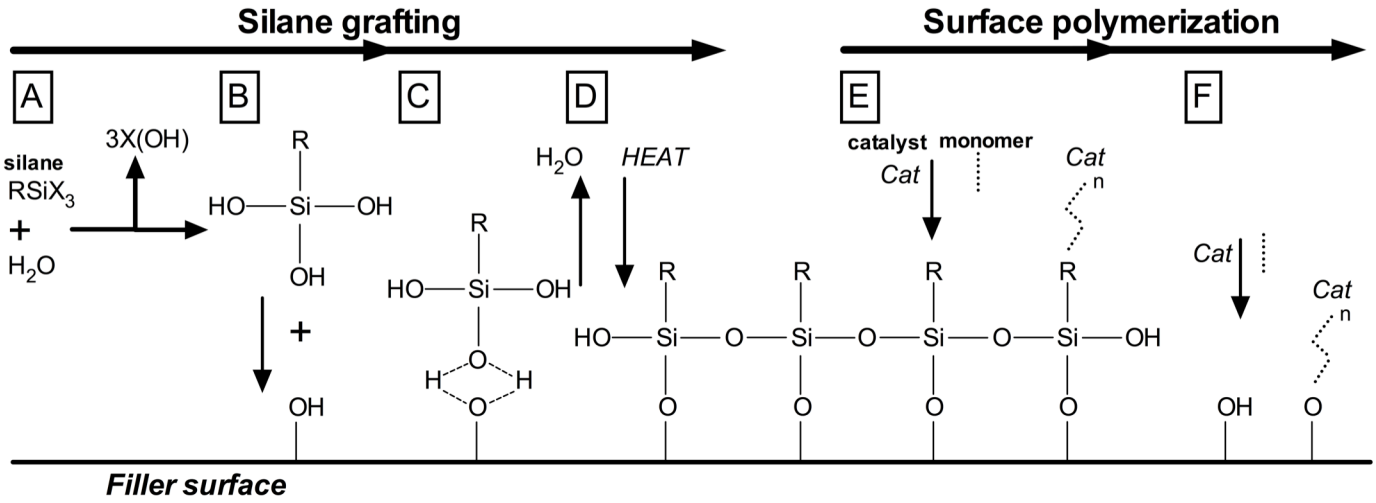

Figure 2.3. Schematics of common surface modification techniques: silane coupling agent grafting and surface

The attachment of these molecules occurs through four generalized steps, as shown in Figure 2.3. First (Figure 2.3A) hydrolysis of the labile groups occurs, followed by (Figure 2.3B) condensation to oligomers. Next (Figure 2.3C), oligomers hydrogen bond to exposed hydroxyl groups on the solid surface. Lastly (Figure 2.3D), a covalent linkage is formed between the silicon and filler particle, with the loss of water during curing and drying steps [188]. Subsequently, there is usually one bond from each organosilane silicon to the surface, with the two remaining silanol groups present in the condensed (to other silanols to form siloxane linkages) or free form. Theoretically, a monolayer is sufficient to provide the desired result. However, due to the reactive nature and mechanism of silane molecules, multi-layer silane coverage can be attained. In order to ensure uniform coverage, often more than one layer is applied to portions (if not all) of the desired surface. The end result is a siloxane polymeric network close to the inorganic surface typically <5 nm thick. The result of silane surface modification is dependent on the chemical composition of the end group of the silane and the interacting organic phase, as well as their relative chemical compatibility. Potential results include a change in wetting and adhesion characteristics of the solid, as well as the ability to catalyze chemical transformations at a heterogeneous interface.

There are various applications of silane grafting within a polymer composite system, such as a coupling or dispersal agent, as well as an adhesion promoter or water repellent, or a combination thereof. Surface modification by a silane is often used as a coupling agent between two components linked by the silane molecule, such as organic and inorganics. Within polymer biocomposites, any molecule that enhances adhesion with the polymer phase is technically a coupling agent, but ideally these agents form a covalent bond between an inorganic (usually the solid phase) and organic (polymer) compounds through an intermediary silane [188]. Although theoretically the covalent coupling is achieved by matching the reactivity of a (thermoset) polymer with that of the silane, this is difficult to accomplish due to the presence of functional groups that can react with unintended species present in the system. Additionally, silane coverage provides a method for controlling the surface energy (wetting) of a substrate, and thus can be described as an adhesion promoter. By altering the critical surface tension of a solid, liquids with a surface tension below this critical value will wet the surface, where as those above will not [188]. In polymer biocomposite systems, it is often desired to allow the uncured polymer binder to wet the solid phase component. The hydrophobicity of the organic group from the silanes will be imparted to polymers phase. This interaction is leveraged to increase the dispersion of particles within a polymer or to make a polymer more free flowing for injectable systems, thus decreasing its apparent viscosity [189]. Additionally, organosilanes are frequently used to repel water from a surface or within a composite system. This has been shown through the decreased water uptake of composites made with silanized-HA, compared to those made with unmodified HA [98].

Silane molecules are often required for the covalent attachment of additional molecules to the surface of inorganic components. After silanization, various molecules can be chemically bound to the inorganic surface depending on the functional end-group of the silane-coupling agent. These molecules include enzymes immobilized on the surface, but more often are synthetic polymer chains.

Surface polymerized polymer surface modification of solid fillers

Polymer attachment can be achieved by the "grafting-to" or "grafting-from" methods. Grafting-to occurs when a polymer is first synthesized and then attached, whereas grafting-from occurs when a polymer is grown from an active surface site through *in situ* polymerization [190]. There are benefits and drawbacks to both methods. The polymer attached in the grafting-to method must have an appropriate anchor sequence that will preferentially attach compared to the rest of the polymer. In contrast, surface-polymerized polymers created by the grafting-from method are not constrained by delivering the polymer to the surface or by the sequence of the polymer. This is because the density of the attached polymer is controlled by the density of initiation sites, often attached silane molecules. Attaching polymer chains to the surface removes the exposed reactive end-group (inherently present or via an attached silane), while still altering the surface properties of the inorganic solid.

The most common polymer family to be attached to solid inorganic materials is aliphatic polyesters, such as poly(ε-caprolactone) (PCL). PCL is a thermoplastic, bioresorbable (via hydrolysis), and semi-crystalline polymer that is synthesized by the ring opening polymerization (ROP) of ε-caprolactone monomer [94]. As depicted in Figure 2.3E, this *in situ* polymerization scheme can be catalyzed by tin (II) 2-ethylhexanoate ($Sn(Oct)_2$) or boron trifluoride dimethyl etherate ($BF_3O(CH_3)_2$) [94, 95]. A silane-coupling agent is used to polymerize the ε-caprolactone monomer from inorganic solids. The molecular weight of both the surface-polymerized and also bulk PCL is dependent on the polymerization time [96]. Depending on the reaction scheme, a continuous PCL phase can be formed surrounding the inorganic solid of interest. However, the PCL chains remain covalently bound to the surface of silane-modified inorganic solids after solvent dilution of the surrounding continuous PCL phase, as supported by x-ray photoelectron spectroscopy (XPS) analysis. Thus PCL surface polymerization is a useful method for modifying inorganic solids [95].

In a similar fashion, others have shown the ability to graft oglio(lactone)s to an inorganic surface without a silane coupling agent, as depicted in Figure 2.3F. This was demonstrated through protonation of a

TCP surface in an aqueous solution of phosphoric acid, followed by the *in situ* surface polymerization of lactones, such as PCL or L-lactide [29]. In this surface modification method, surface-polymerized chains were directly attached to exposed hydroxyl reactive groups inherent on the TCP surface.

Effects of Surface Modification on Filler Properties

Attachment of molecules to the surface of a solid filler in polymeric biocomposites affects a variety of innate properties, particular those related to the surface of the filler material. An overview of the surface modification techniques and how they alter specific filler properties is outlined in Table 2.3. The attachment of molecules affects the immediate physical and chemical composition of a surface, which can alter secondary surface properties. These primary and secondary properties do not necessarily alter how the filler interacts with polymer binders in a biocomposite setting, but these properties can change the inherent overall properties of the resultant filler.

Depending on the density, length, and steric effects of molecules attached to the surface, the apparent chemical composition of the filler has been changed. Not surprisingly, physical attachment of molecules can also alter the topography, or arrangement of physical features, of solid fillers' surfaces. However, molecular attachment does not necessarily preclude an observed increase in roughness. The attachment of silane molecules to fillers used for orthopaedic applications has been reported to smooth surfaces [93]. This is relevant to polymeric biocomposites because theoretically after the surrounding polymer binder has degraded and a filler surface is exposed, the surface topography can affect protein adsorption as well as cell adhesion and spreading.

Table 2.3. Effects of surface modification on material and polymeric biocomposite properties

Category	Surface modification	Parameter	Effect
Filler properties	Silane	Surface topography	Smoothed [93]
		Surface zeta potential	Increased [100]
		Surface wetting, apparent interfacial adhesion with polymer	Increased [97]
		Degradation rate	Decreased [92]
		Cell attachment	No effect [93]
		Bioactivity	Limited effect [100]
	Silane-polymer	Bioactivity	Decreased [102, 191]
Resultant Polymeric Biocomposite	Silane	Mechanical properties	Increased strength/stiffness [92, 93, 97, 192]
		Mechanical properties (post aqueous incubation)	Maintained [92]
		Uncured viscosity	Decreased [189]
		Filler incorporation into polymer binder	Improved [191]
		Filler surface-polymer adhesion	Improved [92, 189]
		Degradation rate	Decreased [92]
		Water absorption	Decreased [93, 98]
	Polymer	Filler surface-polymer adhesion	Improved [29]
		Mechanical properties	Increased strength/modulus [96, 103, 104, 193]

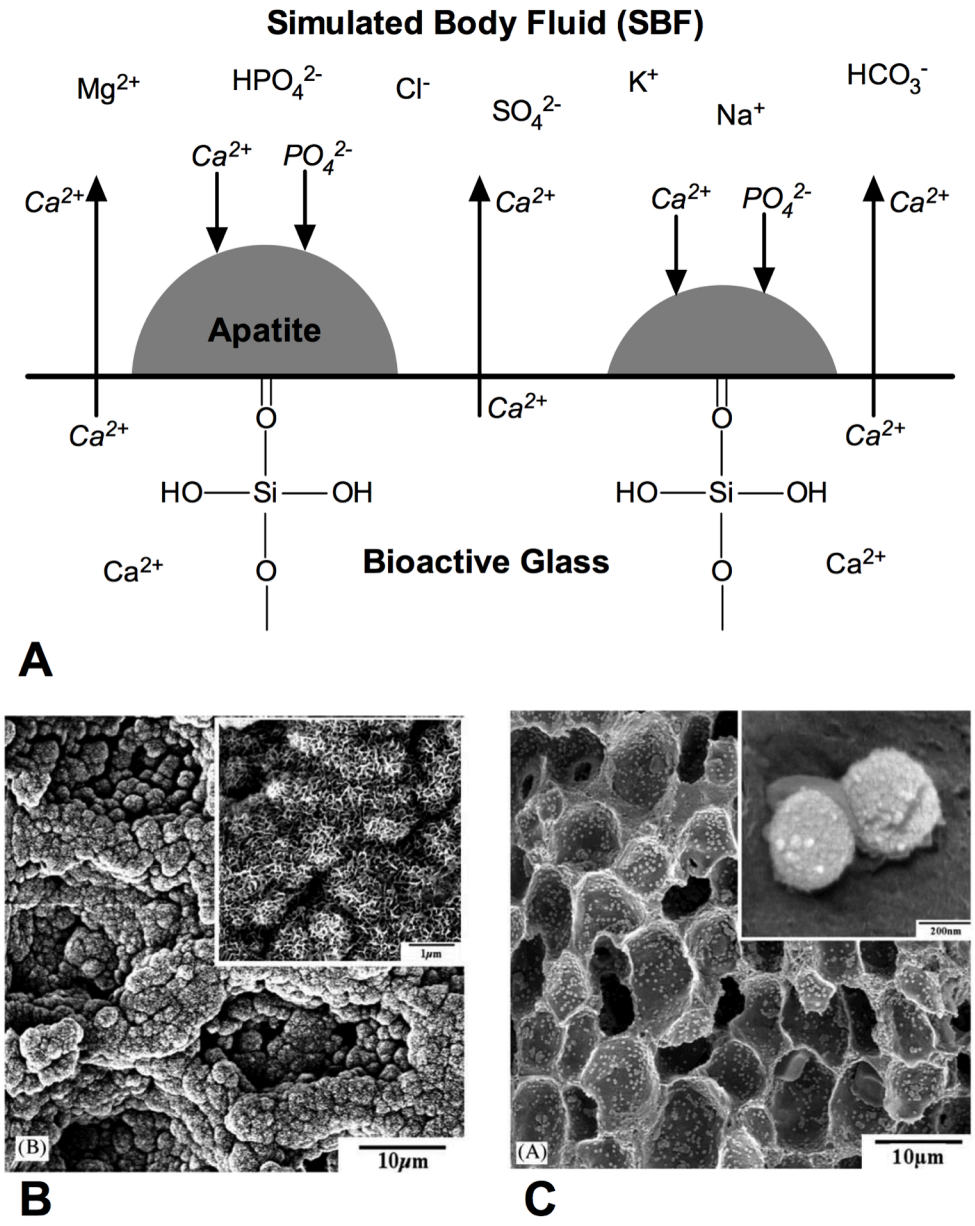

Figure 2.4. Effect of surface modification on solid filler properties: bioactivity. A) Schematic of surface reaction and subsequent nucleation of apatite on bioactive filler surface. Images from SEM of porous poly(L-lactide) composites made with A) un-modified BG and (c) silane treated BG, after 7 days in SBF, showing effect on nucleation of apatite.

Secondary surface properties that are affected by the attachment of surface molecules are related to surface interactions such as cellular interactions, wetting, and surface solution reactions including dissolution/degradation. Solid bioactive fillers in polymeric biocomposites ideally would not only produce an

environment conducive to osteoblast activity via ion release, but would also provide a surface conducive for cell attachment, integration, and proliferation. The presence of 3-(trimethoxysilyl) propyl methacrylate on the surface of sol-gel BG did not alter cell attachment of osteoblast-like cells to composites[93]. Wetting, the ability of a liquid to maintain contact with a solid surface, is an indicator of intermolecular interactions between and relative surface energy of the two phases. Wetting is important in the adhesion between a solid and liquid (e.g. a solid filler and polymer binder). As defined from the Young-Dupré relationship, increasing the wettability of a material increases the thermodynamic work of adhesion [187]. Adhesion between phases in a composite material is one factor that is presumed to alter the mechanical properties of the overall composite. It has been shown that surface modification of HA particles with the silane 3-aminopropyltriethoxy improved wetting of the particles by high density polyethylene (HDPE) polymer binder, and thus the apparent interfacial adhesion between the two phases [97]. With respect to tissue regeneration applications, bioactivity refers to controlled chemical release synchronized with the sequence of cellular changes occurring in repair [168]. Optimal rates of dissolution and reaction are key to stimulating cellular proliferation and differentiation. There are two classes of bioactive materials related to bone repair: Class A bioactivity leads to osteo-conduction (bone migration along a surface) and -production, while Class B bioactivity includes only osteoconduction [168]. Bioactivity is a direct result of surface reactions on a surface of the bioactive material, such as solid fillers utilized in polymeric biocomposites, and is quantified by the release of ions into solution as well as the formation of bone-like apatite onto a surface when in simulated body fluid (SBF) [100]. The surface reactions and subsequent nucleation of bone-like apatite onto a bioactive glass surface submerged in SBF is depicted in Figure 2.4A.

Surface modifications, via attachment of surface molecules, can affect the ability for surface reactions to occur between a solid surface and fluid within the body. This in turn can alter the overall properties of the bioactive material, the biocomposite, and their combined ability to aid in bone remodeling. It has been shown that the presence of aminosilane coatings on HA particles initially hindered the release of Ca and P ions in

aqueous solution, whereas vinyl- and methacryloxy- silane agents showed no effect compared to unmodified HA [100]. Similarly, porous poly(L-lactide) (PLLA) and surface-modified (with 3-amino propyltrimethoxy silane) BG composites formed less apatite compared to those with non-modified glass when incubated in SBF [191]. It is hypothesized that the observed delay is due to decreased diffusivity of released ions from the filler surface through the silane coating to the surrounding fluid. It is important to note that these surface modifications did not completely prevent ionic dissolution or apatite formation, but rather delayed such events.

The majority of solid fillers utilized in polymeric biocomposites for orthopaedic applications are capable of being resorbed or degrading after implantation in the body. The ability to degrade, often by dissolution, is often an advantageous quality when its degradation rate is appropriate. For instance, if the mechanical stability of the polymeric biocomposite is dependent on the solid filler, a fast degradation rate may not be desired. It has been reported that silane modification (with 3-aminopropyl triethoxysilane) decreased the overall cumulative degradation and degradation rate of phosphate glass fibers incubated in water [92]. This decreased degradation rate was attributed to the presence of a polysiloxane coating on the fiber surface.

Effects of Surface-modified Fillers on the Properties of Resultant Polymeric Biocomposites

Modifying the surface of solid fillers used in polymeric biocomposites controls the surface properties (both primary and secondary), which affects both the mechanical and physical properties of the resultant polymeric biocomposite as well as its ability to remodel *in vivo*. An overview of the surface modification techniques and how they alter the resultant biocomposite properties is outlined in Table 2.3. The fundamental theory of composite design is to obtain physical properties that lie between those of the individual components. As previously outlined, a primary motivator to modify the surface of a solid filler is to increase adhesion between the solid filler and polymer components, and thus the overall mechanical properties of the biocomposite. This observation has been supported by numerous studies citing an increase in tensile properties.

Other overall biocomposite properties that are affected by surface modification of filler components include binding to polymer phase, solid filler incorporation into polymer binder, water uptake, and degradation.

Surface modification has been noted to improve interaction between the surface of the solid filler and the polymer binder. As outlined previously, this is likely due to improved matching of surface tension and improved wetting by the (initially) liquid polymer. Proper matching can lead to homogenous distribution and improved incorporation of solid fillers into polymer binder, which has been hypothesized to improve related biocomposite properties, such as mechanical strength [92, 97]. One method utilized to determine the interaction between a liquid polymer and solid filler is by calculating the thermodynamic work of adhesion (W_{ad}) from the Young-Dupré relationship [187, 194]:

$$W_{ad} = \gamma(1 + \cos\theta) \quad (1)$$

where γ is the surface tension of the liquid polymer and θ is the equilibrium contact angle between the polymer and solid filler. This calculation is reliable for biocomposites in which dispersion forces are dominant [195]. In HDPE biocomposites, the viscosity of the overall uncured biocomposite were noted to decrease when [γ-methacrloxy)propyl]trimethoxysilane-modified TiO_2 particles were utilized compared to unmodified particles[189].

The overall mechanical properties of the resultant biocomposite are the properties most significantly altered by surface modification of the solid filler surface. In multiple biocomposite systems made with a variety of polymer binders, the presence of surface molecules (silane- and polymer-based) on the solid fillers increased the overall stiffness of the biocomposite, as shown by an increase in the tensile [92, 93, 97, 104, 191] and compressive moduli [96]. In a similar fashion, the presence of surface silane and polymer-based molecules on solid fillers increased the ultimate tensile [92, 97, 104, 191] and compressive strengths [96] of the various biocomposite systems.

The outlined surface modification techniques have been cited to minimize hydrolytic affects on the solid fillers, polymer binders, the adhesion between these phases, and thus the overall biocomposite properties. *In vitro* degradation experiments in aqueous solution provide information related to the mechanism and rate of degradation of the biocomposite once placed in the body. In PCL biocomposites with silane-modified phosphate glass fibers, a decreased rate of mass loss (overall composite degradation) was reported compared to biocomposites made with unmodified phosphate glass [92]. This altered rate was attributed to an increase in adhesion between the solid filler and polymer binder caused by the presence of siloxane bonds formed at the fiber surface. In the same PCL/BG biocomposite system, inclusion of silane-modified fibers was shown to improve overall biocomposite bending strength when incubated in an aqueous environment (analogous to being in the body) [92]. Qualitative observations from this study focused on appeared-adhesion between the polymer binder and fibers after subjection to degradation incubation followed by mechanical testing. It was noted that biocomposites made with unmodified fibers showed gaps of separation between the polymer and solid phases, where as the biocomposites made with modified fibers maintained their original integrity with respect to adhesion [92]. Other systems have reported a decrease in water absorption in composites with surface-modified filler, which could contribute to maintaining mechanical properties after implantation into the body[93, 98]. This may be due to a decrease in porosity and a reduction in water accumulation at the interface caused by an improved adhesion between the solid and polymer phases.

Large-animal defect models

There are several motivations for utilizing a large-animal, such as ovine, defect model for evaluating biomaterials. Data related the critical parameters used to evaluated the ultimate efficiency of the biocomposites can be obtained from these models, particularly a significant amount related to the biomechanical properties of the implant [196]. This is in large part because the bone biology, mineral composition, turnover and remodeling,

and the mechanical loading environment are similar to human conditions [196]. Since no major differences in bone mineral composition are evident, and both metabolic and remodeling rates are similar to humans [197], sheep are considered a valuable model for human bone turnover and remodeling activity [196]. Additionally, the bodyweight of mature sheep is comparable to adult humans, and their long bone dimensions enable the use of implants designed for applications in humans [198]. Lastly, the large bone and subsequent areas of interest allow bone defects to be explanted and biomechanical testing to be conducted on these specimens *ex vivo,* which is not feasible in small-animal models such as rat [199]. This provides a true evaluation of the mechanical properties of implanted materials and the surrounding native tissue throughout the healing and bone remodeling process.

References

1. M. Szpalski and R. Gunzburg: Applications of calcium phosphate-based cancellous bone void fillers in trauma surgery *Orthopedics.* **25**(5), S601 (2002).

2. S.S. Bajammal, M. Zlowodzki, A. Lelwica, P. Tornetta, III, T.A. Einhorn, R. Buckley, R. Leighton, T.A. Russell, S. Larsson and M. Bhandari: The use of calcium phosphate bone cement in fracture treatment *Journal of Bone and Joint Surgery-American Volume.* **90A**(6), 1186 (2008).

3. D.N. Yetkinler, R.T. McClellan, E.S. Reindel, D. Carter and R.D. Poser: Biomechanical comparison of conventional open reduction and internal fixation versus calcium phosphate cement fixation of a central depressed tibial plateau fracture *Journal of Orthopaedic Trauma.* **15**(3), 197 (2001).

4. A.J. Harmata, C.L. Ward, K. Zienkiewicz, J.C. Wenke and S.A. Guelcher: Investigating the Effects of Surface-Initiated Polymerization of ε-Caprolactone to Bioactive Glass Particles on the Mechanical Properties of Settable Polymer/Ceramic Composites *Journal of Materials Research.* **29**(20), 2398 (2014).

5. C.J. Damien and J.R. Parsons: Bone-Graft and Bone-Graft Substitutes - a Review of Current Technology and Applications *Journal of Applied Biomaterials.* **2**(3), 187 (1991).

6. S. Deb, M. Wang, K.E. Tanner and W. Bonfield: Hydroxyapatite polyethylene composites: Effect of grafting and surface treatment of hydroxyapatite *Journal of Materials Science-Materials in Medicine.* **7**(4), 191 (1996).

7. D. Simpson and J.F. Keating: Outcome of tibial plateau fractures managed with calcium phosphate cement *Injury-International Journal of the Care of the Injured.* **35**(9), 913 (2004).

8. S.R. Shah, K.F. Kurtis and A.G. Mikos: Perspectives on the prevention and treatment of infection for orthopedic tissue engineering applications *Chinese Science Bulletin.* **58**(35), 4342 (2013).

9. C.f.D.C.a.P. (CDC): Septic arthritis following anterior cruciate ligament reconstruction using tendon allografts - Florida and Louisiana *MMWR Morb Mortal Wkly Rep.* **50**, 1081 (2001).

10. C.f.D.C.a.P. (CDC): Update: allograft-associated bacterial infections - United States *MMWR Morb Mortal Wkly Rep.* **51**, 207 (2002).

11. L.O. Conterno and M.D. Turchi: Antibiotics for treating chronic osteomyelitis in adults *Cochrane Database of Systematic Reviews.* (9), (2013).

12. S.F. El-Amin, Y. Khan and C. Laurencin: Bone graft substitutes *Expert Review of Medical Devices.* **3**(1), (2006).

13. D.P. Lew and F.A. Waldvogel: Osteomyelitis *Lancet.* **364**(9431), 369 (2004).

14. E. Johnson, T. Burns, R. Hayda, D. Hospenthal and C. Murray: Infectious complications of open type III tibial fractures among combat casualties. *Clin Infect Dis.* **45**(4), 409 (2007).

15. A.S. Greenwald, S.D. Boden, V.M. Goldberg, Y. Khan, C.T. Laurencin and R.N. Rosier: Bone-graft substitutes: Facts, fictions, and applications *Journal of Bone and Joint Surgery-American Volume.* **83A**, 98 (2001).

16. A.J.W. Johnson and B.A. Herschler: A review of the mechanical behavior of CaP and CaP/polymer composites for applications in bone replacement and repair *Acta Biomaterialia.* **7**(1), 16 (2011).

17. B.D. Ratner and S.J. Bryant: Biomaterials: where we have been and where we are going *Annu. Rev. Biomed. Eng.* **6**, 41 (2004).

18. L.G. Donaruma: Definitions in biomaterials, D. F. Williams, Ed., Elsevier, Amsterdam, 1987, 72 pp *Journal of Polymer Science Part C: Polymer Letters.* **26**(9), 414 (1988).

19. ASTM F2150-02, in Standard Guide for Characterization and Testing of Biomaterial Scaffolds Used in Tissue-Engineered Medical Products (ASTM International, City).

20. C. Migliaresi, A. Motta and A.T. DiBenedetto: Injectable Scaffolds for Bone and Cartilage Regeneration *Engineering of Functional Skeletal Tissues.* 95 (2007).

21. D.F. Williams: On the nature of biomaterials *Biomaterials.* **30**(30), 5897 (2009).

22. J.M. Page, A.J. Harmata and S.A. Guelcher: Design and development of reactive injectable and settable polymeric biomaterials *Journal of Biomedical Materials Research Part A.* **101**(12), 3630 (2013).

23. A.E. Hafeman, K.J. Zienkiewicz, A.L. Zachman, H.-J. Sung, L.B. Nanney, J.M. Davidson and S.A. Guelcher: Characterization of the degradation mechanisms of lysine-derived aliphatic poly(ester urethane) scaffolds *Biomaterials.* **32**(2), 419 (2011).

24. J.M. Page, E.M. Prieto, J.E. Dumas, K.J. Zienkiewicz, J.C. Wenke, P. Brown-Baer and S.A. Guelcher: Biocompatibility and chemical reaction kinetics of injectable, settable polyurethane/allograft bone biocomposites *Acta Biomaterialia.* **8**(12), 4405 (2012).

25. M. Bohner: Design of ceramic-based cements and putties for bone graft substitution *Eur Cells Mater.* **20**, 1 (2010).

26. J.E. Dumas, T. Davis, G.E. Holt, T. Yoshii, D.S. Perrien, J.S. Nyman, T. Boyce and S.A. Guelcher: Synthesis, characterization, and remodeling of weight-bearing allograft bone/polyurethane composites in the rabbit *Acta Biomaterialia.* **6**(7), 2394 (2010).

27. D. Campoccia, L. Montanaro and C.R. Arciola: The significance of infection related to orthopedic devices and issues of antibiotic resistance *Biomaterials.* **27**(11), 2331 (2006).

28. A.G. Gristina: Biomaterial-centered infection: microbial adhesion versus tissue integration *Science.* **237**(4822), 1588 (1987).

29. C. Kunze, T. Freier, E. Helwig, B. Sandner, D. Reif, A. Wutzler and H.J. Radusch: Surface modification of tricalcium phosphate for improvement of the interfacial compatibility with biodegradable polymers *Biomaterials.* **24**(6), 967 (2003).

30. M.J. Lysaght, A. Jaklenec and E. Deweerd: Great expectations: private sector activity in tissue engineering, regenerative medicine, and stem cell therapeutics *Tissue Eng. Part A.* **14**(2), 305 (2008).

31. I. Kolodkin-Gal, D. Romero, S. Cao, J. Clardy, R. Kolter and R. Losick: D-Amino Acids Trigger Biofilm Disassembly *Science.* **328**(5978), 627 (2010).

32. A.J. Domb and N. Kumar: Biodegradable Polymers in Clinical Use and Clinical Development (Wiley, City, 2011).

33. B. Vernon: Injectable Biomaterials: Science and Applications (Woodhead Publishing, City, 2011).

34. Y. Li, J. Rodrigues and H. Tomas: Injectable and biodegradable hydrogels: gelation, biodegradation and biomedical applications *Chemical Society Reviews.* **41**(6), 2193 (2012).

35. M.K. Nguyen and D.S. Lee: Injectable Biodegradable Hydrogels *Macromolecular Bioscience.* **10**(6), 563 (2010).

36. S.A. Guelcher: Biodegradable polyurethanes: Synthesis and applications in regenerative medicine *Tissue Engineering Part B-Reviews.* **14**(1), 3 (2008).

37. H.C. Kolb, M.G. Finn and K.B. Sharpless: Click Chemistry: Diverse Chemical Function from a Few Good Reactions *Angewandte Chemie International Edition.* **40**(11), 2004 (2001).

38. L.S. Moreira Teixeira, J. Feijen, C.A. van Blitterswijk, P.J. Dijkstra and M. Karperien: Enzyme-catalyzed crosslinkable hydrogels: Emerging strategies for tissue engineering *Biomaterials.* **33**(5), 1281 (2012).

39. D.R. Omstead, L.G. Baird, L. Christenson, G.D. Moulin, R. Tubo, D.D. Maxted, J. Davis and F.T. Gentile: Voluntary guidance for the development of tissue-engineered products *Tissue Engineering.* **4**(3), 239 (1998).

40. J.M. Anderson: Mechanisms of inflammation and infection with implanted devices *Cardiovascular Pathology.* **2**(3), 33 (1993).

41. H. Belt, D. Neut, W. Schenk, J.R. Horn, H.C. Mei and H.J. Busscher: Infection of orthopedic implants and the use of antibiotic-loaded bone cements: a review *Acta Orthopaedica.* **72**(6), 557 (2001).

42. J.M. Schierholz and J. Beuth: Implant infections: a haven for opportunistic bacteria *Journal of Hospital Infection.* **49**(2), 87 (2001).

43. L. Rimondini, M. Fini and R. Giardino: The microbial infection of biomaterials: A challenge for clinicians and researchers. A short review *J Appl Biomater Biomech.* **3**(1), 1 (2005).

44. M.E. Fray, A. Bartkowiak, P. Prowans and J. Slonecki: Physical and mechanical behavior of electron-beam irradiated and ethylene oxide sterilized multiblock polyester *Journal of Materials Science: Materials in Medicine.* **11**(11), 757 (2000).

45. G.C.C. Mendes, T.R.S. Brandão and C.L.M. Silva: Ethylene oxide sterilization of medical devices: A review *American Journal of Infection Control.* **35**(9), 574 (2007).

46. R.S. Benson: Use of radiation in biomaterials science *Nuclear Instruments and Methods in Physics Research Section B: Beam Interactions with Materials and Atoms.* **191**(1–4), 752 (2002).

47. S.B. Adams Jr, M.F. Shamji, D.L. Nettles, P. Hwang and L.A. Setton: Sustained release of antibiotics from injectable and thermally responsive polypeptide depots *Journal of Biomedical Materials Research Part B: Applied Biomaterials.* **90**(1), 67 (2009).

48. S.A. Guelcher, K.V. Brown, B. Li, T. Guda, B.-H. Lee and J.C. Wenke: Dual-Purpose Bone Grafts Improve Healing and Reduce Infection *Journal of Orthopaedic Trauma.* **25**(8), 477 (2011).

49. A.E. Hafeman, K.J. Zienkiewicz, E. Carney, B. Litzner, C. Stratton, J.C. Wenke and S.A. Guelcher: Local delivery of tobramycin from injectable biodegradable polyurethane scaffolds *Journal of Biomaterials Science, Polymer Edition.* **21**(1), 95 (2010).

50. Q.X. Ji, X.G. Chen, Q.S. Zhao, C.S. Liu, X.J. Cheng and L.C. Wang: Injectable thermosensitive hydrogel based on chitosan and quaternized chitosan and the biomedical properties *Journal of Materials Science: Materials in Medicine.* **20**(8), 1603 (2009).

51. S. Leprêtre, F. Chai, J.C. Hornez, G. Vermet, C. Neut, M. Descamps, H.F. Hildebrand and B. Martel: Prolonged local antibiotics delivery from hydroxyapatite functionalised with cyclodextrin polymers *Biomaterials.* **30**(30), 6086 (2009).

52. B. Li, K.V. Brown, J.C. Wenke and S.A. Guelcher: Sustained release of vancomycin from polyurethane scaffolds inhibits infection of bone wounds in a rat femoral segmental defect model *Journal of Controlled Release.* **145**(3), 221 (2010).

53. G.D. Prestwich and Y. Luo: Novel biomaterials for drug delivery *Expert Opinion on Therapeutic Patents.* **11**(9), 1395 (2001).

54. M. Shi, J.D. Kretlow, P.P. Spicer, Y. Tabata, N. Demian, M.E. Wong, F.K. Kasper and A.G. Mikos: Antibiotic-releasing porous polymethylmethacrylate/gelatin/antibiotic constructs for craniofacial tissue engineering *J. Control. Release.* (2011).

55. J.C. Wenke and S.A. Guelcher: Dual delivery of an antibiotic and a growth factor addresses both the microbiological and biological challenges of contaminated bone fractures *Expert Opinion on Drug Delivery.* **8**(12), 1555 (2011).

56. D. Campoccia, L. Montanaro, P. Speziale and C.R. Arciola: Antibiotic-loaded biomaterials and the risks for the spread of antibiotic resistance following their prophylactic and therapeutic clinical use *Biomaterials.* **31**(25), 6363 (2010).

57. J.L. Martin, B.J. Norris, E. Murphy and J.A. Crowe: Medical device development: The challenge for ergonomics *Applied Ergonomics.* **39**(3), 271 (2008).

58. G. Baroud, E. Cayer and M. Bohner: Rheological characterization of concentrated aqueous β-tricalcium phosphate suspensions: The effect of liquid-to-powder ratio, milling time, and additives *Acta Biomaterialia.* **1**(3), 357 (2005).

59. J.E. Dumas, P.B. BrownBaer, E.M. Prieto, T. Guda, R.G. Hale, J.C. Wenke and S.A. Guelcher: Injectable reactive biocomposites for bone healing in critical-size rabbit calvarial defects *Biomedical Materials.* **7**(2), 024112 (2012).

60. C. Liu, H. Shao, F. Chen and H. Zheng: Rheological properties of concentrated aqueous injectable calcium phosphate cement slurry *Biomaterials.* **27**(29), 5003 (2006).

61. M. Habib, G. Baroud, F. Gitzhofer and M. Bohner: Mechanisms underlying the limited injectability of hydraulic calcium phosphate paste *Acta Biomaterialia.* **4**(5), 1465 (2008).

62. J.M. Page, E.M. Prieto, J.E. Dumas, K.J. Zienkiewicz, J.C. Wenke, P.B. Baer and S.A. Guelcher: Biocompatibility and Chemical Reaction Kinetics of Injectable, Settable Polyurethane/Allograft Bone Biocomposites *Acta Biomaterialia.* **8**(12), 4405 (2012).

63. A.S. Sarvestani, X. He and E. Jabbari: Viscoelastic characterization and modeling of gelation kinetics of injectable in situ cross-linkable poly (lactide-co-ethylene oxide-co-fumarate) hydrogels *Biomacromolecules.* **8**(2), 406 (2007).

64. J.A. Hubbell: Biomaterials in tissue engineering *Nature Biotechnology.* **13**(6), 565 (1995).

65. A. Göpferich: Mechanisms of polymer degradation and erosion *Biomaterials.* **17**(2), 103 (1996).

66. M. Vert, S. Li, G. Spenlehauer and P. Guerin: Bioresorbability and biocompatibility of aliphatic polyesters *Journal of Materials Science: Materials in Medicine.* **3**(6), 432 (1992).

67. H. Antheunis, J.-C. van der Meer, M. de Geus, W. Kingma and C.E. Koning: Improved Mathematical Model for the Hydrolytic Degradation of Aliphatic Polyesters *Macromolecules.* **42**(7), 2462 (2009).

68. P.A. Gunatillake and R. Adhikari: Biodegradable synthetic polymers for tissue engineering *Eur Cell Mater.* **5**(1), 1 (2003).

69. R.Z. Legeros, A. Chohayeb and A. Schulman: Apatitic Calcium Phosphates Possible Dental Restorative Materials *Journal of Dental Research.* **61**(SPEC. ISSUE), 343 (1982).

70. K.L. Low, S.H. Tan, S.H. Zein, J.A. Roether, V. Mourino and A.R. Boccaccini: Calcium phosphate-based composites as injectable bone substitute materials: A review *J Biomed Mater Res B Appl Biomater.* **94**(1),273 (2010)

71. H. Chim and A.K. Gosain: Biomaterials in Craniofacial Surgery Experimental Studies and Clinical Application *J. Craniofac. Surg.* **20**(1), 29 (2009).

72. C. Liu, W. Wang, W. Shen, T. Chen, L. Hu and Z. Chen: Evaluation of the biocompatibility of a nonceramic hydroxyapatite *J Endod.* **23**(8), 490 (1997).

73. E. Fernandez, M.P. Ginebra, M.G. Boltong, F.C. Driessens, J. Ginebra, E.A. De Maeyer, R.M. Verbeeck and J.A. Planell: Kinetic study of the setting reaction of a calcium phosphate bone cement *J Biomed Mater Res.* **32**(3), 367 (1996).

74. M. Bohner: Calcium orthophosphates in medicine: from ceramics to calcium phosphate cements *Injury.* **31**(Supplement 4), S (2000).

75. M. Bohner, P. Van Landuyt, H.P. Merkle and J. Lemaitre: Composition effects on the pH of a hydraulic calcium phosphate cement *J Mater Sci Mater Med.* **8**(11), 675 (1997).

76. P. Frayssinet, L. Gineste, P. Conte, J. Fages and N. Rouquet: Short-term implantation effects of a DCPD-based calcium phosphate cement *Biomaterials.* **19**(11-12), 971 (1998).

77. B.R. Constantz, B.M. Barr, I.C. Ison, M.T. Fulmer, J. Baker, L. McKinney, S.B. Goodman, S. Gunasekaren, D.C. Delaney, J. Ross and R.D. Poser: Histological, chemical, and crystallographic analysis of four calcium phosphate cements in different rabbit osseous sites *J Biomed Mater Res.* **43**(4), 451 (1998).

78. J.D. Kretlow, S. Young, L. Klouda, M. Wong and A.G. Mikos: Injectable Biomaterials for Regenerating Complex Craniofacial Tissues *Adv Mater Deerfield.* **21**(32-33), 3368 (2009).

79. M.L. Shindo, P.D. Costantino, C.D. Friedman and L.C. Chow: Facial skeletal augmentation using hydroxyapatite cement *Arch Otolaryngol Head Neck Surg.* **119**(2), 185 (1993).

80. B.M.J. Hall J. A., McKee M. D.: Open reduction and internal fixation compared with circular fixator application for bicondylar tibial plateau fractures. *Surgical technique. J Bone Joint Surg Am.* **91A Suppl 2 Pt 1**, 74 (2009).

81. M. Bohner: Design of Ceramic-Based Cements and Putties for Bone Graft Substitution *European Cells & Materials.* **20**, 1 (2010).

82. G.D. Brown, B.L. Mealey, P.V. Nummikoski, S.L. Bifano and T.C. Waldrop: Hydroxyapatite cement implant for regeneration of periodontal osseous defects in humans *J Periodontol.* **69**(2), 146 (1998).

83. D.P. Link, J. van den Dolder, W.J. Jurgens, J.G. Wolke and J.A. Jansen: Mechanical evaluation of implanted calcium phosphate cement incorporated with PLGA microparticles *Biomaterials.* **27**(28), 4941 (2006).

84. W.J. Habraken, L.T. de Jonge, J.G. Wolke, L. Yubao, A.G. Mikos and J.A. Jansen: Introduction of gelatin microspheres into an injectable calcium phosphate cement *Journal of biomedical materials research. Part A.* **87**(3), 643 (2008).

85. W.J. Habraken, Z. Zhang, J.G. Wolke, D.W. Grijpma, A.G. Mikos, J. Feijen and J.A. Jansen: Introduction of enzymatically degradable poly(trimethylene carbonate) microspheres into an injectable calcium phosphate cement *Biomaterials.* **29**(16), 2464 (2008).

86. R.B. Martin, M.W. Chapman, R.E. Holmes, D.J. Sartoris, E.C. Shors, J.E. Gordon, D.O. Heitter, N.A. Sharkey and A.G. Zissimos: Effects of bone ingrowth on the strength and non-invasive assessment of a coralline hydroxyapatite material *Biomaterials.* **10**, 481 (1989).

87. C. Trojani, F. Boukhechba, J.C. Scimeca, F. Vandenbos, J.F. Michiels, G. Daculsi, P. Boileau, P. Weiss, G.F. Carle and N. Rochet: Ectopic bone formation using an injectable biphasic calcium phosphate/Si-HPMC hydrogel composite loaded with undifferentiated bone marrow stromal cells *Biomaterials.* **27**(17), 3256 (2006).

88. O. Gauthier, R. Muller, D. von Stechow, B. Lamy, P. Weiss, J.M. Bouler, E. Aguado and G. Daculsi: In vivo bone regeneration with injectable calcium phosphate biomaterial: a three-dimensional micro-computed tomographic, biomechanical and SEM study *Biomaterials.* **26**(27), 5444 (2005).

89. R.M. Urban, T.M. Turner, D.J. Hall, S. Infanger, N. Cheema and T.H. Lim: Healing of large defects treated with calcium sulfate pellets containing demineralized bone matrix particles *Orthopedics.* **26**(5), S581 (2003).

90. J.R. Porter, T.T. Ruckh and K.C. Popat: - Bone tissue engineering: A review in bone biomimetics and drug delivery strategies**25**(6), 1539 (2009).

91. P. Sepulveda, J.R. Jones and L.L. Hench: Bioactive Materials for Tissue Engineering Scaffolds, in Future Strategies for Tissue and Organ Replacement, edited by J. M. Polak, L. L. Hench and P. Kemp (Imperial College Press, City, 2002), pp. 3.

92. R.A. Khan, A.J. Parsons, I.A. Jones, G.S. Walker and C.D. Rudd: Effectiveness of 3-Aminopropyl-Triethoxy-Silane as a Coupling Agent for Phosphate Glass Fiber-Reinforced Poly(caprolactone)-based Composites for Fracture Fixation Devices *Journal of Thermoplastic Composite Materials.* **24**(4), 517 (2011).

93. V.A. Koleganova, S.M. Bernier, S.J. Dixon and A.S. Rizkalla: Bioactive glass/polymer composite materials with mechanical properties matching those of cortical bone *Journal of Biomedical Materials Research Part A.* **77A**(3), 572 (2006).

94. R.A. Khan, A.J. Parsons, I.A. Jones, G.S. Walker and C.D. Rudd: Preparation and Characterization of Phosphate Glass Fibers and Fabrication of Poly(caprolactone) Matrix Resorbable Composites *Journal of Reinforced Plastics and Composites.* **29**(12), 1838 (2010).

95. G. Jiang, G.S. Walker, I.A. Jones and C.D. Rudd: XPS identification of surface-initiated polymerisation during monomer transfer moulding of poly(epsilon-caprolactone)/Bioglass (R) fibre composite *Applied Surface Science.* **252**(5), 1854 (2005).

96. A.J. Harmata, C.L. Ward, K. Zienkiewicz, J.C. Wenke and S.A. Guelcher: Investigating the Effects of Surface-Initiated Polymerization of ε-Caprolactone to Bioactive Glass Particles on the Mechanical

Properties of Settable Polymer/Ceramic Composites *Journal of Materials Research.* **29**(20), 2398 (2014).

97. R.A. Sousa, R.L. Reis, A.M. Cunha and M.J. Bevis: Coupling of HDPE/hydroxyapatite composites by silane-based methodologies *Journal of Materials Science-Materials in Medicine.* **14**(6), 475 (2003).

98. C. Santos, R.L. Clarke, M. Braden, F. Guitian and K.W.M. Davy: Water absorption characteristics of dental composites incorporating hydroxyapatite filler *Biomaterials.* **23**(8), 1897 (2002).

99. S. Deb, L. Aiyathurai, J.A. Roether and Z.B. Luklinska: Development of high-viscosity, two-paste bioactive bone cements *Biomaterials.* **26**(17), 3713 (2005).

100. A.M.P. Dupraz, J.R. deWijn, S.A.T. vanderMeer and K. deGroot: Characterization of silane-treated hydroxyapatite powders for use as filler in biodegradable composites *Journal of Biomedical Materials Research.* **30**(2), 231 (1996).

101. M. Wang and W. Bonfield: Chemically coupled hydroxyapatite-polyethylene composites: structure and properties *Biomaterials.* **22**(11), 1311 (2001).

102. Q. Liu, J.R. deWijn and C.A. vanBlitterswijk: Nano-apatite/polymer composites: Mechanical and physicochemical characteristics *Biomaterials.* **18**(19), 1263 (1997).

103. Q. Liu, J.R. de Wijn and C.A. van Blitterswijk: Covalent bonding of PMMA, PBMA, and poly(HEMA) to hydroxyapatite particles *Journal of Biomedical Materials Research.* **40**(2), 257 (1998).

104. Q. Liu, J.R. de Wijn and C.A. van Blitterswijk: Composite biomaterials with chemical bonding between hydroxyapatite filler particles and PEG/PBT copolymer matrix *Journal of Biomedical Materials Research.* **40**(3), 490 (1998).

105. T. Yoshii, J.E. Dumas, A. Okawa, D.M. Spengler and S.A. Guelcher: Synthesis, characterization of calcium phosphates/polyurethane composites for weight-bearing implants *Journal of Biomedical Materials Research Part B-Applied Biomaterials.* **100B**(1), 32 (2012).

106. J.E. Dumas, K. Zienkiewicz, S.A. Tanner, E.M. Prieto, S. Bhattacharyya and S.A. Guelcher: Synthesis and Characterization of an Injectable Allograft Bone/Polymer Composite Bone Void Filler with Tunable Mechanical Properties *Tissue Eng. Part A.* **16**(8), 2505 (2010).

107. P. Vermette, H.J. Griesser, G. Laroche and R. Guidoin: Biomedical applications of polyurethanes (Landes Bioscience, City, 2001).

108. S.A. Guelcher, V. Patel, K.M. Gallagher, S. Connolly, J.E. Didier, J.S. Doctor and J.O. Hollinger: Synthesis and in vitro biocompatibility of injectable polyurethane foam scaffolds *Tissue Engineering.* **12**(5), 1247 (2006).

109. S.A. Guelcher, A. Srinivasan, J.E. Dumas, J.E. Didier, S. McBride and J.O. Hollinger: Synthesis, mechanical properties, biocompatibility, and biodegradation of polyurethane networks from lysine polyisocyanates *Biomaterials.* **29**(12), 1762 (2008).

110. M.C. Tanzi, P. Verderio, M.G. Lampugnani, M. Resnati, E. Dejana and E. Sturani: Cytotoxicity of some catalysts commonly used in the synthesis of copolymers for biomedical use *Journal of Materials Science: Materials in Medicine.* **5**(6), 393 (1994).

111. M.C. Tanzi, P. Verderio, M.G. Lampugnani, M. Resnati, E. Dejana and E. Sturani: CYTOTOXICITY OF SOME CATALYSTS COMMONLY USED IN THE SYNTHESIS OF COPOLYMERS FOR BIOMEDICAL USE *Journal of Materials Science-Materials in Medicine.* **5**(6-7), 393 (1994).

112. J.M. Page, E.M. Prieto, J.E. Dumas, K.J. Zienkiewicz, J.C. Wenke, P. Brown-Baer and S.A. Guelcher: Biocompatibility and chemical reaction kinetics of injectable, settable polyurethane/allograft bone biocomposites *Acta Biomaterialia.* **8**(12), 4405 (2012).

113. M. Szycher: Szycher's Handbook of Polyurethanes (CRC Press LLC, City, 1999).

114. S. Guelcher, A. Srinivasan, A. Hafeman, K. Gallagher, J. Doctor, S. Khetan, S. McBride and J. Hollinger: Synthesis, In vitro degradation, and mechanical properties of two-component poly(ester urethane)urea scaffolds: Effects of water and polyol composition *Tissue Engineering.* **13**(9), 2321 (2007).

115. J.Y. Zhang, E.J. Beckman, N.P. Piesco and S. Agarwal: A new peptide-based urethane polymer: synthesis, biodegradation, and potential to support cell growth in vitro *Biomaterials.* **21**(12), 1247 (2000).

116. S. Bennett, K. Connolly, D.R. Lee, Y. Jiang, D. Buck, J.O. Hollinger and E.A. Gruskin: Initial biocompatibility studies of a novel degradable polymeric bone substitute that hardens in situ *Bone.* **19**(1), S101 (1996).

117. P. Bruin, G.J. Veenstra, A.J. Nijenhuis and A.J. Pennings: DESIGN AND SYNTHESIS OF BIODEGRADABLE POLY(ESTER-URETHANE) ELASTOMER NETWORKS COMPOSED OF NON-TOXIC BUILDING-BLOCKS *Makromolekulare Chemie-Rapid Communications.* **9**(8), 589 (1988).

118. G. Skarja and K. Woodhouse: Structure-property relationships of degradable polyurethane elastomers containing an amino acid-based chain extender *Journal of Applied Polymer Science.* **75**(12), 1522 (2000).

119. J. Pauluhn: Inhalation Toxicity of 1,6-Hexamethylene Diisocyanate Homopolymer (HDI-IC) Aerosol: Results of Single Inhalation Exposure Studies *Toxicological Sciences.* **58**(1), 173 (2000).

120. M.H. Karol and J.H. Dean: Respiratory effects of inhaled isocyanates *CRC critical reviews in toxicology.* **16**(4), 349 (1986).

121. H. Kobayashi, S.-H. Hyon and Y. Ikada: Water-curable and biodegradable prepolymers *Journal of Biomedical Materials Research.* **25**(12), 1481 (1991).

122. B.T. Butcher, J.E. Salvaggio, H. Weill and M.M. Ziskind: Toluene diisocyanate (TDI) pulmonary disease: immunologic and inhalation challenge studies *Journal of allergy and clinical immunology.* **58**(1), 89 (1976).

123. E.H. Vock and W.K. Lutz: Distribution and DNA adduct formation of radiolabeled methylenediphenyl-4, 4'-diisocyanate (MDI) in the rat after topical treatment *Toxicology letters.* **92**(2), 93 (1997).

124. C. Bolognesi, X. Baur, B. Marczynski, H. Norppa, O. Sepai and G. Sabbioni: Carcinogenic risk of toluene diisocyanate and 4, 4'-methylenediphenyl diisocyanate: epidemiological and experimental evidence *CRC critical reviews in toxicology.* **31**(6), 737 (2001).

125. M.-N. Kim, J.-C. Jang, I.-M. Lee, H.-S. Lee and J.-S. Yoon: TOXICITY AND BIODEGRADATION OF DIAMINES *Journal of Environmental Science and Health, Part B.* **37**(1), 53 (2002).

126. C. Batich, J. Williams and R. King: Toxic hydrolysis product from a biodegradable foam implant *Journal of Biomedical Materials Research.* **23**(S14), 311 (1989).

127. R. Schoental: Carcinogenic and chronic effects of 4, 4′-diaminodiphenylmethane, an epoxyresin hardener, (1968).

128. K. Gorna and S. Gogolewski: Biodegradable porous polyurethane scaffolds for tissue repair and regeneration *J. Biomed. Mater. Res. Part A.* **79A**(1), 128 (2006).

129. J.Y. Zhang, E.J. Beckman, J. Hu, G.G. Yang, S. Agarwal and J.O. Hollinger: Synthesis, biodegradability, and biocompatibility of lysine diisocyanate-glucose polymers *Tissue Engineering.* **8**(5), 771 (2002).

130. W.N. Sivak, I.F. Pollack, S. Petoud, W.G. Zamboni, J.Y. Zhang and E.J. Beckman: Catalyst-dependent drug loading of LDI-glycerol polyurethane foams leads to differing controlled release profiles *Acta Biomaterialia.* **4**(5), 1263 (2008).

131. W.N. Sivak, J.Y. Zhang, S. Petoud and E.J. Beckman: Degradative-release as a function of drug structure from LDI-glycerol polyurethanes *Bio-Med. Mater. Eng.* **20**(5), 269 (2010).

132. E.J. Adolph, A.E. Hafeman, J.M. Davidson, L.B. Nanney and S.A. Guelcher: Injectable polyurethane composite scaffolds delay wound contraction and support cellular infiltration and remodeling in rat excisional wounds *J. Biomed. Mater. Res. Part A.* **100A**(2), 450 (2012).

133. S. Guelcher, A. Srinivasan, A. Hafeman, K. Gallagher, J. Doctor, S. Khetan, S. McBride and J. Hollinger: Synthesis, In vitro degradation, and mechanical properties of two-component poly(ester urethane)urea scaffolds: Effects of water and polyol composition *Tissue Engineering.* **13**, 2321 (2007).

134. A. Hafeman, B. Li, T. Yoshii, K. Zienkiewicz, J. Davidson and S. Guelcher: Injectable Biodegradable Polyurethane Scaffolds with Release of Platelet-derived Growth Factor for Tissue Repair and Regeneration *Pharm. Res.* **25**(10), 2387 (2008).

135. A.P. Duarte, J.F. Coelho, J.C. Bordado, M.T. Cidade and M.H. Gil: Surgical adhesives: Systematic review of the main types and development forecast *Progress in Polymer Science.* **37**(8), 1031 (2012).

136. T.W. Gilbert, S.F. Badylak, E.J. Beckman, D.M. Clower and J.P. Rubin: Prevention of seroma formation with TissuGlu((R)) surgical adhesive in a canine abdominoplasty model: Long term clinical and histologic studies *Journal of plastic, reconstructive & aesthetic surgery : JPRAS.* (2012).

137. T.W. Gilbert, S.F. Badylak, J. Gusenoff, E.J. Beckman, D.M. Clower, P. Daly and J.P. Rubin: Lysine-derived urethane surgical adhesive prevents seroma formation in a canine abdominoplasty model *Plastic and reconstructive surgery.* **122**(1), 95 (2008).

138. K.J. Walgenbach, H. Bannasch, S. Kalthoff and J.P. Rubin: Randomized, prospective study of TissuGlu(R) surgical adhesive in the management of wound drainage following abdominoplasty *Aesthetic plastic surgery.* **36**(3), 491 (2012).

139. Q.W. Lu, T.R. Hoye and C.W. Macosko: Reactivity of common functional groups with urethanes: Models for reactive compatibilization of thermoplastic polyurethane blends *Journal of Polymer Science Part a-Polymer Chemistry.* **40**(14), 2310 (2002).

140. E.J. Adolph, A.E. Hafeman, J.M. Davidson, L.B. Nanney and S.A. Guelcher: Injectable polyurethane composite scaffolds delay wound contraction and support cellular infiltration and remodeling in rat excisional wounds *Journal of Biomedical Materials Research Part A.* **100**(2), 450 (2012).

141. A.E. Hafeman, K.J. Zienkiewicz, A.L. Zachman, H.J. Sung, L.B. Nanney, J.M. Davidson and S.A. Guelcher: Characterization of the degradation mechanisms of lysine-derived aliphatic poly (ester urethane) scaffolds *Biomaterials.* **32**(2), 419 (2011).

142. C.E. Nelson, M.K. Gupta, E.J. Adolph, J.M. Shannon, S.A. Guelcher and C.L. Duvall: Sustained local delivery of siRNA from an injectable scaffold *Biomaterials.* **33**(4), 1154 (2012).

143. A.E. Hafeman, K.J. Zienkiewicz, A.L. Zachman, H.J. Sung, L.B. Nanney, J.M. Davidson and S.A. Guelcher: Characterization of the degradation mechanisms of lysine-derived aliphatic poly(ester urethane) scaffolds *Biomaterials.* **32**(2), 419 (2011).

144. K.J. Walgenbach, H. Bannasch, S. Kalthoff and J.P. Rubin: Randomized, Prospective Study of TissuGluA (R) Surgical Adhesive in the Management of Wound Drainage Following Abdominoplasty *Aesthet. Plast. Surg.* **36**(3), 491 (2012).

145. R. Adhikari, P.A. Gunatillake, I. Griffiths, L. Tatai, M. Wickramaratna, S. Houshyar, T. Moore, R.T.M. Mayadunne, J. Field, M. McGee and T. Carbone: Biodegradable injectable polyurethanes: Synthesis and evaluation for orthopaedic applications *Biomaterials.* **29**(28), 3762 (2008).

146. Y. Marois and R. Guidoin: Biocompatibility of Polyurethanes, (2000).

147. T. Yoshii, J.E. Dumas, A. Okawa, D.M. Spengler and S.A. Guelcher: Synthesis, characterization of calcium phosphates/polyurethane composites for weight-bearing implants *Journal of Biomedical Materials Research Part B: Applied Biomaterials.* **100B**(1), 32 (2012).

148. E.D. Jerald, B.B. Pamela, M.P. Edna, G. Teja, G.H. Robert, C.W. Joseph and A.G. Scott: Injectable reactive biocomposites for bone healing in critical-size rabbit calvarial defects *Biomedical Materials.* **7**(2), 024112 (2012).

149. B. Li, T. Yoshii, A.E. Hafeman, J.S. Nyman, J.C. Wenke and S.A. Guelcher: The effects of rhBMP-2 released from biodegradable polyurethane/microsphere composite scaffolds on new bone formation in rat femora *Biomaterials.* **30**(35), 6768 (2009).

150. J.E. Dumas, P.B. BrownBaer, E.M. Prieto, T. Guda, R.G. Hale, J.C. Wenke and S.A. Guelcher: Injectable reactive biocomposites for bone healing in critical-size rabbit calvarial defects *Biomedical Materials.* **7**(2), (2012).

151. K.V. Brown, B. Li, T. Guda, D.S. Perrien, S.A. Guelcher and J.C. Wenke: Improving Bone Formation in a Rat Femur Segmental Defect by Controlling Bone Morphogenetic Protein-2 Release *Tissue Eng. Part A.* **17**(13-14), 1735 (2011).

152. W.N. Sivak, J.Y. Zhang, S. Petoud and E.J. Beckman: Incorporation of ionic ligands accelerates drug release from LDI-glycerol polyurethanes *Acta Biomaterialia.* **6**(1), 144 (2010).

153. W.N. Sivak, J.Y. Zhang, S. Petoud and E.J. Beckman: Simultaneous drug release at different rates from biodegradable polyurethane foams *Acta Biomaterialia.* **5**(7), 2398 (2009).

154. W.N. Sivak, I.F. Pollack, S. Petoud, W.C. Zamboni, J.Y. Zhang and E.J. Beckman: LDI-glycerol polyurethane implants exhibit controlled release of DB-67 and anti-tumor activity in vitro against malignant gliomas *Acta Biomaterialia.* **4**(4), 852 (2008).

155. E. Johnson, T. Burns, R. Hayda, D. Hospenthal and C. Murray: Infectious complications of open type III tibial fractures among combat casualties.
Clin Infect Dis. **45**(4), 409 (2007).

156. J.W. Costerton: Introduction to biofilm *Int J Antimicrob Agents* **11**((3-4)), 217 (1999).

157. L. Hall-Stoodley, J.W. Costerton and P. Stoodley: Bacterial biofilms: from the Natural environment to infectious diseases *Nature Reviews Microbiology.* **2**, 95 (2004).

158. R. Brady, J. Leid, J. Calhoun, J.W. Costerton and M. Shirtliff: Osteomyelitis and the role of biofilms in chronic infection. *FEMS Immunol Med Microbiol.* **52**(1), 13 (2008).

159. T. Marrie and J.W. Costerton: Mode of growth of bacterial pathogens in chronic polymicrobial human osteomyelitis. *J Clin Microbiol.* **22**(6), 924 (1985).

160. A.G. Gristina, M. Oga, L.X. Webb and C.D. Hobgood: Adherent Bacterial-Colonization in the Pathogenesis of Osteomyelitis *Science.* **228**(4702), 990 (1985).

161. S.A. Guelcher, K.V. Brown, B. Li, T. Guda, B.H. Lee and J.C. Wenke: Dual-Purpose Bone Grafts Improve Healing and Reduce Infection *J. Orthop. Trauma.* **25**(8), 477 (2011).

162. J.W. Costerton: Biofilm theory can guide the treatment of device-related orthopaedic infections *Clinical Orthopaedics and Related Research.* (437), 7 (2005).

163. C.R. Rathbone, J.D. Cross, K.V. Brown, C.K. Murray and J.C. Wenke: Effect of Various Concentrations of Antibiotics on Osteogenic Cell Viability and Activity *Journal of Orthopaedic Research.* **29**(7), 1070 (2011).

164. A.I. Hochbaum, I. Kolodkin-Gal, L. Foulston, R. Kolter, J. Aizenberg and R. Losick: Inhibitory Effects of D-Amino Acids on Staphylococcus aureus Biofilm Development *Journal of Bacteriology.* **193**(20), 5616 (2011).

165. C.J. Sanchez, E.M. Prieto, C.A. Krueger, K.J. Zienkiewicz, D.R. Romano, C.L. Ward, K.S. Akers, S.A. Guelcher and J.C. Wenke: Effects of local delivery of D-amino acids from biofilm-dispersive scaffolds on infection in contaminated rat segmental defects *Biomaterials.* **34**(30), 7533 (2013).

166. Defintions in biomaterials (Elsevier, City, 1987).

167. T. Kokubo and H. Takadama: How useful is SBF in predicting in vivo bone bioactivity? *Biomaterials.* **27**(15), 2907 (2006).

168. L.L. Hench: The story of Bioglass (R) *Journal of Materials Science-Materials in Medicine.* **17**(11), 967 (2006).

169. P. Saravanapavan, J.R. Jones, R.S. Pryce and L.L. Hench: Bioactivity of gel-glass powders in the CaO-SiO2 system: A comparison with ternary (CaO-P2O5-SiO2) and quaternary glasses (SiO2-CaO-P2O5-Na2O) *J. Biomed. Mater. Res. Part A.* **66A**(1), 110 (2003).

170. L.L. Hench and J.M. Polak: Third-generation biomedical materials *Science.* **295**(5557), 1014 (2002).

171. P. Ducheyne: Bioceramics: materials characteristics versus in vivo behavior *J Biomed Mater Res* **21 (A2 Suppl)**, 219 (1987).

172. Q.-Z. Chen, Y. Li, L.-Y. Jin, J.M.W. Quinn and P.A. Komesaroff: A new sol-gel process for producing Na(2)O-containing bioactive glass ceramics *Acta Biomaterialia.* **6**(10), 4143 (2010).

173. S.M. Best, A.E. Porter, E.S. Thian and J. Huang: Bioceramics: Past, present and for the future *Journal of the European Ceramic Society.* **28**(7), 1319 (2008).

174. A.R. Boccaccini and J.J. Blaker: Bioactive composite materials for tissue engineering scaffolds *Expert Review of Medical Devices.* **2**(3), 303 (2005).

175. L.L. Hench and J. Wilson: Bioceramics *Mrs Bulletin.* **16**(9), 62 (1991).

176. L. Hench, Splinter, R., Allen, W., Greenlee Jr T.: Bonding mechanisms at the interface of ceramic prosthetic materials *J Biomed Mater Res.* **5**, 117 (1971).

177. M.N. Rahaman, D.E. Day, B.S. Bal, Q. Fu, S.B. Jung, L.F. Bonewald and A.P. Tomsia: Bioactive glass in tissue engineering *Acta Biomaterialia.* **7**(6), 2355 (2011).

178. H. Kobayashi, A.S. Turner, H.B. Seim, III, T. Kawamoto and T.W. Bauer: Evaluation of a silica-containing bone graft substitute in a vertebral defect model *J. Biomed. Mater. Res. Part A.* **92A**(2), 596 (2010).

179. A. Moreira-Gonzalez, C. Lobocki, K. Barakat, L. Andrus, M. Bradford, M. Gilsdorf and I.T. Jackson: Evaluation of 45S5 bioactive glass combined as a bone substitute in the reconstruction of critical size calvarial defects in rabbits *J. Craniofac. Surg.* **16**(1), 63 (2005).

180. I.A. Silver and M. Erecinska: Interactions of osteoblastic and other cells with bioactive glasses and silica in vitro and in vivo *Materialwissenschaft Und Werkstofftechnik.* **34**(12), 1069 (2003).

181. O. Bretcanu, S. Misra, I. Roy, C. Renghini, F. Fiori, A.R. Boccaccini and V. Salih: In vitro biocompatibility of 45S5 Bioglass (R)-derived glass-ceramic scaffolds coated with poly(3-hydroxybutyrate) *Journal of Tissue Engineering and Regenerative Medicine.* **3**(2), 139 (2009).

182. L.-C. Gerhardt and A.R. Boccaccini: Bioactive Glass and Glass-Ceramic Scaffolds for Bone Tissue Engineering *Materials.* **3**(7), 3867 (2010).

183. H.Y. Li and J. Chang: In vitro degradation of porous degradable and bioactive PHBV/wollastonite composite scaffolds *Polymer Degradation and Stability.* **87**(2), 301 (2005).

184. Q.Z. Chen and A.R. Boccaccini: Coupling mechanical competence and bioresorbability in Bioglass (R)-derived tissue engineering scaffolds *Advanced Engineering Materials.* **8**(4), 285 (2006).

185. C. Chan, I. Thompson, P. Robinson, J. Wilson and L. Hench: Evaluation of Bioglass/dextran composite as a bone graft substitute *International Journal of Oral and Maxillofacial Surgery.* **31**(1), 73 (2002).

186. Z. Wang, B. Lu, L. Chen and J. Chang: Evaluation of an osteostimulative putty in the sheep spine *J. Mater. Sci.-Mater. Med.* **22**(1), 185 (2011).

187. R.E. Neuendorf, E. Saiz, A.P. Tomsia and R.O. Ritchie: Adhesion between biodegradable polymers and hydroxyapatite: Relevance to synthetic bone-like materials and tissue engineering scaffolds *Acta Biomaterialia.* **4**(5), 1288 (2008).

188. B. Arkles: Tailoring Surfaces with Silanes *Chemtech.* **7**(12), 766 (1977).

189. M. Hashimoto, H. Takadama, M. Mizuno and T. Kokubo: Enhancement of mechanical strength of TiO2/high-density polyethylene composites for bone repair with silane-couple treatment *Materials Research Bulletin.* **41**(3), 515 (2006).

190. W.K.J. Mosse, M.L. Koppens, T.R. Gengenbach, D.B. Scanlon, S.L. Gras and W.A. Ducker: Peptides Grafted from Solids for the Control of Interfacial Properties *Langmuir.* **25**(3), 1488 (2009).

191. K. Zhang, Y.B. Wang, M.A. Hillmyer and L.F. Francis: Processing and properties of porous poly(L-lactide)/bioactive glass composites *Biomaterials.* **25**(13), 2489 (2004).

192. R.Y. Zhang and P.X. Ma: Biomimetic polymer/apatite composite scaffolds for mineralized tissue engineering *Macromolecular Bioscience.* **4**(2), 100 (2004).

193. Q. Liu, J.R. de Wijn and C.A. van Blitterswijk: A study on the grafting reaction of isocyanates with hydroxyapatite particles *J Biomed Mater Res* **40**(3), 358 (1998).

194. A.W. Adamson and A.P. Gast: Physical Chemistry of Surfaces (Wiley, City, 1997).

195. V. Mangipudi, M. Tirrell and A.V. Pocius: Direct Measurement of Molecular-Level Adhesion between Poly(Ethylene-Terephthalate) and Polyethylene Films - Determination of Surface and Interfacial Energies *Journal of Adhesion Science and Technology.* **8**(11), 1251 (1994).

196. J.C. Reichert, D.R. Epari, M.E. Wullschleger, S. Saifzadeh, R. Steck, J. Lienau, S. Sommerville, I.C. Dickinson, M.A. Schuetz, G.N. Duda and D.W. Hutmacher: Establishment of a Preclinical Ovine Model for Tibial Segmental Bone Defect Repair by Applying Bone Tissue Engineering Strategies *Tissue Engineering Part B-Reviews.* **16**(1), 93 (2010).

197. A. Ravaglioli, A. Krajewski, G.C. Celotti, A. Piancastelli, B. Bacchini, L. Montanari, G. Zama and L. Piombi: Mineral evolution of bone *Biomaterials.* **17**(6), 617 (1996).

198. E. Newman, A.S. Turner and J.D. Wark: The Potential of Sheep for the Study of Osteopenia - Current Status and Comparison with Other Animal-Models *Bone.* **16**(4), S277 (1995).

199. G. Liu, Z. Li, W. Zhang, C. Lei, L. Wei and Y. Cao: Repair of goat tibial defects with bone marrow stromal cells and ss-tricalcium phosphate *J. Mater. Sci.-Mater. Med.* **19**(6), 2367 (2008).

CHAPTER III

D-AMINO ACID BIOFILM DISPERSAL AGENTS' EFFECT ON BONE-RELATED CELL ACTIVITY

Introduction

Infectious complications are a significant factor contributing to patient morbidity and limiting the success of clinical management of complex trauma. Treatment of musculoskeletal trauma involves operative debridement of necrotic bone followed by several weeks of systemic antibiotics, temporary fixation, and/or implantation of devices to promote bone regeneration. For orthopaedic infections, *Staphylococcus aureus* is the most commonly isolated agent, accounting for more than half of all infections [1-3]. In addition to growing trends of antimicrobial resistance, the ability of bacteria to develop and persist within biofilms, on implanted biomedical devices is recognized as a significant factor contributing to chronic-relapsing infections and non-osseous union.

Bacterial biofilms represent a protected mode of growth conferring resistance to antimicrobials, thereby limiting the effectiveness of current treatment strategies. Biofilm-derived bacteria are largely insensitive to antimicrobials due to the low permeability of the extracellular matrix surrounding the bacteria and the reduced metabolic state of the persister cells surviving antibiotic treatment [6, 7]. Preventing the formation of a biofilm may represent an alternative strategy for improving the management of infections and patient outcomes. Recent reviews have highlighted the need for biomaterials that deter the establishment of an infection by concurrently dispersing biofilms and promoting tissue integration and regeneration [10]. The D-isomers of amino acids (D-AAs) prevent and disperse biofilms formed by a broad range of bacterial species, including *S. aureus* [13]. In contrast to other dispersal agents, D-AAs promote the dispersion of biofilms through multiple mechanisms and have minimal toxicity toward eukaryotic cells [9, 14]. Previously, we reported that biofilm-dispersive scaffolds

augmented with a 1:1:1 mixture of D-Pro:D-Met:D-Trp reduced the incidence of infection and microbial burden when implanted into rat segmental defects contaminated with clinical isolates of *S. aureus*.

The primary goal of the present study was to evaluate the effects of D-AAs on osteoblast and osteoclast differentiation *in vitro* and on bone cellular activity *in vivo*. In this pilot study, D-AAs were delivered *in vivo* through a settable low-viscosity (LV) bone graft composite composed of MASTERGRAFT® Mini Granules (MG), a lysine triisocyanate-poly(ethylene glycol) (LTI-PEG) prepolymer, a polyester triol, and a tertiary amine catalyst. LV grafts were augmented with 0 or 200 mM D-AAs and injected into ovine femoral condyle defects. New bone formation was measured by micro-computed tomography (μCT) and histology to assess the effects of D-AAs on bone remodeling.

The following research questions were addressed: (1) does increasing doses of D-AAs hinder differentiation of osteoblasts (as determined by Alkaline Phosphatase-positive Colony Forming Unit (CFU-AP) and osteoblast Colony Forming Unit (CFU-OB) assays) and osteoclasts (as determined by Tartrate-resistant acid phosphatase staining (TRAP)) *in vitro*; (2) does local delivery of D-AAs from LV bone grafts hinder bone accretion (as determined by μCT and histological analysis) in a large animal model *in vivo*?

Experimental

In vitro cell culture

To assess the effects of D-AAs on osteoblast and osteoclast differentiation *in vitro*, bone marrow stromal cells (BMSCs) and osteoclast precursor cells were treated with 0 – 81 mM total D-AAs in a 1:1:1 mixture by weight of D-methionine (Met):D-phenylalanine (Phe):D-proline (Pro). D-AAs were dissolved in culture medium (final pH=7.5) containing α-minimum essential medium supplemented with 10% fetal bovine serum, 100 IU/ml

penicillin, and 100 μg/ml streptomycin. BMSCs were isolated from long bones of adult C57 WT mice [15]. For osteoblast differentiation, BMSCs isolated from 3 mice were plated separately at a density of 1.5×10^6 cells/ml. 50 μg/ml of ascorbic acid and 5mM glycerophosphate were added to culture medium 7 and 14 days following plating. Fourteen and 21 days following plating, alkaline phosphatase (ALP) and Von Kossa staining were performed and the numbers of ALP-positive colony forming units (CFU-ALP) and osteoblastic colony forming units (CFU-OB) counted. For BMSC proliferation, BMSCs isolated from 2 mice were plated separately at a density of 2×10^6 cells/ml. After BMSCs reached 80% confluence, cells were trypsinized and re-plated separately into 24-well plates at a density of 1×10^5 cells/ml. D-AA treatment was started one day following platting. Crystal violet staining was performed at different time points and the optical density of the released dye (OD570 nm) was used to quantify cell number. Culture medium and D-AAs were refreshed every other day.

Osteoclast precursor cells were prepared from spleens of 4 adult C57 WT mice by the ficoll (LSM, MP Biomedicals, Solon, OH, USA) gradient method [9] and plated separately at a density of 2.5×10^6 cells/ml. Osteoclast differentiation was induced with 30 ng/ml of macrophage colony-stimulating factor (MCSF, Sigma, St Louis, MO, USA) and 50 ng/ml of receptor activator of nuclear factor B ligand (Rankl, R& D Systems, Minneapolis, MN, USA). Osteoclast differentiation induction and the D-AA treatment started the day cells were plated. Culture medium and D-AA treatment was refreshed every other day. At day 6, Tartrate-resistant acid phosphatase (TRAP) staining was performed. The percentage of TRAP positive area (%) was quantified by MetaMorph Image analysis software.

In vivo large-animal ovine model

LV grafts implanted *in vivo* were prepared with the following polymer composition: LTI-PEG prepolymer (21.7% NCO), a poly(ε-caprolactone (70%)-*co*-glycolide (20%)-*co*-$_{D,L}$-lactide (10%)) triol (450

Da), and a triethylene diamine (TEDA) catalyst (10% solution in dipropylene glycol). To test the effects of D-AAs *in vivo*, a 1:1:1 mixture (by weight) of D-Met:D-Phe:D-Pro was mixed with the reactive polymer prior to injection. LV grafts were prepared by mixing LTI-PEG prepolymer (index 115 [16]), polyester triol, the mixture of D-AAs (0 – 200 mM), TEDA, and MASTERGRAFT® Mini Granules (MG) (40 – 45 wt%).

Four healthy domestic crossbred, adult, female, non-pregnant sheep (*Ovis Aries,* 54-88 kg) were used to evaluate the effects of D-AAs on bone formation. All surgical and care procedures were carried out at IBEX Preclinical Research Inc. (Logan, UT) under aseptic conditions per Institutional Animal Care and Use Committee (IACUC) approval. Pre-operative butorphanol and atropine were administered. Morphine was administered as an epidural injection prior to surgery to provide pre-emptive analgesia. A semi-circular incision was created in the periosteum and the periosteal flap was removed. Bilateral defects 11 × 18 mm were drilled (Figure 6.3A) via a k-wire guide and reamer in the distal aspect of the lateral femoral condyle of each sheep. Before graft application, gauze was used to reduce defect hemorrhaging. Two grafts were investigated (n=4 for each): (1) LV (control) and (2) LV+ D-AAs (200 mM, based on defect volume). Each sheep was implanted with one of each graft, with two grafts implanted into the right and two into the left of four utilized condyles for each graft. LV components were gamma-irradiated (25-40 kGY) by Sterigenics International, mixed, and injected into the defects. Wounds were closed 15 min after implantation. The primary outcome was BV/TV measured by μCT in the middle region of the defect. An *a priori* power analysis indicated that a sample size of 4 would detect a 7.5% difference of BV/TV between groups assuming a mean and standard deviation of 30% and 5%, respectively. This is with a power of 80% and an alpha level of 0.05 using a two-tailed test.

A μCT 50 (SCANCO Medical, Basserdorf, Switzerland) was used to acquire images of the extracted femurs at 16 weeks and cured LV grafts (n=4) fabricated independent of the *in vivo* study. μCT scans were performed in 10% neutral buffered formalin at 70 kVp energy, 200 μA source current, 1000 projections per rotation, 800 ms integration time, and an isotropic voxel size of 24.2 μm. Four concentric annular volumes of

interest 1.83 mm thick and 14 mm long (from the outer cortical surface of the femur) were defined for each sample. The three inner regions incorporated the composites, while the outer region included the host bone interface. Ossified tissue was segmented using a threshold of 340 mg HA cm^{-3} to include both bone and MASTERGRAFT® (MG). Bone volume fraction (BV/TV), trabecular separation (Tb.Sp), trabecular number (Tb.N), and trabecular thickness (Tb.Th) were measured for each annular region and plotted versus the mean radial distance from the core of the defect (R_m) [17]. These morphometric parameters were chosen in order to quantitatively assess the remodeling of trabecular bone architecture in three-dimensions assuming a fixed-structure model [6]. Previously published morphometric parameters for ovine femur trabecular bone were included as a native control [9].

Sheep femora were maintained in 10% neutral buffered formalin for three weeks following dehydration in ethanol. Specimens were embedded in poly(methyl methacrylate) and longitudinal cross-sections were cut, ground, and polished (<100 μm) in the middle of the defect from the blocks using an Exakt system. Sections were stained with Stevenel's Blue and Van Gieson and imaged at 2X and 20X magnification with an Olympus camera (DP71) and SZX16 microscope. New bone formation and residual MG was quantified using Metamorph software (Version 7.0.1) in an area of interest (6 × 14.6 mm) located in the center of the defect. The rectangular area of interest was subdivided into regions 1.83 mm wide corresponding to the size and location of the μCT regions of interest [6, 9].

The *in vitro* cell culture results (CFU-AP and OB colonies, OD570, and TRAP positive area) were compared between the treated and control groups by one-way ANOVA ($\alpha = 0.05$). The μCT morphometric parameters, and area% new bone data were compared between the two groups with the t-test for all comparisons between LV control and LV+D-AAs ($\alpha = 0.05$).

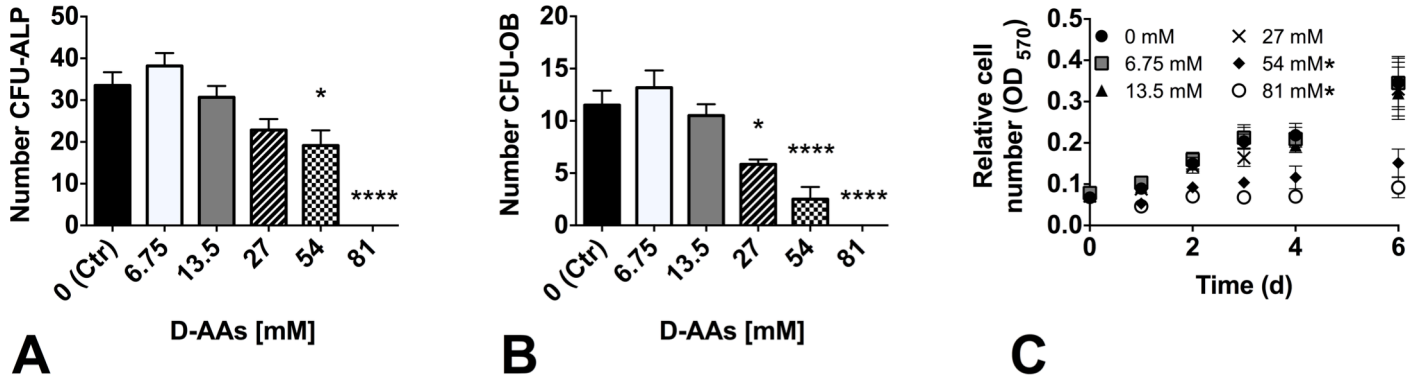

Figure 3.1. Number of (A) CFU-ALP after 14 days and (B) CFU-OB after 21 days of culture in osteogenic medium supplemented with D-AA concentrations from 0-81 mM. Values are reported as mean ± SEM of n=6 samples. (C) Relative cell number (OD570) in BMSCs treated with D-AA concentrations from 0-81 mM for 6 days. Values are reported as mean ± SEM of n=2 samples. * and **** denotes significant differences to control, $p < 0.05$and $p < 0.0001$, respectively, as determined by one-way ANOVA.

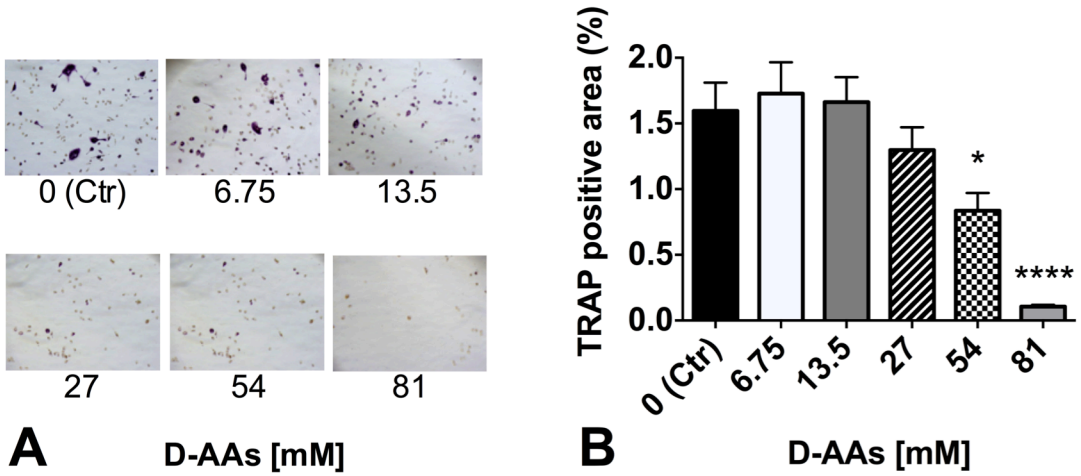

Figure 3.2. (A) Images and (B) corresponding percentage TRAP positive stained surface area of osteoclast cultures treated with D-AA concentrations from 0-81 mM. Values are reported as mean ± SEM of n=24 samples. * and **** denotes significant differences to control, $p < 0.05$), and $p < 0.0001$, respectively, as determined by one-way ANOVA.

Results

The number of CFU-AP colonies formed in cultures exposed to D-AAs concentrations ≤ 27 mM was similar to the non-treated control group (Figure 3.1A) whereas, exposure of BMSCs to ≥54 mM significantly decreased CFU-AP number compared to non-treated controls after 14d. In a similar fashion, the number of CFU-OB was not affected following exposure to D-AAs concentrations ≤ 13.5 mM (Figure 3.1B). Exposure of BMSCs to D-AAs concentrations ≤ 27 mM did not significantly hinder proliferation, whereas the 54 and 81mM concentrations did (Figure 3.1C). The effect of D-AAs on osteoclast precursor cell differentiation was evaluated by TRAP staining. The percent area positively stained for TRAP in osteoclast cultures exposed to D-AAs concentrations ≤ 27 mM was similar to the non-treated control group (Figure 3.2A and B), indicating normal differentiation. However, doses >27nM reduced osteoclast differentiation.

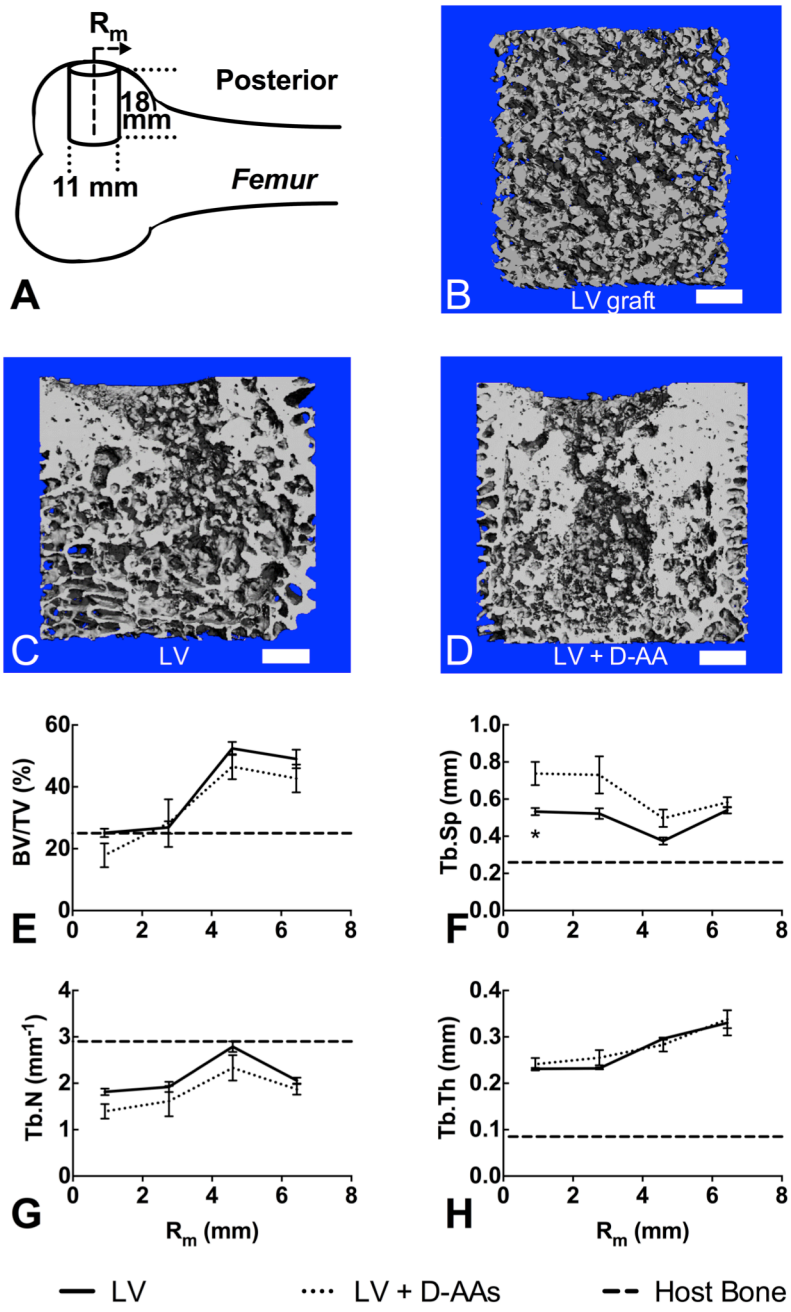

Figure 3.3. (A) Schematic of femoral condyle plug defect. Representative μCT 3D reconstructions (scale bars = 2 mm) of (B) LV graft before *in vivo* implantation, and defects filled with (C) LV or (D) LV+D-AAs, at 16 weeks, show similar morphologies throughout the defect site and increased density at the graft/host bone interface. The morphological parameters (E) BV/TV, (F) Tb.Sp., (G) Tb.N., and (H) Tb.Th. plotted versus the mean radius of the region of interest (R_m) show insignificant differences between defects filled with LV or LV+D-AAs (with the exception of Tb.Sp. at 0.92 mm). The dashed line represents the mean of each parameter as previously reported for native femur trabecular bone. Values are reported as mean ± SEM of n=4 samples. * denotes significant differences ($p < 0.05$) as determined by an unpaired t test compared at each R_m, with Welch's correction for unequal standard deviations.

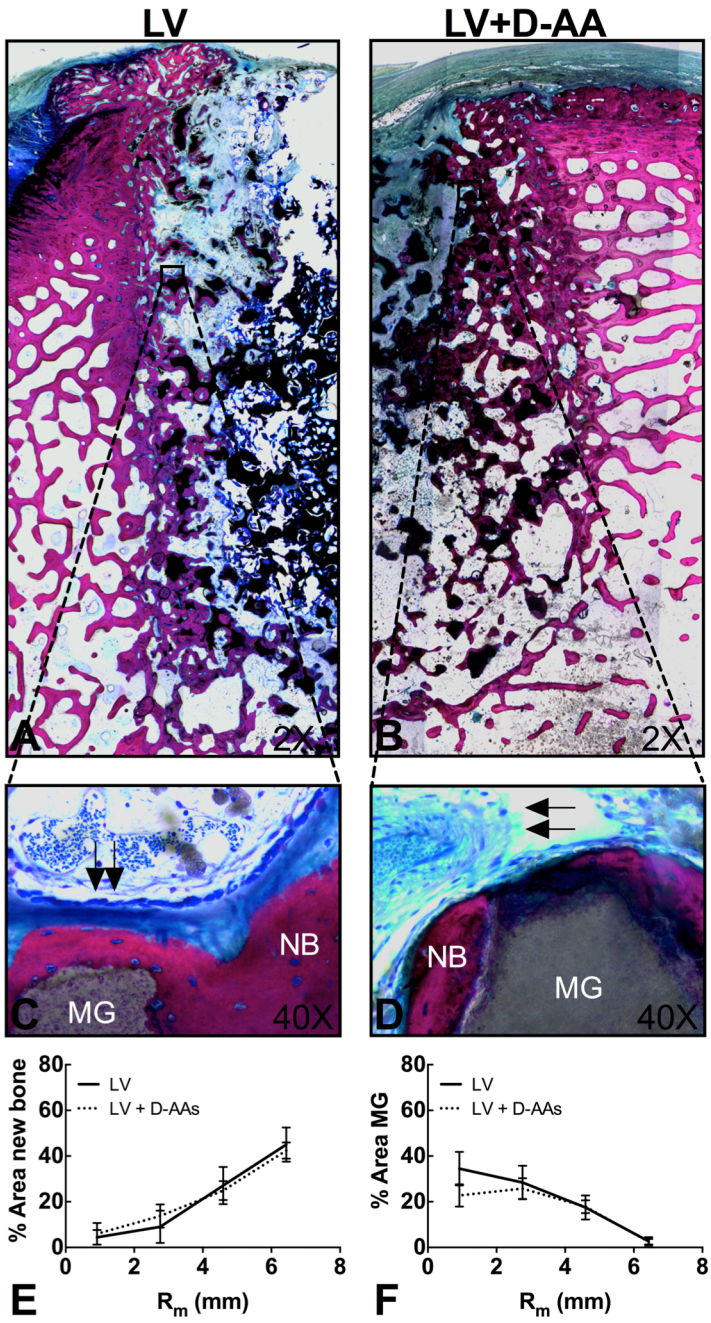

Figure 3.4. Half-view (of entire slide analyzed) low (2X) magnification images of histological cross-sections of defects filled with (A) LV or (B) LV+ D-AAs at 16 weeks show active remodeling. Sections were stained with Stevenel's Blue and Van Gieson. Corresponding high (40X) magnification images of highlighted portions of defects filled with (C) LV or (D) LV+ D-AAs show residual MASTERGRAFT® (MG) particles, new bone (NB), and vascular development (indicated by arrows). Area% (E) new bone and (F) MG, at four regions in the defect measured by histomorphometry shows no significant differences in new bone formation or MG degradation between LV and LV+ D-AAs. Values are reported as mean ± SEM of n=4 samples. * denotes significant differences ($p < 0.05$) as determined by an unpaired t test compared at each R_m, with Welch's correction for unequal standard deviations.

Representative μCT 3D images of LV before *in vivo* implantation (Figure 3.3B) compared to femoral condyle plug defects treated with LV +/- D-AAs at 16 weeks post-implantation (Figure 3.3C-D) show mineral content non-characteristic of MG particles alone, indicating new bone formation and remodeling at the outer region of the defect site (as compared to the inner region) for both groups. BV/TV, Tb.Sp, Tb.N, and Tb.Th. were measured by μCT and plotted versus the radial distance from the center (R_m) (Figure 3.3E-H). BV/TV (which includes new bone and residual MG particles) for each region exceeded that of the host bone (14.6 ± 0.6%). Differences between morphometric parameters measured for the two groups at each R_m were not statistically significant except for Tb.Sp at R_m=0.92 mm.

Histological sections of defects treated with LV +/- D-AAs at 16 weeks post-implantation showed significant cellular infiltration as well as new bone formation and integration of the grafts with host tissue, with lamellar bone similar to native trabecular architecture. Low-magnification images (2X, Figure 3.4A-B) of the defect sites show residual MG particles (black) and bone (pink) ingrowth at the outer regions for both test groups. There was minimal evidence of residual polymer (turquoise). Additionally, the morphology of the surrounding host trabecular bone was similar for both groups, with increased bone density at the composite/defect interface compared to host bone or the center of the graft. Defects filled in both test groups show similar osteocyte densities throughout mineralized bone (both new and surrounding host bone) as well as some signs of fibrous tissue near the center of defect sites. High magnification images (20X, Figure 3.4C-D) show new mineralized bone (NB) growth along the MG particle surface, active cuboidal-shaped osteoblasts along bone surfaces, and blood vessels filled with erythrocytes (indicated by black arrows). For both composites tested, radial histomorphometric analysis (Figure 3.4E-F) showed new bone formation increased from approximately 6 to 40 area% new bone as R_m increased from 1 to 6.5 mm (Figure 3.4E). Minimal differences in mean new bone formation between test groups were quantified for each region. Additionally, differences

between mean area% MG (Figure 3.4F) measured by histomorphometric radial analysis for the two groups at each R_m were not statistically significant.

Discussion

Bone grafts implanted in contaminated open fractures can function as a nidus for infection due to the formation of a biofilm on the surface. Antibiotic treatment needed to eliminate sessile bacteria within biofilms requires concentrations more than 500 times those required to kill planktonic bacteria. While local delivery of antibiotics can achieve bactericidal concentrations, many clinically used antibiotics, including rifampin, doxycycline, and penicillin, are either cytotoxic or inhibit osteogenic differentiation *in vitro* at therapeutically relevant concentrations [9]. Alternatives to antibiotics include agents that have inhibitory and/or dispersive activity against biofilms, such as bismuth thiols, recombinant DNAses [9], quorum sensing inhibitors [9], and D-AAs [9], which have been reported to disperse biofilms *in vitro* and improve healing of biofilm-associated infections *in vivo* [9]. D-AAs are active against a broad spectrum of bacterial species, and local delivery of D-AAs from bone grafts has been shown to reduce the frequency of infection of open fractures contaminated with *S. aureus in vivo*. While previous studies demonstrated that D-Phe, D-Pro, and D-Met were not cytotoxic (>70% viability) to osteoblasts and fibroblasts *in vitro* [19], their effects on osteoblast and osteoclast differentiation and proliferation *in vitro* and on new bone formation *in vivo* have not been investigated. Thus, the goal of the present study was to evaluate the effect of D-AAs on bone cell proliferation and differentiation *in vitro* and bone formation *in vivo*.

A limitation of this pilot study is that *in vivo* bone healing was evaluated only at one time point. At 4 months, local delivery of D-Phe, D-Pro, and D-Met did not hinder bone formation at delivered concentrations exceeding levels that provide anti-biofilm activity. We have reported that the burst release of D-AAs ranges from 20 – 60%, and that the majority of the drug is released in the first 30 days [20]. Thus, the effects of long-

term (>30 days) release of D-AAs on bone healing may warrant further investigation. A second limitation of this study was the inability to distinguish new bone from residual MG via μCT due to their similar densities. Histological and histomorphometric radial analysis (Figure 3.4E-F) were conducted in addition to μCT to independently quantify the Area % new bone and MG.

We have previously reported that the anti-biofilm activity of D-Met, D-Pro, D-Phe, and D-Trp for *S. aureus and P. aeruginosa* increases as the concentration of D-AAs increases from 0.1 – 5 mM, and that concentrations >5 mM result in minimal increases in activity [19, 21]. In contrast, adverse effects of D-AAs on osteoblast proliferation and differentiation, as well as osteoclastogenesis, were observed at concentrations 5 times higher (>27 mM). These results parallel a previous result reporting that the biofilm dispersal agent cis-2-decenoic acid inhibited biofilm formation at concentrations >125 μg/ml, while concentrations >250 μg/ml inhibited fibroblast proliferation *in vitro*. Thus, our findings indicate that D-AAs exhibit anti-biofilm activity at concentrations below levels that hinder osteoblast and osteoclast differentiation *in vitro*.

LV grafts were augmented with D-AAs and injected into ovine femoral condyle plug defects to assess their effect on bone healing *in vivo*. We have previously shown that PUR scaffolds incorporating ≥50 mM (based on defect volume) total D-AAs (mixture of D-Met, D-Pro, and D-Trp) significantly reduced bacterial counts *in vivo* [19]. In the present study, the effects of D-Met, D-Pro, and D-Phe on bone healing were evaluated using grafts augmented with 200 mM D-AAs. D-Phe was utilized instead of D-Trp due to its *in vitro* anti-biofilm activity and lower toxicity compared to D-Trp [22]. The concentration of 200 mM was the maximum possible value that could be delivered from the LV graft while maintaining injectability. As shown by μCT (Figure 3.3) and histological (Figure 3.4) analyses, an increase in BV/TV and Area % new bone was observed at the outer region of both groups receiving the LV grafts (R_m > 4 mm). Thus, bone ingrowth initiated near the host bone/composite interface and progressed toward the interior of the composite, as evidenced by the increase in BV/TV near the interface and monotonic decrease in BV/TV from the interface to the inner core. This

mechanism differs from the remodeling of polymer/allograft bone composites implanted in rabbit femoral plug defects, which exhibited BV/TV values closer to that of host bone near the interface. This difference in bone ingrowth may be due to differences in porosity between the LV grafts (27-28%) and allograft (2-6%)[3-5] composites. Thus, the higher porosity of LV grafts may have supported faster cellular infiltration compared to low-porosity allograft composites. Furthermore, allograft bone resorbs significantly faster than calcium phosphates such as MG, further increasing the potential for faster cellular infiltration.

Sustained release of antibiotics at concentrations exceeding the minimal bacterial concentration is required for at least 4 weeks to control infection of contaminated bone defects [6-8], but the optimal concentration and duration of release for biofilm dispersal agents are unknown. Longitudinal studies investigating bacterial burden, bone formation, and bone remodeling in contaminated defects as a function of D-AA dose and release kinetics during healing are now required to further support the use of D-AAs in the clinical management of infected open fractures.

References

1. L.O. Conterno and M.D. Turchi: Antibiotics for treating chronic osteomyelitis in adults *Cochrane Database of Systematic Reviews.* (9), (2013).

2. S.R. Shah, K.F. Kurtis and A.G. Mikos: Perspectives on the prevention and treatment of infection for orthopedic tissue engineering applications *Chinese Science Bulletin.* **58**(35), 4342 (2013).

3. D.P. Lew and F.A. Waldvogel: Osteomyelitis *Lancet.* **364**(9431), 369 (2004).

4. M. Palmer, W. Costerton, J. Sewecke and D. Altman: Molecular Techniques to Detect Biofilm Bacteria in Long Bone Nonunion: A Case Report *Clinical Orthopaedics and Related Research.* **469**(11), 3037 (2011).

5. E. Tuomanen, R. Cozens, W. Tosch, O. Zak and A. Tomasz: The Rate of Killing of Escherichia-Coli by Beta-Lactam Antibiotics Is Strictly Proportional to the Rate of Bacterial-Growth *Journal of General Microbiology.* **132**, 1297 (1986).

6. I. Kolodkin-Gal, D. Romero, S. Cao, J. Clardy, R. Kolter and R. Losick: D-Amino Acids Trigger Biofilm Disassembly *Science.* **328**(5978), 627 (2010).

7. A.I. Hochbaum, I. Kolodkin-Gal, L. Foulston, R. Kolter, J. Aizenberg and R. Losick: Inhibitory Effects of D-Amino Acids on Staphylococcus aureus Biofilm Development *Journal of Bacteriology.* **193**(20), 5616 (2011).

8. A.E. Hafeman, B. Li, T. Yoshii, K. Zienkiewicz, J.M. Davidson and S.A. Guelcher: Injectable biodegradable polyurethane scaffolds with release of platelet-derived growth factor for tissue repair and regeneration *Pharmaceutical Research.* **25**(10), 2387 (2008).

9. C.J. Sanchez, E.M. Prieto, C.A. Krueger, K.J. Zienkiewicz, D.R. Romano, C.L. Ward, K.S. Akers, S.A. Guelcher and J.C. Wenke: Effects of local delivery of D-amino acids from biofilm-dispersive scaffolds on infection in contaminated rat segmental defects *Biomaterials.* **34**(30), 7533 (2013).

10. M.L. Bouxsein, S.K. Boyd, B.A. Christiansen, R.E. Guldberg, K.J. Jepsen and R. Müller: Guidelines for assessment of bone microstructure in rodents using micro–computed tomography**25**(7), 1486 (2010).

11. R. Bindl, R. Oheim, P. Pogoda, F.T. Beil, K. Gruchenberg, S. Reitmaier, T. Wehner, E. Calcia, P. Radermacher, L. Claes, M. Amling and A. Ignatius: Metaphyseal Fracture Healing in a Sheep Model of Low Turnover Osteoporosis Induced by Hypothalamic-Pituitary Disconnection (HPD) *Journal of Orthopaedic Research.* **31**(11), 1851 (2013).

12. E. Mittra, C. Rubin and Y.X. Qin: Interrelationship of trabecular mechanical and microstructural properties in sheep trabecular bone *Journal of Biomechanics.* **38**(6), 1229 (2005).

13. J. Dumas, E. Prieto, K. Zienkiewicz, T. Guda, J. Wenke, J. Bible, G. Holt and S. Guelcher: Remodeling of Settable Allograft Bone/Polymer Composites with Initial Bone-like Mechanical Properties in Rabbit Femora. *Tissue Eng Part A.* **20**(1-2), 115 (2014).

14. J.W. Costerton, Z. Lewandowski, D.E. Caldwell, D.R. Korber and H.M. Lappinscott: Microbial Biofilms *Annu. Rev. Microbiol.* **49**, 711 (1995).

15. J.P. Folsom, B. Baker and P.S. Stewart: In vitro efficacy of bismuth thiols against biofilms formed by bacteria isolated from human chronic wounds *J Appl Microbiol* **111**(4), 989 (2011).

16. M. Hentzer and M. Givskov: Pharmacological inhibition of quorum sensing for the treatment of chronic bacterial infections *Journal of Clinical Investigation.* **112**(9), 1300 (2003).

17. C.R. Rathbone, J.D. Cross, K.V. Brown, C.K. Murray and J.C. Wenke: Effect of Various Concentrations of Antibiotics on Osteogenic Cell Viability and Activity *Journal of Orthopaedic Research.* **29**(7), 1070 (2011).

18. T. Winkler, E. Hoenig, R. Gildenhaar, G. Berger, D. Fritsch, R. Janssen, M.M. Morlock and A.F. Schilling: Volumetric analysis of osteoclastic bioresorption of calcium phosphate ceramics with different solubilities *Acta Biomaterialia.* **6**(10), 4127 (2010).

19. B. Li, K.V. Brown, J.C. Wenke and S.A. Guelcher: Sustained release of vancomycin from polyurethane scaffolds inhibits infection of bone wounds in a rat femoral segmental defect model *Journal of Controlled Release.* **145**(3), 221 (2010).

20. J.A. Niska, J.A. Meganck, J.R. Pribaz, J.H. Shahbazian, E. Lim, N. Zhang, B.W. Rice, A. Akin, R.I. Ramos, N.M. Bernthal, K.P. Francis and L.S. Miller: Bacterial Burden, Inflammation and Bone Damage Longitudinally Using
Optical and mCT Imaging in an Orthopaedic Implant Infection in Mice. *PLoS ONE.* **7**(10), e47397. doi:10.1371/journal.pone.0047397 (2012).

21. A.J. Harmata, C.L. Ward, K. Zienkiewicz, J.C. Wenke and S.A. Guelcher: Investigating the Effects of Surface-Initiated Polymerization of ε-Caprolactone to Bioactive Glass Particles on the Mechanical Properties of Settable Polymer/Ceramic Composites *Journal of Materials Research.* **29**(20), 2398 (2014).

22. J.R. Jones: Review of bioactive glass: from Hench to hybrids *Acta Biomater.* **9**(1), 4457 (2013).

CHAPTER IV

INVESTIGATING THE EFFECTS OF SURFACE-INITIATED POLYMERIZATION OF E-CAPROLACTONE TO 45S5 BIOACTIVE GLASS ON BIOACTIVE PROPERTIES

Introduction

Bioactive glasses have been used for bone regeneration due to their bioactive properties [1-3]. The brittle nature [4-6] of this type of biomaterial restricts its use alone in weight-bearing anatomical locations, and thus is often blended with polymers for designing biomaterials with bone-like properties. Several bioactive/polymer composites have been investigated for bone regeneration; however, their initial strength was also substantially less than that of trabecular bone [1, 4, 7-9 10]. Recently, a polymer composite comprising a settable, degradable lysine-derived polyurethane (PUR) and surface-modified 45S5 bioactive glass (BG) exhibited initial quasi-static compressive and torsional properties exceeding those of native human trabecular bone [11]. The achieved mechanical properties were attributed to improved interfacial bonding between the polymer and BG phases, which was conjectured to result from chain entanglements formed between the surface polymerization of ε-caprolactone, via surface-initiated ring-opening polymerization (ROP)[12, 13], and the *in situ* formed polyurethane mesh network.

Silane molecules are often utilized as coupling agents between ceramic solids and polymer phases [14]. Grafting silanes to ceramics has been shown to enhance the mechanical strength of polymer composites [15-18]. While silanes are useful for promoting interfacial binding resulting from interactions between the terminal amine and the bulk polymer phase [19], their utility with settable PUR systems may be limited by their high reactivity with polyisocyanates [20], which can result in excessively short working times. Consequently, validating additional surface modification techniques, such as surface polymerization of ε-caprolactone is desired. Additionally, while grafting molecules to the surface of solid fillers, in appropriate systems, has been

shown to improve the overall mechanical properties of resultant polymer composites, the effect of the presence of these surface molecules on the surface bioactivity of bioactive ceramics is not well understood. A range of observations have been made, showing that the presence of aminosilane coatings initially hindered the release of Ca and P ions in aqueous solution, whereas vinyl- and methacryloxy- silane agents showed no effect compared to unmodified substrate [16, 21]. A utilized surface modification technique should not be a detriment to the long-term bioactive properties of bioactive materials.

In this study, the effects of silane functionalization and surface polymerization of ε-caprolactone on 45S5 bioactive glass disks on the *in vitro* biomineralization was investigated. We hypothesized the grafted surface layer thickness, from silane and PCL chains, would control the diffusivity of Ca^{2+} and PO_4^{3-} ions near the BG surface, and thus the addition of PCL would hinder surface reactions and overall bioactivity more than the (3-aminopropyl)triethoxysilane (APTES) molecule alone, as assessed by bone-like hydroxycarbonate apatite (HCA) formation on the BG surface when incubated in physiological solution for up to 21 days. The molecular weight, and consequently the layer thickness, of the surface-initiated PCL was varied by adjusting the polymerization time. The amount of HCA nucleation was assessed qualitatively by scanning electron microscopy (SEM), quantitatively by energy dispersive spectroscopy (EDS), and its maturity was assessed by X-ray diffraction (XRD). Poly(ε-caprolactone) surface-polymerized on APTES-grafted BG disks did not substantially delay the nucleation of HCA on the BG surface, when conditioned in simulated body fluid (SBF), compared to grafting APTES alone. The *in vitro* bioactivity of APTES-PCL grafted BG disks underscores the potential of a APTES-PCL BG fillers in polymeric biocomposites with maintained long-term bioactive properties, improved polymeric adhesion, and thus overall mechanical properties.

Methods

Materials

Melt-derived 45S5 bioactive rods (10 mm diameter by 50 mm length) were purchased from Mo-Sci Corp. (Rolla, MO). APTES, ε-caprolactone, deuterated dimethyl sulfoxide (DMSO), dipropylene glycol, and all components of SBF were purchased from Sigma-Aldrich (St. Louis, MO). Magnesium sulfate, stannous octoate ($Sn(Oct)_2$), and phosphate-buffered saline (PBS) were acquired from Thermo Fisher Scientific (Waltham, MA). SiO_2 wafers were purchased from University Wafer (South Boston, MA).

Surface modification

Study design

Four treatment groups were evaluated to investigate the effects of surface-initiated PCL layer thickness on bioactivity (Table 4.1): (1) cleaned and unmodified (U-BG), (2) cleaned and silanized with APTES (Sil-BG), (3) Sil-BG polymerized with ε-caprolactone for 5 h (5 h PCL-BG), and (4) Sil-BG polymerized with ε-caprolactone for 24 h (24 h PCL-BG). BG disks were used as a model to characterize the surface properties of the BG particles that would be utilized in a polymeric biocomposite [11]. SiO_2 wafers were used as a model for the BG disk surface due to their smooth surface, which was required for atomic force microscopy (AFM) and ellipsometry techniques.

BG disk cleaning

Melt-derived 45S5 bioactive glass disks (3-mm thick) (used to evaluate the effects of surface treatments) were obtained by cutting rods with a Buehler® IsoMet® Low Speed saw. The disks were polished with silicon

carbide paper under aqueous conditions until a mean roughness (R_a) below 1 μm was obtained. The surface roughness was measured by a Veeco Dektak 150 Stylus Surface profilometer (Plainview, NY). BG disks were sonicated for 5 min in a solution of acetone in deionized (DI) water (95 volume %) at room temperature followed by rinsing in DI water under sonication for 5 min [12]. A total of three washing cycles were performed.

Surface-initiated polymerization of ε-caprolactone

After cleaning, discs were contacted with a 2 μM solution of APTES in 9:1 (v/v) ethanol:DI water for 5 h at room temperature [22], rinsed with ethanol, and annealed at 100°C for 1 h. For surface-initiated ring-opening polymerization, ε-caprolactone was dried in the presence of magnesium sulfate. A mixture comprising a 1:1000 molar ratio of $Sn(Oct)_2$:ε-caprolactone [22] and 3 g ε-caprolactone mixture was reacted with Sil-BG disks under static conditions 110°C. The polymerization time (5 or 24 h) was controlled to vary the number-average molecular weight (M_n) and layer thickness (Table 4.1) of the surface-polymerized PCL. Treatment groups were denoted by the polymerization time (e.g., 5 h PCL-BG denotes BG disks polymerized with ε-caprolactone for 5 hours). PCL-modified BG disks were extracted with chloroform to remove non-grafted PCL and dried at 40°C for 24 h.

Surface characterization of bioactive glass disks

Gel permeation chromatography (GPC)

A Waters Breeze GPC (Milford, MA) was used to measure the number-average molecular weight (M_n) of the extracted non-grafted PCL, which has been reported to approximate the M_n of the grafted polymer [23]. Two MesoPore 300 x 7.5 mm columns (Polymer Laboratories) were used in series with stabilized tetrahydrofuran as the mobile phase at a flow rate of 1 mL min^{-1} at 35°C.

Atomic force microscopy (AFM)

A Jeol JSPM-5200 was used to obtain AFM images of surface-modified SiO_2 wafers under ambient laboratory environment. Images (5 μm squares) were obtained using a Si cantilever in AC (tapping) mode, plane-fitted and filtered to remove noise, and processed using Gwyddion software.

X-ray photoelectron spectroscopy (XPS)

XPS measurements were performed using an ULVAC-PHI 5000 VersaProbe spectrometer (Kanagawa, Japan). Dried BG disk specimens were irradiated with a 25 W monochromatic Al Kα x-ray beam (1486.6 eV) and a 100-μm spot size. An electron neutralizer of 1.1 eV and an Ar+ ion neutralizer of 10 eV were used to counteract charging effects. XPS survey scans were accumulated over a binding energy range from 0-1300 eV with a pass energy of 187.85 eV and a take-off angle of 45°. Data were processed using CasaXPS Version 2.3.15 software to calculate the atomic percentages.

Surface tension and contact angle measurements

Wetting experiments were conducted using the sessile drop method. Equilibrium contact angles were measured with a Rame-Hart goniometer on static ~10 μL drops of water. A syringe was used to apply the liquid to the BG disk surface specimens. Reported errors represent the averages and standard deviations, respectively, from three independent measurements.

Ellipsometry

To measure the thickness of the surface-polymerized PCL layer, SiO_2 wafers were treated as described in Section 2.2 for bioactive glass discs. Measured values of M_n for PCL were comparable to those measured for BG disks. Dry ellipsometric thicknesses on SiO_2 wafers were determined from a J. A. Wollam XLS-100 variable angle spectroscopic ellipsometer. Thicknesses were fit to data taken at 75° from the surface over wavelengths from 200 to 1000 nm. The sample surface was modeled as a Si substrate with a native oxide layer and a Cauchy layer. The thickness of the oxide layer was measured from a water and ethanol-cleaned silicon-oxide wafer each time samples were prepared. The thickness of the film was calculated using the software's Cauchy film fit.

In vitro apatite-forming bioactivity assay

The procedure for the apatite-forming test conducted was based on published protocols [24]. Bioactive glass disks were cut in half, creating a hemi-circular shape. Each sample was submerged in 10 mL SBF in a plastic tube and maintained in a incubator at 37°C [24]. The SBF fluid was completely replenished for each sample every 2 days, while the altered SBF was retained for further analysis. At designated time points, samples were removed from the SBF and rinsed with ion-exchanged, distilled water and dried in a desiccator.

Scanning electron microscopy (SEM) and Energy Dispersive Spectroscopy (EDS).

Disks were characterized before and after immersion in SBF. Energy dispersive X-ray spectra of surfaces (n=3) were recorded for randomly chosen locations of broad full field-of-views at 1,000X magnification and 10 kV using a Hitachi S-4200 SEM (Finchampstead, UK). The spectra were processed by "INCA" (Oxford instruments) software using standard reference spectra. After EDS analysis, samples were

sputter-coated with gold and images were obtained and processed using the Quartz PCI system software.

X-ray diffraction (XRD)

XRD scans were performed on a Scintag X_1 θ/θ automated powder X-ray diffractometer in the range of 15-50 in 2θ using a Cu Kα radiation source and a zero-background Si(510) sample support [24]. Scans were taken in step mode with a step size of 0.05 and a preset time of 30 s.

Nuclear magnetic resonance (NMR)

The SBF solutions recovered from the *in vitro* apatite-forming assay were lyophilized and the residues were reconstituted in deuterated DMSO. Nuclear magnetic resonance spectroscopy (NMR) was performed with a Bruker 300 MHz NMR (Billerica, MA) to determine the structure of the residues.

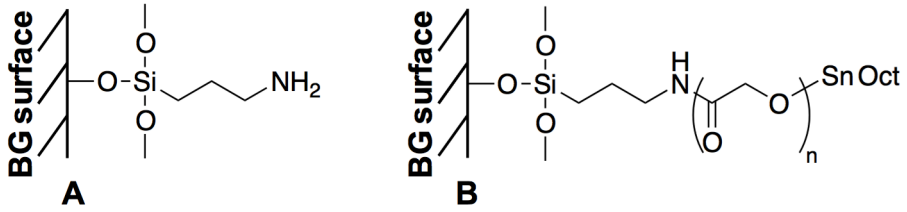

Figure 4.1 Schematic of BG surface modifications. (A) APTES silanol group. (B) Surface-initiated ring-opening polymerization, resulting in PCL chain attached to pre-attached silanol group.

Table 4.1. Characterization of the surface-initiated ring opening polymerization (ROP) of ε-caprolactone. Representative values of M_n and PDI (determined by GPC) and layer thickness (measured by ellipsometry).

Treatment Group	Surface Treatment	PCL M_n (g mol^{-1})	Polydispersity Index (PDI)	Layer thickness *L* (nm)
U-BG	Unmodified	0	N/A	-
Sil-BG	APTES	0	N/A	1.9 ± 0.3
5 h PCL-BG	5h polymerization with ε-caprolactone	7,512	1.1	6.9 ± 0.4
24 h PCL-BG	24h polymerization with ε-caprolactone	26,654	1.9	12.8 ± 0.3

Results

Due to their 2D geometry, disks were used to characterize the effects of the surface treatments. The surface of the BG disks and SiO_2 wafers was modified using established protocols for the grafting of a chemically anchored amine group to the surface using APTES, which was subsequently used to initiate the surface-initiated ROP of PCL. In the presence of ε-caprolactone and $Sn(Oct)_2$, the amine group on the surface-anchored APTES undergoes an exchange reaction with the carboxylate group of the stannous octoate to form the activate catalyst, allowing ε-caprolactone molecules to initiate polymerization of polymer molecules grafted to the BG surface [22, 25]. A schematic illustrating the products of the silanization and polymerization reactions are shown in Figure 4.1.

Table 4.2. Composition of surface-modified bioactive glass discs. Values are reported as atomic percent as measured by X-ray photoelectron spectroscopy (XPS). ND denotes none detected.

Group	C 1s	O 1s	Si 2p	Ca 2p	Na 1p	N 1s	Sn 3d
U-BG	10.1	62.0	17.7	2.9	7.3	ND	ND
Sil-BG	37.6	42.4	13.2	0.7	1.2	5.0	ND
5 h PCL-BG	69.2	28.5	2.0	ND	0.1	ND	0.4
24 h PCL-BG	69.2	27.7	3.0	ND	ND	ND	0.1

Table 4.3. Contact angles measured for surface-modified bioactive glass disks. Values are reported as the mean ± standard deviation of triplicate samples. Water contact angles for PCL surface-polymerized disks approach published values for PCL (73°).

Treatment Group	Water contact angle θ (deg.)
U-BG	14.7 ± 0.6
Sil-BG	45.0 ± 2.7
5 h PCL-BG	66.7 ± 2.5
24 h PCL-BG	66.0 ± 3.6

The properties of the surface-grafted PCL BG disks and silicon wafers, including polymerization time, M_n, PDI, layer thickness (*L*) (on wafers), are listed in Table 4.1. As anticipated, the molecular weight of PCL increased with increasing reaction time. The surfaces characterized by XPS and the water contact angles of the BG discs are listed in Tables 4.2 and 4.3, respectively. Prior to surface treatment, oxygen (62.0%), silicon (17.6%), carbon (10.1%), sodium (7.3%) and calcium (2.9%) were present. When the discs were treated with the amino silane-coupling agent (Sil-BG), the surface concentration of carbon increased (37.6%) and nitrogen

was detected (5.0%), confirming that surface was covered with amino silane (Table 4.2). When Sil-BG was subjected to PCL polymerization, Sn was present at 0.37% and 0.11% for low (5 h PCL-BG) and high molecular weight (24 h PCL-BG) PCL, respectively, suggesting that the $Sn(Oct)_2$ catalyst was bound to the grafted PCL. Additionally, for the PCL-grafted groups, the amount of carbon increased to 69.2% compared to BG (10.1% C) and Sil-BG (37.6% C), while calcium and nitrogen were not detected. These results suggest that PCL polymerized from the aminosilane molecule grafted to the BG surface. As shown in Table 4.3, the surface modifications were further confirmed by water contact angle measurements, which paralleled previously published results and showed an increase in hydrophobicity of the U-BG surface (14.7°) after grafting a silane layer (45.0°)[26] and surface PCL polymerization (66.0°)[27].

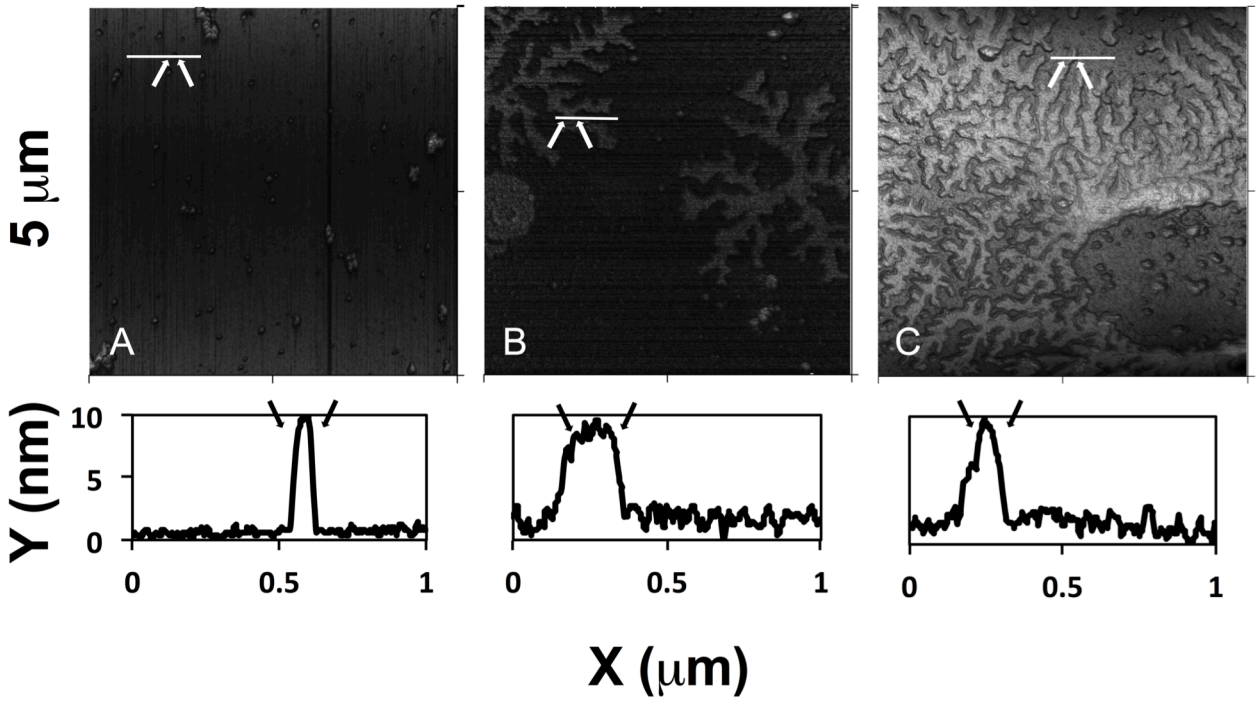

Figure 4.2. Images from atomic force microscopy (AFM) and corresponding layer thickness analysis of silicon

The mean surface thicknesses on silicon oxide wafers for the silane, 5 h PCL, and 24 h PCL grafted layers measured by ellipsometry were 1.9 ± 0.3 nm, 6.9 ± 0.4 nm, and 12.8 ± 0.3 nm, respectively (Table 4.1). Similar to the results for molecular weight, the mean surface layer thickness (L) on silicon oxide wafers increased from 6.9 ± 0.4 nm to 12.8 ± 0.3 nm as polymerization time increased from 5 to 24 hours (Table 4.1). Figure 4.2 shows representative AFM images of the same groups. Silanized surfaces featured islands approximately 10 nm in height that are conjectured to be aggregates of polymerized APTES. 5 h PCL modification showed partial coverage by nodular structures of the PCL brush layer that form lamellae. The difference in height between the lamellae and surrounding surface was approximately 8 nm, which is consistent with previous reports [28, 29]. Similarly, 24 h PCL modification showed increased coverage density of flat-on lamellae compared to the 5 h PCL group with similar height.

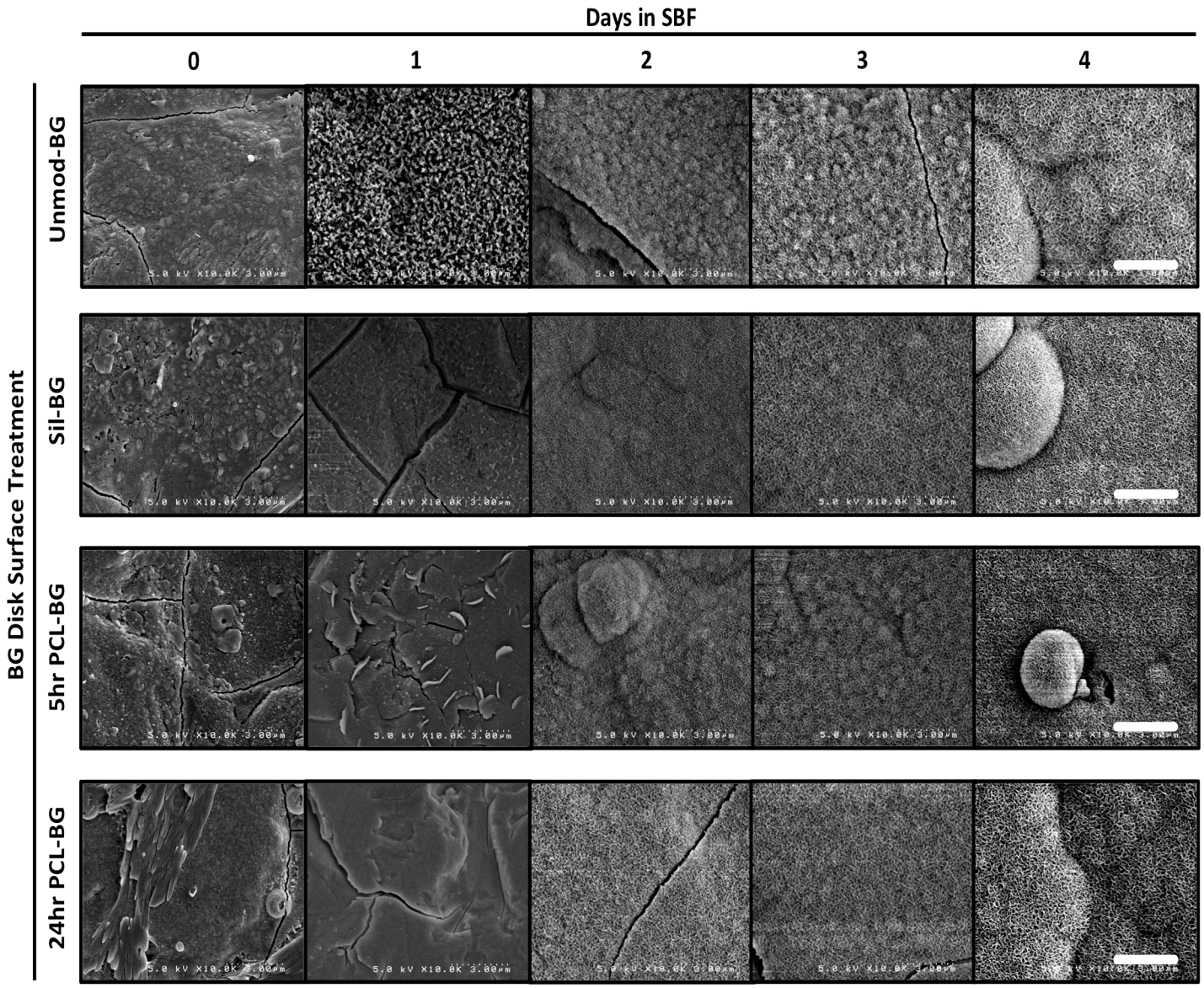

Figure 4.3. *In vitro* apatite formation assay. SEM images of BG disks submerged in SBF for 0,1, 2, 3, and 4 days are shown at high (10,000X) magnification for U-, Sil-, 5 h PCL-, and 24 h PCL-BG disks (Scale bar= 3 μm).

The kinetics of HCA formation upon immersion in SBF was measured for U-, Sil-, 5 h PCL-, and 24 h PCL-BG disks by SEM imaging (Figure 4.3) and EDS (Figure 4.4) analysis. High- (10,000X) magnification images of the surfaces immersed in SBF for 0, 1, 2, 3, and 4 days are shown in Figure 4.3 [24]. Initially (day 0), there is no evidence of HCA nucleated on any of the surfaces. After 1 day in SBF, substantial apatite nucleation was observed on the surface of U-BG disks, while minimal apatite nucleation was present on Sil-, 5 h PCL-, and

24 h PCL-BG disks. After 2 days in SBF, apatite appears to have nucleated on the surface of all groups with a spherulitic micro-morphology formed by 4 days in SBF.

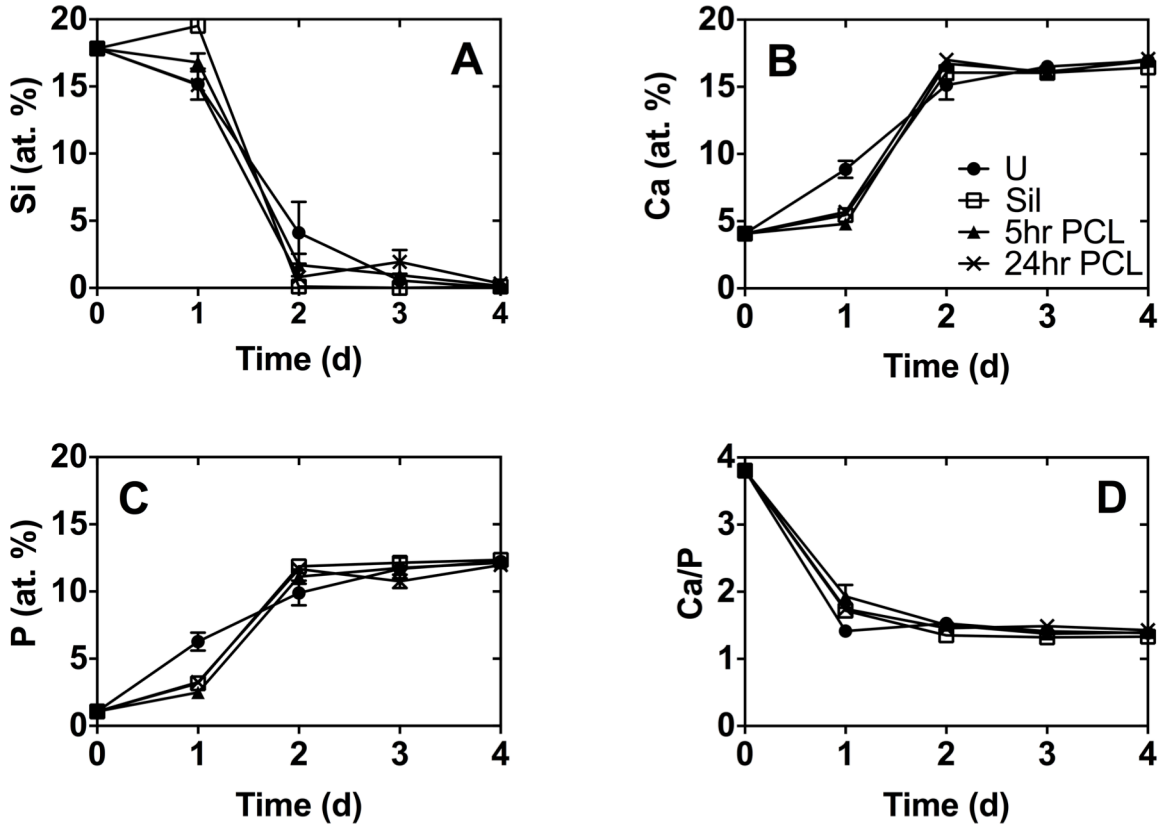

Figure 4.4. Elemental analysis of various BG disk surfaces by EDS. Atomic percent of (A) silicon, (B) calcium, (C) phosphorus, and (D) calculated Ca/P on surfaces of U-, Sil-, 5 h PCL-, and 24 h PCL-BG disks, post 0, 1, 2, 3, and 4 days immersed in SBF.

The one-day delay in HCA nucleation on the surface-modified disk groups observed by SEM was further supported by EDS analysis. The atomic % of Si, Ca, and P, as well as the Ca/P ratio, were measured at the same time points (Figure 4.4). After 1 day in SBF, U-BG disks showed significantly greater amounts of Ca and P (8.86% and 6.27%, respectively) compared to surface-modified BG disk groups (4.80-5.69% and 2.49-3.26%, respectively). The Ca/P ratio was similar for all groups and approached a value of 1.5-1.67 that is

representative of HCA formation [30]. After ≥2 days in SBF, there were no significant differences in % Ca, % P, or Ca/P ratio between any of the groups.

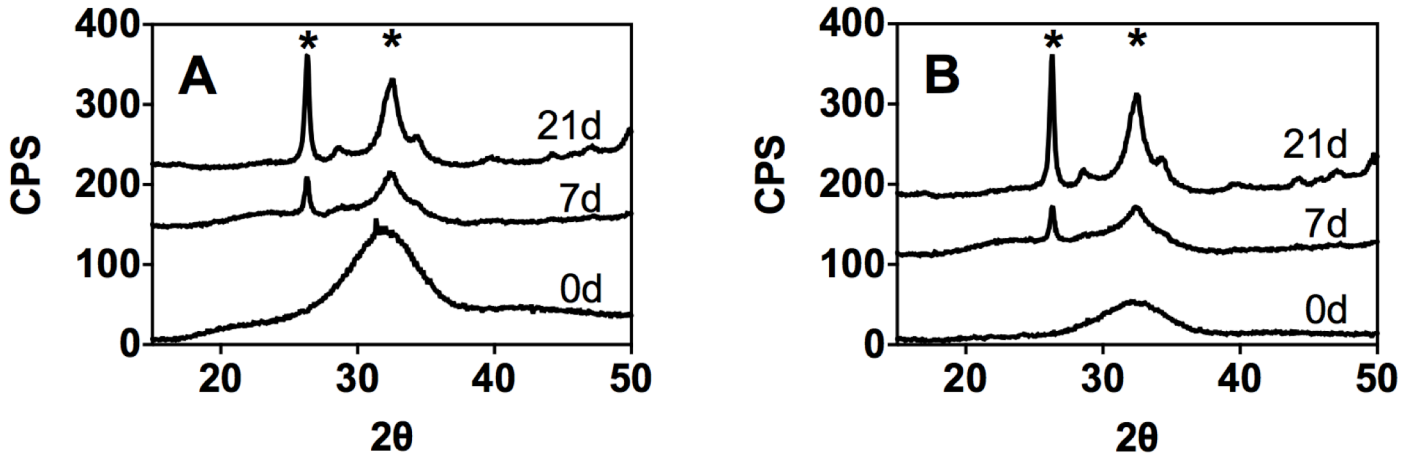

Figure 4.5. XRD spectra of BG disks not submerged (0 d control) or submerged in SBF for 7 or 21 days for (A) unmodified BG and (B) 24 h PCL-BG. The two major peaks for HCA (26° and 33°) are marked by *.

The maturity of the nucleated HCA was evaluated by analyzing the crystallinity of the disks before and after immersion in SBF by XRD (Figure 4.5). Spectra for U-BG and 5 h PCL-BG after immersion in SBF for 0, 7, and 21 days show two major peaks for HCA (diffraction angle 2θ = 26° and 33°) for both BG groups at 7 and 21 days, [3, 31] but absent at 0 day. After 7 days in SBF, peaks at 2θ = 26° and 33° appear for both U- and 24 h PCL-BG disks, implying the formation of a polycrystalline HCA layer [3]. After 21 days in SBF, these peaks representative of crystalline HCA (JCPDS pattern 9-432) began to appear [31].

Discussion

Surface nucleation of bone-like HCA is induced *in vitro* when bioactive glass is immersed in SBF [24, 32, 33], and can be detected within hours [3, 24, 34]. Some studies have reported that grafting APTES to BG delays the kinetics of HCA formation for up to 2 days [35, 36], while others have reported no effect of silanization on bioactivity [34, 37]. Considering that PCL chains could further hinder diffusion of soluble ions to/from the BG surface, we investigated the effects of both APTES alone as well as the thickness of the PCL layer on the rate of HCA formation. NMR analysis (not shown) revealed that no PCL was present in the conditioned SBF, suggesting that the grafted PCL layer was stable throughout the incubation period (21 days) in SBF.

BG disks were used as a model to characterize the surface properties of the BG particles that would be utilized in a polymeric biocomposite [11]. Characterization of surface-modified materials via XPS, ellipsometry, and water contact angle, showed that previously established protocols [22,12, 13] for APTES and PCL grafting were successfully adapted to BG disks and silicon oxide wafer substrates. As shown in Table 4.2, successful grafting of APTES was confirmed by the increase in carbon and nitrogen observed for Sil-BG compared to BG. Polymerization of PCL onto the grafted APTES was confirmed by the increase in carbon observed for 5 h and 24 h PCL-BG compared to Sil-BG. An advantage of the "grafting-from" compared to the "grafting-to" method is that the density of the polymer layer is controlled by the density of initiation sites (i.e., reactive amines from APTES) and is thus not constrained by the conformation of the polymer [38]. The presence of Sn in the XPS spectra suggests that the $Sn(Oct)_2$ catalyst was bound to the grafted PCL, which is consistent with a previous study reporting covalent bonding of $Sn(Oct)_2$ to PCL grafted to APTES-modified BG fiber surfaces [22]. $Sn(Oct)_2$ is the most commonly used initiator in ROP processes because of its approval by the U.S. Food and Drug Administration in food stabilizers. Verification of surface modifications was further obtained via AFM analysis (Figure 4.2). Unexpectedly, based on images obtained from AFM, it appeared that increased

polymerization time not only increased the M_n of resultant polymer and mean layer thickness (L) of grafted polymer but also the surface coverage and altered the resultant polymer morphology, on silicon oxide wafers.

From biomineralization experiments of surface-modified BG in SBF, the effect of silane and PCL surface modification on HCA nucleation was investigated. The presence of APTES delayed the rate of HCA formation at days 0 – 1, which parallels observations made in previous studies [35, 36]. Despite this confirmed trend, it is difficult to compare the length of time of the delay between studies. The surface reactions that result in HCA nucleation are highly sensitive and dependent on numerous factors, including the amount of BG surface area exposed to incubation physiological fluids, BG surface morphology, the volume of incubation fluid and frequency of fluid changed which both alter number of free ions in solution, and composition of the incubation container [24]. Unless the biomineralization method is identical, the rate of HCA nucleation should not be directly compared between studies, but rather used as an approximation.

Surface-initiated PCL, both 5 h and 24 h polymerization times, did not further hinder HCA nucleation kinetics (Figures 4.3 – 5) compared to BG with APTES grafted alone. While 24 h PCL-BG exhibited slightly delayed (i.e., <2 days) nucleation of HCA, after 7 days there were no significant differences in the crystallinity of the HCA layer between groups (Figures 4.5). Taken together, these data suggest that the presence of a grafted polymer layer results in only a temporal delay in mineralization that is resolved by day 7. Since surface-initiated PCL is attached to solid surfaces by the grafting-from mechanism, it is presumed that PCL chains attach to the BG surface (at this temperature) via a previously attached APTES molecule[22, 39]. AFM images (Figure 4.2) show that increased PCL polymerization time increases coverage of silanized surface with PCL chains. Consequently, APTES molecules are conjectured to have been present in a near monolayer form with nearly complete covered in order to provide PCL active attachment sites. The biomineralization results from this study support the hypothesis that attached APTES molecules prevent surface reaction between BG surface and physiological fluid by physically blocking reactive surface sites, which delays HCA nucleation in the first

day, and that increasing the grafted surface layer thickness by addition of PCL chains does not further delay HCA nucleation by decreasing the diffusivity of Ca^{2+} and PO_4^{3-} ions near the BG surface.

These results support further investigation of the effect of APTES-PCL surface modification on *in vivo* properties. Although the APTES-PCL surface modification has been shown to significantly increase the quasi-static compression and torsion mechanical properties of overall BG/polymer composites [11], the cytotoxicity of residual stannous octoate catalyst from the surface-initiated polymerization *in vivo* is unknown. The presence of Sn in the XPS spectra suggests that the $Sn(Oct)_2$ catalyst was bound to the grafted PCL, which is consistent with a previous study [22]. Thus, more effective approaches for removing the residual tin catalyst are needed to minimize potential cytotoxicity *in vivo*. Additionally, the effects of APTES-PCL surface modification on the delay of new bone formation are not known and merit further investigation *in vivo*. Evaluating bioactivity by *in vitro* biomineralization techniques has been accepted as the standard method for evaluating bioactivity of materials. In the future, it will be important to validate that the observed 2 day delay in HCA formation *in vitro* does not significantly hinder the ability for polyurethane polymer and PCL surface-modified BG particle composite to aid in the remodeling of bone defects *in vivo*.

We hypothesize the observed delay in HCA nucleation on silane-modified (with or without additional PCL) bioactive glass surfaces is either caused by the presence of a cross-linked silane network[14] that is preventing ions diffusing to/from the BG surface or physical blocking of potential reactive sites needed to participate in surface reactions with the surrounding physiological fluid. The attachment of silane molecules to a ceramic surface usually results in the formation of one bond from each organosilane silicon to the surface, with the two remaining silanol groups present in the condensed (to other silanols to form siloxane linkages) or free form [14]. The end result is a siloxane polymeric network close to the inorganic surface typically <5 nm thick. If the BG surface is completely covered with attached silanes that are in the condensed form, the resultant polymeric network may be able to alter diffusion of ions at the surface. If the first hypothesis is true, alternative

approaches for surface-initiated polymerization of ε-caprolactone that do not require silane treatment may reduce the delay in biomineralization. A previous study showed the ability to attach oligo(lactones) (specifically L-lactide and ε-caprolactone) to activated tricalcium phosphate (TCP) filler particles at 150°C without any additional catalysts or the use of a silane coupling agent [13]. Although, if the second hypothesis is true, the attachment of any surface molecule will physically block reactive sites on the BG surface and thus cause a short-term delay in HCA nucleation. Subsequently, further investigation on the effect of surface coverage of the BG surface on the bioactive properties, and subsequent overall mechanical properties of resultant polymeric composite made with surface-modified BG particles, will be needed.

Conclusion

In this study, the effect of surface-initiated polymerization of ε-caprolactone on bioactive glass disks on the *in vitro* biomineralization was investigated. The increased polymerization time increased the number-average molecular weight of resultant polymer, mean layer thickness, and the surface coverage of grafted PCL layer, as well as altered the resultant polymer layer morphology, on silicon oxide wafers. The presence of grafted silane (APTES) alone delayed the rate of HCA formation at days 0 – 1, when conditioned in SBF. The presence of PCL chains did not delay the nucleation of HCA on the surface of bioactive glass disks compared to silane-treated disks. Additionally, after 7 days in SBF, the maturity of nucleated HCA on un-modified and APTES-PCL modified BG was indistinguishable, suggesting that the observed temporal delay in mineralization was resolved at later time points. The ability for PCL surface-modified BG to support biomineralization *in vitro* points to its potential use for future development in an injectable, settable, synthetic polyurethane composite graft for bone defects.

References

1. J.R. Jones: Review of bioactive glass: from Hench to hybrids *Acta Biomater.* **9**(1), 4457 (2013).

2. A.R. Boccaccini and J.J. Blaker: Bioactive composite materials for tissue engineering scaffolds *Expert Review of Medical Devices.* **2**(3), 303 (2005).

3. L.L. Hench and J. Wilson: Bioceramics *Mrs Bulletin.* **16**(9), 62 (1991).

4. O. Bretcanu, S. Misra, I. Roy, C. Renghini, F. Fiori, A.R. Boccaccini and V. Salih: In vitro biocompatibility of 45S5 Bioglass (R)-derived glass-ceramic scaffolds coated with poly(3-hydroxybutyrate) *Journal of Tissue Engineering and Regenerative Medicine.* **3**(2), 139 (2009).

5. M.N. Rahaman, D.E. Day, B.S. Bal, Q. Fu, S.B. Jung, L.F. Bonewald and A.P. Tomsia: Bioactive glass in tissue engineering *Acta Biomaterialia.* **7**(6), 2355 (2011).

6. L.-C. Gerhardt and A.R. Boccaccini: Bioactive Glass and Glass-Ceramic Scaffolds for Bone Tissue Engineering *Materials.* **3**(7), 3867 (2010).

7. K.E. Tanner: Bioactive composites for bone tissue engineering *Proceedings of the Institution of Mechanical Engineers Part H-Journal of Engineering in Medicine.* **224**(H12), 1359 (2010).

8. M. Bil, J. Ryszkowska, J.A. Roether, O. Bretcanu and A.R. Boccaccini: Bioactivity of polyurethane-based scaffolds coated with Bioglass((R)) *Biomedical Materials.* **2**(2), 93 (2007).

9. J.L. Ryszkowska, M. Auguscik, A. Sheikh and A.R. Boccaccini: Biodegradable polyurethane composite scaffolds containing Bioglass (R) for bone tissue engineering *Composites Science and Technology.* **70**(13), 1894 (2010).

10. C. Chan, I. Thompson, P. Robinson, J. Wilson and L. Hench: Evaluation of Bioglass/dextran composite as a bone graft substitute *International Journal of Oral and Maxillofacial Surgery.* **31**(1), 73 (2002).

11. A.J. Harmata, C.L. Ward, K. Zienkiewicz, J.C. Wenke and S.A. Guelcher: Investigating the Effects of Surface-Initiated Polymerization of ε-Caprolactone to Bioactive Glass Particles on the Mechanical Properties of Settable Polymer/Ceramic Composites *Journal of Materials Research.* **29**(20), 2398 (2014).

12. E. Verne, C. Vitale-Brovarone, E. Bui, C.L. Bianchi and A.R. Boccaccini: Surface functionalization of bioactive glasses *J. Biomed. Mater. Res. Part A.* **90A**(4), 981 (2009).

13. C. Kunze, T. Freier, E. Helwig, B. Sandner, D. Reif, A. Wutzler and H.J. Radusch: Surface modification of tricalcium phosphate for improvement of the interfacial compatibility with biodegradable polymers *Biomaterials.* **24**(6), 967 (2003).

14. B. Arkles: Tailoring Surfaces with Silanes *Chemtech.* **7**(12), 766 (1977).

15. R.A. Sousa, R.L. Reis, A.M. Cunha and M.J. Bevis: Coupling of HDPE/hydroxyapatite composites by silane-based methodologies *Journal of Materials Science-Materials in Medicine.* **14**(6), 475 (2003).

16. K. Zhang, Y.B. Wang, M.A. Hillmyer and L.F. Francis: Processing and properties of porous poly(L-lactide)/bioactive glass composites *Biomaterials.* **25**(13), 2489 (2004).

17. V.A. Koleganova, S.M. Bernier, S.J. Dixon and A.S. Rizkalla: Bioactive glass/polymer composite materials with mechanical properties matching those of cortical bone *Journal of Biomedical Materials Research Part A.* **77A**(3), 572 (2006).

18. R.A. Khan, A.J. Parsons, I.A. Jones, G.S. Walker and C.D. Rudd: Effectiveness of 3-Aminopropyl-Triethoxy-Silane as a Coupling Agent for Phosphate Glass Fiber-Reinforced Poly(caprolactone)-based Composites for Fracture Fixation Devices *Journal of Thermoplastic Composite Materials.* **24**(4), 517 (2011).

19. V.A. Koleganova, S.M. Bernier, S.J. Dixon and A.S. Rizkalla: Bioactive glass/polymer composite materials with mechanical properties matching those of cortical bone *J Biomed Mater Res A.* **77**(3), 572 (2006).

20. G. Oertel: Polyurethane Handbook, 2nd ed. (Hanser Gardner Publications, City, 1994).

21. A.M.P. Dupraz, J.R. deWijn, S.A.T. vanderMeer and K. deGroot: Characterization of silane-treated hydroxyapatite powders for use as filler in biodegradable composites *Journal of Biomedical Materials Research.* **30**(2), 231 (1996).

22. G. Jiang, G.S. Walker, I.A. Jones and C.D. Rudd: XPS identification of surface-initiated polymerisation during monomer transfer moulding of poly(epsilon-caprolactone)/Bioglass (R) fibre composite *Applied Surface Science.* **252**(5), 1854 (2005).

23. M. Barsbay, G. Gueven, M.H. Stenzel, T.P. Davis, C. Barner-Kowollik and L. Barner: Verification of controlled grafting of styrene from cellulose via radiation-induced RAFT polymerization *Macromolecules.* **40**(20), 7140 (2007).

24. T. Kokubo and H. Takadama: How useful is SBF in predicting in vivo bone bioactivity? *Biomaterials.* **27**(15), 2907 (2006).

25. S. Penczek, A. Duda, A. Kowalski, J. Libiszowski, K. Majerska and T. Biela: On the mechanism of polymerization of cyclic esters induced by Tin(II) octoate *Macromolecular Symposia.* **157**, 61 (2000).

26. P.A. Heiney, K. Gruneberg, J.Y. Fang, C. Dulcey and R. Shashidhar: Structure and growth of chromophore-functionalized (3-aminopropyl)triethoxysilane self-assembled on silicon *Langmuir.* **16**(6), 2651 (2000).

27. K.R. Yoon, K.B. Lee, Y.S. Chi, W.S. Yun, S.W. Joo and I.S. Choi: Surface-initiated, enzymatic polymerization of biodegradable polyesters *Advanced Materials.* **15**(24), 2063 (2003).

28. X. Wang, J. Yang and J. Zhou: Crystallization behavior of poly(epsilon-caprolactone) grafted on silicon surface *E-Polymers.* (2011).

29. A. Olivier, J.-M. Raquez, P. Dubois and P. Damman: Semi-crystalline poly(epsilon-caprolactone) brushes on gold substrate via "grafting from" method New insights with AFM characterization *European Polymer Journal.* **47**(1), 31 (2011).

30. N.L. D'Elía, A.N. Gravina, J.M. Ruso, J.A. Laiuppa, G.E. Santillán and P.V. Messina: Manipulating the bioactivity of hydroxyapatite nano-rods structured networks: Effects on mineral coating morphology and growth kinetic *Biochimica et biophysica acta.* **1830: 5014-5026**, (2013).

31. M.R. Saeri, A. Afshar, M. Ghorbani, N. Ehsani and C.C. Sorrell: The wet precipitation process of hydroxyapatite *Materials Letters.* **57**(24-25), 4064 (2003).

32. P. Saravanapavan, J.R. Jones, R.S. Pryce and L.L. Hench: Bioactivity of gel-glass powders in the CaO-SiO2 system: A comparison with ternary (CaO-P2O5-SiO2) and quaternary glasses (SiO2-CaO-P2O5-Na2O) *J. Biomed. Mater. Res. Part A.* **66A**(1), 110 (2003).

33. L.L. Hench: The story of Bioglass (R) *Journal of Materials Science-Materials in Medicine.* **17**(11), 967 (2006).

34. Q.-Z. Chen, K. Rezwan, V. Francon, D. Armitage, S.N. Nazhat, F.H. Jones and A.R. Boccaccini: Surface functionalization of Bioglass((R))-derived porous scaffolds *Acta Biomaterialia.* **3**(4), 551 (2007).

35. K. Zhang, Y. Wang, M.A. Hillmyer and L.F. Francis: Processing and properties of porous poly(L-lactide)/bioactive glass composites *Biomaterials.* **25**(13), 2489 (2004).

36. A.M. Dupraz, J.R. de Wijn, S.A. v d Meer and K. de Groot: Characterization of silane-treated hydroxyapatite powders for use as filler in biodegradable composites *J Biomed Mater Res.* **30**(2), 231 (1996).

37. Q.Z. Chen, K. Rezwan, D. Armitage, S.N. Nazhat and A.R. Boccaccini: The surface functionalization of 45S5 Bioglass (R)-based glass-ceramic scaffolds and its impact on bioactivity *J. Mater. Sci.-Mater. Med.* **17**(11), 979 (2006).

38. W.K.J. Mosse, M.L. Koppens, T.R. Gengenbach, D.B. Scanlon, S.L. Gras and W.A. Ducker: Peptides Grafted from Solids for the Control of Interfacial Properties *Langmuir.* **25**(3), 1488 (2009).

39. G. Jiang, M.E. Evans, I.A. Jones, C.D. Rudd, C.A. Scotchford and G.S. Walker: Preparation of poly(epsilon-caprolactone)/continuous bioglass fibre composite using monomer transfer moulding for bone implant *Biomaterials.* **26**(15), 2281 (2005).

CHAPTER V

INVESTIGATING THE EFFECTS OF SURFACE-INITIATED POLYMERIZATION OF E-CAPROLACTONE TO 45S5 BIOACTIVE GLASS PARTICLES ON THE MECHANICAL PROPERTIES OF SETTABLE HIGH-VISCOSITY COMPOSITES

Introduction

Injectable and settable synthetic bone grafts that possess initial mechanical strength exceeding that of host bone and maintain strength comparable to bone while remodeling could improve the clinical management of a number of orthopaedic conditions, such as repair of open tibial plateau fractures[1, 2], screw augmentation[3-5], and vertebroplasty[6]. Since their discovery in 1982[7], calcium phosphate cements (CPCs) were successfully introduced into clinical applications due to their osteoconductivity and fast setting times[8]. While the initial compressive strength of CPCs is comparable to that of trabecular bone, they undergo brittle fracture at strains less than the yield strain of trabecular bone, resulting in failure under physiologically relevant loads with a substantial shear component[9-11]. Thus, the brittleness of CPCs precludes their use in many weight-bearing applications. Combining ceramics with polymers has been investigated as an approach to designing materials with tougher mechanical properties. However, a recent review of the ceramic/polymer composite literature reported that the compressive strength of most composites is substantially weaker than both trabecular bone and CPCs[10].

Low-porosity (<10%), settable composites incorporating a degradable lysine-derived prepolymer, a polyester triol, a tertiary amine catalyst, and allograft bone particles exhibited initial compressive strength exceeding that of trabecular bone and remodeled by creeping substitution of the allograft particles[12]. However, the torsional strength of the composites was less than that of trabecular bone. Furthermore, allograft bone has low bioactivity, is limited in supply, and can present risks of disease transmission. Thus, there is a compelling

need for high-viscosity, settable ceramic/polymer composites with initial mechanical properties exceeding those of host bone, particularly under loadings with a significant shear component[13].

45S5 Bioactive glass (BG) has been widely used for bone regeneration due to its bioactivity[13-15], as assessed by the formation of a hydroxycarbonate apatite (HCA) layer on its surface in physiological solution[16]. Dissolution of ions from BG alters the local environment and promotes cellular responses critical for both new bone formation as well as the formation of an apatite layer on the surface[17, 18]. BG/polymer composites have been investigated for bone regeneration[13, 19-22]. In a previous study, BG/dextran composites remodeled to form new bone when injected into rabbit femoral condyle plug defects[23]. However, BG/dextran composites are not settable and thus the initial strength is substantially less than that of trabecular bone. While settable polymers offer the advantages of increased strength, interfacial bonding between the polymer and BG phases is required to prevent nucleation of cracks and premature failure[13, 24]. Using monomer transfer molding, glass fiber/poly(ε-caprolactone) (PCL) composites have been fabricated in which polymerization was initiated from an amine-terminated silane grafted to the fiber surface, resulting in chemical bonding between the glass and the PCL phases and enhanced mechanical properties[25, 26]. However, thermoplastic polymers such as PCL must be processed by melt- or solvent-casting and are not suitable for injectable and settable systems.

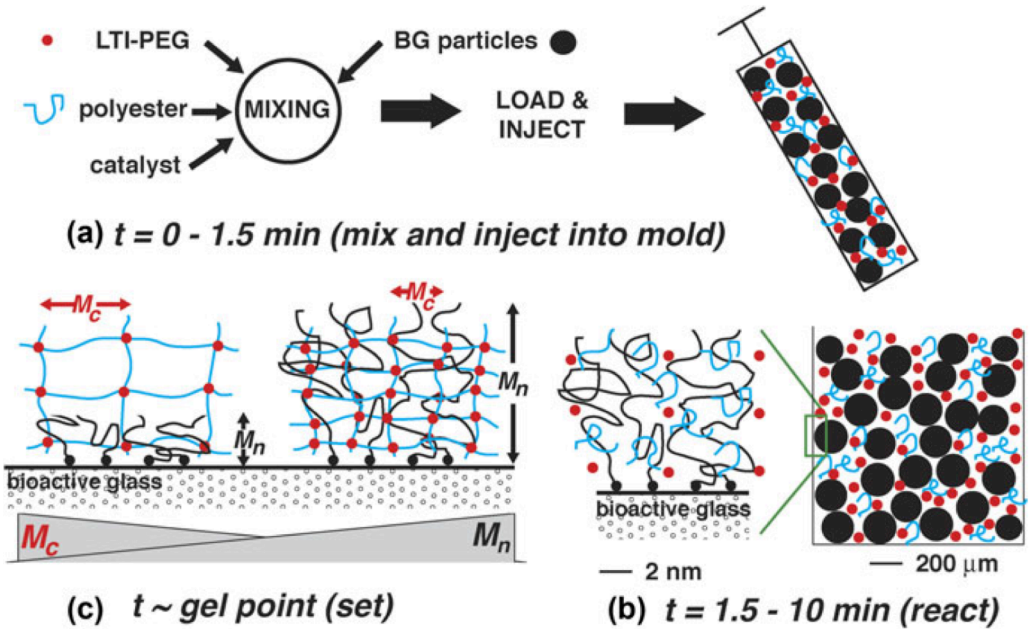

Figure 5.1. Schematic illustrating the synthesis of bioactive glass/polyurethane composites by reactive liquid molding. (a) At the length scale of the bioactive glass particles, the reactive mixture initially (t = 0) comprises LTI-PEG prepolymer (red circles), polyester polyol chains (blue lines), and bioactive glass particles (black circles). At the length scale of the interphase, the interfacial region near the surface of the bioactive glass particles initially comprises PCL chains (black lines) anchored to the surface by an APTES linker (small black circle), LTI-PEG prepolymer, and polyester polyol. (b) At the gel point (~10 min), the prepolymer and polyol have reacted to form a PUR network with molecular weight between cross-links M_c. For low molecular weight grafted PCL and high molecular weight polyol, $M_n < M_c$, resulting in a low degree of inter-penetration between grafted PCL chains and the PUR network. For high molecular weight PCL and low molecular weight polyol, $M_n > M_c$, resulting in a high degree of inter-penetration between the chains.

In this study, we investigated an alternative approach in which mechanical properties are enhanced by chain entanglements between surface-initiated PCL chains on the BG particles and an *in situ*-formed polymer network (Figure 5.1C). To prepare the composites, a lysine triisocyanate (LTI)-poly(ethylene glycol) (PEG) prepolymer was mixed with a polyester triol, a tertiary amine catalyst, and BG particles (Figure 5.1A). The LTI-PEG prepolymer and the polyester triol react to form a polymer network with a gel time of ~10 min and molecular weight between crosslinks M_c (Figure 5.1B and C). Prior to mixing with the reactive polymer, BG particles were functionalized with the silane-coupling agent 3-aminopropyl-triethoxysilane (APTES) followed by surface polymerization of ε-caprolactone via surface-initiated ring-opening polymerization (ROP)[27, 28]. The

molecular weight of the surface-initiated PCL (M_n, Fig. 5.1C) was varied by adjusting the polymerization time. We hypothesized that under conditions where $M^* = M_n/M_c >> 1$, surface-initiated PCL chains are physically entangled in the polymer network as the reaction progresses toward the gel point (Figure 5.1C), which enhances interfacial bonding and mechanical properties. To test this hypothesis, the effects of M^* on the compressive properties of the composites were investigated by varying the molecular weight of both the surface-initiated PCL (M_n) and the polyester triol component of the polymer network (M_c). Additionally, the torsional strength was measured to evaluate the feasibility of the composites as weight-bearing bone grafts under more physiologically relevant loads incorporating a shear component. Finally, the ability of the strongest composite to remodel *in vivo* was evaluated in a rat femoral condyle defect model.

Experimental

Materials

Melt-derived 45S5 bioactive glass particles (150-212 μm diameter) were purchased from Mo-Sci Corp. (Rolla, MO). APTES, ε-caprolactone, dipropylene glycol, PCL triol (M_n ~300 g mol^{-1}, referred to as PCL300), deuterated dimethyl sulfoxide (DMSO), glycerol, ε–caprolactone, and iron acetylacetonate (FeAA) catalyst were purchased from Sigma-Aldrich (St. Louis, MO). Magnesium sulfate, stannous octoate ($Sn(Oct)_2$), and phosphate-buffered saline (PBS) were acquired from Thermo Fisher Scientific (Waltham, MA). Technovit 4000 (Heraeus Kulzer) was purchased from Electron Microscopy Sciences (Hatfield, PA). Triethylenediamine (TEDA) was purchased from Evonik (Parsipanny, NJ). A lysine triisocyanate (LTI)-polyethylene glycol (PEG) prepolymer (21% NCO) was supplied by Medtronic (Memphis, TN). $_{D,L}$-lactide and glycolide were supplied by Polysciences (Warrington, PA).

Surface modification and characterization of bioactive glass particles

In vitro study design

BG/polymer composites with adjustable $M^* = M_n/M_c$ were prepared by independently varying the values of M_n and M_c. To vary M_c, polymer networks were synthesized from a 300 g mol^{-1} (7C300) or 3000 g mol^{-1} (7C3000) poly(ε-caprolactone (70%)-*co*-glycolide (20%)-*co*-$_{D,L}$-lactide (10%)) triol and either an FeAA or TEDA catalyst. Copolyester triols were used to ensure that they were amorphous, viscous liquids at room temperature. The value of M_n was varied by three BG surface treatments (Table 5.1): (1) cleaned and unmodified (U-BG), (2) Silanized with APTES (Sil-) and polymerized with ε-caprolactone for 5 hr (5hr PCL-BG), and (3) Sil-BG polymerized with ε-caprolactone for 24 hr (24hr PCL-BG). BG polyurethane composites are denoted by the following notation: *BG surface treatment*-BG/*polyol-catalyst* (e.g., a composite made with 24hr PCL-BG, 7C300 polyester triol, and FeAA catalyst is denoted 24hr PCL-BG/7C300-F).

Cleaning

Melt-derived 45S5 bioactive glass particles were sonicated for 5 min in a solution of acetone in deionized (DI) water (95 volume %) at room temperature followed by rinsing in DI water under sonication for 5 min, based on previous optimization[27]. A total of three washing cycles were performed.

Surface-initiated polymerization of ε-caprolactone

After cleaning, particles were contacted with a 2 μM solution of APTES in 9:1 (v/v) ethanol:DI water for 5 h at room temperature[26], rinsed with ethanol, and annealed at 100°C for 1 h. For surface-initiated ring-opening polymerization (ROP), ε-caprolactone was dried in the presence of magnesium sulfate. A mixture

comprising a 1:1000 molar ratio of $Sn(Oct)_2$:ε-caprolactone[25] and a 0.83:1 weight ratio of Sil-BG: ε-caprolactone was reacted with Sil-BG particles while stirring at 110°C. The polymerization time (5 or 24 h) was controlled to vary the number-average molecular weight M_n (Table 5.1) of the surface-polymerized PCL. Treatment groups were denoted by the polymerization time as noted above. PCL-modified BG particles were extracted with chloroform to remove non-grafted PCL and dried at 40°C for 24 h.

Gel permeation chromatography (GPC)

A Waters Breeze GPC (Milford, MA) was used to measure the number-average molecular weight (M_n) of the extracted non-grafted PCL, which has been reported to approximate the M_n of the grafted polymer[29]. Two MesoPore 300 x 7.5 mm columns (Polymer Laboratories) were used in series with stabilized tetrahydrofuran as the mobile phase at a flow rate of 1 mL min^{-1} at 35°C.

Thermogravimetric Analysis (TGA)

TGA analyses were performed to quantified the amount of PCL on the BG surface, with a heating at a rate of 10°C min^{-1} over the temperature range of 25-600°C under a nitrogen flow of 40 mL min^{-1}. A TA Instruments Q500 instrument with the corresponding TA Instruments Universal Analysis 2000 (Version 4.5A) software was used. The sample masses were 20 mg.

Table 5.1. Characterization of the surface-initiated ring opening polymerization (ROP) of ε-caprolactone, by M_n and PDI (determined by GPC), and wt% PCL (determined by TGA).

Treatment group	Surface treatment	PCL M_n (g mol^{-1})	Polydispersity index (PDI)	Wt% PCL
U-BG	Unmodified	0	N/A	0
5 h PCL-BG	5 h polymerization with ε-caprolactone	5,026 ± 3,351	1.14 ± 0.04	0.058 ± 0.023
24 h PCL-BG	24 h polymerization with ε-caprolactone	19,225 ± 2,526	1.32 ± 0.19	0.158 ± 0.029

Synthesis and characterization of BG/polymer composites with varying molecular weight between PUR crosslinks and surface layer molecular weight

Synthesis

BG/polymer composites were prepared by mixing the LTI-PEG prepolymer, polyester triol, surface-modified BG particles, and catalyst (Figure 5.1A). The polyester triol and catalyst were varied to modify the molecular weight between cross-links of the polymer network (M_c), while the composition of the bioactive glass particles was modified to vary the surface-initiated PCL molecular weight (M_n). Polyester triols with number-average molecular weights of 300 or 3000 g mol^{-1} and a backbone comprising 70% ε-caprolactone, 20% glycolide, and 10% $_{D,L}$-lactide (7C300 and 7C3000) were synthesized by ROP in the presence of stannous octoate catalyst as described previously[30]. The appropriate polyester triol (7C300 or 7C3000) and the amount of catalyst (7C300: 0.015- 0.098 wt% and 7C3000: 0.023-0.150 wt% for FeAA and TEDA, to yield same gel points added as a dipropylene glycol solution were weighed in one side of a small plastic cup and mixed until homogenous. The LTI-PEG prepolymer was added to the clean half of the cup and the appropriate amount of BG particles spread over the entire surface of the cup. The relative amounts of LTI-PEG prepolymer and

polyester were calculated assuming an isocyanate index of 140 (i.e., 40% excess isocyanate)[30]. The amount of BG was based on a density of 2.7 g cm^{-3} and a targeted volume percent (56.7%) in the final composite. All components were hand-mixed, loaded into a 5 mL syringe, and injected into a mold at room temperature and 40-50% relative humidity. The mixture was cured under a load of 0.96 kg for 5 min to simulate compacting the material in a confined defect space, followed by curing at unloaded conditions at 37°C for 24 h to simulate curing in the human body.

Rheology

Rheological properties of the non-catalyzed composites were measured using a TA Instruments AR2000ex rheometer to determine the initial viscosity. After mixing the components, the sample was loaded between 40-mm diameter steel cross-hatch plates and compressed to a gap of 2.6 mm. Viscosity measurements were completed at a constant strain of 1% as a function of shear rate.

Polymer swelling and composite porosity

The polymer network molecular weight between cross-links M_c was calculated using the Flory-Rehner equation from swelling experiments[31]. The dimensionless surface molecular weight M^* was defined as the surface layer number-average molecular weight M_n (measured by GPC) divided by M_c:

$$M^* = \frac{M_n}{M_C} \tag{1}$$

M_n was adjusted by the varying the surface PCL polymerization time and M_c was adjusted by varying the polyol molecular weight or catalyst during composite fabrication. Thus, a family of composites with $0 \leq M^* \leq 28$ was

fabricated from the four polymer network compositions and three BG surface treatments (U-BG, 5hr PCL-BG, 24hr PCL-BG) to investigate the effect of M^* on mechanical properties. The porosity of the composites was computed from SEM cross-sectional images at 60X magnification and 5 kV using a Hitachi S-4200 SEM (Finchampstead, UK). The pore area in each image was quantified using MetaMorph Offline (Version 7.7.0.0) software. The porosity was calculated as the pore area fraction.

Quasi-static compressive mechanical testing of BG/polymer composites

Cylindrical specimens (6 x 12 mm) samples were prepared and compressive mechanical testing was conducted using an MTS 858 Bionix Servohydraulic Test System. Composites were conditioned in PBS at room temperature for 24 h immediately before testing and pre-loaded to approximately 12 N followed by continuous compression until failure at a rate of 25 mm min^{-1}. The load and position were recorded every 0.01 s. The compressive stress was calculated by dividing the load by the cross sectional area of the samples post-hydration. Compressive modulus (E) was calculated as the slope of the initial linear section of the stress-strain curve, compressive strength (σ) as the maximum stress achieved, and compressive ultimate yield strain (UYS) as the strain at the compressive strength.

Synthesis and torsion testing of BG/polymer composites with bone-like torsional strength

To evaluate the feasibility of BG/polymer composites for bone regeneration in weight-bearing defects, specimens fabricated from the three BG surface treatment groups (U-, 5hr PCL-, and 24hr PCL-BG) and the 7C300-F polymer network (FeAA catalyst and 7C300 polyester triol) were tested under torsion. Quasi-static torsion testing was performed using an Instron Dynamite 8841 fatigue tester equipped with a 1.7 Nm torque cell. Approximately 4 mm of each end of the cylindrical specimens (6 x 20 mm) was potted in larger

cylindrical molds made from Technovit 4000. The gage length (i.e., the gap between the potted ends) was approximately 12 mm. Specimens were conditioned in PBS at room temperature for 24 h and secured to the Instron with one end attached to a stationary torque transducer that measured the torque (T). The crosshead speed was 0.035 rad s^{-1} in order to minimize viscoelastic effects[32, 33]. The shear stress (τ) was determined from the torque/angle unit length ($\theta = \alpha/L$) curve using the equation:

$$\tau = \tau = \frac{1}{2\pi r^3}\left(\theta \frac{dT}{d\theta} + 3T\right) \quad (2)$$

where r is the radius of the cylindrical specimen, $dT/d\theta$ was determined by fitting a 5th order polynomial to the experimental torque curve (from zero up to the maximum T and corresponding θ values), and T is the interpolated torque [32]. The shear modulus (G) was defined as the slope of the linear portion of the stress/angular deformation curve ($G = \tau/\gamma$), the torsion strength as the maximum shear stress achieved, and the torsion *UYS* as the strain at the torsion strength.

One-way ANOVA and Tukey HSD test were performed using JMP 9.0 to determine whether statistical differences existed between the means of groups of interest. For all experiments, $p < 0.05$ was considered statistically significant.

Rat femoral condyle defect in vivo model

Animal study

Three rats were used in the femoral condyle defect *in vivo* model. All surgical and care procedures were carried out under aseptic conditions based on IACUC approval. After rats were placed under anesthesia, bilateral defects approximately 3 mm diameter × 5 mm deep were drilled in the distal aspect of each lateral femoral condyle. Composite precursors were gamma-irradiated using a dose of approximately 25 kGY. The

lead-candidate composite (24hr PCL-BG/ PCL 300-F) was mixed, injected into the cylindrical defect, and followed by closure of the wound 5 min after implantation. A slower degrading polyol (PCL300 instead of 7C300)[34] was utilized in the *in vivo* study in order to maintain polymer in the defect site for an extended period of time and investigate the effect of the presence of BG on bone remodeling. Implanted femurs were harvested 16 wk after composite implantation.

Histological analysis

Rat femora were maintained in a solution of 10% neutral buffered formalin for less than two weeks followed by a series of ethanol dehydrations. Specimens were embedded in poly(methyl methacrylate) and longitudinal cross-sections were cut, ground, and polished (<100 μm) in the middle of the defect from the resultant blocks using an Exakt system. The sections were stained with Sanderson's Rapid Bone Stain and Van Gieson counterstain. BG particles stained light brown, residual polymer stained turquoise, and new bone stained red. The sections were imaged at 2X and 10X magnification with an Olympus camera (DP71) and SZX16 microscope.

Results

Characterization of surface-modified bioactive glass and BG/polymer composites

The properties of the surface-modified particles, including polymerization time, M_n, polydispersity index (PDI), and wt% PCL, are listed in Table 5.1. As anticipated, the mean molecular weight of PCL increased with increasing reaction time, from 5,026 to 19,225 g mol^{-1} when time was increased from 5 to 24 hr. The wt% PCL

paralleled the increase in M_n as 5 and 24 hr polymerization times added 0.058 and 0.158 wt% on to the unmodified BG particle surfaces.

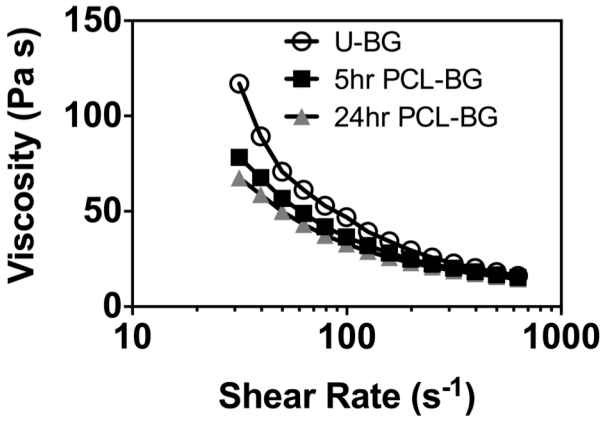

Figure 5.2. Viscosity of non-catalyzed BG/polymer composites fabricated with T7C2G1L300 polyol and U-BG, 5hr PCL-BG and 24hr PCL-BG particles, as a function of shear rate.

As shown in Figure 5.2, composites made with 7C300 non-catalyzed polymer and the three BG surface treatment groups of interest (one representative from each group displayed) showed shear-thinning properties, as evidenced by the decrease in viscosity with shear rate. All groups exhibited a viscosity approaching 15 Pa-s at a high shear rate (above 400 s^{-1}). The rheological properties of non-catalyzed BG/polymer composites did not appear to be dependent on the surface properties of the BG at high shear rates.

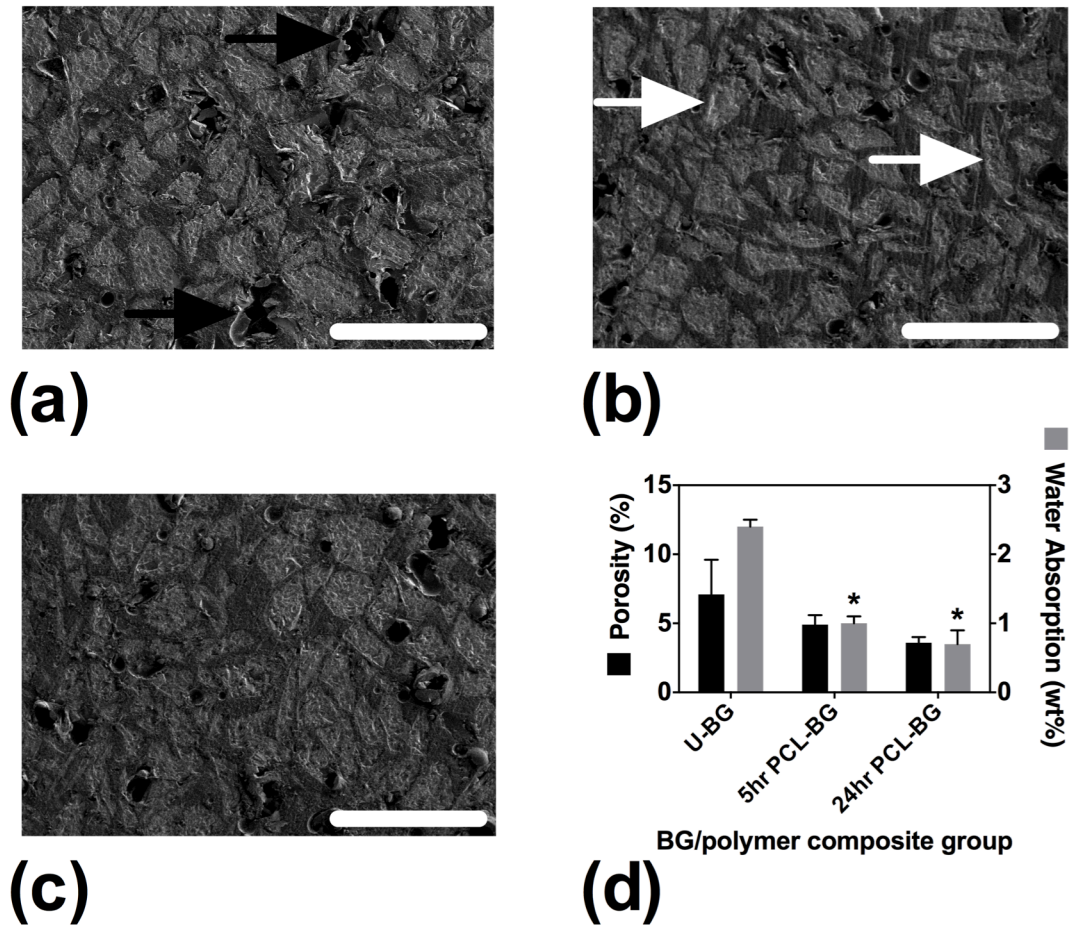

Figure 5.3. SEM images of cross-section of BG/polymer composites fabricated with T7C2G1L300 polyol, FeAA catalyst, and (a) U-BG, (b) 5hr PCL-BG and (c) 24hr PCL-BG particles (Scale bar= 500 μm, white and black arrows point to representative BG particles and voids, respectively) and their subsequent (d) overall porosity (volume fraction pores) and water absorption (wt%) after 24 h incubation in PBS. * indicates $p < 0.05$ compared to composites made with U-BG, with respect to water absorption.

BG particles can be identified in the images of the cross-sections of U-, 5hr PCL-, and 24hr PCL-BG/7C300-F composites shown in Figures 5.3A, 3B and 3C, respectively, with white arrows pointing to representative particles in Figure 5.3A. Surface modification did not appear to alter the shape and size of the BG particles. BG/polymer composites made with all three BG groups exhibited few dispersed irregularly shaped voids. Voids can be seen in Figures 5.3A, 3B and 3C, with black arrows pointing to a representative void in Figure 5.3A. The porosity and change in mass of the composites after conditioning in PBS (water

absorption) are shown in Figure 5.3D. Composites made with U-BG exhibited significantly higher water absorption compared to those made with 5hr and 24hr PCL-BG. While the porosity of U-BG/7C300-F composites was also higher compared to the other two groups, the differences were not significant. Similar observations were made for U-, 5hr PCL-, and 24hr PCL-BG/7C300-F composites (data not shown).

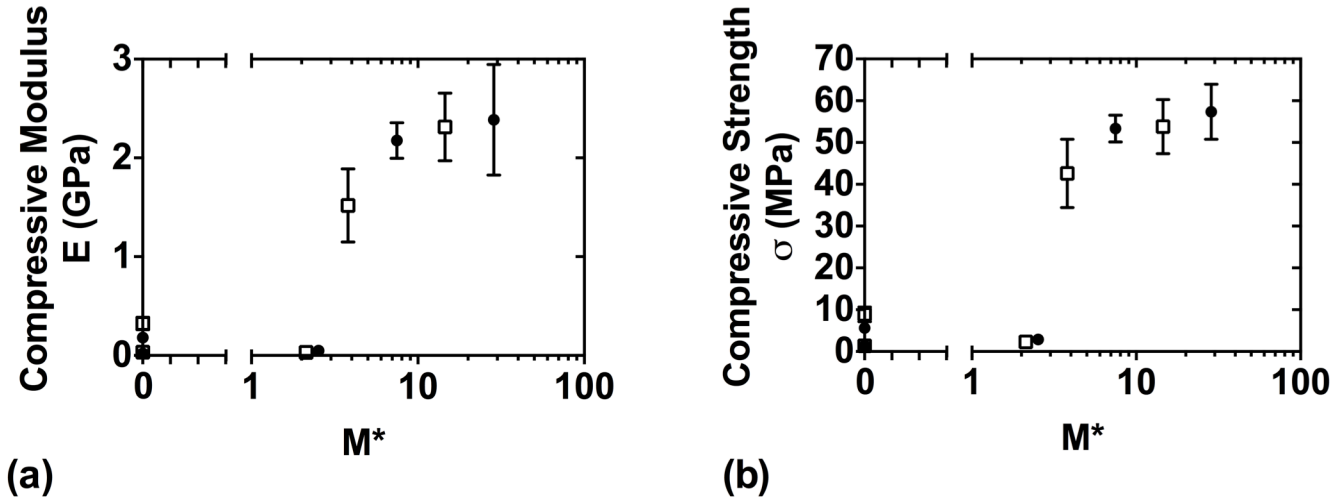

Figure 5.4. Effects of surface-initiated PCL number-average molecular weight (M_n) and PUR network molecular weight between crosslinks (M_c) on quasi-static compressive mechanical properties of BG/polymer composites. M_n values are provided in Table 5.1. In swelling experiments, M_c values were measured for PUR networks catalyzed by FeAA or TEDA with T7C2G1L300 (673 g mol-1 and 1,319 g mol-1 for FeAA and TEDA catalyzed composites, respectively) and T7C2G1L3000 (7,595 g mol-1 and 9,041 g mol-1 for FeAA and TEDA catalyzed composites, respectively). Compressive (a) modulus and (b) strength plotted versus dimensionless surface layer molecular weight $M^* = M_n / M_c$. Values reported as mean ± standard deviation of triplicate samples. An M^*=0 x-axis value was manually added to the semi-log plot in order to allow for values corresponding to M^*=0 (composites made with U-BG) to be plotted.

Compressive properties

To investigate the structure-property relationships governing compressive modulus and strength, BG/polymer composites were prepared from polyester triols with varying molecular weight (300 and 3000 g mol^{-1}) and different catalysts (FeAA and TEDA) to yield polymer networks with tunable molecular weight between crosslinks (M_c) (673–9,041 g mol^{-1}). The molecular weight of surface-initiated PCL on the BG particles (M_n) was varied over the range 0 – 19,225 g mol^{-1} by varying the polymerization time (0, 5, or 24 hr, Table 5.1). The compressive modulus (E) and strength (σ) of the composites are plotted against the dimensionless layer molecular weight $M^* = M_n/M_c$ in Figures 5.4A and B, respectively. Interestingly, data for E and σ for both TEDA and FeAA catalysts lie approximately on the same curve. For both catalysts, E attains 50% of its maximum value (E_m) at M^* = 3.8 – 7.5 and 90% of E_m at M^* = 7.5 – 10.0. Similarly, σ reaches 50% of its maximum value (σ_m) at M^* = 2.5 – 3.8 and 90% of σ^*_m at M^* = 7.5 – 10.0. Above $M^* \cong 20$, the compressive properties asymptotically approach the maximum value. Taken together, these data suggest that the effects of interfacial bonding on mechanical properties saturates at $M^* \geq 20$. The composite with the highest compressive mechanical properties, 24hr PCL-BG/7C300-F, had mean compressive modulus and strength values of 2.39 GPa and 57.4 MPa, respectively.

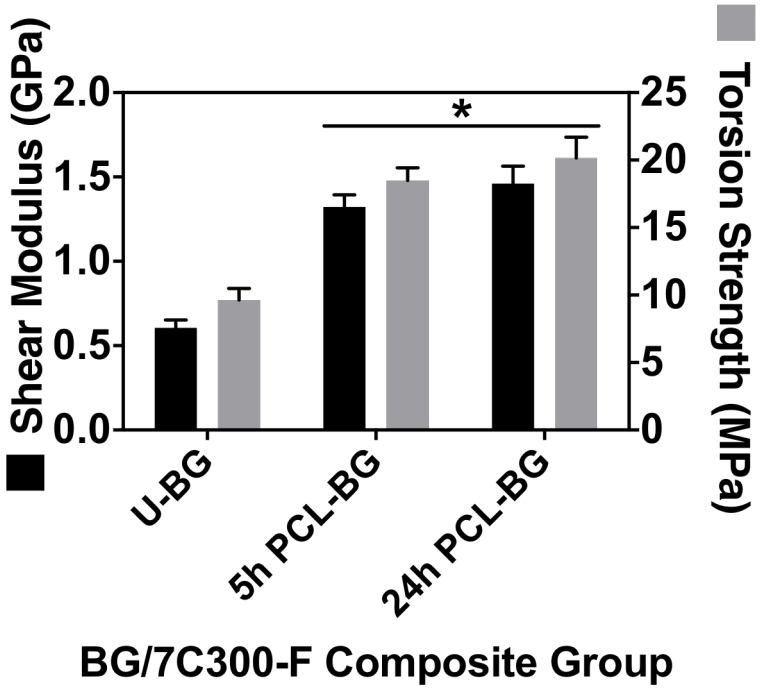

Figure 5.5. Surface-polymerization of PCL on bioactive glass particles significantly increases the quasi-static torsional properties of BG/polymer composites fabricated with T7C2G1L300 polyol and FeAA catalyst. Values reported as mean ± standard deviation of triplicate samples. Statistical analysis performed by one-way ANOVA and Tukey HSD. * indicates $p < 0.05$ compared to composites made with U-BG.M^*=0 x-axis value was manually added to the semi-log plot in order to allow for values corresponding to M^*=0 (composites made with U-BG) to be plotted.

Table 5.2. Torsion mechanical properties of 24 h PCL-BG/T7C2G1L300-F composites.

Composite group	**Toughness (kJ m-3)**	**Ultimate yield strain (%)**
U-BG/7C300-F	279.3 ± 18.9	5.9 ± 4.5
5 h PCL-BG/7C300-F	383.1 ± 143.2	2.3 ± 0.3
24 h PCL-BG/7C300-F	512.3 ± 79.6	3.0 ± 0.6

Torsional properties

To investigate the feasibility of BG/polymer composites as weight-bearing bone grafts, the torsional properties of the lead-candidate composite (24hr PCL-BG/7C300-F) were measured under quasi-static loading (Figure 5.5). Both U-BG/7C300-F and 5hr PCL-BG/7C300-F composites were also tested to investigate the effects of layer thickness on torsional strength. U-BG/7C300-F showed the weakest mechanical properties, with a shear modulus and torsional strength of 0.61 GPa and 9.6 MPa, respectively. PCL surface-polymerization significantly increased the torsional properties of the composite compared to U-BG/300-F. 24hr PCL-BG/7C300-F exhibited a shear modulus and torsional strength of 1.46 GPa and 20.2 MPa. Differences between 24hr and 5hr PCL-BG/7C300-F were not significant. The torsional toughness and *UYS* of the three composites tested are listed in Table 5.2. Despite a decrease in the *UYS* between BG/polymer composites made with PCL-grafted BG compared to those with U-BG, the overall toughness of these composites significantly increased. The lead-candidate composite (24hr PCL-BG/7C300-F) had the highest mean torsional toughness, 512.3 kJ m^{-3}.

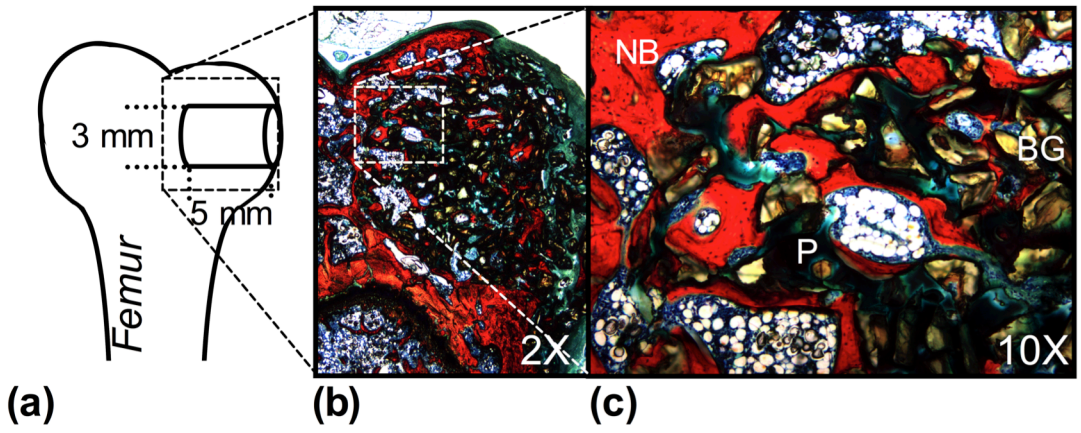

Table 5.6. Histological sections of lead-candidate BG/polymer composite (24hr PCL-BG/T7C2G1L300-F) implanted into rat femoral condyle defect *in vivo* model. (a) Illustration of shape and size (3 mm diameter X 5 mm length) of cylindrical plug defect. (b) Low- (2X) and (c) high- (10X) magnification images of histological section at 16 weeks. NB: new mineralized bone, BG: 45S5 bioactive glass, P: polyurethane polymer.

In vivo remodeling

The overall bone remodeling capability of the lead-candidate BG/polymer composite (24hr PCL-BG/PCL300-F) was evaluated in a rat femoral condyle defect *in vivo* 8 weeks after implantation. To provide orientation with respect to histological analysis, an illustration of the defect is shown in Figure 5.6A. The low magnification (2X) image of an embedded histological section (Figure 5.6B) shows new mineralized bone growth (red), dispersed between remaining BG particles and residual PUR polymer (turquoise), throughout the entire defect site. The high magnification (10X) image of the same histological section (Figure 5.6C) highlights appositional mineralized bone growth (NB) on the surfaces of residual BG particles and residual polymer (P). Osteocytes can be seen dispersed throughout the new mineralized bone. No negative signs of a sustained inflammatory response were noted in any of the analyzed defects.

Discussion

Injectable composites incorporating 45S5 bioactive glass particles and a flowable polymer remodeled to form new bone when implanted in metaphyseal bone defects in rabbits[23, 35]. Appositional bone growth was observed near the surface of the BG particles, followed by remodeling of the BG to form new bone at later time points. While dextran, glycerin, and polyethylene glycol improve the flowability of the composite, these polymers are non-settable, and consequently their weak mechanical properties preclude their use as weight-bearing bone grafts. In addition to settability, interfacial bonding between the polymer and particle phases is another important factor regulating mechanical properties[13]. Amine-terminated silanes have been effectively used to promote bonding between mineral and polymer phases[25, 36], but their high reactivity with isocyanate-terminated prepolymers (~1,000 times faster than hydroxyl groups[37]) limits their utility for injectable applications. In the present study, we investigated a novel approach for enhancing interfacial bonding by

physical entanglements of surface-initiated PCL chains on the BG surface within a polymer network formed *in situ* through the reaction of the LTI-PEG prepolymer with the polyester triol. The presence of surface-initiated PCL chains significantly increased the strength of the composites when the dimensionless surface layer molecular weight $M^* > 3$.

Physical chain entanglements between polymer phases are known to enhance interfacial bonding. As shown in Figure 5.4, σ and E increase sigmoidally with M^*, asymptotically approaching their maximum values when $M^* \geq 20$. This dependence is conjectured to result from entanglements between the surface-initiated PCL chains and the PUR network formed *in situ*. Interestingly, these observations contrast with a previous study reporting that composites comprising α-tricalcium phosphate (α-TCP) particles dispersed in poly(L,DL-lactide) did not show a significant improvement in mechanical properties when L-lactide was grafted to the protonated surface of the α-TCP particles[28]. For linear polymers, physical crosslinks due to chain entanglements result as the molecular weight of the polymer approaches the entanglement molecular weight (M_e)[38], which for PCL is 15,000 g mol^{-1} [39]. Thus, our finding that mechanical properties are enhanced when $M^* > 3$ suggests that the molecular weight of the surface-initiated PCL must exceed 45,000 g mol^{-1} to produce substantial entanglements within the bulk PCL phase. Considering the molecular weight of the surface-polymerized L-lactide was only 390 – 1,050 g mol^{-1}, entanglements and the consequent increase in mechanical properties would not be expected.

To modify the 45S5 BG particles, a surface-initiated ε-caprolactone polymerization technique was modified from a monomer transfer molding process in which polymerization of ε-caprolactone is initiated on the surface of a bioactive glass fiber preform[25, 26]. In this process, a continuous polymer phase comprising high (>125,000 g mol^{-1}) molecular weight PCL was covalently bound to the bioactive glass fibers, resulting in a significant enhancement in mechanical properties. However, due to the high temperature (110°C) required for ε-caprolactone polymerization, the monomer transfer molding process is not suitable to fabricate the bulk

polymer for injectable composites. The monomer transfer molding approach contrasts with the reactive liquid molding process reported in the present study, in which lower (<20,000 g mol^{-1}) molecular weight surface-initiated PCL chains inter-penetrate with the polymer network formed *in situ* (Figure 5.1C). Furthermore, the reactive liquid molding process was carried out at physiological temperature (37°C) in the presence of BG particles modified by surface-initiated polymerization of ε-caprolactone, thereby rendering the composites suitable for injectable applications.

While the compressive strength of CPCs (~50 MPa) and many ceramic/polymer composites exceeds that of trabecular bone (4-12 MPa)[40], there is a paucity of data on the strength of CPCs under more physiologically relevant loading conditions, such as torsion or shear[11]. Due to the brittleness of CPCs, their tensile strength is at least an order of magnitude lower than the compressive strength[11]. The brittleness and weak shear properties of CPCs have been suggested to contribute to their poor performance in applications where only modest weight-bearing properties are required, such as kyphoplasty[11, 41, 42]. While the shear modulus (0.61 GPa) and torsional strength (9.6 MPa) of the U-BG/7C300-F composite only slightly exceed the corresponding values for trabecular bone (0.29 GPa and 6.1 MPa, respectively[32]), the torsional properties of 5hr PCL- and 24hr PCL-BG/7C300-F composites exceed the values reported for trabecular bone and calcium phosphate cements by a factor of >3 [43]. Mechanical testing was performed on materials made in 40-50% relative humidity, cured for 24 h at 37°C, and soaked in PBS 24 h prior to testing. While the humidity in bone defects is anticipated to be higher than 40-50% due to the presence of body fluids, in a previous study we reported that environmental water has minimal impact on the cure profile of allograft bone/polymer composites[44]. However, further studies are necessary to assess the effects of body fluids on the mechanical properties of BG/polymer composites cured *in vivo*.

We have previously reported that injectable, settable allograft/polymer composites catalyzed by TEDA did not release cytotoxic components during cure and promoted new bone formation in a rabbit femoral condyle

plug defect model[12, 44]. In another study, polyurethane scaffolds synthesized using the FeAA catalyst were shown to be non-cytotoxic and support mineralization *in vitro* and new bone formation *in vivo*[45, 46]. While TEDA and FeAA catalysts have been reported to be non-cytotoxic *in vivo*, the cytotoxicity of residual stannous octoate catalyst from the surface-initiated polymerization *in vivo* is unknown. The presence of Sn in the XPS spectra suggests that the $Sn(Oct)_2$ catalyst was bound within the grafted PCL, which is consistent with a previous study[25, 26]. Rat femoral condyle defects filled with the lead-candidate BG/polymer composite did not show evidence of toxicity (Figure 5.6). However, longer-term studies are needed to evaluate the biocompatibility and safety of the settable bone grafts. To reduce the risk of toxicity, the tin catalyst could be eliminated by surface-initiated polymerization of PCL on phosphoric acid-treated BG without the intermediate step of silanization[43].

BG/polymer composites showed ingrowth of new bone, residual BG, and residual polymer at 8 weeks when injected into femoral condyle plug defects in rats (Figure 5.6). These observations are in agreement with a previous study reporting remodeling of BG/dextran composites injected into femoral condyle plug defects in rabbits[23]. However, dextran is a water-soluble polymer functioning as a temporary carrier that diffused away from the defect site after injection. In contrast, the reactive polymer investigated in the present study must degrade in order for cells to infiltrate the composites. Previous studies have reported that the lysine-derived poly(ester urethane) networks investigated in the present study break down by hydrolytic and oxidative degradation[34, 47]. Similarly, BG breaks down by dissolution and/or osteoclast-mediated degradation[48, 49]. While additional studies at later time points and in larger animal models are required to elucidate the mechanism, it is anticipated that cells infiltrate and remodel the composite by degradation of the polymer and BG phases[43].

The results from the present study elucidate the interfacial structure-property relationships governing the mechanical properties of surface-modified ceramic/polymer composites. The molecular weight of the surface-initiated polymer layer on the ceramic particle must exceed the molecular weight between crosslinks of the bulk

polymer phase by at least a factor of 3 to achieve effective interfacial bonding and enhanced mechanical properties. Further *in vivo* studies are necessary to assess the ability of settable BG/polymer composites to maintain torsional strength exceeding that of trabecular bone during remodeling of the grafts.

Conclusions

In this study, the effects of the surface-initiated polymerization of ε-caprolactone on the mechanical properties of BG/polymer composites were investigated. Surface-initiated PCL chains increased the compressive strength of BG/polymer composites 6- to 10-fold compared to unmodified BG particles. Furthermore, compressive strength was dependent on the ratio of the molecular weight of the surface-initiated PCL layer to the mesh size of the polymer network formed *in situ*. The torsional strength of the lead-candidate composite exceeded that of human trabecular bone and calcium phosphate cements by a factor of 3. When injected into femoral condyle plug defects in rats, the lead-candidate BG/polymer composite supported cellular infiltration and remodeling. The initial bone-like strength of BG/polymer composites, as well as their ability to support bone remodeling *in vivo*, points to their potential for future development as injectable, settable grafts for repair of weight-bearing bone defects.

References

1. T.A. Russell and R.K. Leighton: Comparison of Autogenous Bone Graft and Endothermic Calcium Phosphate Cement for Defect Augmentation in Tibial Plateau Fractures *Journal of Bone and Joint Surgery-American Volume.* **90A**(10), 2057 (2008).

2. D. Simpson and J.F. Keating: Outcome of tibial plateau fractures managed with calcium phosphate cement *Injury-International Journal of the Care of the Injured.* **35**(9), 913 (2004).

3. L. Amendola, A. Gasbarrini, M. Fosco, C.E. Simoes, S. Terzi, F. Delure and S. Boriani: Fenestrated pedicle screws for cement-augmented purchase in patients with bone softening: a review of 21 cases *J Orthop Traumatol.* **12**(4), 193 (2011).

4. S. Larsson, V.A. Stadelmann, J. Arnoldi, M. Behrens, B. Hess, P. Procter, M. Murphy and D.P. Pioletti: Injectable calcium phosphate cement for augmentation around cancellous bone screws. In vivo biomechanical studies *Journal of Biomechanics.* **45**(7), 1156 (2012).

5. S. Larsson and P. Procter: Optimising implant anchorage (augmentation) during fixation of osteoporotic fractures: Is there a role for bone-graft substitutes? *Injury-International Journal of the Care of the Injured.* **42**, S72 (2011).

6. J.J. Verlaan, F.C. Oner and W.J.A. Dhert: Anterior spinal column augmentation with injectable bone cements *Biomaterials.* **27**(3), 290 (2006).

7. R.Z. Legeros, A. Chohayeb and A. Schulman: Apatitic Calcium Phosphates Possible Dental Restorative Materials *Journal of Dental Research.* **61**(SPEC. ISSUE), 343 (1982).

8. H. Chim and A.K. Gosain: Biomaterials in Craniofacial Surgery Experimental Studies and Clinical Application *J. Craniofac. Surg.* **20**(1), 29 (2009).

9. J.A. Hall, M.J. Beuerlein and M.D. McKee: Open reduction and internal fixation compared with circular fixator application for bicondylar tibial plateau fractures. Surgical technique *J Bone Joint Surg Am.* **91 Suppl 2 Pt 1**, 74 (2009).

10. A.J. Wagoner Johnson and B.A. Herschler: A review of the mechanical behavior of CaP and CaP/polymer composites for applications in bone replacement and repair *Acta Biomater.* **7**(1), 16 (2011).

11. M. Bohner: Design of ceramic-based cements and putties for bone graft substitution *Eur Cell Mater.* **20**, 1 (2010).

12. J.E. Dumas, E.M. Prieto, T. Guda, K.J. Zienkiewicz, J. Garza, J. Bible, G.E. Holt and S.A. Guelcher: Remodeling of Settable Allograft Bone/Polymer Composites with Initial Bone-like Mechanical Properties in Rabbit Femora *Tissue Eng Part A.* **[Epub ahead of print]**, (2013).

13. J.R. Jones: Review of bioactive glass: from Hench to hybrids *Acta Biomater.* **9**(1), 4457 (2013).

14. A.R. Boccaccini and J.J. Blaker: Bioactive composite materials for tissue engineering scaffolds *Expert Review of Medical Devices.* **2**(3), 303 (2005).

15. L.L. Hench and J. Wilson: Bioceramics *Mrs Bulletin.* **16**(9), 62 (1991).

16. P. Saravanapavan, J.R. Jones, R.S. Pryce and L.L. Hench: Bioactivity of gel-glass powders in the CaO-SiO2 system: A comparison with ternary (CaO-P2O5-SiO2) and quaternary glasses (SiO2-CaO-P2O5-Na2O) *J. Biomed. Mater. Res. Part A.* **66A**(1), 110 (2003).

17. L.L. Hench: The story of Bioglass (R) *Journal of Materials Science-Materials in Medicine.* **17**(11), 967 (2006).

18. A. Hoppe, N.S. Gueldal and A.R. Boccaccini: A review of the biological response to ionic dissolution products from bioactive glasses and glass-ceramics *Biomaterials.* **32**(11), 2757 (2011).

19. K.E. Tanner: Bioactive composites for bone tissue engineering *Proceedings of the Institution of Mechanical Engineers Part H-Journal of Engineering in Medicine.* **224**(H12), 1359 (2010).

20. O. Bretcanu, S. Misra, I. Roy, C. Renghini, F. Fiori, A.R. Boccaccini and V. Salih: In vitro biocompatibility of 45S5 Bioglass (R)-derived glass-ceramic scaffolds coated with poly(3-hydroxybutyrate) *Journal of Tissue Engineering and Regenerative Medicine.* **3**(2), 139 (2009).

21. M. Bil, J. Ryszkowska, J.A. Roether, O. Bretcanu and A.R. Boccaccini: Bioactivity of polyurethane-based scaffolds coated with Bioglass((R)) *Biomedical Materials.* **2**(2), 93 (2007).

22. J.L. Ryszkowska, M. Auguscik, A. Sheikh and A.R. Boccaccini: Biodegradable polyurethane composite scaffolds containing Bioglass (R) for bone tissue engineering *Composites Science and Technology.* **70**(13), 1894 (2010).

23. C. Chan, I. Thompson, P. Robinson, J. Wilson and L. Hench: Evaluation of Bioglass/dextran composite as a bone graft substitute *International Journal of Oral and Maxillofacial Surgery.* **31**(1), 73 (2002).

24. R.E. Neuendorf, E. Saiz, A.P. Tomsia and R.O. Ritchie: Adhesion between biodegradable polymers and hydroxyapatite: Relevance to synthetic bone-like materials and tissue engineering scaffolds *Acta Biomater.* **4**, 1288 (2008).

25. G. Jiang, M.E. Evans, I.A. Jones, C.D. Rudd, C.A. Scotchford and G.S. Walker: Preparation of poly(epsilon-caprolactone)/continuous bioglass fibre composite using monomer transfer moulding for bone implant *Biomaterials.* **26**(15), 2281 (2005).

26. G. Jiang, G.S. Walker, I.A. Jones and C.D. Rudd: XPS identification of surface-initiated polymerisation during monomer transfer moulding of poly(epsilon-caprolactone)/Bioglass (R) fibre composite *Applied Surface Science.* **252**(5), 1854 (2005).

27. E. Verne, C. Vitale-Brovarone, E. Bui, C.L. Bianchi and A.R. Boccaccini: Surface functionalization of bioactive glasses *J. Biomed. Mater. Res. Part A.* **90A**(4), 981 (2009).

28. C. Kunze, T. Freier, E. Helwig, B. Sandner, D. Reif, A. Wutzler and H.J. Radusch: Surface modification of tricalcium phosphate for improvement of the interfacial compatibility with biodegradable polymers *Biomaterials.* **24**(6), 967 (2003).

29. M. Barsbay, G. Gueven, M.H. Stenzel, T.P. Davis, C. Barner-Kowollik and L. Barner: Verification of controlled grafting of styrene from cellulose via radiation-induced RAFT polymerization *Macromolecules.* **40**(20), 7140 (2007).

30. S.A. Guelcher, V. Patel, K.M. Gallagher, S. Connolly, J.E. Didier, J.S. Doctor and J.O. Hollinger: Synthesis and in vitro biocompatibility of injectable polyurethane foam scaffolds *Tissue Engineering.* **12**(5), 1247 (2006).

31. N.S. Ruppender, A.R. Merkel, T.J. Martin, G.R. Mundy, J.A. Sterling and S.A. Guelcher: Matrix Rigidity Induces Osteolytic Gene Expression of Metastatic Breast Cancer Cells *Plos One.* **5**(11), (2010).

32. K.B. Garnier, R. Dumas, C. Rumelhart and M.E. Arlot: Mechanical characterization in shear of human femoral cancellous bone: torsion and shear tests *Medical Engineering & Physics.* **21**(9), 641 (1999).

33. C.M. Ford and T.M. Keaveny: The dependence of shear failure properties of trabecular bone on apparent density and trabecular orientation *Journal of Biomechanics.* **29**(10), 1309 (1996).

34. A.E. Hafeman, K.J. Zienkiewicz, A.L. Zachman, H.-J. Sung, L.B. Nanney, J.M. Davidson and S.A. Guelcher: Characterization of the degradation mechanisms of lysine-derived aliphatic poly(ester urethane) scaffolds *Biomaterials.* **32**(2), 419 (2011).

35. Z. Wang, B. Lu, L. Chen and J. Chang: Evaluation of an osteostimulative putty in the sheep spine *J. Mater. Sci.-Mater. Med.* **22**(1), 185 (2011).

36. R.A. Khan, A.J. Parsons, I.A. Jones, G.S. Walker and C.D. Rudd: Effectiveness of 3-aminopropyl-triethoxy-silane as a Coupling Agent for Phosphate Glass Fiber-Reinforced Poly(caprolactone)-based Composites for Fracture Fixation Devices *J Thermoplastic Composite Materials.* **24**, 517 (2011).

37. G. Oertel: Polyurethane Handbook, 2nd ed. (Hanser Gardner Publications, City, 1994).

38. H.R. Brown and T.P. Russell: Entanglements at polymer surfaces and interfaces *Macromolecules.* **29**(2), 798 (1996).

39. A. Gurarslan, J. Shen and A.E. Tonelli: Behavior of Poly(epsilon-caprolactone)s (PCLs) Coalesced from Their Stoichiometric Urea Inclusion Compounds and Their Use as Nucleants for Crystallizing PCL Melts: Dependence on PCL Molecular Weights *Macromolecules.* **45**(6), 2835 (2012).

40. M.R. Allen, H.A. Hogan, W.A. Hobbs, A.S. Koivuniemi, M.C. Koivuniemi and D.B. Burr: Raloxifene enhances material- level mechanical properties of femoral cortical and trabecular bone *Endocrinology.* **148**(8), 3908 (2007).

41. M. Libicher, J. Hillmeier, U. Liegibel, U. Sommer, W. Pyerin, M. Vetter, H.P. Meinzer, I. Grafe, P. Meeder, G. Noldge, P. Nawroth and C. Kasperk: Osseous integration of calcium phosphate in

osteoporotic vertebral fractures after kyphoplasty: initial results from a clinical and experimental pilot study *Osteoporos Int.* **17**(8), 1208 (2006).

42. G. Maestretti, C. Cremer, P. Otten and R.P. Jakob: Prospective study of standalone balloon kyphoplasty with calcium phosphate cement augmentation in traumatic fractures *Eur Spine J.* **16**(5), 601 (2007).

43. J. Dumas, E. Prieto, K. Zienkiewicz, T. Guda, J. Wenke, J. Bible, G. Holt and S. Guelcher: Remodeling of Settable Allograft Bone/Polymer Composites with Initial Bone-like Mechanical Properties in Rabbit Femora. *Tissue Eng Part A.* **20**(1-2), 115 (2014).

44. J.M. Page, E.M. Prieto, J.E. Dumas, K.J. Zienkiewicz, J.C. Wenke, P. Brown-Baer and S.A. Guelcher: Biocompatibility and Chemical Reaction Kinetics of Injectable, Settable Polyurethane/Allograft Bone Biocomposites *Acta Biomaterialia.* **8**(12), 4405 (2012).

45. K. Gorna and S. Gogolewski: Preparation, degradation, and calcification of biodegradable polyurethane foams for bone graft substitutes *J Biomed Mater Res.* **67A**, 813 (2003).

46. S. Gogolewski and K. Gorna: Biodegradable polyurethane cancellous bone graft substitutes in the treatment of iliac crest defects *J Biomed Mater Res.* **80A**, 94 (2007).

47. J.M. Page, E.M. Prieto, J.E. Dumas, K.J. Zienkiewicz, J.C. Wenke, P. Brown-Baer and S.A. Guelcher: Biocompatibility and chemical reaction kinetics of injectable, settable polyurethane/allograft bone biocomposites *Acta Biomaterialia.* **8**(12), 4405 (2012).

48. T.J. Lehtonen, J.U. Tuominen and E. Hiekkanen: Resorbable composites with bioresorbable glass fibers for load-bearing applications. In vitro degradation and degradation mechanism *Acta Biomaterialia.* **9**(1), 4868 (2013).

49. S. Midha, W. van den Bergh, T.B. Kim, P.D. Lee, J.R. Jones and C.A. Mitchell: Bioactive Glass Foam Scaffolds are Remodelled by Osteoclasts and Support the Formation of Mineralized Matrix and Vascular Networks In Vitro *Advanced Healthcare Materials.* **2**(3), 490 (2013).

CHAPTER VI

COMPRESSIVE FATIGUE AND FRACTURE TOUGHNESS BEHAVIOR OF INJECTABLE, SETTABLE BONE CEMENTS

Introduction

Tibial plateau fractures involve a weight-bearing joint and often have depressed portions that require extensive open reduction and internal fixation approaches along with subchondral grafting to maintain articular congruence. Bone grafts utilized in the clinical management of these fractures are subjected to repetitive, dynamic physiological loading from everyday activities, such as sitting, standing, and walking [1]. Anatomic reduction and maintenance of the joint is important for both bone healing and articular regeneration, since lack of articular congruence after fractures increases the likelihood of osteoarthritis [2]. The use of calcium phosphate cements (CPCs) mitigates the loss of the reduction compared to autograft [3]. However, the brittleness and low shear strength of CPCs adversely impact their ability to bear mechanical loads, requiring the use of large internal fixation devices, which have been suggested to increase complications [4]. Consequently, ~25% of the repairs of severe tibial plateau fractures fail, requiring rehospitalization which results in an increased risk of a poor outcome at 2 years post-injury [5]. These clinical observations underscore the clinical need for an injectable, settable, and weight-bearing graft that will prevent catastrophic failure of the fixation and subsequent morbidity of severe tibial plateau fractures.

While the need for materials that can be used to repair weight-bearing bone defects is apparent [6], the specific mechanical requirements of these materials to optimize structural compatibility with the native bone have yet to be established [1, 7]. Quasi-static mechanical testing, often in compressive mode, is frequently utilized to evaluate a material's 'weight-bearing' ability. However, compressive strength alone is a poor indicator of *in vivo* performance since physiologic loads typically include shear components and are dynamic [8, 9]. Although

quasi-static testing is adequate to assess material behavior as it relates to daily occurrences such as one-legged stances, there is a distinct gap between the manner in which materials are mechanically evaluated and the mechanics to which they are subjected post-implantation *in vivo*. For example, fatigue failure is a predominant *in vivo* failure mode of bone cements [1], but the assessment of the mechanical properties of bone void fillers often involves monotonic, load-to-failure tests. This is a potential concern because strength is not necessarily predictive of fatigue resistance as fatigue failure occurs at stresses below the yield strength of the material [10].

Reporting only the mean quasi-static strength is often misleading as materials fail under a cyclic load that is a fraction of the reported strength [8]. Previous studies have infrequently reported properties such as fatigue life or fracture toughness for CPCs or polymer/ceramic composites due to their brittle behavior [7, 9, 11-13]. Brittle materials are susceptible to micro-cracking when subjected to repetitive subcritical loading, as is often applied in dynamic fatigue [11, 14-16]. Micro-crack growth or general damage accumulation can lead to a degradation of material properties and is difficult to detect because it often forms internally within the microstructure. Thus, the assessment of fracture and fatigue mechanics provides a more complete evaluation of whether a biomaterial will sustain *in vivo* service loads over time [8, 9, 11, 17].

Previously we showed that surface-modification of 45S5 bioactive glass (BG) particles via surface-initiated polymerization of ε-caprolactone significantly increased the quasi-static compressive and torsional strength of lysine-derived polyurethane (PUR) polymer/BG composites, to levels exceeding that of human trabecular bone [18]. In the present study, we evaluated the dynamic compressive fatigue properties of PUR polymer/BG composites when subjected to physiologically relevant (5-15 MPa) [1, 19] or supra-physiological (15-30 MPa) loads, and compare their properties to a commercially available biphasic CPCs (CaS/P). The fatigue life (N_f) was determined for three independent definitions of failure, which were chosen to represent three potential mechanisms of clinical failure, including accumulation of internal micro-crack defects, plastic deformation, and subsidence. In order to evaluate the ability of the composites to resist crack growth, fracture

toughness testing of single edge-notched beam specimens in mode I was conducted. The stress intensity factor (K) and J-integral values were calculated to determine the toughness to initiate cracking and the additional contribution of inelastic deformation (e.g., plasticity) as well as the toughness of a growing crack, respectively[20].

Experimental

Materials

Melt-derived 45S5 bioactive glass particles (150-212 μm diameter) were purchased from Mo-Sci Corp. (Rolla, MO). (3-Aminopropyl)triethoxyilane (APTES) and ε-caprolactone were purchased from Sigma-Aldrich (St. Louis, MO). Magnesium sulfate, stannous octoate ($Sn(Oct)_2$), and phosphate-buffered saline (PBS) were acquired from Thermo Fisher Scientific (Waltham, MA). Triethylenediamine (TEDA) was purchased from Evonik (Parsipanny, NJ). A lysine triisocyanate (LTI)-polyethylene glycol (PEG) prepolymer (21% NCO) was supplied by Medtronic (Memphis, TN). $_{D,L}$-lactide and glycolide were supplied by Polysciences (Warrington, PA). Polyester triol of 300 Da was synthesized with a backbone comprising 70% ε-caprolactone, 20% glycolide, and 10% $_{D,L}$-lactide (T7C2G1L300). Commercially available PRO-DENSE®, a biphasic bone cement composed of calcium sulfate and calcium phosphate (CaS/P) was obtained from Wright Medical (Memphis, TN).

Table 6.1. Compressive fatigue study design. The numbers corresponding to each maximum stress applied (σ_{max}) and specimen tested refer to the interval length (number of cycles) between recorded cycles. '-' indicates the specimen was not subjected to corresponding stress

σ_{max} (MPa)	PCL-BG/PUR	CaS/P	U-BG/PUR
5	1000	1000	1
10	1000	1	-
15	1000	1	-
20	10	-	-
25	10	-	-
30	1	-	-

Preparation of experimental specimens

The study design included comparing the fatigue life of three synthetic bone grafts at multiple stress levels, although not all materials could withstand more than 1 cycle at higher levels (Table 6.1). The two BG/polyurethane (PUR) composites investigated incorporated either: (a) cleaned and unmodified BG particles (U-BG), or (b) cleaned BG particles subsequently modified by surface-initialed polymerization of ε-caprolactone (PCL-BG) [18]. For cleaning, BG particles were sonicated for 5 min in a solution of acetone and deionized (DI) water (5/95 by volume %, respectively) at room temperature, followed by rinsing in DI water under sonication for 5 min [21]. A total of three washing cycles were performed. PCL-BG were modified by adsoprtion of APTES molecules, incubated in a 2 μM solution of APTES in 9:1 (v/v) ethanol:DI water for 5 h at room temperature [18, 22], and annealed at 100°C for 1 h, followed by ring-opening polymerization (ROP) ε-caprolactone. A mixture comprising a 1:1000 molar ratio of $Sn(Oct)_2$:ε-caprolactone[22] and a 0.83:1 weight ratio

of Sil-BG: ε-caprolactone was reacted with silane-modified BG particles while stirring at 110°C for 24h. The PCL-BG particles were extracted with chloroform to remove non-grafted PCL and dried at 40°C for 24 h [18].

BG/polymer composites were prepared by mixing the LTI-PEG prepolymer, polyester triol, BG particles, and TEDA catalyst as previously described [18]. The relative amounts of LTI-PEG prepolymer and polyol were calculated assuming an isocyanate index of 140 (i.e., 40% excess isocyanate) [23]. The amount of BG was based on a density of 2.7 g cm^{-3} and a targeted volume percent (56.7%) in the final composite. All components were hand-mixed, loaded into a 1 mL syringe, and injected into a mold at room temperature and 40-50% relative humidity.

Composites created for compressive fatigue testing were injected into a cylindrical mold (6 mm diameter) and cured under a load of 0.96 kg for 5 min to simulate compaction of the material in a confined defect space. Composites were further cured at 37°C for 24 h while not loaded. After curing, the ends of the composites were cut to ensure parallel faces and a length:diameter ratio of 2:1. Composites created for fracture toughness testing were injected into a rectangular metal mold with dimensions 7.4 mm x 3.7 mm x 36.9 mm (W x B x L), with $B = 0.5W$, as per the fracture toughness test standard ASTM E1820. To fabricate the commercially available CaS/P cement specimen, the mixing protocol provided in a 20 CC kit was followed. The mixed CaS/P paste was injected into the same cylindrical or rectangular mold as the BG/PUR composites, and allowed to cure at 37°C for 24 h, and cut in the same fashions. All specimens were conditioned in PBS at room temperature for 24 h immediately before testing.

Compressive fatigue mechanical testing

Following ASTM F2118-10, cylindrical specimens were loaded in dynamic compressive fatigue using a servohydraulic material testing instrument (MTS 858 Bionix, Eden Prairie, MN). Compressive fatigue was

employed because bone grafts are primarily subjected to compression *in vivo*. Specimens were loosely wrapped in medical gauze in order to distribute and maintain constant hydration during testing, as adapted from previous methods [24]. Specimens were placed between two rigid compression platens. The upper platen, which was attached to the actuator, was lowered until it made contact with the specimen as determined by a detected force of 1 N transmitted through the lower stationary platen attached to a load cell (Tovey Engineering Inc., SWT14-5K-000, with a maximum capacity of 14 kN). A calibrated MTS extensometer (634.31F-24) with a gage length of 20 mm was attached to both platens via razor edge adaptors, cut notches cut in the platens, and silicon elastic bands, to track the overall strain experienced by the specimens. Specimens were cyclic-loaded in sinusoidal compressive testing under load control at a frequency of 5 Hz [12]. Specimens were loaded from the nominal compressive preload and set to a minimum stress of 0.03 MPa to a varied maximum stress level (σ_{max}), from 5 to 30 MPa (Table 6.1), which correspond to physiologically relevant service loads. All testing was performed at room temperature and specimens were hydrated with water via a drip-system. When the overall strain on the specimen reached 5% or it reached 1 million load cycles, whichever occurred first, the specimen was unloaded and the testing was stopped. The MTS material testing instrument was tuned (adjusting Proportional, Integral, and Derivative terms) for each of the material to ensure that the cyclic loading sine wave reached the maximum stress (peak) and minimum stress (valley) levels. The same tuning parameters were applied to all the specimens tested within each group.

During the cyclic testing, the force vs. displacement data were recorded for the first cycle and then for one complete cycle at intervals determined by projected fatigue life (Table 6.1). The MTS control software acquired data at 50 Hz for the test parameters of load, displacement, strain and number of load cycles. The following properties were then calculated using standard mechanical equations for fatigue testing of cylindrical specimens. The compressive engineering stress (σ) was calculated by dividing the load by the cross sectional area of the samples post-hydration. Secant modulus (E) was defined as the ratio in change in stress ($\Delta\sigma$) by

change in strain ($\Delta\varepsilon$) (Figure 6.1). The number of cycles (N), overall creep strain (relative to initial strain) (c_k), loading secant modulus (E), and maximum displacement (d_m) were measured for each specimen (Figure 6.1). Mechanical fatigue failure was defined based on three different criteria: 1) 10% decrease in secant modulus, 2) 1% creep deformation (c_k), and 3) 3% maximum displacement (d_m). The initial modulus was defined as the average of the moduli of the first 10 cycle intervals (Table 6.1), when >10 intervals occurred, otherwise the modulus of the first cycle interval. Cycle intervals were defined differently for each material based on projected fatigue failure. The strains c_k and d_m were defined based on the initial height of the specimen (set as the maximum potential c_k and d_m). The three failure definitions were chosen to represent three potential mechanisms of clinical failure, accumulation of internal crack defects, plastic deformation, and subsidence. The fatigue life (N_f) was defined as the number of cycles achieved until mechanical failure per definition. The run-out maximum for N_f was set at 1 million cycles. The mean fatigue life of groups at each corresponding stress level were statistically compared by individual t-tests utilizing nonparametric setting with Mann-Whitney test.

Fracture toughness mechanical testing

After removing materials from the rectangular molds (size and fabrication method described above), single-edge notched beam (SENB) specimens were created using a low-speed diamond wheel saw (SouthBay Technology Inc.) and sharpened further into a pre-crack by means of a razor blade lubricated with 1 μm Buehler MetaDi diamond particulate solution to give original crack size a_0 = 1.4-2.2 mm (approximately $0.25W$). The a_0 length was chosen (as compared to $a_0 = 0.5W$, as required by ASTM E1820) in order to provide greater opportunity for more stable cracking events in the brittle materials. A VanGuard 12424MM series confocal microscope, at 10X magnification, measured the exact length of the starter notch. After positioning the SENB specimens horizontally on two 1 mm diameter supports with a ~30 mm span S (equal to $4\times W$), they were loaded mid-span (in-line opposite to the notch) in three-point bending clamps (Instron Fixtures Series 2810-413) using

another axial servo-hydraulic testing system (DynaMight 8841, Instron, Norwood, MA) with 1 kN load cell (Honeywell). The force vs. displacement (LVDT) data were recorded at 50 Hz as the specimen was tested in displacement control to failure with a progressive, multiple loading (+0.07 mm at 0.01 mm/s)-unloading (-0.04 mm at 0.015 mm/s)-dwell scheme (rising R-curve approach). The time between load/unload sequence was kept as short as possible while allowing sufficient time to adjust the macro focus of the camera macro lens and take a picture of the imparted crack propagation. All testing was performed at room temperature.

The bone cement and composites exhibit non-linear mechanical behavior (i.e., a significant amount of plastic deformation). Thus, the fracture behavior of these materials was studied in the framework of elastic-plastic fracture mechanics. The fracture resistance was characterized in terms of the *J*-integral for all groups tested, without the correction of crack extension (i.e. crack lengths (a) = initial crack length (a_0)). The value of *J* was calculated for each cycle by adding its elastic and plastic components:

$$J = \frac{K(P)(1-\nu^2)^2}{E} + J_{pl} \quad (1).$$

The critical stress intensity required to initiate cracks (K_{init}) was computed as $K_{init} = \sqrt{\frac{J.E}{1-\vartheta^2}}$ at the maximum load ($P = P_{max}$) and *J* was the value of the J-integral at fracture ($P = P_{fail}$). The detailed equations used to compute the stress-intensity *K* and the plastic component of *J* are provided in ASTM E1820 [25]. Additionally, R-curve analysis was conducted on the BG/PUR composites. After correcting J-integral for crack extension, crack growth toughness was determined as the slope of *J* versus corresponding crack extensions (Figure 6.10). Statistical significance between the means of parameters corresponding to each material tested was determined by a one-way ANOVA with Tukey honest significant difference (HSD).

SENB notch and fracture characterization

A Canon EOS 5D Digital SLR camera mounted with a macro photo lens MP-E 65mm 1:2.8 was used to qualitatively characterize the compressive fatigue tested specimens. Additionally, images of starter notch and subsequent crack propagation were taken in between loading cycles during fracture toughness mechanical testing by the SLR camera to qualitatively characterize stable and unstable crack extensions. Scanning electron microscope (SEM) imaging at 45X magnification and 5 kV (Hitachi S-4200 SEM (Finchampstead, UK)) was used to obtain fractography images of the internal cracked surface of specimens post fracture toughness mechanical testing.

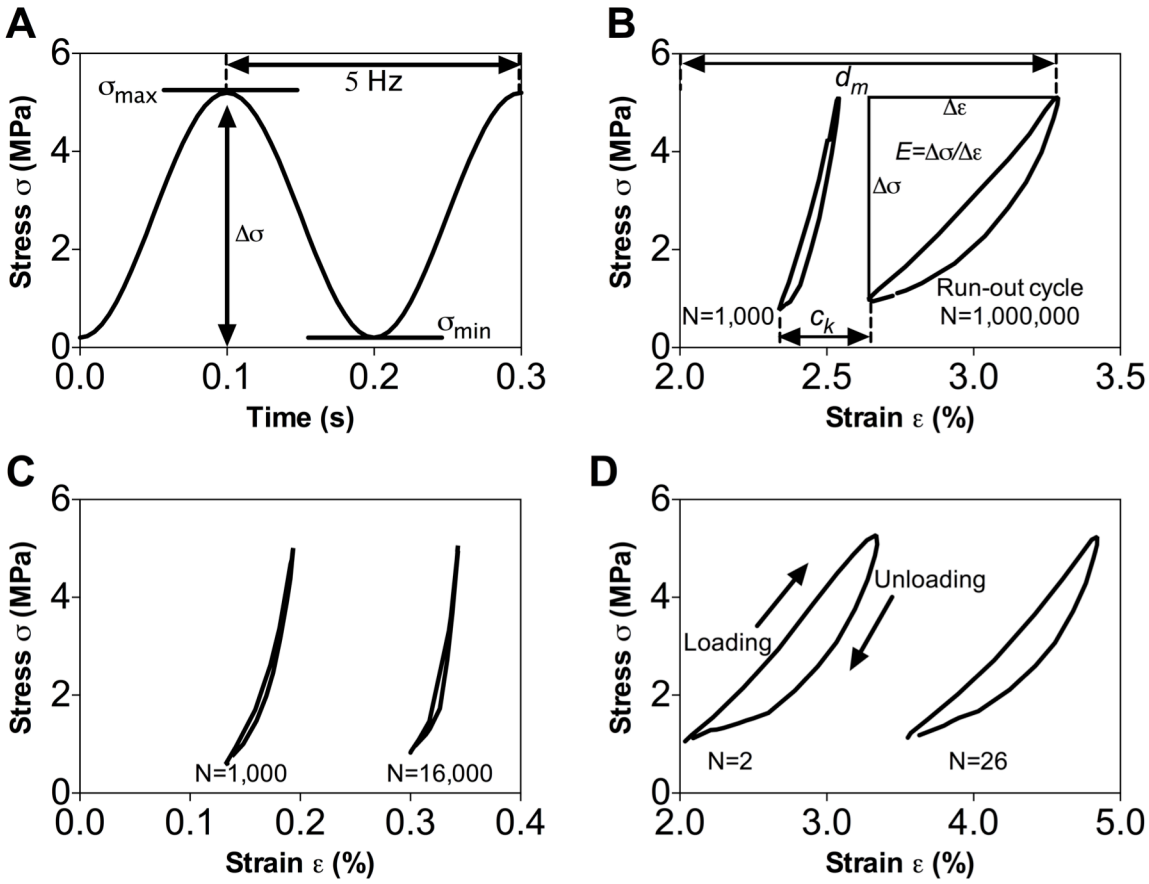

Figure 6.1. Compressive fatigue method and analysis. (A) Sinusoidal loading details for a maximum stress applied (σ_{max})=5 MPa and frequency=5 Hz. Representative stress (σ) vs. strain (ε) curves (σ_{max} =5 MPa), first and last cycles recorded, for (B) PCL surface-modified 45S5 bioactive glass (BG) and polyurethane composite (PCL-BG/PUR), (C) calcium sulfate and phosphate-based bone cement (CaS/P), and (D) un-modified BG and PUR composite (U-BG/PUR). Included in panel B), secant modulus (*E*) was defined at change in stress ($\Delta\sigma$), divided by the change in strain ($\Delta\varepsilon$), between the lowest and highest strain during loading. Creep strain (c_k) and maximum displacement (d_m) were defined by translation along the x-axis.

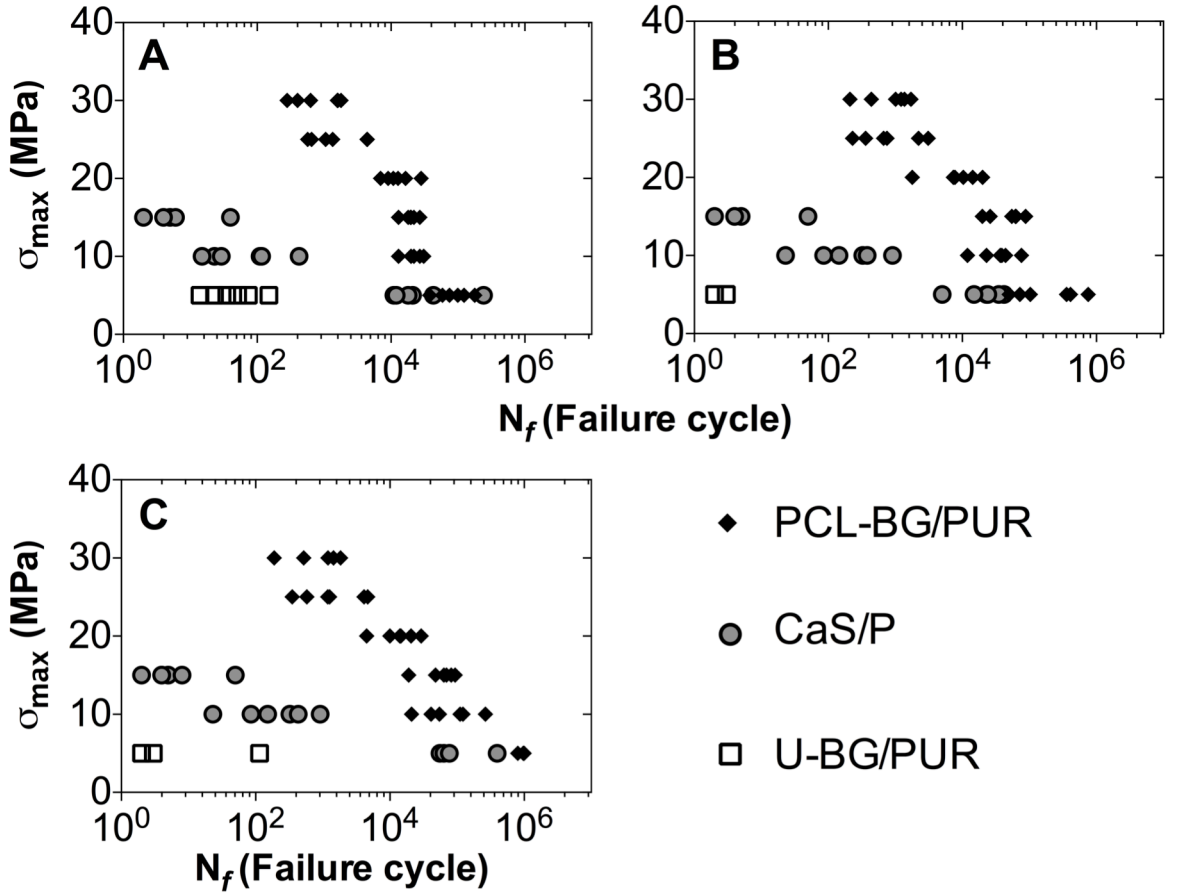

Figure 6.2. Fatigue S-N plot of BG/PUR composites and CaS/P cement. Fatigue life (N_f) was determined based on three different definitions of failure cycle, as the first cycle with (A) 10% decrease in secant modulus (E) compared to average of first 10 segments, (B) 1% creep deformation (c_k), and (C) 3% maximum displacement (d_m). Data shown includes n=6 for each load/specimen group.

Table 6.2. Median fatigue life (N_f) based on 1% creep failure definition, at maximum stress applied (σ_{max}). Values reported as 'median (n=6), (25% percentile, 75% percentile).' '-' indicates the specimen was not subjected to corresponding stress. Mann-Whitney tests were performed to determine statistical significance between the mean of groups.

σ_{max} (MPa)	PCL-BG/PUR	CaS/P	U-BG/PUR
5	230500[a] (66500, 495000)	23500 (12500, 36750)	3 (2, 3) [a,b]
10	38000[a] (20250, 52000)	236 (70, 511)	-
15	58500[a] (24500, 69250)	4 (3, 16)	-
20	9075 (5960, 15735)	-	-
25	710 (327, 2443)	-	-
30	1115 (383, 1458)	-	-

[a] $p<.0022$, at specific σ_{max} relative to CaS/P.

[b] $p<.0022$, at specific σ_{max} relative to PCL-BG/PUR.

Results

A summary of the groups tested in cyclic compressive fatigue, the corresponding maximum stress levels applied (σ_{max}), and cycle intervals between recorded cycles are shown in Table 6.1 (n=6 for each specimen and maximum stress level pairing). Cyclic compression test data for BG/PUR composites and CaS/P bone cement showed progressive loss of secant modulus (and thus broadening of hysteresis loop) and accumulation of

residual strains (cyclic creep). For the PCL-BG/PUR composite and CaS/P cement groups (Figure 6.1B and C, respectively), there was creep and damage accumulation (modulus loss) during a relatively long fatigue life, whereas U-BG/PUR composite showed primarily viscoelastic behavior over a short fatigue life (Figure 6.1D). Additionally, there was less overall creep exhibited by CaS/P cement compared to BG/PUR composites. Fatigue resistance of PCL-BG/PUR was superior to that of U-BG/PUR and CaS/P at the higher stress levels for each of fatigue failure definition: A) 10% decrease in secant modulus, B) 1% creep (c_k), C) 3% maximum displacement (d_m) (Figure 6.2). Overall, the fatigue behavior of each sample type at each failure definition exhibited the expected linear relationship with a negative slope between the maximum stress level applied (σ_{max}) and fatigue life (log scale). At σ_{max}=5 MPa, surface-modified PCL-BG composites and the CaS/P cement had a similar fatigue life when failure was defined with respect to secant modulus degradation (damage), but the fatigue life was higher for PCL-BG than for CaS/P when failure was based on overall creep and maximum displacement (Figure 6.2B and 2C). Unmodified BG/PUR composites had a substantially lower fatigue life for all definitions of failure compared to both the surface-modified BG composite and CaS/P cement (Figure 6.2). In addition, the PCL-BG/PUR composite had longer fatigue life compared to the CaS/P cement at σ_{max} =10-15 MPa irrespective of failure definition (Figure 6.2). The median number of cycles until failure (creep-based failure definition) tested at σ_{max} = 5 MPa for PCL-BG/PUR composite, CaS/P cement, and U-BG/PUR composite was 230500, 23500, and 3, respectively (Table 6.2). The difference in mean fatigue life between PCL-BG/PUR composite and CaS/P cement was also statistically significant at higher loads of 10 and 15 MPa.

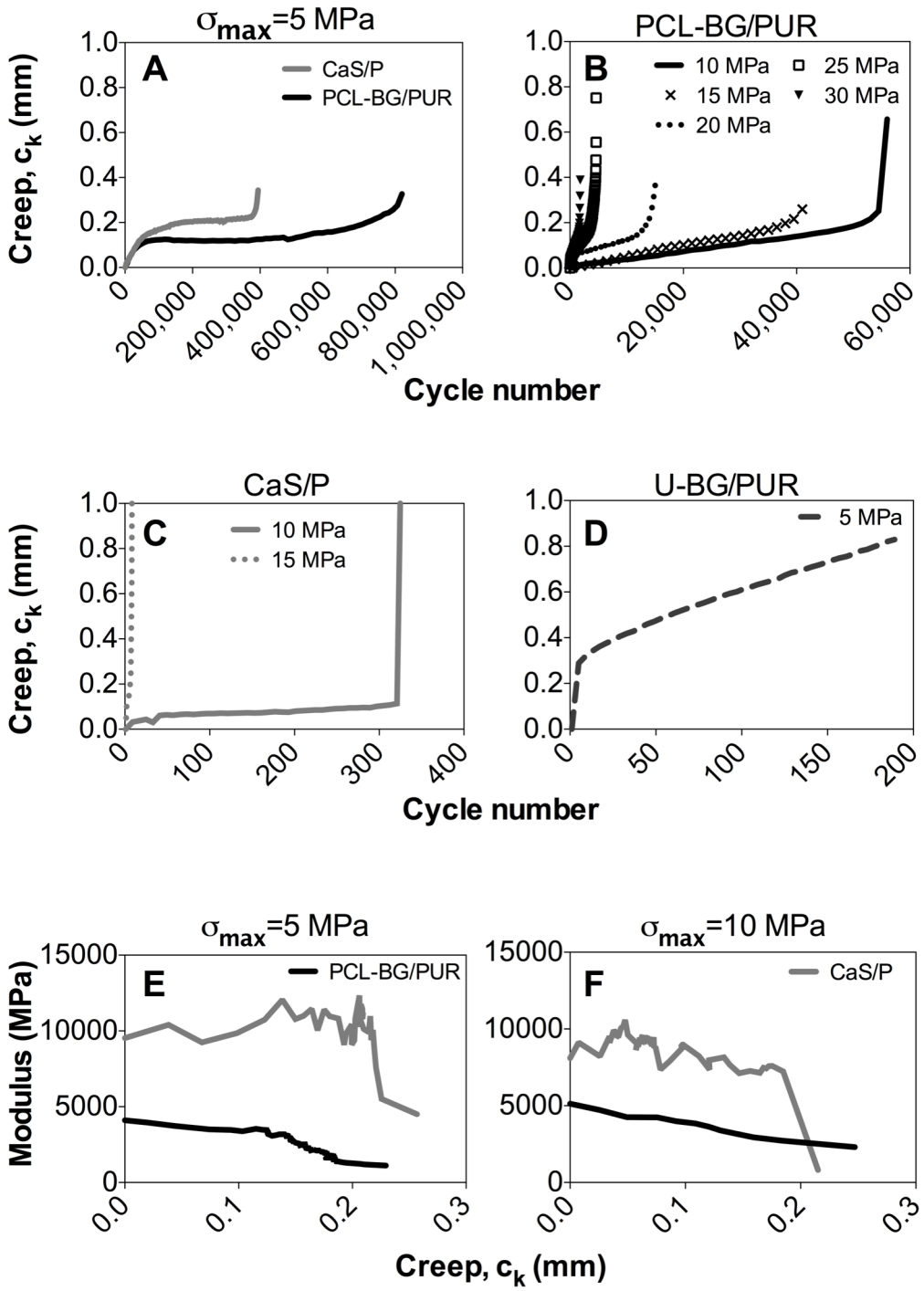

Figure 6.3. Fatigue testing creep (c_k) behavior vs. cycle number. Tested at maximum stress level (σ_{max}) of (A) 5 MPa for PCL-BG/PUR composite and CaS/P cement, (B) 10-30MPa for PCL-BG/PUR, and (C) 10-15 MPa for CaS/P, and (D) 5 MPa for U-BG/PUR. Plots shown are median, representative data of each specimen group/load group (n=6). Note that differences between the groups/stress levels in the value of the final creep data point plotted were due to interval span of cyclic data collected. Modulus (*E*) vs. creep (c_k) for PCL-BG/PUR and CaS/P at σ_{max}= (E) 5 MPa and (F) 10 MPa.

Creep strains developed throughout cyclic fatigue loading in force control, and PCL-BG/PUR composite and CaS/P cement exhibited the three stages of creep for a viscoelastic material: primary rapid strain increase in the first loading cycles, steady state-creep over the majority of the fatigue life, and a rapid increase in deformation near the end of the fatigue life (Figure 6.3). The non-linear relationship between creep and loading cycle was similar between both surface-modified BG composites and CaS/P cements at σ_{max} = 5 MPa (Figure 6.3A), but the CaS/P cement failed sooner and the steady state creep rate occurred at a higher stain than PCL-BG/PUR composite. This typical creep behavior was maintained with the surface-modified BG composite that was loaded at σ_{max} between 10-30 MPa (Figure 6.3B) as well CaS/P cement loaded at σ_{max} of 10 and 15 MPa (Fig. 6.3C). After a specimen reached a creep of approximately 0.2 mm or strain of 1.7%, complete failure usually occurred shortly thereafter. Also at these stress levels, surface-modified BG composites showed a more gradual transition from the second to third stage of creep compared to the CaS/P cement (Figure 6.3B vs. Figure 6.3C). As for the U-BG/PUR composite, the steady creep state occurred at lower number of cycles and at higher strains leading to fatigue life compared to the other materials (Figure 6.3D vs. Figure 6.3A). The modulus of both surface-modified BG/PUR composite and CaS/P cement degraded throughout the fatigue testing (Figure 6.3E-F). The BG/PUR composite showed a steady decrease in modulus as creep occurred, while CaS/P cement maintained a stiff modulus (within a small range) until failure drastically reduced the overall modulus within a small amount of creep.

Figure 6.4. Macroscopic specimen failure. Images of specimens post-fatigue testing (strain= 5%): (A) PCL-BG/PUR, (B) CaS/P, and (C) U-BG/PUR. Centimeter ruler shown in images.

All specimens showed macroscopic failure at cycles exceeding those defined by failure mechanisms related to modulus, creep, and displacement, which is supported by images of tested specimens at strains >5% (Figure 6.4A-C). PCL-BG composites stayed intact at these high strains, failing primarily at the specimen ends (Figure 6.4A). CaS/P cement showed numerous cracking events throughout the gain region of the specimen, often crumbling apart as fatigue loading completed (Figure 6.4B). U-BG composites often failed in the gage region of specimen but usually disassembled in large fractures rather than complete crumbling (Figure 6.4C).

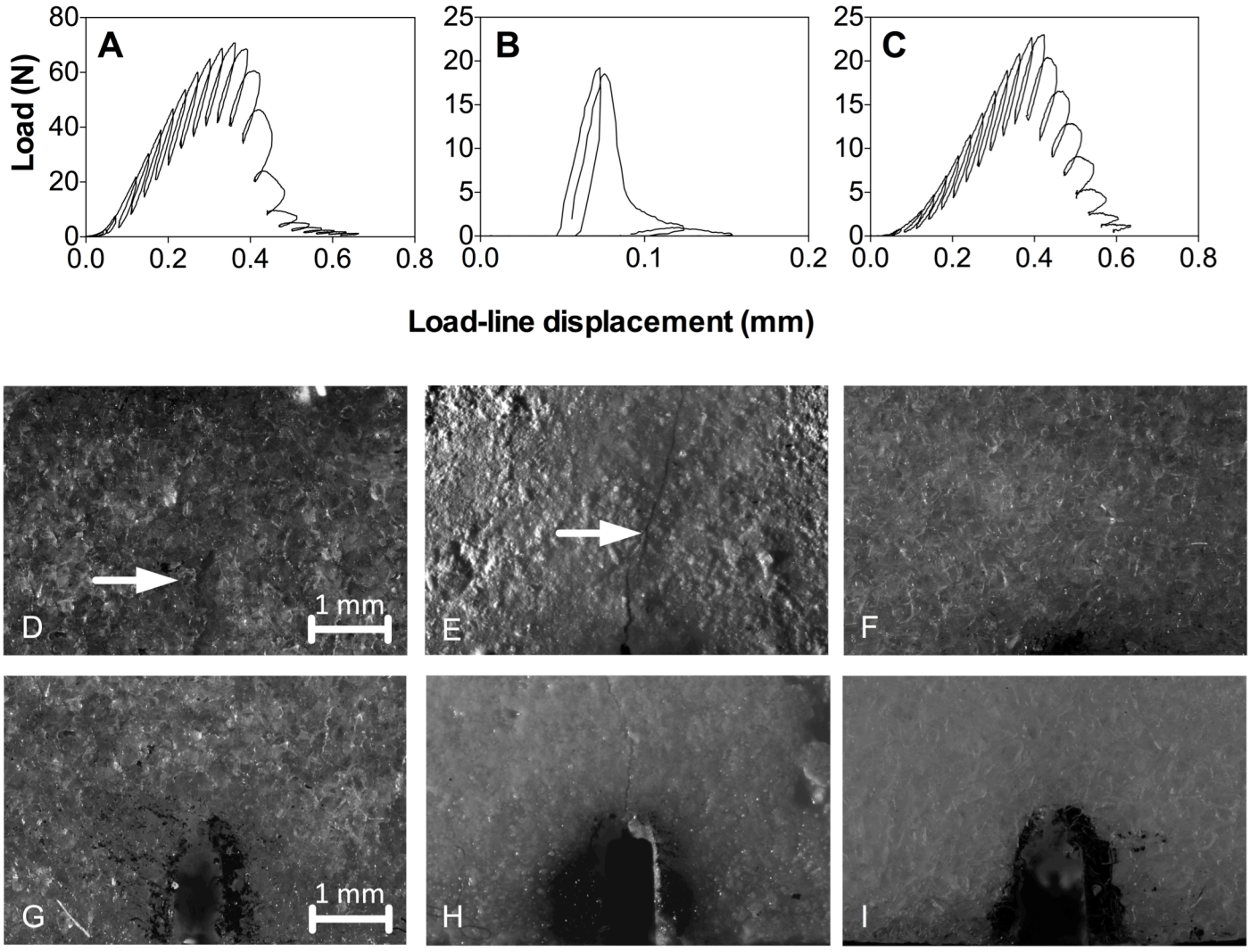

Figure 6.5. Fracture toughness testing. Applied load vs. load-line displacement curves for (A) PCL-BG/PUR, (B) CaS/P, and (C) U-BG/PUR. Images of representative typical crack propagation for each group (n=3) during fracture toughness testing. Displayed images respectively show above/include the starter notch for (D/G) PCL-BG/PUR, (E/H) CaS/P, and (F/I) U-BG/PUR. White arrows point to the propagated crack. All images were taken at the same magnification. Scale bar indicates 1 mm.

Table 6.3. Fracture toughness properties. Statistical significance of quantified value compared to the other groups determined by one-way ANOVA and Tukey HSD. Data shown is mean ± standard deviation (n=3).

Material	K_{init} (MPa $m^{0.5}$)	J (N/mm)
PCL-BG/PUR	1.43 ± 0.04[a]	1.54 ± 0.10[a]
CaS/P	0.32 ± 0.04	0.03 ± 0.01
U-BG/PUR	0.48 ± 0.07	0.62 ± 0.10

[a] $p<0.05$, relative to either remaining material group.

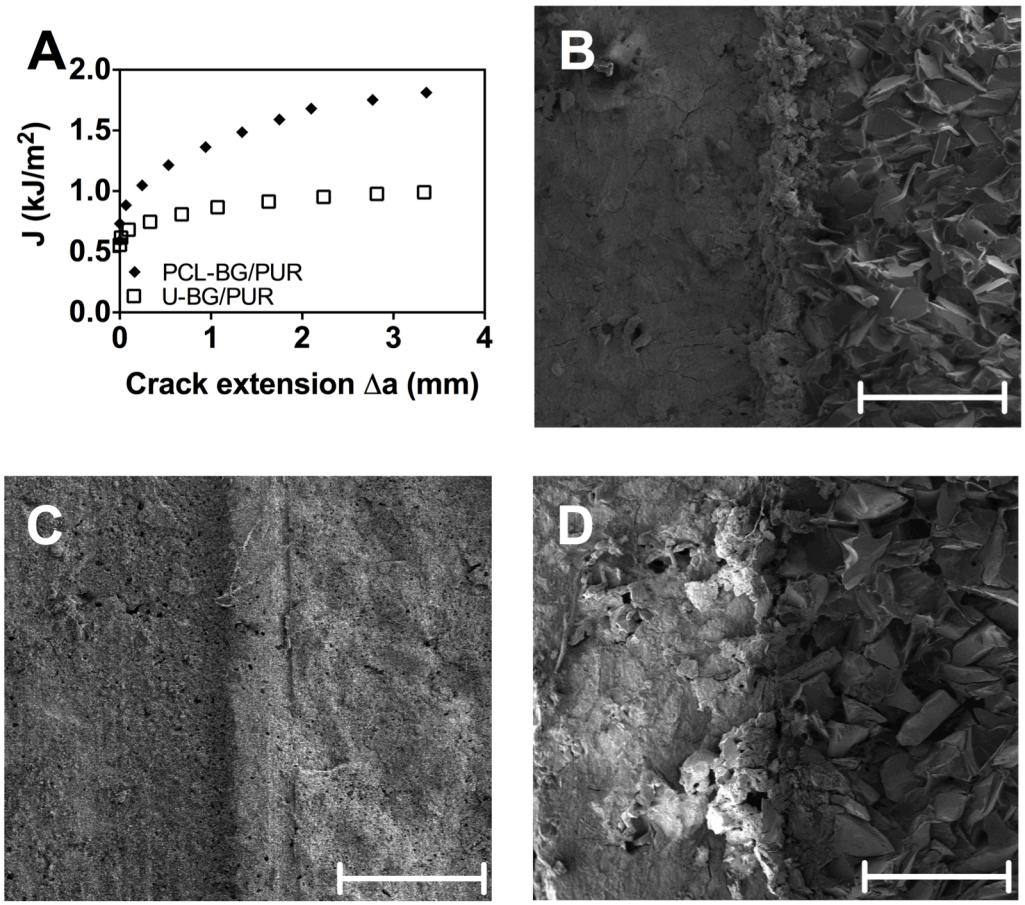

Figure 6.6. Fracture toughness analysis. Plot of (A) *J* vs. crack extension for PCL-BG and U-BG/PUR composites. SEM images of pre-cut micro-notch (left half of image) and interior of cracked specimen (right half of image) for (B) PCL-BG/PUR, (C) CaS/P, and (D) U-BG/PUR, after fracture toughness testing. Scale bar indicates 667 μm.

To critically evaluate the fracture toughness of each material, we determined the stress intensity factor or resistance to crack initiation (K_{init}) and J-integral from the load vs. displacement curves (Figure 6.5A-C). Images of the SENB specimen taken during fracture toughness testing revealed propagation of a crack from the micro-notches in PCL-BG composite and CaS/P cement (as indicated by white arrow in Figure 6.5D-E, respectively). Cracking from the micro-notched was not observed for the exterior of the U-BG/PUR composite specimen, but failure did occur. Fracture toughness properties (K_{init} and J-integral) of PCL-BG composite were significantly higher compared to the other two groups (Table 6.3), but there was no significant differences between the U-BG composite and CaS/P cement. There was a sufficient number of crack events for only the U- and PCL-BG/PUR composites (i.e., rising R-curves behavior), allowing the crack growth toughness of these specimens to be determined. J-integral was plotted against crack extension (Figure 6.6A). The surface modification of the BG before incorporation with the PUR binder significantly increased the elasto-plastic J-integral (Table 6.3) and change in J per crack extension (Figure 6.6A). This crack growth toughness is not existent in the brittle CaS/P material because crack instability occurred early in the loading of SENB specimens. SEM images of fractured surfaces show that BG/PUR composites (Figure 6.6B and D) had substantially rougher fracture surface than the CaS/P cement (Figure 6.6C), suggesting a more tortuous path for crack propagation. No noticeable difference was observed between the fracture surfaces of the two BG/PUR composites tested.

Discussion

Injectable and settable bone grafts that have sufficient fatigue resistance to withstand physiologically relevant dynamic stresses are anticipated to improve clinical management of severe tibial plateau fractures as well as fractures at other weight-bearing sites. Previous studies reported that allograft/ or ceramic/polymer

composites remodel and support new bone formation in preclinical models of bone regeneration in metaphyseal defects [18, 26-29]. Previously we showed that PCL-BG/polymer composites exhibit torsional strengths exceeding those of trabecular bone and support new bone growth when injected into femoral condyle defects in rats [18], but their mechanical properties under dynamic loadings have not been investigated. In this study, we measured the fatigue and fracture toughness properties of U-BG and PCL-BG/polymer composites, as well as an injectable CPC clinical control (CaS/P). While U-BG composites had torsional strength [18] and K_{init} values equal to ~35% of those measured for PCL-BG composites, the fatigue life of U-BG composites was almost 10^5 times shorter than that measured for PCL-BG composites at a 5 MPa. Similarly, CaS/P showed torsional strength [30] and K_{init} values equal to ~20% of the values measured for PCL-BG composites, but the fatigue life of CaS/P was 10^4 shorter at 15 MPa. These observations underscore the importance of fatigue testing under dynamic loads to assess the weight-bearing potential of bone graft substitutes, since materials with similar quasi-static properties can show dramatic differences in fatigue properties. The current recommended clinical management for tibial plateau fracture patients treated with fixation is to limit weight-bearing activities for 10 weeks [31]. Although the use of CPCs has shown to maintain anatomical reduction [32-34], better stability through improved fatigue life and fracture toughness with a BG/polymer composite could reduce the non-weight-bearing postoperative period.

A limited number of studies have evaluated dynamic compressive mechanical properties of synthetic biomaterials for orthopaedic applications. Calcium silicate-gelatin composites were reported to have fatigue life ranging from 10^3-10^5, at a 30 MPa load [35]. Additionally, 13-93 bioactive glass scaffolds made by robotic deposition were reported to have fatigue lives ranging from 10^4-10^6 at loads from 10-30 MPa [36]. Although the fatigue lives of these synthetic biomaterials are slightly longer than the PCL-BG composite in this study, these other materials are not injectable or settable.

The compressive fatigue mechanical properties of both human cortical and trabecular bone display S-N curves with N_f increasing with decreasing applied stress [37], as was observed for all synthetic bone grafts tested

in the present study. PCL-BG/polymer composites exhibited compressive fatigue properties in the range of human trabecular bone tested at physiological and supra-physiological loads [38-40], but not those of cortical bone [24, 41]. CaS/P cement and U-BG/polymer composite did not exhibit compressive fatigue properties in the range of either bone type. PCL-BG composite had an N_f in the range of 10^2-10^4 (Figure 6.2A) for maximum stress levels of 15-30 MPa (modulus-based failure definition, as was used in comparative human bone studies). These stress levels are equivalent to normalized loads of log(σ/averaged E_0)= -2.37 to -2.6. In two previous studies, human vertebral trabecular bone (independently tested healthy and elderly patients) was mechanically tested in dynamic compression fatigue over a range of σ/E_0 values that corresponded to maximum stress levels between 15-30 MPa. The published fatigue lives or these human specimens ranged from approximately 10^2-10^4 [40] and 10^2-10^5 [39] for healthy and elderly patients, respectively. Although it has been shown that higher frequency of applied load increases N_f [37, 42], increasing the frequency from 1 to 20 Hz increased N_f by one order of magnitude [42]. The sinusoidal frequency applied in our study (5 Hz) was slightly higher than the human studies referenced (1.32-2.87 Hz and 0.9-3 Hz, respectively), and the PCL-BG composite N_f exceeded values published in the former study. Thus, we anticipate that an increase in frequency of 2-3 Hz does not prevent the appropriate comparison to these human bone studies.

The creep behavior shown for BG/PUR composites during fatigue testing (Figure 3) matched characteristic creep profiles shown for these human bone specimens. Human specimens were shown to fail not only from modulus degradation but also from height subsidence, which motivated including the creep- and displacement-based failure definitions within the analysis of this study. During applied maximum stress levels of 10-30 MPa, PCL-BG composites exhibited steady state creep during strains from 0.8-1.5% (c_k=0.1-0.2 mm). Previous studies showed human trabecular bone exhibited steady creep during strains <0.6% [39, 40]. Thus, PCL-BG/PUR composite can withstand creep strain equal to or higher than human trabecular bone before entering the third stage of typical creep behavior.

The fracture toughness properties determined for the PCL-BG/PUR composite (K_{init} =1.43 MPa $m^{0.5}$, Table 6.3) were comparable to published values for bone and related orthopaedic biomaterials. Wet trabecular and cortical bone have been shown to have ranges of K_{IC} = 0.1-0.8 MPa $m^{0.5}$ [43, 44] and 2-12 MPa $m^{0.5}$ [11, 43, 45, 46], respectively. For CaS/P cement, K_{init}=0.32 MPa $m^{0.5}$ (Table 6.3) was comparable to the K_{IC} of another calcium phosphate cement (Norian Skeletal Repair System, SRS®) previously reported (K_{IC}=0.14 MPa $m^{0.5}$) [17]. Despite having a similar carbonated apatite composition to the mineral phase of bone, Norian SRS® and CaS/P cements showed considerably lower toughness compared to that of wet bone. Consequently, the fracture toughness of PCL-BG/polymer composite has fracture toughness properties closer to human bone than calcium phosphate cements.

Fatigue creep and fracture toughness results from this study provide mechanistic insight regarding the longer fatigue life of PCL-BG/polymer composite compared to CaS/P cement. PCL-BG composite showed several stable cracking events throughout the fracture toughness testing (Figure 6.5A), whereas CaS/P did not show signs of stable cracking but rather unstable cracking when an event was observed (Figure 6.5B). Although the PCL-BG composite is not immune to microcrack formation, this damage appears to be constrained to small areas of the composite. This is supported by images of composites after complete fatigue failure that showed signs of shear bands with the majority of the composite intact (Figure 6.4A), whereas the CaS/P cement showed numerous end-to-end catastrophic cracks throughout the specimen (Figure 6.4B). CaS/P cement appeared to have better resistance to initial creep deformation compared to PCL-BG composite at loads above 5 MPa (Figure 6.3C), but complete failure occurred at lower overall creep and appeared to happen more rapidly (Figure 6.3 E and F). Thus it appears CaS/P cannot absorb loaded energy in a stable manner. When microcracks formed, these unstable events led to failure of the CaS/P, presumably due to its low fracture toughness.

A recent review reported that the majority of calcium phosphate/polymer composites had quasi-static compressive mechanical properties below those of human trabecular bone and bulk monolithic calcium

phosphates [7]. The reason for these subpar mechanical properties may be due to poor interfacial bonding between phases within the composite. Adequate interfacial bonding is necessary in order to capitalize on the potential benefits of combining a tough ductile polymer phase with a strong brittle phase. The fracture toughness of bone has been attributed to its composite nature, in which apatite is bound to collagen [11, 47]. Similarly, the superior fatigue and fracture toughness properties of PCL-BG composites are conjectured to result from extensive interfacial bonding due to physical entanglements between surface-polymerized PCL chains on the BG particles and the continuous PUR network [18].

To our knowledge, the surface-modified BG/PUR composite from the current study is the first published injectable, settable, synthetic bone graft with initial quasi-static and dynamic compressive mechanical properties equal to or greater than that of native trabecular bone. BG/polymer composites could potentially reduce the period that patients with tibial plateau fractures must limit weight-bearing activities, to times shorter than the current recommendation of 10 weeks [31]. When injected into femoral condyle plug defects in rats, PCL-BG composites exhibited new bone formation, BG degradation, and polymer resorption at 8 weeks [18]. Thus, the mechanical behavior of PCL-BG composites is anticipated to change with time *in vivo*. Consequently, it will be important to verify that PCL-BG composites maintain sufficient fatigue resistance and fracture toughness properties throughout all stages of the remodeling process, from initial injection to final healing. These questions are currently under investigation in a large animal load-bearing model of bone regeneration.

Conclusions

In this study, the dynamic compressive fatigue properties of BG/polymer composites when subjected to physiological or supra-physiological loads were evaluated, and their properties were compared to those of a commercially available biphasic CPC (CaS/P). Poly(ε-caprolactone) surface-modified BG/polymer composite

fatigue resistance was superior to that of CaS/P cement at low and high compressive stress. The fatigue failures of BG/PUR composite and CaS/P biomaterials included both creep and damage accumulation. CaS/P cement reached steady state creep during fatigue testing at a higher stain than PCL-BG/polymer composite but showed catastrophic failure at a lower strain. Additionally, the fracture toughness properties of BG/polymer composites and CaS/P cements were evaluated. PCL surface modified BG/polymer composite showed significantly higher resistance to crack growth than CaS/P and un-modified BG/polymer composite groups.

References

1. S. Ramakrishna, J. Mayer, E. Wintermantel and K.W. Leong: Biomedical applications of polymer-composite materials: a review *Composites Science and Technology.* **61**(9), 1189 (2001).

2. D.D. Anderson, C. Van Hofwegen, J.L. Marsh and T.D. Brown: Is elevated contact stress predictive of post-traumatic osteoarthritis for imprecisely reduced tibial plafond fractures? *J Orthop Res.* **29**(1), 33 (2011).

3. D. Simpson and J.F. Keating: Outcome of tibial plateau fractures managed with calcium phosphate cement *Injury.* **35**(9), 913 (2004).

4. J.A. Hall, M.J. Beuerlein and M.D. McKee: Open reduction and internal fixation compared with circular fixator application for bicondylar tibial plateau fractures. Surgical technique *J Bone Joint Surg Am.* **91 Suppl 2 Pt 1**, 74 (2009).

5. M.J. Bosse, E.J. MacKenzie, J.F. Kellam, A.R. Burgess, L.X. Webb, M.F. Swiontkowski, R.W. Sanders, A.L. Jones, M.P. McAndrew, B.M. Patterson, M.L. McCarthy, T.G. Travison and R.C. Castillo: An analysis of outcomes of reconstruction or amputation after leg-threatening injuries *N Engl J Med.* **347**(24), 1924 (2002).

6. K. Rezwan, Q.Z. Chen, J.J. Blaker and A.R. Boccaccini: Biodegradable and bioactive porous polymer/inorganic composite scaffolds for bone tissue engineering *Biomaterials.* **27**(18), 3413 (2006).

7. A.J.W. Johnson and B.A. Herschler: A review of the mechanical behavior of CaP and CaP/polymer composites for applications in bone replacement and repair *Acta Biomaterialia.* **7**(1), 16 (2011).

8. M. Bohner: Design of Ceramic-Based Cements and Putties for Bone Graft Substitution *European Cells & Materials.* **20**, 1 (2010).

9. A. Gisep, S. Kugler, D. Wahl and B. Rahn: Mechanical characterisation of a bone defect model filled with ceramic cements *Journal of Materials Science-Materials in Medicine.* **15**(10), 1065 (2004).

10. W. Krause and R.S. Mathis: Fatigue Properties of Acrylic Bone Cements - Review of the Literature *Journal of Biomedical Materials Research-Applied Biomaterials.* **22**(A1), 37 (1988).

11. E.F. Morgan, D.N. Yetkinler, B.R. Constantz and R.H. Dauskardt: Mechanical properties of carbonated apatite bone mineral substitute: strength, fracture and fatigue behaviour *Journal of Materials Science-Materials in Medicine.* **8**(9), 559 (1997).

12. J. Slane, J. Vivanco, J. Meyer, H.-L. Ploeg and M. Squire: Modification of acrylic bone cement with mesoporous silica nanoparticles: Effects on mechanical, fatigue and absorption properties *Journal of the Mechanical Behavior of Biomedical Materials.* **29**, 451 (2014).

13. R.A. Latour and J. Black: Development of Frp Composite Structural Biomaterials - Fatigue-Strength of the Fiber-Matrix Interfacial Bond in Simulated in-Vivo Environments *Journal of Biomedical Materials Research.* **27**(10), 1281 (1993).

14. M.R. Kessler, N.R. Sottos and S.R. White: Self-healing structural composite materials *Composites Part a-Applied Science and Manufacturing.* **34**(8), 743 (2003).

15. M.T. Tilbrook, R.J. Moon and M. Hoffman: Crack propagation in graded composites *Composites Science and Technology.* **65**(2), 201 (2005).

16. G. Pinter, E. Ladstätter, W. Billinger and R.W. Lang: Characterisation of the tensile fatigue behaviour of RTM-laminates by isocyclic stress–strain-diagrams *International Journal of Fatigue.* **28**(10), 1277 (2006).

17. G. Lewis: Injectable bone cements for use in vertebroplasty and kyphoplasty: State-of-the-art review *Journal of Biomedical Materials Research Part B-Applied Biomaterials.* **76B**(2), 456 (2006).

18. A.J. Harmata, C.L. Ward, K. Zienkiewicz, J.C. Wenke and S.A. Guelcher: Investigating the Effects of Surface-Initiated Polymerization of ε-Caprolactone to Bioactive Glass Particles on the Mechanical Properties of Settable Polymer/Ceramic Composites *Journal of Materials Research.* **29**(20), 2398 (2014).

19. ASTM: Designation F2118-10. Standard Test Method for Constant Amplitude of Force Controlled Fatigue Testing of Acrylic Bone Cement Materials *ASTM International.* (2010).

20. R.O. Ritchie, K.J. Koester, S. Ionova, W. Yao, N.E. Lane and J.W. Ager, III: Measurement of the toughness of bone: A tutorial with special reference to small animal studies *Bone.* **43**(5), 798 (2008).

21. E. Verne, C. Vitale-Brovarone, E. Bui, C.L. Bianchi and A.R. Boccaccini: Surface functionalization of bioactive glasses *J. Biomed. Mater. Res. Part A.* **90A**(4), 981 (2009).

22. G. Jiang, G.S. Walker, I.A. Jones and C.D. Rudd: XPS identification of surface-initiated polymerisation during monomer transfer moulding of poly(epsilon-caprolactone)/Bioglass (R) fibre composite *Applied Surface Science.* **252**(5), 1854 (2005).

23. S.A. Guelcher, V. Patel, K.M. Gallagher, S. Connolly, J.E. Didier, J.S. Doctor and J.O. Hollinger: Synthesis and in vitro biocompatibility of injectable polyurethane foam scaffolds *Tissue Engineering.* **12**(5), 1247 (2006).

24. W.E. Caler and D.R. Carter: Bone Creep-Fatigue Damage Accumulation *Journal of Biomechanics.* **22**(6-7), 625 (1989).

25. ASTM: Designation: E 1820, Standard Test Method for Measurement of Fracture Tougness *ASTM International* (2005).

26. J.E. Dumas, T. Davis, G.E. Holt, T. Yoshii, D.S. Perrien, J.S. Nyman, T. Boyce and S.A. Guelcher: Synthesis, characterization, and remodeling of weight-bearing allograft bone/polyurethane composites in the rabbit *Acta Biomaterialia.* **6**(7), 2394 (2010).

27. R. Adhikari, P.A. Gunatillake, I. Griffiths, L. Tatai, M. Wickramaratna, S. Houshyar, T. Moore, R.T.M. Mayadunne, J. Field, M. McGee and T. Carbone: Biodegradable injectable polyurethanes: Synthesis and evaluation for orthopaedic applications *Biomaterials.* **29**(28), 3762 (2008).

28. J.E. Dumas, K. Zienkiewicz, S.A. Tanner, E.M. Prieto, S. Bhattacharyya and S.A. Guelcher: Synthesis and Characterization of an Injectable Allograft Bone/Polymer Composite Bone Void Filler with Tunable Mechanical Properties *Tissue Engineering Part A.* **16**(8), 2505 (2010).

29. T. Yoshii, J.E. Dumas, A. Okawa, D.M. Spengler and S.A. Guelcher: Synthesis, characterization of calcium phosphates/polyurethane composites for weight-bearing implants *Journal of Biomedical Materials Research Part B-Applied Biomaterials.* **100B**(1), 32 (2012).

30. J.E. Dumas, E.M. Prieto, K.J. Zienkiewicz, T. Guda, J.C. Wenke, J. Bible, G.E. Holt and S.A. Guelcher: Balancing the Rates of New Bone Formation and Polymer Degradation Enhances Healing of Weight-Bearing Allograft/Polyurethane Composites in Rabbit Femoral Defects *Tissue Engineering Part A.* **20**(1-2), 115 (2014).

31. A.M. Ali, M. El-Shafie and K.M. Willett: Failure of fixation of tibial plateau fractures *Journal of Orthopaedic Trauma.* **16**(5), 323 (2002).

32. R.D. Welch, H. Zhang and D.G. Bronson: Experimental tibial plateau fractures augmented with calcium phosphate cement or autologous bone graft *Journal of Bone and Joint Surgery-American Volume.* **85A**(2), 222 (2003).

33. D. Simpson and J.F. Keating: Outcome of tibial plateau fractures managed with calcium phosphate cement *Injury-International Journal of the Care of the Injured.* **35**(9), 913 (2004).

34. T.A. Russell and R.K. Leighton: Comparison of Autogenous Bone Graft and Endothermic Calcium Phosphate Cement for Defect Augmentation in Tibial Plateau Fractures *Journal of Bone and Joint Surgery-American Volume.* **90A**(10), 2057 (2008).

35. S.-J. Ding, C.-K. Wei and M.-H. Lai: Bio-inspired calcium silicate-gelatin bone grafts for load-bearing applications *Journal of Materials Chemistry.* **21**(34), 12793 (2011).

36. X. Liu, M.N. Rahaman, G.E. Hilmas and B.S. Bal: Mechanical properties of bioactive glass (13-93) scaffolds fabricated by robotic deposition for structural bone repair *Acta Biomaterialia.* **9**(6), 7025 (2013).

37. J.J. Kruzic and R.O. Ritchie: Fatigue of mineralized tissues: Cortical bone and dentin *Journal of the Mechanical Behvaior of Biomedical Materials I* **1**(1), 3 (2008).

38. L. Rapillard, M. Charlebois and P.K. Zysset: Compressive fatigue behavior of human vertebral trabecular bone *Journal of Biomechanics.* **39**(11), 2133 (2006).

39. S.M. Haddock, O.C. Yeh, P.V. Mummaneni, W.S. Rosenberg and T.M. Keaveny: Similarity in the fatigue behavior of trabecular bone across site and species *Journal of Biomechanics.* **37**(2), 181 (2004).

40. S. Dendorfer, H.J. Maier, D. Taylor and J. Hammer: Anisotropy of the fatigue behaviour of cancellous bone *Journal of Biomechanics.* **41**(3), 636 (2008).

41. P. Zioupos, M. Gresle and K. Winwood: Fatigue strength of human cortical bone: Age, physical, and material heterogeneity effects *J. Biomed. Mater. Res. Part A.* **86A**(3), 627 (2008).

42. S. Diel, O. Huber, H. Saage, P. Steinmann and W. Winter: Mechanical behavior of a cellular composite under quasi-static, static, and cyclic compression loading *Journal of Materials Science.* **47**(15), 5635 (2012).

43. Q. Fu, E. Saiz, M.N. Rahaman and A.P. Tomsia: Bioactive glass scaffolds for bone tissue engineering: state of the art and future perspectives *Materials Science & Engineering C-Materials for Biological Applications.* **31**(7), 1245 (2011).

44. M.L. Oyen: The materials science of bone: Lessons from nature for biomimetic materials synthesis *Mrs Bulletin.* **33**(1), 49 (2008).

45. J.W. Melvin: Fracture-Mechanics of Bone *Journal of Biomechanical Engineering-Transactions of the Asme.* **115**(4), 549 (1993).

46. M. Bohner: Calcium orthophosphates in medicine: from ceramics to calcium phosphate cements *Injury-International Journal of the Care of the Injured.* **31**, S37 (2000).

47. M. Wang: Developing bioactive composite materials for tissue replacement *Biomaterials.* **24**(13), 2133 (2003).

CHAPTER VII

CONCLUSIONS

The culmination of this dissertation is the development and characterization of two synthetic, biodegradable, lysine-derived, aliphatic polyurethane systems designed for healing of weight bearing and bacterially contaminated defects. The studies detailed in the previous chapters provide insight into the foundation of polyurethane-based solutions for clinical management of these two related orthopaedic conditions and future potential for a combined formulation that both prevents bacterial biofilm formation and mechanical failure in challenging bone defects.

In Chapter III, a dose dependent *in vitro* investigation on the effect of D-isomers of amino acids (D-AAs) on osteoblast and osteoclast differentiation provided a clear concentration breaking point by which D-AAs begin to hinder cellular activity. Previously, we reported that anti-biofilm activity of D-AAs for *S. aureus* increased with D-AAs concentration from 0.1-5 mM, with minimal increased activity >5 mM [1]. But in the current study, we observed that D-AAs did not hinder osteoblast proliferation and differentiation, as well as osteclastogenesis at local concentrations <27 mM.

A low-viscosity D-AA augmented PUR graft did not significantly hinder bone healing after 16 weeks when injected into ovine femoral condyle plug defects. Comparable healthy bone remodeling, which included cellular infiltration, formation of lamellar bone architecture, and appropriate osteocyte density, occurred between defects filled with a blank PUR graft and the augmented PUR graft, despite a significantly higher initial loading concentration of D-AAs than what was concluded to inhibit cellular activity *in vitro*. We concluded that at local doses effective for preventing biofilm formation, D-AAs do not inhibit osteoblast and osteoclast differentiation *in vitro*, or long-term bone healing *in vivo*. Consequently, based on this study, delivery of D-AAs is an effective anti-biofilm strategy that does not significantly inhibit bone repair.

In Chapter IV, the additional attachment of surface-polymerized ε-caprolactone to silane-grafted BG was shown to not further inhibit the bioactive surface properties of the material, as determined by nucleation of bone-like hydroxycarbonate apatite (HCA) when in physiological fluid. Resultant number-average molecular weight (M_n) of the polymer, mean layer thickness, and surface coverage of the grafted PCL layer all increased with polymerization time, as modeled on silicon oxide wafers. Scanning electron microscopy (SEM) images and elemental surface quantification by energy dispersive spectroscopy (EDS) showed that BG disks modified with (3-aminopropyl)triethoxysilane (APTES) or APTES and PCL both delayed HCA nucleation equally by 1 day, compared to unmodified BG. The long-term (1-3 weeks) maturity of physiological fluid incubation induced nucleated HCA on unmodified and PCL-modified BG was the same. Consequently, surface-polymerization of PCL does not hinder *in vitro* biomineralization of BG enough to elicit concern that innate bioactive properties would be impacted in the long-term when implanted *in vivo*.

Surface polymerization of ε-caprolactone (PCL) on 45S5 bioactive glass (BG) particles not only increased overall mechanical properties of the resultant BG/PUR composite, but also provided insight to the relationship between the surface-initiated layer and polymer network and its effect on mechanical properties. As outlined in Chapter V, despite no significant difference in porosities between tested PUR composites, PCL chains increased the compressive and torsional strength of composites 6- to 10-fold and 2-fold, respectively, compared to composites made with unmodified BG particles [2]. It was determined that the compressive strength and modulus were dependent on the thickness (or molecular weight) of the PCL layer relative to the mesh size of the PUR network formed *in situ* [2]. Additionally, the torsional strength and toughness of the PCL-modified BG/PUR composite exceeded that of human trabecular bone[3] and a calcium phosphate cement[4] by a factor of 3. When implanted into femoral condyle plug defects in rats, the PCL-modified BG/PUR composite supported cellular infiltration and bone remodeling at 8 weeks. These results support conclusions made from *in vitro* biomineralization studies that silane-PCL modification does not inhibit the bioactivity of BG enough to prevent

adequate bone remodeling *in vivo*. Overall, the results from this study clarify the interfacial structure-property relationships governing the mechanical properties of surface-modified ceramic/polymer composites.

Conclusions from Chapters IV and V, and the observation that compressive strength alone is a poor indicator of *in vivo* performance[5, 6], motivated further characterization of the mechanical properties of surface-modified BG/PUR composites through evaluation of dynamic compressive fatigue in Chapter VI. The fatigue resistance of PCL-modified BG/PUR composite was superior to that of a commercially available calcium sulfate and phosphate cement (CaS/P), at both low (5 MPa) and high stresses (10-15 MPa), across all definitions of failure related to damage accumulation, creep, and displacement. Additionally, PCL-BG/polymer composites exhibited compressive fatigue properties in the range of human trabecular bone tested at physiological (5-15 MPa) and supra-physiological (20-30 MPa) loads [7-9]. To our knowledge, the surface-modified BG/PUR composite is the first published injectable, settable, synthetic bone graft with initial quasi-static (Chapter V) and dynamic compressive mechanical properties equal to or greater than that of native trabecular bone.

Analysis of fatigue creep and coupled fracture resistance testing provided insight to the mechanisms of fatigue failure, which included both damage accumulation and creep for BG/PUR composites and for CaS/P. Although less overall creep occurred with the CaS/P, and both cements exhibited characteristic creep profiles shown for human trabecular bone, once steady state creep was reached catastrophic failure occurred at a lower creep strain for CaS/P than PCL-BG/PUR. Additionally, PCL-BG composite showed significantly higher resistance to crack growth than CaS/P and un-modified BG/polymer composite groups. Consequently, the fatigue creep behavior and fracture toughness of PCL-BG/polymer composite has mechanical failure properties closer to human bone than calcium phosphate cements.

References

1. C.J. Sanchez, E.M. Prieto, C.A. Krueger, K.J. Zienkiewicz, D.R. Romano, C.L. Ward, K.S. Akers, S.A. Guelcher and J.C. Wenke: Effects of local delivery of D-amino acids from biofilm-dispersive scaffolds on infection in contaminated rat segmental defects *Biomaterials.* **34**(30), 7533 (2013).

2. A.J. Harmata, C.L. Ward, K. Zienkiewicz, J.C. Wenke and S.A. Guelcher: Investigating the Effects of Surface-Initiated Polymerization of ε-Caprolactone to Bioactive Glass Particles on the Mechanical Properties of Settable Polymer/Ceramic Composites *Journal of Materials Research.* **29**(20), 2398 (2014).

3. K.B. Garnier, R. Dumas, C. Rumelhart and M.E. Arlot: Mechanical characterization in shear of human femoral cancellous bone: torsion and shear tests *Medical Engineering & Physics.* **21**(9), 641 (1999).

4. J. Dumas, E. Prieto, K. Zienkiewicz, T. Guda, J. Wenke, J. Bible, G. Holt and S. Guelcher: Remodeling of Settable Allograft Bone/Polymer Composites with Initial Bone-like Mechanical Properties in Rabbit Femora. *Tissue Eng Part A.* **20**(1-2), 115 (2014).

5. M. Bohner: Design of Ceramic-Based Cements and Putties for Bone Graft Substitution *European Cells & Materials.* **20**, 1 (2010).

6. A. Gisep, S. Kugler, D. Wahl and B. Rahn: Mechanical characterisation of a bone defect model filled with ceramic cements *Journal of Materials Science-Materials in Medicine.* **15**(10), 1065 (2004).

7. L. Rapillard, M. Charlebois and P.K. Zysset: Compressive fatigue behavior of human vertebral trabecular bone *Journal of Biomechanics.* **39**(11), 2133 (2006).

8. S.M. Haddock, O.C. Yeh, P.V. Mummaneni, W.S. Rosenberg and T.M. Keaveny: Similarity in the fatigue behavior of trabecular bone across site and species *Journal of Biomechanics.* **37**(2), 181 (2004).

9. S. Dendorfer, H.J. Maier, D. Taylor and J. Hammer: Anisotropy of the fatigue behaviour of cancellous bone *Journal of Biomechanics.* **41**(3), 636 (2008).

CHAPTER VIII

SUGGESTIONS FOR FUTURE WORK

The results and conclusions from the previously outlined chapters inspired additional research questions and potential studies to further these projects. The following chapter includes preliminary results and related suggestions for future work that will aid in the development of a polyurethane (PUR) graft design to treat weight-bearing and biofilm contaminated bone defects.

TAILORING THE RELEASE KINETICS OF D-AMINO ACIDS FROM BIOFILM-DISPERSIVE POLYURETHANE SCAFFOLDS

Introduction

Infection of bone by bacteria (osteomyelitis) can lead to the destruction of bone tissue and can become chronic, which often leads to poor healing outcomes, extremity amputation, or patient morbidity [2-4]. With >50% of all cases of this condition exhibiting *Staphylococcus aureus*, this microorganism is the most frequently isolated pathogenic organism associated with the condition [5-9]. Biofilm, a protected mode of growth for bacterium, developed by *S. aureus* is prevalent in the infected bone of patients suffering from osteomyelitis and is implicated in development of chronic osteomyelitis [7-9]. Bacteria hidden within surface-attached biofilms are largely insensitive to antibiotics because the film acts as a diffusion barrier, which slows down the penetration rate of nutrients and antimicrobial agents, as well as metabolic and growth rates of subsequent bacteria [2, 3, 12, 13]. Consequently, preventing the formation of biofilm by controlling the interface between an implanted material and the anatomical site is imperative to the success of an implanted device or biomaterial. This “race for the surface” refers to the contest between cell integration and bacterial adhesion to the same surface [13, 14].

Recent studies have shown that D-isomers of amino acids (D-AAs) disperse bacterial biofilms made by *S. aureus*, among other bacterial species. D-AAs promote the disassembly of biofilms through the release of the protein component of the extracellular matrix that holds together bacteria communities in the biofilm structure[15]. A minimum biofilm inhibitory concentration (MBIC) and minimum inhibitory concentration (MIC) for various individual D-AAs has been shown to be approximately 1 mM[4] and 3 μM- 8.5 mM[15], respectively. These amino acids have minimal cellular toxicity and at doses effective for preventing biofilm formation. D-AAs do not inhibit osteoblast and osteoclast cells differentiation *in vitro* or bone repair *in vivo*.

Although synthetic bone grafts or scaffolds can be effective at promoting bone growth, foreign materials implanted into a defect, contaminated or not, could function as a nidus for bacterial infection. The development of a synthetic scaffold that prevents biofilm formation could prevent osteomyelitis. Previously, we showed the ability for biofilm-dispersive PUR scaffolds augmented with a mixture of D-AAs to protect the scaffold from contamination from contiguous wound environment and to reduce microbial burden (of clinical isolate of *S. aureus*) *in vitro* as well as in rat segmental defects *in vivo* [1]. The release of various D-AAs followed a diffusion controlled sustained profile characterized by an initial burst followed by a sustained release, up to 21d. The magnitude of the initial burst release from the PUR scaffold was dependent on the D-AA released[1].

The ability to control the release kinetics of drugs from scaffolds, both degradable and non-degradable, has proven to be vital for development of an effective therapeutic [16]. There are numerous factors that alter the release of drugs or biologics, such as D-AAs, from a polymer matrix, including chemical and physical properties of both the drug as well as matrix carrier. The main driving forces are solute diffusion, polymeric matrix swelling, and material degradation [16]. Methods for altering these properties have been investigated and include altering the biologic's hydrophobicity [17, 18] and thus solubility, adding an excipient [17, 19, 20], or changing the initial concentration of loaded biologic [21, 22]. Previously it was shown that vancomycin-HCl (V-HCl) released from PMMA and other materials resulted in a high burst with minimal sustained release due to high water

solubility of V-HCl [23-25]. When the vancomycin was changed to a free base form and the solubility was decreased, the burst release was decreased and the sustained release was increased [18].

For the prevention and/or dispersal of bacterial biofilm, the most effective treatment dosage and corresponding duration of D-AAs has not been determined. As with the delivery of any drug, the burst effect may be favorable in certain indications, but could also cause negative effects such as toxicity if local levels are exceeded. Additionally, a shortened release profile may require frequent dosing [24, 26, 27]. Due to the surface-attaching nature of biofilms, it is hypothesized that in order to prevent biofilm attachment and subsequent formation, therapeutic levels of dispersal agents should be reached once, or even before, an abiotic surface is introduced *in vivo* [28].

The optimal release profile of D-AAs from an augmented PUR scaffold to model dosage time courses has not been investigated. One objective of the present study was to determine methods to alter the release profile of D-AAs from augmented PUR scaffolds by which the delivered dosage of D-AAs would be above the MBIC for varying amounts of time. PUR scaffolds augmented with various forms of D-Tryptophan (D-Trp), with and without excipients, and at various loadings thereof, were evaluated by *in vitro* incubation in phosphate buffer solution (PBS) in order to characterize D-Trp release kinetics. Although the release profile of D-Trp was not dependent on the biologic's solubility or by the addition of an excipient to the PUR scaffold at early time points (<7d), the overall initial loading of D-Trp in the PUR scaffold was able to significantly alter the released D-Trp dosage duration.

Methods

Materials

D- and L-isomers of amino acids (free base form), including methionine, phenylalanine, proline, and tryptophan were purchased from Sigma Aldrich (St. Louis, MO, USA). For polyurethane scaffold synthesis, D(+)-trehalose dihydrate, ε-caprolactone and stannous octoate were purchased by Sigma Aldrich, and glycolide and D,L-lactide were purchased from Polysciences. Hydrochloric acid and phosphate-buffered saline (PBS) were acquired from Thermo Fisher Scientific (Waltham, MA). An isocyanate-terminated prepolymer (22.7% NCO) comprising polyethylene glycol (PEG) end-capped with lysine triisocyanate (LTI) at a 2:1 M ratio of LTI:PEG was supplied by Medtronic (Memphis, TN, USA). Triethylene diamine was purchased from Evonik (TEGOAMIN 33, Hopewell, VA, USA). Polyester triol of 900 Da was synthesized with a backbone comprising 60% ε-caprolactone, 30% glycolide, and 10% D,L-lactide, as previously described [29, 30].

D-Tryptophan hydrochloride (D-Trp HCl)

D-Trp HCl was synthesized, from D-Trp free base (D-Trp FB, as received from vendor) based on previously described methods for the synthesis of vancomycin hydrochloride [18]. A solution of HCl:methanol (1:11) was made. D-Trp FB was mixed into HCl:MeOH solution, 0.2:1 mL, by vortexing. The liquid in the mixture was evaporated by a rotary evaporator, with water bath temperature set at 47°C. The remaining solid D-Trp HCl was dried for 24 h at 40°C under vacuum.

D-AA solubility

Solubility was defined as the maximum amount of each D-AA, D-Trp HCl and D-Trp FB, to completely

dissolve in DI water at room temperature (21.1°C), without qualitative signs of solid D-AA. DI water (3 mL) was mixed in a V-bottom glass vial with a fitting triangular stir bar by a magnetic stir plate. D-AA was added to the water, in increments of 0.01 g, until maximum solubility had been reached.

Table 8.1. Study design of PUR scaffolds, indicating additive and amount included in formulation.

Additive	Loading (wt%)
D-Trp FB	0.1,1,5 and 10
D-Trp HCl	5, 8
D-Trp HCl, +trehalose	8, 5 (respectively)

Synthesis of D-AA augmented polyurethane (PUR) scaffolds

PUR scaffolds augmented with D-AA (D-Trp FB or D-Trp HCl) with or without trehalose (study design outlined in Table 8.1) were fabricated as previously described [1]. The appropriate amounts of each D-AA (Table 8.1) were pre-mixed. The polyester triol, LTI-PEG prepolymer (excess isocyanate 15%), 2.0 parts per hundred parts polyol (pphp) tertiary catalyst, 3.0 pphp water, 4.0 pphp calcium stearate pore opener, and additive loaded into a 20 ml cup and mixed for 1 min using a Hauschild SpeedMixer DAC 150 FVZ-K vortex mixer (FlackTek). The reactive mixture was allowed to cure and foam at room temperature for 24 h.

D-AA release kinetics

D-AA release kinetics from PUR scaffolds (0.5 g batch) was determined in the same fashion as previously described [1]. Cured PUR scaffolds augmented with D-AA were incubated in PBS, under rotating motion at 37°C for up to 2 weeks. The medium was sampled at various time points, at which time 53% (10 mL of total 19 mL) of medium was removed and replaced with fresh PBS, and analyzed for D-AAs by high-

performance liquid chromatography (HPLC) using a system equipped with a Waters 1525 binary pump and a 2487 Dual-Absorbance Detector at 200 nm. Samples of released D-AAs were eluted through an Atlantis HILIC Silica column (5 mm particle size, 4.6 mm diameter x 250 mm length) using an isocratic mobile phase flowing at 1 mL/min. The mobile phase contained 2.5 mM potassium dihydrogen phosphate with pH 2.85 (A) and Acetonitrile (B) at a ratio of A25:B75. The column oven temperature was maintained at 30°C. Sample concentration was determined in reference to an external standard curve using the Waters Breeze system.

Results

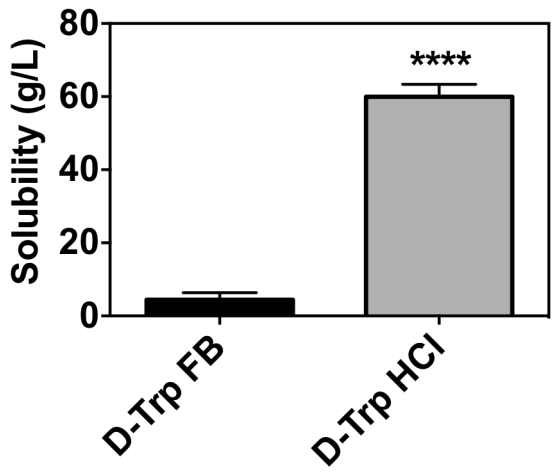

Figure 8.1. Solubility of D-Tryptophan free base (D-Trp FB) and D-Tryptophan hydrochloride (D-Trp HCl) in DI water at 21.1°C. **** indicates $p < 0.0001$.

The solubility of two D-Tryptophan forms, free base and hydrochloride, were determined for water (Figure 8.1). D-Trp HCl was significantly more water soluble than the free base form, with each having a solubility of 4.4 ± 1.9 g/L and 60.0 ± 3.3 g/L, respectively.

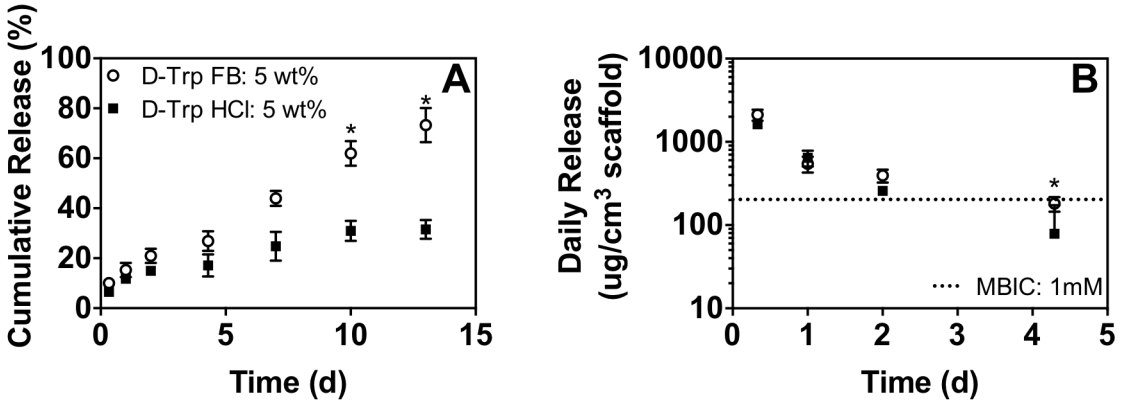

Figure 8.2. *In vitro* release of D-Tryptophan free base (D-Trp FB) or D-Tryptophan hydrochloride (D-Trp HCl) from augmented PUR scaffold (5 wt% of total scaffold mass). (A) Cumulative % release (% of initial loading) of indicated D-AA (symbols) versus time. (B) Daily release of indicated D-AA (symbols, same as A) versus time. For both plots: mean plotted (n=3) ± standard deviation. * indicates $p<0.002$. Minimum biofilm inhibitory concentration (MBIC) set at 1 mM or 204 μg/cm^3, based on previous results [7].

D-AAs were released into PBS from PUR scaffolds, augmented with 5 wt% D-Trp FB or D-Trp HCl, over a two week period. Based on the cumulative release percentage, D-Trp FB and D-Trp HCl showed similar release kinetics at time points <10d (Figure 8.2A). At day 10 and 12, the cumulative release of scaffold with D-Trp FB was significantly higher than the D-Trp HCL scaffold. The cumulative release of D-Trp HCl began to remain steady after 10 days in PBS, plateauing at ~30%, where as the cumulative release of D-Trp FB continued a near linear release profile throughout the entire 14 day period. Although the % cumulative release was not different before 10d, the daily release amount from the D-Trp FB scaffold was significantly more than the D-Trp HCL scaffold after 4d (Figure 8.2B). Despite this difference, there was minimal difference between the daily release of the two D-Trp forms before 4d when both D-AAs had a daily release above the minimum biofilm inhibitory concentration (MBIC).

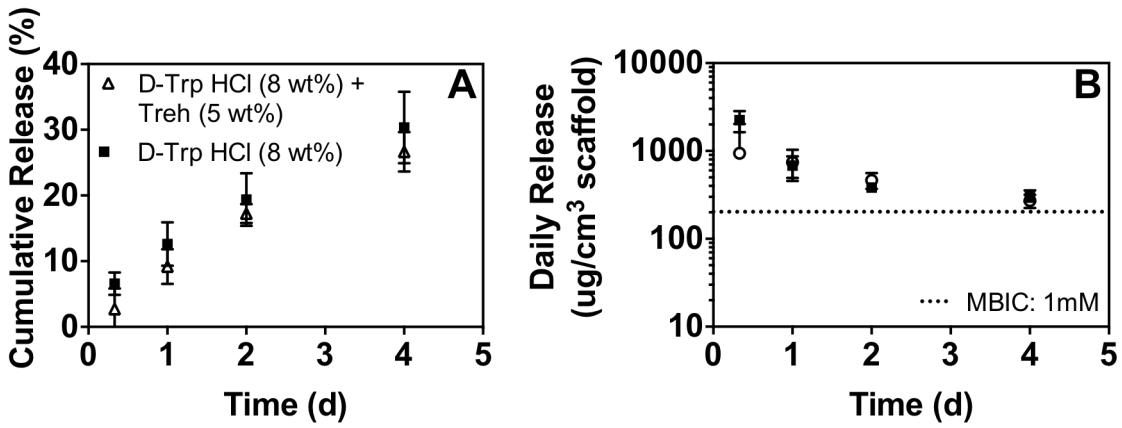

Figure 8.3. *In vitro* release of D-Tryptophan hydrochloride (D-Trp HCl) (8 wt% of total scaffold mass) with or without trehalose (5 wt% of total PUR mass) from augmented PUR scaffold. (A) Cumulative % release (% of initial loading) of indicated D-AA group (symbols) versus time. (B) Daily release of indicated D-AA group (symbols, same as A) versus time. For both plots: mean plotted (n=3) ± standard deviation. Minimum biofilm inhibitory concentration (MBIC) set at 1 mM or 204 μg/cm^3, based on previous results [1].

D-Trp HCL was released into PBS from PUR scaffolds, augmented with 8 wt% D-Trp HCl, with or without an additional 5 wt% trehalose, over a five day period. Based on the cumulative release percentage, no difference was seen between the releases of D-Trp HCL from the PUR scaffolds at any time point (Figure 8.3A). Similarly, the daily release amount of D-Trp HCL was not significantly different between the two groups at any time point (Figure 8.3B).

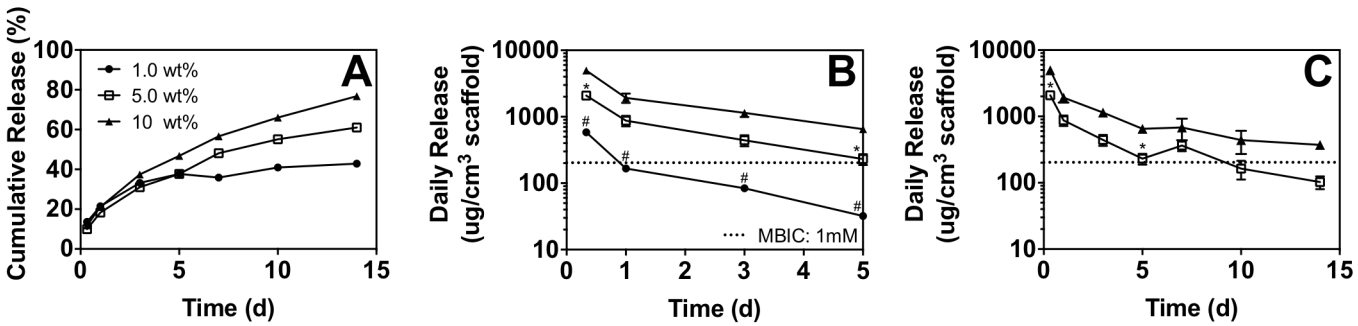

Figure 8.4. *In vitro* release of various loadings amounts (1-10 wt% of total scaffold mass) of D-Tryptophan free base (D-Trp FB) from augmented PUR scaffold. (A) Cumulative % release (% of initial loading) of indicated D-Trp FB loading (symbols) versus time. (B) Daily release of indicated D-Trp FB loading (symbols, same as A) versus time (0-5 d). (C) Daily release of 5 and 10 wt% D-Trp FB (symbols, same as A) versus time (0-15 d). For all plots: mean plotted (n=3) ± standard deviation. Minimum bactericidal concentration (MBC) set at 1 mM or 204 μg/cm^3, based on previous results [1].

D-Trp FB was released into PBS from PUR scaffolds, augmented with 1-10 wt% D-Trp FB, over a 14 day period. The shapes of the % cumulative release profiles were similar, particularly before 5d. By 14d, scaffolds loaded with 1 wt%, 5 wt%, and 10 wt% D-Trp FB released 42.9%, 61.0%, and 76.7% of their initial loading, respectively (Figure 8.4A). Despite similarly shaped curves and cumulative release percentages, the daily release profiles showed differences before day 5 (Figure 8.4B). At each time point, the daily release from the 1 wt% scaffold was significantly less than the 10 wt%. The 5 wt% and 10 wt% scaffolds' daily release remained above the MBIC for the first 7 days of incubation, and at 1/3 day and 5d time points the daily release from the 10 wt% scaffold was significantly more than the 5 wt% scaffold (Figure 8.4C).

Discussion

D-AAs have been investigated as biofilm-dispersal and -preventative agents against several bacterial biofilm species, include *S. aureus.* In recent studies, MBIC have been determined for various specific D-AAs, which are in the range of 1 mM [1]. Lysine derived, biodegradable polyurethane-based materials have been extensively investigated for tissue engineering applications, particularly those related to bone remodeling.

Recently, we utilized PUR biomaterials for the delivery of D-AAs to contaminated and healthy bone defects, both in small and large animals, respectively [1]. Although the effect of specific D-AA on cumulative release profile was characterized, the release profile of D-AAs in relation to targeted MBIC dosage and potential durations was not. In the current study, we hypothesized that D-AA release kinetics could be tailored to fit various release profiles by increasing the water solubility of the D-AA, adding excipients, or altering the initial loading concentration of D-AAs in the PUR scaffold. We chose to focus on releasing one D-AA, D-Trp, due to varying burst profiles[1] as well as dispersal potencies of different D-AAs [32].

The time course of characterized release kinetics paralleled our hypothesis that maintaining a dosage above MBIC for the initial days (<5 days) after implantation or incubation is vital to preventing biofilm formation, both over short and long time (>14 days) courses. Additionally, characterizing early time points prevents PUR degradation at later times from altering the characterized release from the scaffold. Consequently, release studies were not conducted beyond 14 days and the ability to tailor the kinetics of released D-Trp from PUR scaffolds at these time points were not investigated. Discrepancies comparing effects between these time periods were observed. The cumulative release of D-Trp HCl was significantly higher than D-Trp FB after >10 days in PBS, but their daily release before this time point did not show significant differences. Future studies should be done to characterize the release profiles of various loadings of D-Trp HCl and FB in PUR scaffolds, as these results may show significant differences in the amount released daily over short and long time spans.

The effect of hydrophobicity of D-AAs on their release from polymer materials has not conclusively been determined. Previously it was shown that the order of cumulative release for D-AAs (10 wt%) independently released, from the same PUR scaffold that was used in the current study, was D-Methionine (D-Met) > D-Proline (D-Pro) > D-Trp [1]. This order holds true for the initial (<2d) burst release, where approximately 75%, 55%, and 30%, respectively, of the initial loading was released, as well as the sustained release (>14d). The order of solubility for these D-AAs was D-Pro >> D-Met > D-Trp [33]. Even though the

solubility of D-Pro >> D-Met, the resultant cumulative release of these D-AAs from the PUR scaffold did not parallel this property, but the increased solubility of D-Met compared to D-Trp parallels the cumulative released order. Similarly, in the current study, increased solubility (Figure 8.1) decreased the sustained release of D-Trp (5 wt%) (Figure 8.2). From these two studies, it appears hydrophobicity is not a dominant factor that can predict the release kinetics of D-AAs from PUR scaffolds as it has been used in other systems [17, 18].

Trehalose, a naturally derived alpha-linked disaccharide, has been used to stabilize peptides and proteins for encapsulation and alter the release kinetics of proteins from various delivery systems [20, 34-36]. In this study, trehalose was mixed into the non-cured PUR precursors and thus physically entrapped within the formed PUR mesh network. Adding trehalose as an excipient to the PUR scaffold in this fashion did not alter the amount or the release kinetics of D-Trp (Figure 8.3). In previous studies, trehalose was co-lyophilized with the delivered drug via a water solution [20, 37, 38]. This co-lyophilization technique has been shown to increase the size of the burst [38] in some studies, and in other studies increase the sustained release but not the burst size [20]. Trehalose, and any drug in close proximity to this excipient, may potentially be released from polymer systems by an osmotic pressure gradient [27, 37-39].

An increase in particle loading within a delivery vehicle increases the potential amount of drug released at any given time. In the current study, this theory was supported as an increased loading from 1 wt% to 10 wt% D-Trp increased the daily release (Figure 8.4B). Increasing the initial loading also increased the initial burst release and the sustained % cumulative release (Figure 8.4A), as was shown previously [40]. A significant number of previous studies focused on release from monolithic materials have also shown that increasing the drug loading increased the initial burst, which was theorized to be a result of increased particles dispersed on the surface of the polymer matrix immediately exposed to physiological fluid [20, 41, 42]. Base on this theory, in the current study the increased loading would significantly increase D-AAs exposed on PUR surface due to high volumetric porosity, and thus increase burst release [1].

Theories developed and explained in terms of the percolation theory for the release of particles from monolithic materials may provide insight to why the techniques do or do not affect the release of D-AAs from a PUR scaffold. In a monolithic system, drug particles are releasable if they are connected to a pore that leads to the surface[41] and the total fraction released by diffusion is dependent on the volumetric drug loading. Above a critical loading, the fraction of initially loaded particles can be released rapidly. In effect, the particle loading in the PUR scaffold is always above the critical loading of monolithic PUR because of the porosity. Thus, increasing the D-AA's hydrophobicity or adding an excipient may not have significantly changed the release kinetics of the loaded D-AAs. In a monolithic system, the total amount of drug released comprises the fraction released by osmotic rupturing of the polymer (F_{II}) and the fraction released by diffusion and dissolution (F_D). Since the augment PUR scaffolds in this study had a porosity of nearly 90%[1], it is hypothesized that the majority of D-AAs released were from F_D. Co-lyophilizing D-AAs with trehalose may prevent D-AAs from immediately being released from exposed PUR surface at pore walls and relased by $F_{D,}$ and thus significantly delay the release of a portion of the initially loaded D-AAs by releasing from F_{II}.

Additional *in vitro* release studies may provide insight to the exact mechanism of release and how it can be better tailored. It would be advantageous to visualize where D-AAs are being released from within a PUR-based material. Similarly, conducting a release study from monolithic PUR molds may answer the previous questions posed related to D-AAs released from the polymer surface versus those embedded in the PUR network. Most importantly, there have been concerns in the controlled release field with *in vitro* release studies due to the lack of correlation between *in vitro* and *in vivo* release profiles [26, 43, 44]. Therefore, in the future, testing materials with various release profiles of D-AAs in a contaminated model will need to be evaluated before fully accepting that the previous *in vitro* release studies accurately model the *in vivo* kinetics.

Conclusions

Porous biodegradable polyurethane scaffolds have been shown to support tunable release of D-amino acids *in vitro*. The burst release of D-Tryptophan freebase, and subsequent time above a projected minimal biofilm inhibitory concentration, were increased when the initial loading was increased. Therefore, PUR scaffolds augmented with D-AAs can be tailored to meet future optimal dosing profiles of the local delivery of biofilm dispersing D-AAs.

SURFACE POLYMERIZATION OF ε-CAPROLACTONE WITHOUT A SILANE COUPLING AGENT

As outlined in the discussion section of Chapter IV, the presence of grafted silane (and additional PCL) molecules to the BG surface delays the nucleation of HCA, and thus the overall bioactivity of the material. The HCA nucleation was delayed 1 day *in vitro*, but this is not an absolute timeline that will necessarily correlate to a 1 day delay *in vivo*. Since we (the Guelcher Lab) view HCA nucleation as an indicator of the presence of surface bioactivity rather than the ability for bone to physically bind to the BG particles (although this may be an additional benefit for the BG/PUR composite in direct contact with native bone), I do not believe the actual delay of HCA nucleation is a deterrent. But, this delay indicates that ions from the BG surface are not being released into the local environment at the same initial rate as those on the surface of unmodified BG. The ions released from bioactive glass have been shown to create a local micro-environment, or in many ways a niche, that is conducive to cellular activity related to bone remodeling and growth [45]. From this perspective, BG as a solid particle can more accurately be thought of as a delivery vehicle for these ions. Consequently, preventing the timely delivery and release of these ions to a bone defect will delay formation of this environment and potentially the delay of bone remodeling and growth.

As described in Chapter IV, a previous study showed the ability to attach oligo(lactones) (specifically L-lactide and ε-caprolactone) to activated tricalcium phosphate (TCP) filler particles at 150°C without any additional catalysts or the use of a silane coupling agent [46]. The grafting of ε-caprolactone to the BG surface without a silane-coupling agent may prevent the delay of the surface reaction, which releases desired ions. It is important to understand if the presence of PCL chains alone delays HCA nucleation for a mechanistic understanding of the surface reaction between the BG and surrounding physiological fluid. Similarly, for the purposes of this research project, it is necessary to validate that this surface modification technique will result in surface-modified particles that increases the overall resultant mechanical properties of the BG/PUR composite in which it would be utilized. The ultimate goal of the project is to develop a synthetic graft that can bear weight

at early time points after implantation. If this surface modification technique can not aid in meeting this goal it should not be implemented, even if it does not hinder BG bioactivity.

Preliminary work validated (by ellipsometry, atomic force microscopy, and water contact angle) that this technique (surface polymerization of ε-caprolactone at 150°C) can be adapted to modify the surface of silicon oxide wafers under static conditions through the use of a heating block (as done in Chapter IV). Initial attempts to graft PCL to BG disks using this method resulted in the internal fracturing of the BG disks. Further investigation in heated atmospheric air indicated that this was not caused by simply heating the disks to 150°C or from the thermal shock of a rapid change in BG temperature (from room temperature to 150°C). In order to test the rate of HCA nucleation on the BG surface modified with this method, the same size and shaped BG discs must be used for all tested groups. Consequently, any form of fracturing is not acceptable for this study.

Future work should focus on preventing fracture, validating (via X-ray spectroscopy) that PCL chains have grafted to the BG surface, and comparing the rate of HCA nucleation on BG disks surface-modified to corresponding groups with the same two number-average molecular weights (M_n) of PCL grafted from the original silane-dependent method, as done previously. All surface and biomineralization analysis techniques utilized in Chapter IV should be applied to this surface modification group. Additionally, this surface polymerization method must be transferred to the dynamic stirring method in order to modify the surface of BG particles and test their effect on the mechanical properties of resultant PUR biocomposites, as outlined in Chapter V [47]. The M_n can be analyzed by gel permeation chromatography (GPC) and the mechanical properties can be evaluated by quasi-static compression.

BIOMECHANICAL AND HISTOLOGICAL EVALUATION OF POLYURETHANE COMPOSITE GRAFT IN LARGE ANIMAL SHEEP WEIGHT- AND NONWEIGHT-BEARING DEFECT MODELS

Introduction

Experimental models in small animals have shown that cement bone graft substitutes are capable of providing similar structural support and biocompatibility when compared to autogenous bone grafts [11, 48-51]. However, clinical studies in humans and *in vivo* studies in large animals at higher levels of stress have shown that these same cements have inadequate biomechanical properties and frequently fail due to their decreased resiliency and faster resorption than autogenous bone grafting, when combined with poor patient compliance [49, 52-54]. As outlined in Chapters V and VI, we have shown that a polyurethane (PUR) lysine triisocyanate (LTI)-polyethylene glycol (PEG) based composite comprising poly(ε-caprolactone) surface-modified 45S5 bioactive glass particles has initial quasi-static compression and torsion[47] as well as dynamic compressive fatigue properties comparable to native human bone. The ability for this BG/PUR or any PUR/matrix graft to hold weight bearing capacity *in vivo* has not been investigated.

In a previous study, a stringent weight-bearing tibial slot defect model in sheep that evaluated the weight bearing properties of calcium sulfate derivatives was developed [54]. The developed model allowed for mechanical loads and physiologic properties more similar to those seen in humans compared to small animal models. This study found that the bone graft substitutes, which had previously shown adequate mechanical properties in small animals, failed at the higher mechanical loads used in this study that approximated human weights. Additionally, recent studies have highlighted the effects of mechanical loading on the osteoconductivity of biomaterials such as calcium phosphate granule [55]. A mechano-regulating theory has been

applied to bone remodeling driven by biomechanical parameters [56, 57]. Thus, mechanical forces regulate the activities of osteoblasts and osteoclasts during remodeling.

In the currently outlined and future on going study, our goal is to answer two questions: (a) How does mechanical loading affect remodeling of PUR/matrix grafts, and (b) Do PUR/matrix grafts maintain mechanical properties comparable to bone while remodeling in weight-bearing and non-weight-bearing defects? First, the goal of the *in vivo* model development is to reproduce a clinical model in sheep to evaluate weight bearing bone graft substitutes in order to utilize this model for future procedures at the United States Army Institute of Surgical Research (USAISR). Eventually, PUR/matrix grafts will be evaluated in mechanically challenging ovine tibial plateau slot and non weight bearing femoral condyle plug defects. The bilateral sheep defect model enables testing of the same material in both a weight-bearing slot tibial plateau defect and a nonweight bearing femoral condyle plug defect. The plateau slot defect will validate that the grafts support earlier weight bearing compared to CPCs. This model will enable us to answer the question whether PUR/matrix grafts are functionally weight bearing in a stringent preclinical model in which the clinical standard of care (i.e. CPCs) fails [10, 54].

We hypothesize that PUR/matrix composites will exhibit initial mechanical properties exceeding those of trabecular bone, and will maintain mechanical properties comparable to bone during remodeling of the graft in both nonweight bearing and weight bearing defects. In the sheep tibial plateau slot defect, the hydroxyapatite (HA) bone cement (Norian SRS, Synthes) failed mechanically after 5 weeks post-implantation, which was attributed to incomplete cure, brittle fracture, and/or excessive resorption [10, 54]. Due to their favorable bone-like initial mechanical properties and balanced remodeling *in vivo*, PUR/matrix grafts will be functionally weight bearing in the ovine tibial slot defect model, while the CPC standard of care will not. We anticipate that PUR/matrix composites will maintain the mechanical integrity of the defect due to their substantially greater energy-to-failure (toughness), as outlined in Chapter V [47], and their greater fatigue resistance properties as

outlined in Chapter VI, compared to CPCs. We further hypothesize that the rate of remodeling in the weight-bearing defect will be faster than that in the non-weight-bearing defect.

Previous characterization of the mechanical properties of PUR composites conditioned materials in PBS for 24 h before mechanical testing [47, 58, 59]. The goal of the current *in vivo* study is to maintain the initial mechanical properties of the PUR graft composite for an extended period of time (>2 weeks) when implanted *in vivo*. Although degradation of the PUR component should be minimal during short time spans, [60] extended incubation in physiological fluid may affect the interfacial bonding between the BG particles and PUR network. In order to determine the effect of incubation in physiological fluid on the quasi-static compressive mechanical properties of the BG/PUR composite, an *in vitro* longitudinal study was conducted in conjunction with the *in vivo* model development as an iterative investigation and development of the PUR/matrix graft.

Figure 8.5. Image from previous development of non weight bearing femoral condyle plug defect (above) and weight bearing tibial slot defect models in sheep [10].

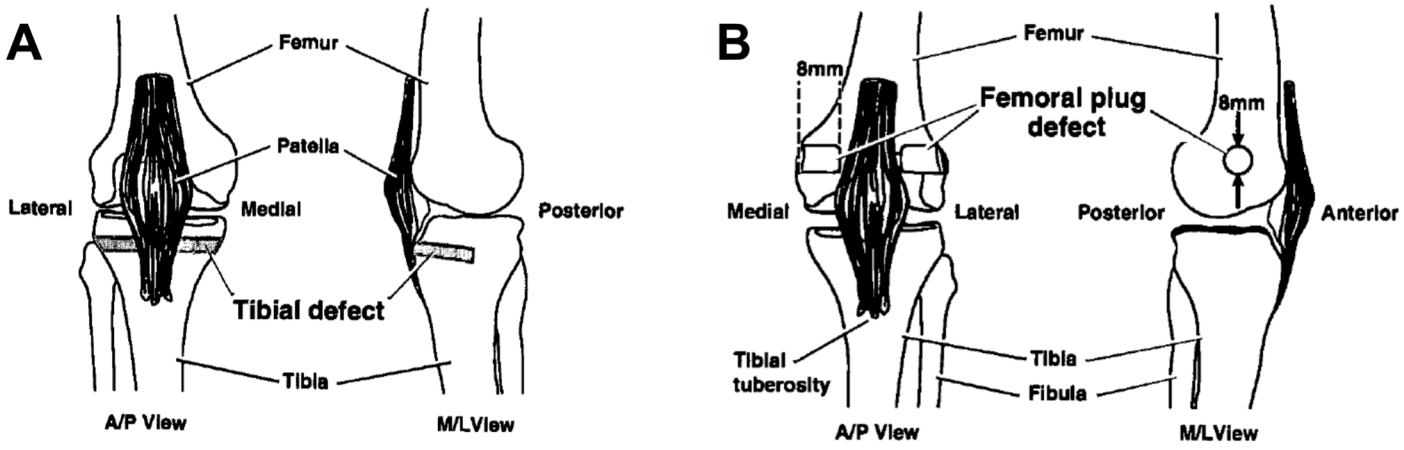

Figure 8.6. Drawing showing the location of (A) slot defect previously created in the proximal part of tibia and (B) plug defect in medial and lateral femoral condyles [11].

Experimental

Methods

In vivo model development

Polyurethane graft composite comprising LTI-PEG, T7C2G1L300, and 24 h polymerized poly(ε-caprolactone) surface-modified 45S5 bioactive glass particles[47] and a commercially available calcium phosphate cement (CPC) (Norian Skeletal Repair System, SRS®) were evaluated in a non weight bearing femoral condyle plug defect and a weight bearing tibial plateau defect model, in sheep. The same lead-candidate BG/PUR formulation[47] outlined in Chapter V was tested, but two changes to the formulation were made. In order to minimize *in vivo* expansion, the relative amounts of lysine triisocyanate (LTI)-polyethylene glycol (PEG) prepolymer and polyester triol (300 Da, backbone comprising 70% ε-caprolactone, 20% glycolide, and 10% $_{D,L}$-lactide (T7C2G1L300) [29, 30] were calculated assuming an isocyanate index of 110 (i.e., 10% excess isocyanate)[30] and a 5 wt% iron acetylacetonate (FeAA) in ε-caprolactone monomer catalyst was used. BG/PUR

composite was sterilized as previously described [47], whereas Norian SRS cement came pre-sterilized by manufacturer.

Two skeletally mature (1.2-3 years) female sheep *(Ovis aries)*, weighing 57-62 Kg were used in the first trial of model development. The foundational surgical protocol was outlined by the principal investigator (David J. Tennent, CPT, MD) in protocol A-14-036 (US AISR). Bilateral posterial tibia and femur defects were prepared, as previously developed (Figure 8.5)[10, 11]. Under general anesthesia, each limb was shaved, aseptically prepped with a series of betadine and alcohol, and draped. Two separate bony defects were prepared in each posterior extremity under tourniquet. Two 8mm circumference by 16mm depth defects were created using a trephine on the medial and lateral distal femoral condyles of each posterior extremity (Figure 8.6). This represented a protected, non weight bearing corticocancellous region to evaluate resorption properties and mechanical integrity in a protected region of bone as a control. For the tibial defect, a single slot defect measuring 6mm high and to a depth of approximately 50% of the total anterior to posterior tibial depth was created proximal to the patella tendon underneath the tibial plateau (Figure 8.6). This defect represents a region of high mechanical stresses that are more akin to those seen in a clinical tibial plateau depressed fracture.

Each of these defects was then filled with one of two bone cements, Norian SRS or BG/PUR composite, prepared separately per manufacturing guidelines. The bony defects were dried with thrombin gauze, to provide additional hemostasis, and the cement was placed into each of the defects (in the following order: tibial slot defect, lateral femoral condyle, then medial femoral condyle), and allowed to harden for approximately 5-10 minutes post-mixing. Each animal will have both cements in separate extremities. The placement of bone graft substitutes in each extremity was alternated so that one had Norian SRS in the right posterior extremity and one had BG/PUR cement in the right posterior extremity.

Immediately following surgery, post-op radiographs and computed tomography (CT) scans were taken. The animals remained in a sling for one-week post operatively and then were transitioned to weight bearing as

tolerated. The primary outcomes for this pilot study included the ability for animal to tolerate procedure and recovery as well as implanted material's ability to maintain structural integrity during two week period. Two weeks following the surgery, the study development animals were euthanized, radiographs were performed and CT was obtained to evaluate early construct failure and/or animal harm prior to initiating our full trial.

Longitudinal in vitro incubation quasi-static compressive mechanical testing

Polyurethane graft composite comprising either 24 h polymerized poly(ε-caprolactone) surface-modified 45S5 bioactive glass particles or unmodified, cleaned (U-) MASTERGRAFT® Mini Granules (MG) were fabricated for quasi-static compressive mechanical testing, as before [47]. The same base lead-candidate BG/PUR formulation[47] outlined in Chapter V was tested, but various changes to the formulation were made. The relative amounts of isocyanate (from LTI-PEG or LTI) and polyester triol (300 Da, backbone comprising 70% ε-caprolactone, 20% glycolide, and 10% $_{D,L}$-lactide (T7C2G1L300) or 100% ε-caprolactone (PCL300)) were calculated assuming an isocyanate index of 110-160[30] and a 5 wt% iron acetylacetonate (FeAA) in ε-caprolactone monomer catalyst was used. Cylindrical specimens (6 x 12 mm) samples were prepared and compressive mechanical testing was conducted using an MTS 858 Bionix Servohydraulic Test System, as previously described [47]. Composites were conditioned in phosphate buffer solution (PBS) at 37°C for various time points, exceeding 24 h, in order to determine the effect of incubation in physiological fluid on the compressive mechanical properties of the composite. The change in mass and volume of the composites, after PBS conditioning, were measured and correlated to water absorption and swelling. Composites were pre-loaded to approximately 12 N followed by continuous compression until failure at a rate of 25 mm min^{-1}. The load and position were recorded every 0.01 s. The compressive stress was calculated by dividing the load by the cross sectional area of the samples post-hydration. Compressive modulus (E) was calculated as the slope of the initial linear section of the stress-strain curve, compressive strength (σ) as the maximum stress achieved, and

compressive ultimate yield strain (*UYS*) as the strain at the compressive strength.

Table 8.2. Study design for longitudinal incubation mechanical testing.

Isocyanate source	Polyol	Index	Solid Filler	Volume % Filler	Time pt (days)	Abbreviation	Figure
LTI-PEG	T7C2G1L300	120	PCL-BG	57	0, 3, 6	LTI-PEG 120	7.8
LTI	T7C2G1L300	120	PCL-BG	57	0, 3, 6	LTI 120	7.8
LTI-PEG	T7C2G1L300	120	U-MG	30	1, 2, 3, 6	U-MG/LTI-PEG	7.9
LTI	T7C2G1L300	140	PCL-BG	45	3	140-7C300	7.10
LTI	PCL300	140	PCL-BG	45	3	140-PCL300	7.10
LTI	PCL300	140	PCL-BG	57	3, 6	LTI 140	7.11

Preliminary Results and Discussion

Detailed observations were made throughout the surgical procedures. Both animals tolerated the procedures well without immediate complications. All materials appeared to have set prior to closing with adequate gross mechanical strength. The exposed surfaces of all implanted materials cured and hardened in the appropriate time period. Overexpansion was not noted for any of the BG/PUR composites or CPC cement.

Animals tolerated the slings reasonably well, although one sheep developed a pressure sore under the front right forelimb that required it being taken out of the sling 3 days early. Both animals were able to ambulate independently with adequate pain control. The following week proceeded uneventfully with both animals being able to weight bear independently at the end of two weeks prior to the end of the model development study period.

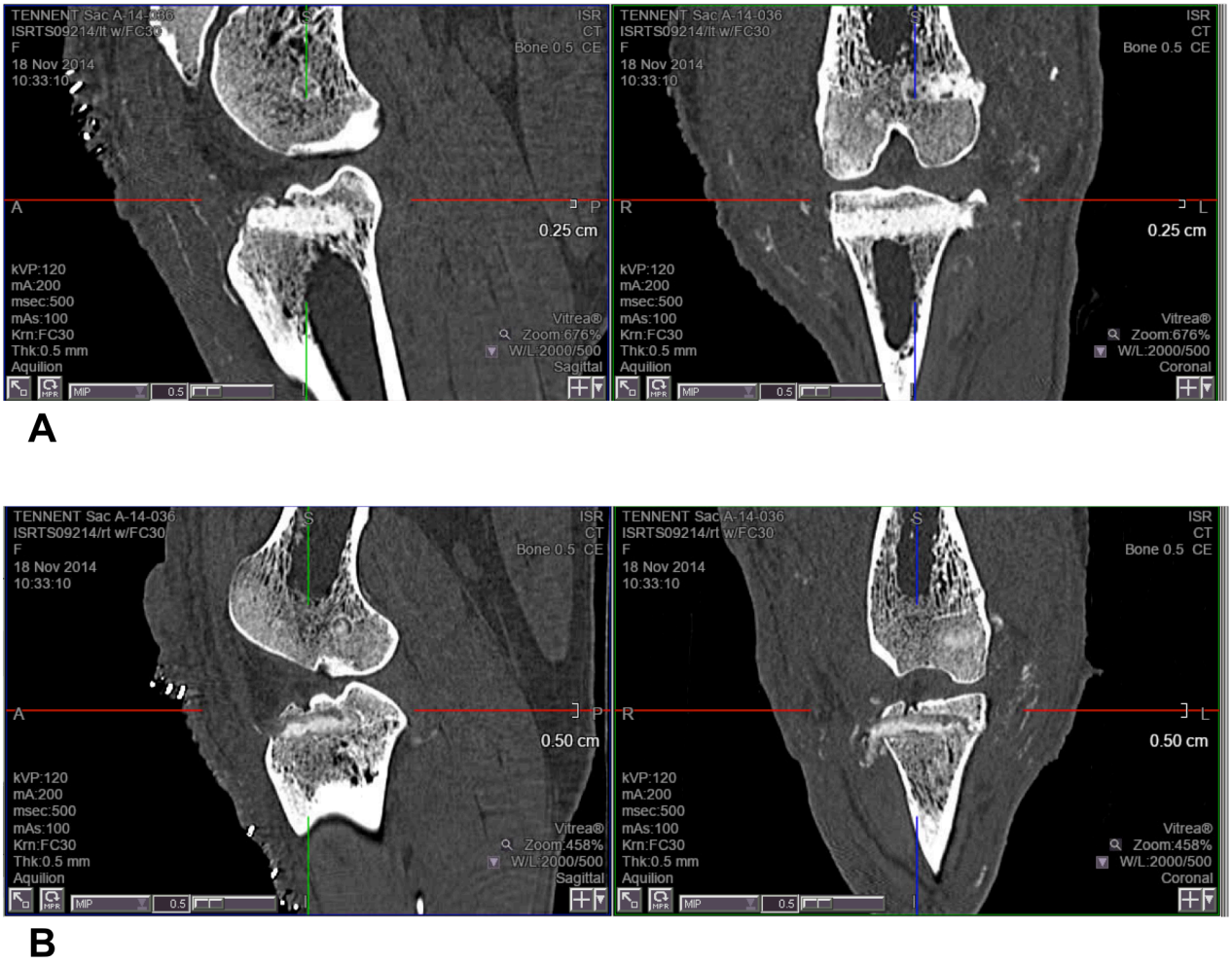

Figure 8.7. Images from CT scans taken 2 weeks post implantation for defects filled with (A) Norian SRS and (B) BG/PUR composite, show femoral condyle plug defects (above) and tibial slot defects (below).

On post-mortem examination, it appeared the properties of the implanted materials changed over the two week period. BG/PUR composite filled the defect fully, however, it appeared soft, gritty with a spongy consistency and was easily penetrated with a scalpel, both at the exposed surface as well as inside all (both weight and non weight bearing) defects. The BG/PUR appeared to be less dense than Norian overall with questionable central impaction. The Norian maintained its integrity and remained hard grossly. Imaging showed an anterior fracture of all plateaus at an angle consistent with anterior loading while standing or direct impact on the ground when on all fours (Figure 8.7). For the Norian-filled defects, no critical failure of the plateau was identified, although some failure of the anterior tibia plateau was noted. Overall, with mild modifications, it

appears we had a viable model that can be changed slightly to alter the amount of stress provided to a study material. The animals tolerated the procedure well. Some concerns over the integrity of the PUR at two weeks were noted.

Longitudinal in vitro incubation mechanical testing

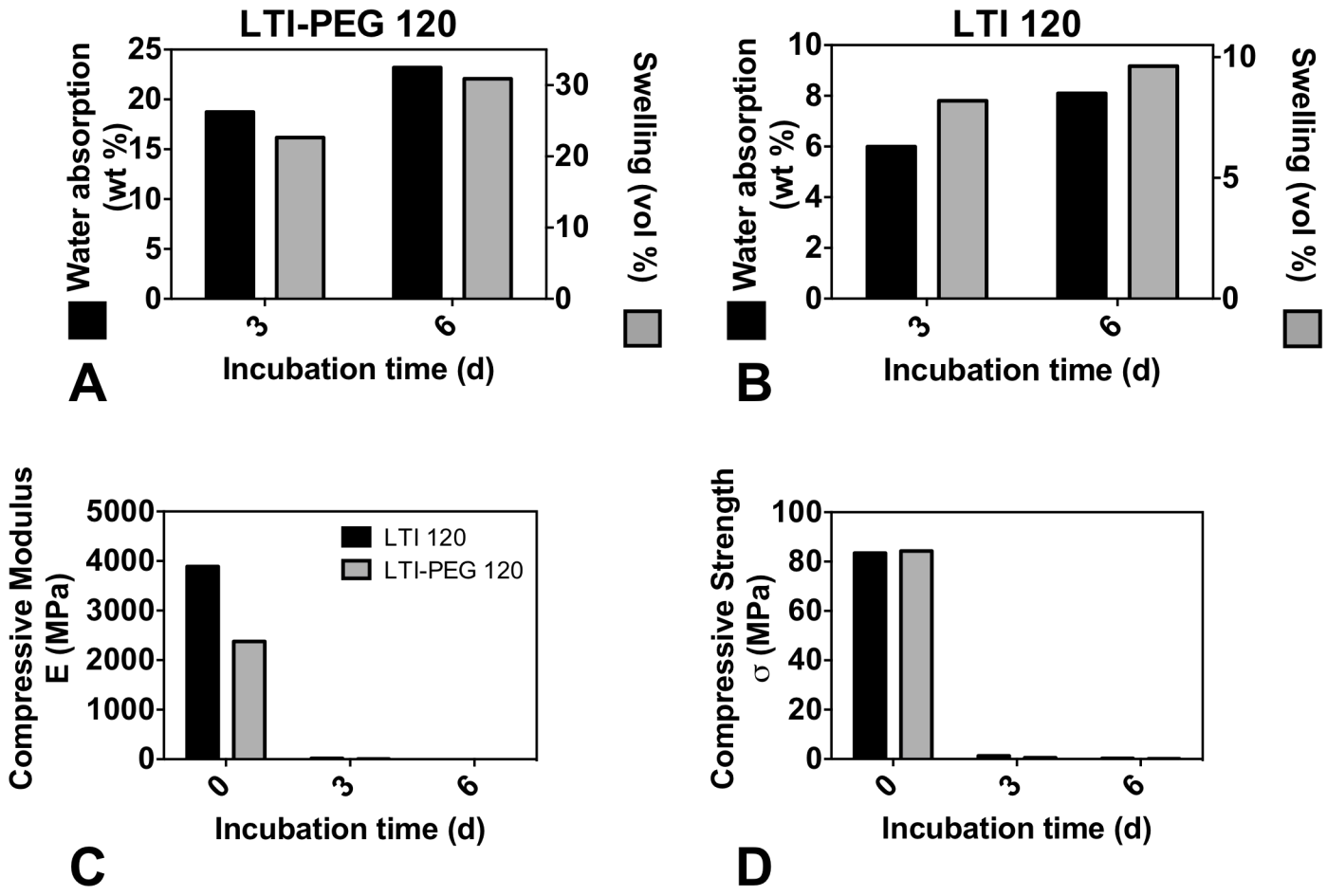

Figure 8.8. Post-incubation swelling and water absorption properties for (A) LTI-PEG 120 and (B) LTI 120 composites, both made with PCL-modified BG at 57 vol% and T7C2G1L300 polyol. Also, quasi-static compression properties, including (C) compressive modulus and (D) compressive strength. Values reported from one sample at each incubation time point.

After incubation for up to 6 days in PBS, the overall volumetric swelling (vol %) and change in mass (water absorption, wt %) of the composites with either LTI or LTI-PEG at an index of 120 were measured (Figure 8.8A and B). The composite made with LTI-PEG had more water absorption and swelling after both 3 and 6 days. The quasi-static compression properties of LTI 120 and LTI-PEG 120 composites were also determined (Figure 8.8C and D). At day 0 (not incubated in PBS), LTI 120 had a higher modulus than LTI-PEG 120, but the compressive strengths were nearly identical. After at least 3 days incubated in PBS, both composites lost all mechanical integrity, as shown by extremely low compressive moduli and strengths. Despite absorbing less water and swelling less, LTI 120 did not maintain mechanical properties any better than LTI-PEG 120.

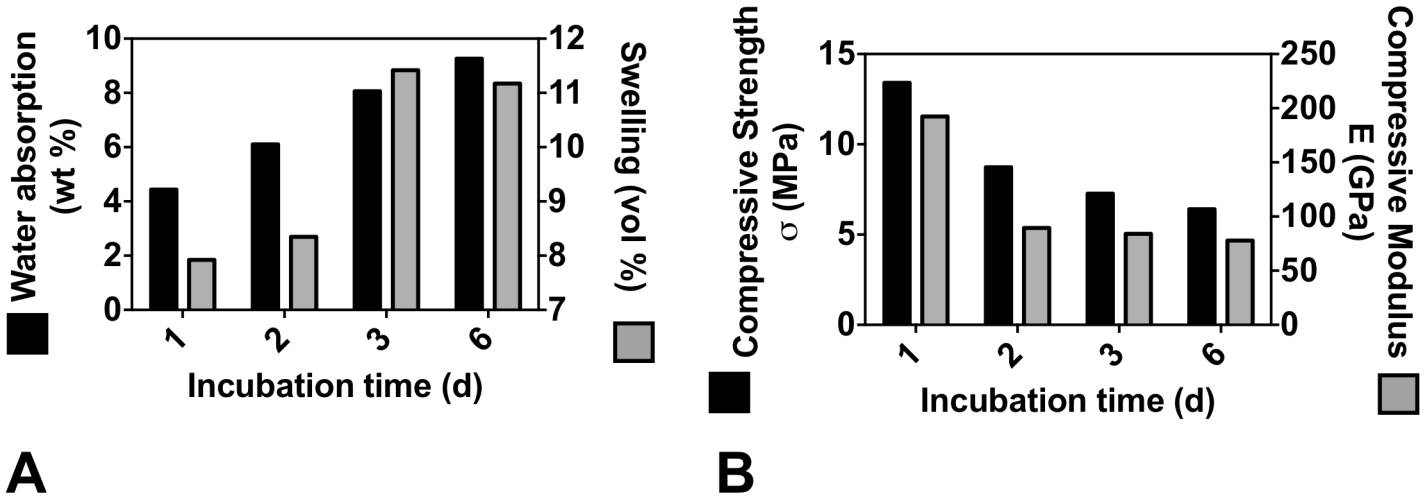

Figure 8.9. Post-incubation (A) swelling and water absorption properties as well as (B) quasi-static compression properties of U-MG/PUR composites fabricated with LTI-PEG and T7C2G1L300 polyol, at an index=120. Values reported from one sample at each incubation time point.

In the same fashion, the overall volumetric swelling (vol %) and change in mass (water absorption, wt %) of the composites made with U-MG/LTI-PEG and an index of 120 were measured (Figure 8.9A). An additional 5 days of incubation increased the U-MG/LTI-PEG composite swelling and water absorption each by only ~4%. Compared to LTI-PEG 120 (which had a PCL-BG filler), U-MG/LTI-PEG appeared to have

absorbed less water and swelled less after at least 3 days incubation. The quasi-static compression properties of U-MG/LTI-PEG composites were also determined (Figure 8.9B). After 6 days of incubation, the U-MG/LTI-PEG composites maintained ~33% of their initial strength. This was a higher percentage of the initial mechanical properties (1 day incubation) of the composite compared to those made with surface-modified BG (Figure 8.8C and D), although the initial properties are significantly less. It appeared that decreasing the amount of water absorption, and thus swelling, may have prevented a loss of mechanical properties. Additionally, these results suggest that the composite with MG better prevented water absorption than those made with BG. The compressive modulus and strength (192 MPa and 13.4 MPa, respectively) were approximately 25-45% of those of composites made previously with the same isocyanate and polyol source (but at index=140) and U-BG (approximately 750 MPa and 30 MPa, respectively) after one day of incubation in PBS. The lower initial mechanical properties of U-MG/LTI-PEG compared to U-BG/PUR composites are presumably due to the lower strength of MG filler, which may be caused by MG's highly meso-porous structure. Alternatively, BG particles are fabricated by a melt-derived process and thus have no pores.

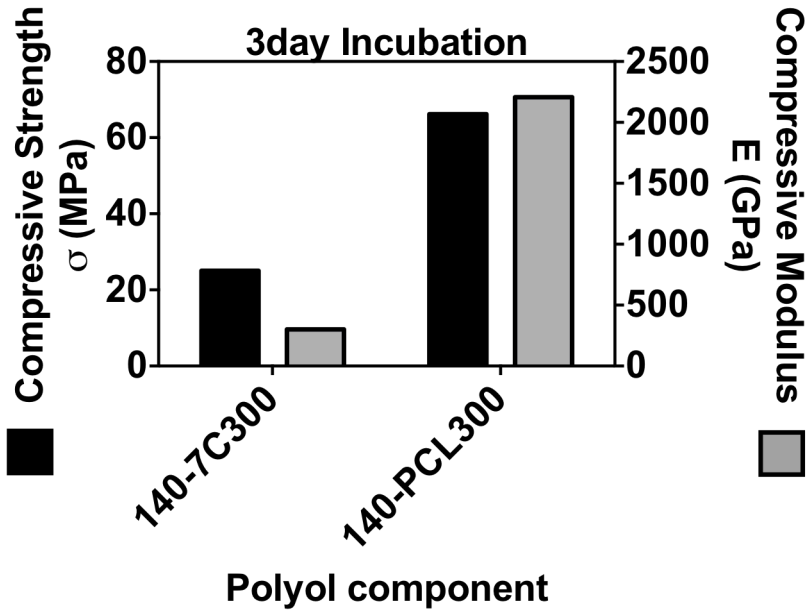

Figure 8.10. Post-incubation (3 days) quasi-static compression properties of PCL-BG/PUR composites fabricated with LTI and either PCL300 or T7C2G1L300 polyol, at an index=140. Values reported from one sample at each incubation time point.

In comparing the quasi-static compression mechanical properties of LTI-based composites (index=140), those fabricated with the PCL300 (100% caprolactone) polyol (140-PCL300) had a higher modulus and strength than those fabricated with the T7C2G1L300 polyol (140-7C300) (Figure 8.10), after 3 days of incubation in PBS. It should be noted that the purity of these polyols may not be equal as PCL300 was purchased from Sigma Aldrich and the T7C2G1L300 polyol was made in the Guelcher laboratory [29, 31]. Previously it was shown that LTI-based scaffolds comprising a polyol component with 60% caprolactone degraded faster (~10 days) *in vitro* than those with 70% caprolactone [60]. Although polymer degradation should not occur within the first three days of aqueous incubation, the increased hydrophobicity of a 100% caprolactone polyol component (compared to 70%) may affect the ability for a composite to maintain interfacial bonding between BG parrticles and PUR by inhibiting infiltration of water, and thus maintain its mechanical properties over a period of time.

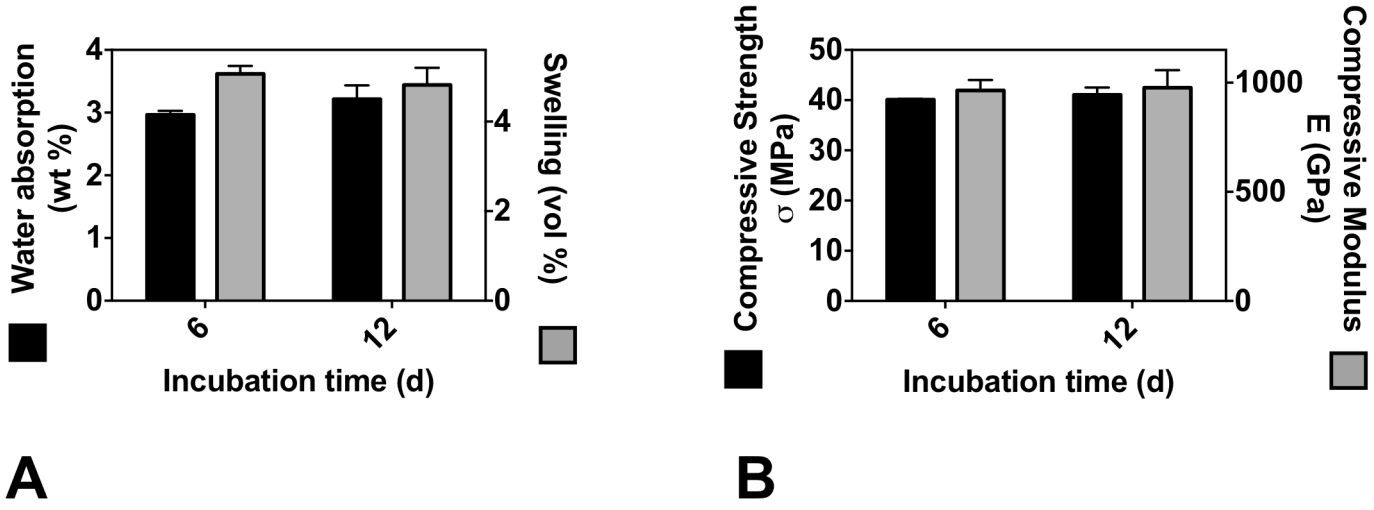

Figure 8.11. Post-incubation (A) swelling and water absorption properties as well as (B) quasi-static compression properties of PCL-BG/PUR composites fabricated with LTI and PCL300 polyol, at an index=140 (LTI-140). Values reported from one sample at each incubation time point.

The lead-candidate composite, LTI-140, comprising LTI isocyanate, PCL300 polyol (index=140), and 57 vol% PCL-BG (Table 8.2) was incubated in PBS for up to 12 days. There was no significant difference between the composites incubated for 6 and 12 days, with respect to their water absorption and swelling vol% (Figure 8.11A). Similarly, there was no difference between 6 and 12 day time points with respect to their quasi-static compression mechanical properties (Figure 8.11B). Although the mechanical properties are ~60% of the LTI-140's initial (incubated for 1d) compressive properties, this is the highest maintained fraction of a composite's strength over the longest incubation period out of any formulation characterized. More importantly, after 12 days in PBS, the compressive modulus and strength still exceeded those of native human trabecular bone [61].

Although some of these results are from studies with a single representative group at each time point (n=1), some trends began to show. First, the presence of the polyethylene glycol (PEG) in the prepolymer isocyanate source (LTI-PEG) increased the resultant composite's water absorption and swelling (Figure 8.8A

and B). This is a logical result from including this neutral, generally hydrophilic polyether [62, 63]. In order to prevent substantial water absorption and the correlated swelling, isocyanate sources with a PEG component should be avoided. Composites made with LTI alone showed the ability to maintain mechanical properties after incubation in PBS for a up to 12 days (Figure 8.11). Thus, LTI may be an appropriate isocyanate source in the future, although safety concerns related to utlizing a monomer in this fashion must be investigated. Alternatively, the potential to replace the PEG component with a more hydrophobic polymer chain or a cell-degradable poly(thioketal)-based[64] component could provide additional positive attributes, while preserving the higher viscosity (than LTI monomer) of the prepolymer precursor, which provide desired handling properties.

Secondly, it appeared that composites with a stoichiometric index <140 lost their mechanical integrity after <3 days in PBS. It is hypothesized that a portion of the available isocyanate reactive groups within the pre-cured composite quickly reacted with water in the local environment [65], and thus decreased the overall effective index and isocyanates available to react with hydroxyl groups needed to form the polyurethane network. Consequently, the resultant PUR network may have had a substantial number of unreacted hydroxyl groups or a large sol content, and thus potentially a larger mesh size than anticipated for a corresponding polyol molecular weight [66], decreased interfacial adhesion with surface molecules on solid fillers [47], and thus decreased overall mechanical properties. Previous studies showed that in poly(ester-urethane) networks comprising L-lysine diisocyanate (LDI) and polyester triols the index with the least sol content was 105 [67]. The optimized index for triisocyanates is likely higher due to a higher functionality (of three) and consequently less effective mobility of the isocyanate functional groups to physically match free hydroxyls. Additionally, in the previous LDI study, when the index was set below 100 the sol content rose to >10% (up to 25% at index=95), whereas when the index was >120 the sol content never surpassed 10%. It is my suggestion that more detailed studies be conducted to characterize the effect of the stoichiometric index on the curing profile of LTI-based PUR

materials, the resultant PUR mesh size and sol content, and that future formulations for high viscosity, low porosity, PUR graft composites should be indexed ≥140.

There are several other variables within this weight bearing PUR graft system that can be investigated and optimized to achieve the desired goals. Melt-derived 45S5 bioactive glass has been the lead-candidate filler within this system for some time. Similarly to the meso-porous MG, attempts to incorporate sol-gel BG did not improve the overall mechanical properties of the composite. Other formulations of melt-derived bioactive glass, such as silicate 13-93 or borosilicate 13-93B1 [68], may possess appealing attributes that could change the overall remodeling capability and mechanical properties of the graft [69]. For instance, if it is observed that resorption gaps are present at late time points in future large animal *in vivo* models, a slower degrading bioactive glass may solve this potential problem. Collaboration with one of many research laboratories that are dedicated to the development of bioactive glasses, such as Dr. Aldo R. Boccaccini's, may be fruitful. Additionally, incorporation of meso-porous fillers, like MG, may prevent water absorption and swelling during the first phases of solution incubation. In order for this type of filler to be viable in this system, the initial mechanical properties of resultant composites must be increased. This may be achieved through surface modification with silane coupling agents [70]. Similarly, a low viscosity isocyanate source (such as LTI) may be able to penetrate MG's mesoporous structure and further improve the adhesion between MG and PUR, compared to a high viscosity isocyanate source (such as LTI-PEG) that can not penetrate this structure. Although composites made with this surface-modified filler alone may not possess initial mechanical properties strong enough for weight bearing applications, a portion of the total filler content could be mixed with melt-derived bioactive glasses in order to benefit from the positive attributes of both fillers.

FUTURE DEVELOPMENT OF A BIOFILM-PREVENTING AND

WEIGHT-BEARING PUR GRAFT

To date, the research projects related to the development of a weight-bearing matrix/PUR graft and a biofilm-preventing D-AA/PUR graft have largely been conducted independently, but in parallel. In the future, after major milestones have been independently achieved for each project, the key features from each lead-candidate graft should be combined to develop a biofilm-preventing weight-bearing graft. The key hurdle or milestone for the weight-bearing project will be the ability support physiological load in a weight-bearing large animal defect for an extended period of time.

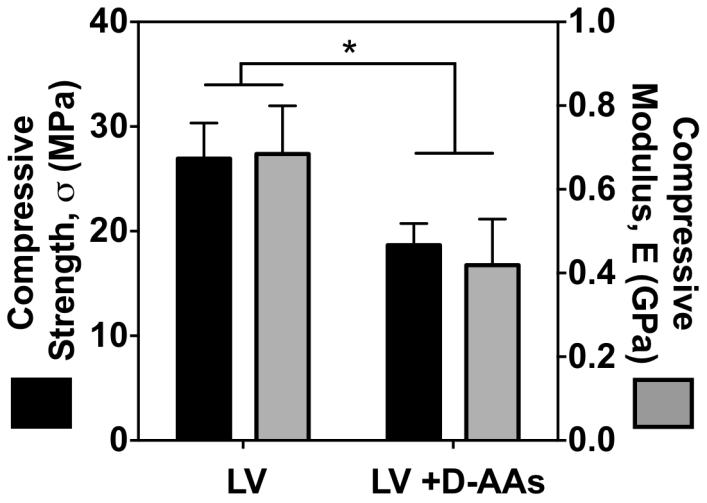

Figure 8.12. Augmentation of LV bone grafts with D-AAs modifies the mechanical properties of the composites. Augmentation of LV grafts with D-AA decreased the quasi-static compressive mechanical properties (strength and modulus). The values reported are mean ± standard deviation of triplicate samples, with * indicating $p<0.05$ between quantified parameter, as determined by unpaired t test.

Previously, we showed that the addition of D-AAs (10 wt%) to a high porosity (~90%) PUR scaffold decreased the quasi-static compressive modulus and strength by ~67% [1]. Unpublished results from the study presented in Chapter III, showed that the low-viscosity (LV) PUR graft had significantly higher quasi-static

compressive modulus and strength compared to the LV graft augmented with 5 wt% D-AAs (LV+ D-AAs) (Figure 8.12). In this system, the addition of D-AAs decreased the mechanical properties ~30%. Additionally, the PUR scaffold and LV+D-AAs graft had porosities of ~90%[1] and ~27%, respectively. The PUR LV graft contained 45 wt% (27 vol%) MASTERGRAFT® Mini Granules (MG) and the LV+D-AAs contained 5 wt% less, which was replaced with D-AAs. From these results, it appears that the addition of D-AAs may not affect lower porosity PUR grafts as much compared to high porosity PUR scaffolds. Also, as discussed in Chapter III, the LV+D-AAs graft contained a higher initial concentration of D-AAs than what was originally formulated in the PUR scaffold. Thus, the wt% of D-AAs loaded in a low porosity graft may be decreased, based on future results related to the D-AAs release study outlined previously in this Chapter. Consequently, the addition of D-AAs to the current lead-candidate BG/PUR graft would require replacing a lower percentage of the overall matrix filler, compared to the previously developed LV system. Thus, I hypothesize that the addition of D-AAs to the weight-bearing matrix/PUR graft will decrease the overall mechanical properties of the resultant graft as well, but less than that of the LV graft system.

Further characterization of a biofilm-preventing and weight-bearing PUR graft would be needed. Particularly, the release kinetics of D-AAs and any potential interaction between the delivered D-AAs and bioactive matrix filler (such as BG) would need to be characterized. To my knowledge, there are no weight-bearing bacterially contaminated defects *in vivo* models. As the field improves the complexity of reliable animal models and more attention is focused on these two independently difficult orthopaedic conditions, hopefully such a model will be developed. Ideally, promising results from combining these two concepts would motivate others to include biofilm-dispersing agents, like D-AAs, as a standard prerequisite component in the formulation and development of all future synthetic bone grafts.

References

1. C.J. Sanchez, E.M. Prieto, C.A. Krueger, K.J. Zienkiewicz, D.R. Romano, C.L. Ward, K.S. Akers, S.A. Guelcher and J.C. Wenke: Effects of local delivery of D-amino acids from biofilm-dispersive scaffolds on infection in contaminated rat segmental defects *Biomaterials.* **34**(30), 7533 (2013).

2. D.P. Lew and F.A. Waldvogel: Osteomyelitis *Lancet.* **364**(9431), 369 (2004).

3. L.O. Conterno and M.D. Turchi: Antibiotics for treating chronic osteomyelitis in adults *Cochrane Database of Systematic Reviews.* (9), (2013).

4. J. Huh, D.J. Stinner, T.C. Burns and J.R. Hsu: Infectious Complications and Soft Tissue Injury Contribute to Late Amputation After Severe Lower Extremity Trauma *Journal of Trauma-Injury Infection and Critical Care.* **71**, S47 (2011).

5. L. Hall-Stoodley, J.W. Costerton and P. Stoodley: Bacterial biofilms: from the Natural environment to infectious diseases *Nature Reviews Microbiology.* **2**, 95 (2004).

6. J.W. Costerton: Biofilm theory can guide the treatment of device-related orthopaedic infections *Clinical Orthopaedics and Related Research.* (437), 7 (2005).

7. R. Brady, J. Leid, J. Calhoun, J.W. Costerton and M. Shirtliff: Osteomyelitis and the role of biofilms in chronic infection. *FEMS Immunol Med Microbiol.* **52**(1), 13 (2008).

8. T. Marrie and J.W. Costerton: Mode of growth of bacterial pathogens in chronic polymicrobial human osteomyelitis. *J Clin Microbiol.* **22**(6), 924 (1985).

9. A.G. Gristina, M. Oga, L.X. Webb and C.D. Hobgood: Adherent Bacterial-Colonization in the Pathogenesis of Osteomyelitis *Science.* **228**(4702), 990 (1985).

10. A. Gisep, R. Wieling, M. Bohner, S. Matter, E. Schneider and B. Rahn: Resorption patterns of calcium-phosphate cements in bone *Journal of Biomedical Materials Research Part A.* **66A**(3), 532 (2003).

11. E.P. Frankenburg, S.A. Goldstein, T.W. Bauer, S.A. Harris and R.D. Poser: Biomechanical and histological evaluation of a calcium phosphate cement *Journal of Bone and Joint Surgery-American Volume.* **80A**(8), 1112 (1998).

12. E. Tuomanen, R. Cozens, W. Tosch, O. Zak and A. Tomasz: The Rate of Killing of Escherichia-Coli by Beta-Lactam Antibiotics Is Strictly Proportional to the Rate of Bacterial-Growth *Journal of General Microbiology.* **132**, 1297 (1986).

13. S.R. Shah, K.F. Kurtis and A.G. Mikos: Perspectives on the prevention and treatment of infection for orthopedic tissue engineering applications *Chinese Science Bulletin.* **58**(35), 4342 (2013).

14. A.G. Gristina: Biomaterial-Centered Infection - Microbial Adhesion Versus Tissue Integration *Science.* **237**(4822), 1588 (1987).

15. I. Kolodkin-Gal, D. Romero, S. Cao, J. Clardy, R. Kolter and R. Losick: D-Amino Acids Trigger Biofilm Disassembly *Science.* **328**(5978), 627 (2010).

16. D.Y. Arifin, L.Y. Lee and C.-H. Wang: Mathematical modeling and simulation of drug release from microspheres: Implications to drug delivery systems. *Advanced Drug Delivery Reviews.* **58**(12–13), 1274 (2006).

17. R.W. Korsmeyer, R. Gurny, E. Doelker, P. Buri and N.A. Peppas: Mechanisms of Solute Release from Porous Hydrophilic Polymers *International Journal of Pharmaceutics.* **15**(1), 25 (1983).

18. B. Li, K.V. Brown, J.C. Wenke and S.A. Guelcher: Sustained release of vancomycin from polyurethane scaffolds inhibits infection of bone wounds in a rat femoral segmental defect model *Journal of Controlled Release.* **145**(3), 221 (2010).

19. L. Illum: Chitosan and its use as a pharmaceutical excipient *Pharmaceutical Research.* **15**(9), 1326 (1998).

20. A. Sukarto and B.G. Amsden: Low melting point amphiphilic microspheres for delivery of bone morphogenetic protein-6 and transforming growth factor-β3 in a hydrogel matrix *Journal of Controlled Release.* **158**(1), 53 (2012).

21. M. Fresta, G. Puglisi, G. Giammona, G. Cavallaro, N. Micali and P. Furneri.: Pefloxacine mesilate- and ofloxacin-loaded polyethylcyanoacrylate nanoparticles: characterization of the colloidal drug carrier formulation. *J Pharm Sci.* **84**(7), 895 (1995).

22. M. Polakovič, T. Görner, R. Gref and E. Dellacherie: Lidocaine loaded biodegradable nanospheres: II. Modelling of drug release *Journal of Controlled Release.* **60**(2–3), 177 (1999).

23. O.S. Kluin, H.C. van der Mei, H.J. Busscher and D. Neut: A surface-eroding antibiotic delivery system based on poly-(trimethylene carbonate). *Biomaterials.* **30**(27), 4742 (2009).

24. J.-C. Ruiz, C. Alvarez-Lorenzo, P. Taboada, G. Burillo, E. Bucio, K. De Prijck, H.J. Nelis, T. Coenye and A. Concheiro: Polypropylene grafted with smart polymers (PNIPAAm/PAAc) for loading and controlled release of vancomycin *Eur J Pharm Biopharm.* **70**(2), 467 (2008).

25. C.S. Adams, V. Antoci, G. Harrison, P. Patal, T.A. Freeman, I.M. Shapiro, J. Parvizi, N.J. Hickok, S. Radin and P. Ducheyne: Controlled release of vancomycin from thin sol-gel films on implant surfaces successfully controls osteomyelitis *J Orthop Res.* **27**(6), 709 (2009).

26. Y. Fu and W.J. Kao: Drug release kinetics and transport mechanisms of non-degradable and degradable polymeric delivery systems *Expert Opinion on Drug Delivery.* **7**(4), 429 (2010).

27. X. Huang and C.S. Brazel: On the importance and mechanisms of burst release in matrix-controlled drug delivery systems *Journal of Controlled Release.* **73**(2-3), 121 (2001).

28. A.S. Lynch and D. Abbanat: New antibiotic agents and approaches to treat biofilm-associated infections *Expert Opinion on Therapeutic Patents.* **20**(10), 1373 (2010).

29. A.S. Sawhney and J.A. Hubbell: Rapidly degraded terpolymers of dl-lactide, glycolide, and epsilon-caprolactone with increased hydrophilicity by copolymerization with polyethers. *J Biomed Mater Res.* **24**(10), 1397 (1990).

30. S.A. Guelcher, V. Patel, K.M. Gallagher, S. Connolly, J.E. Didier, J.S. Doctor and J.O. Hollinger: Synthesis and in vitro biocompatibility of injectable polyurethane foam scaffolds *Tissue Engineering.* **12**(5), 1247 (2006).

31. S.A. Guelcher, V. Patel, K.M. Gallagher, S. Connolly, J.E. Didier, J.S. Doctor and J.O. Hollinger: Synthesis and In Vitro Biocompatibility of Injectable Polyurethane Foam Scaffolds *Tissue Engineering.* **12** (5), 1247 (2006).

32. C.J. Sanchez, K.S. Akers, D.R. Romano, R.L. Woodbury, S.K. Hardy, C.K. Murray and J.C. Wenke: D-Amino Acids Enhance the Activity of Antimicrobials Against Biofilms of Clinical Wound Isolates of Staphylococcus aureus and Pseudomonas aeruginosa. *Antimicrobial Agents and Chemotherapy.* **58**(8), 4353 (2014).

33. Y. Nozaki and C. Tanford: The solubility of amino acids and two glycine peptides in aqueous ethanol and dioxane olutions. Establishment of a hydrophobicity scale. *J Biol Chem* **246**, 2211 (1971).

34. P. Johansen, Y. Men, R. Audran, G. Corradin, H.P. Merkle and B. Gander: Improving stability and release kinetics of microencapsulated tetanus toxoid by co-encapsulation of additives *Pharmaceutical Research.* **15**(7), 1103 (1998).

35. K. Fu, K. Griebenow, L. Hsieh, A.M. Klibanov and R. Langer: FTIR characterization of the secondary structure of proteins encapsulated within PLGA microspheres' *Journal of Controlled Release.* **58**(3), 357 (1999).

36. K.G. Carrasquillo, A.M. Stanley, J.C. Aponte-Carro, P. De Jesus, H.R. Costantino, C.J. Bosques and K. Griebenow: Non-aqueous encapsulation of excipient-stabilized spray-freeze dried BSA into poly(lactide-co-glycolide) microspheres results in release of native protein *Journal of Controlled Release.* **76**(3), 199 (2001).

37. B.G. Amsden, L. Timbart, D. Marecak, R. Chapanian, M.Y. Tse and S.C. Pang: VEGF-induced angiogenesis following localized delivery via injectable, low viscosity poly(trimethylene carbonate) *Journal of Controlled Release.* **145**(2), 109 (2010).

38. S. Sharifpoor and B. Amsden: In vitro release of a water-soluble agent from low viscosity biodegradable, injectable oligomers *European Journal of Pharmaceutics and Biopharmaceutics.* **65**(3), 336 (2007).

39. F. Gu, R. Neufeld and B. Amsden: Osmotic-driven release kinetics of bioactive therapeutic proteins from a biodegradable elastomer are linear, constant, similar, and adjustable *Pharmaceutical Research.* **23**(4), 782 (2006).

40. R.A. Siegel and R. Langer: Controlled release of polypeptides and other macromolecules *Pharmaceutical Research.* **1**(1), 2 (1984).

41. B.G. Amsden and Y.L. Cheng: Enhanced Fraction Releasable above Percolation-Threshold from Monoliths Containing Osmotic Excipients *Journal of Controlled Release.* **31**(1), 21 (1994).

42. R.A. Siegel and R. Langer: Controlled Release of Polypeptides and Other Macromolecules *Pharmaceutical Research.* (1), 2 (1984).

43. W.H. Liu, J.L. Song, K. Liu, D.F. Chu and Y.X. Li: Preparation and in vitro and in vivo release studies of Huperzine A loaded microspheres for the treatment of Alzheimer's disease *Journal of Controlled Release.* **107**(3), 417 (2005).

44. J. Kelm, T. Regitz, E. Schmitt, W. Jung and K. Anagnostakos: In vivo and in vitro studies of antibiotic release from and bacterial growth inhibition by antibiotic-impregnated polymethylmethacrylate hip spacers *Antimicrobial Agents and Chemotherapy.* **50**(1), 332 (2006).

45. A. Hoppe, N.S. Gueldal and A.R. Boccaccini: A review of the biological response to ionic dissolution products from bioactive glasses and glass-ceramics *Biomaterials.* **32**(11), 2757 (2011).

46. C. Kunze, T. Freier, E. Helwig, B. Sandner, D. Reif, A. Wutzler and H.J. Radusch: Surface modification of tricalcium phosphate for improvement of the interfacial compatibility with biodegradable polymers *Biomaterials.* **24**(6), 967 (2003).

47. A.J. Harmata, C.L. Ward, K. Zienkiewicz, J.C. Wenke and S.A. Guelcher: Investigating the Effects of Surface-Initiated Polymerization of ε-Caprolactone to Bioactive Glass Particles on the Mechanical Properties of Settable Polymer/Ceramic Composites *Journal of Materials Research.* **29**(20), 2398 (2014).

48. B.R. Constantz, I.C. Ison, M.T. Fulmer, R.D. Poser, S.T. Smith, M. Vanwagoner, J. Ross, S.A. Goldstein, J.B. Jupiter and D.I. Rosenthal: Skeletal Repair by in-Situ Formation of the Mineral Phase of Bone *Science.* **267**(5205), 1796 (1995).

49. R.D. Welch, H. Zhang and D.G. Bronson: Experimental tibial plateau fractures augmented with calcium phosphate cement or autologous bone graft *Journal of Bone and Joint Surgery-American Volume.* **85A**(2), 222 (2003).

50. D. Simpson and J.F. Keating: Outcome of tibial plateau fractures managed with calcium phosphate cement *Injury-International Journal of the Care of the Injured.* **35**(9), 913 (2004).

51. A. Trenholm, S. Landry, K. McLaughlin, K.J. Deluzio, J. Leighton, K. Trask and R.K. Leighton: Comparative Fixation of Tibial Plateau Fractures Using [alpha]-BSM(TM), a Calcium Phosphate Cement, Versus Cancellous Bone Graft *Journal of Orthopaedic Trauma.* **19**(10), 698 (2005).

52. A.M. Ali, M. El-Shafie and K.M. Willett: Failure of fixation of tibial plateau fractures *Journal of Orthopaedic Trauma.* **16**(5), 323 (2002).

53. M.J. Bosse, E.J. MacKenzie, J.F. Kellam, A.R. Burgess, L.X. Webb, M.F. Swiontkowski, R.W. Sanders, A.L. Jones, M.P. McAndrew, B.M. Patterson, M.L. McCarthy, T.G. Travison and R.C. Castillo: An analysis of outcomes of reconstruction or amputation of leg-threatening injuries *New England Journal of Medicine.* **347**(24), 1924 (2002).

54. A. Gisep, S. Kugler, D. Wahl and B. Rahn: Mechanical characterisation of a bone defect model filled with ceramic cements *Journal of Materials Science-Materials in Medicine.* **15**(10), 1065 (2004).

55. E.F. Morgan and T.M. Keaveny: Dependence of yield strain of human trabecular bone on anatomic site *Journal of Biomechanics.* **34**(5), 569 (2001).

56. J.J. Verlaan, F.C. Oner and W.J.A. Dhert: Anterior spinal column augmentation with injectable bone cements *Biomaterials.* **27**(3), 290 (2006).

57. C.J. Du, H.S. Ma, M. Ruo, Z.J. Zhang, X.J. Yu and Y.J. Zeng: An experimental study on the biomechanical properties of the cancellous bones of distal femur *Bio-Medical Materials and Engineering.* **16**(3), 215 (2006).

58. J.E. Dumas, T. Davis, G.E. Holt, T. Yoshii, D.S. Perrien, J.S. Nyman, T. Boyce and S.A. Guelcher: Synthesis, characterization, and remodeling of weight-bearing allograft bone/polyurethane composites in the rabbit *Acta Biomaterialia.* **6**(7), 2394 (2010).

59. J.E. Dumas, E.M. Prieto, K.J. Zienkiewicz, T. Guda, J.C. Wenke, J. Bible, G.E. Holt and S.A. Guelcher: Balancing the Rates of New Bone Formation and Polymer Degradation Enhances Healing of Weight-Bearing Allograft/Polyurethane Composites in Rabbit Femoral Defects *Tissue Engineering Part A.* **20**(1-2), 115 (2014).

60. A.E. Hafeman, K.J. Zienkiewicz, A.L. Zachman, H.-J. Sung, L.B. Nanney, J.M. Davidson and S.A. Guelcher: Characterization of the degradation mechanisms of lysine-derived aliphatic poly(ester urethane) scaffolds *Biomaterials.* **32**(2), 419 (2011).

61. A.J.W. Johnson and B.A. Herschler: A review of the mechanical behavior of CaP and CaP/polymer composites for applications in bone replacement and repair *Acta Biomaterialia.* **7**(1), 16 (2011).

62. J. Israelachvili: The different faces of poly(ethylene glycol) *Proc. Natl. Acad. Sci.* **94**, 8378 (1997).

63. K. Miki, P. Westh and Y. Koga: **109**(41), 19541 (2005).

64. J.R. Martin, M.K. Gupta, J.M. Page, F. Yu, J.M. Davidson, S.A. Guelcher and C.L. Duvall: A porous tissue engineering scaffold selectively degraded by cell-generated reactive oxygen species *Biomaterials.* **35**(12), 3766 (2014).

65. J.M. Page, E.M. Prieto, J.E. Dumas, K.J. Zienkiewicz, J.C. Wenke, P. Brown-Baer and S.A. Guelcher: Biocompatibility and chemical reaction kinetics of injectable, settable polyurethane/allograft bone biocomposites *Acta Biomaterialia.* **8**(12), 4405 (2012).

66. N.S. Ruppender, A.R. Merkel, T.J. Martin, G.R. Mundy, J.A. Sterling and S.A. Guelcher: Matrix Rigidity Induces Osteolytic Gene Expression of Metastatic Breast Cancer Cells *Plos One.* **5**(11), (2010).

67. R.F. Storey, J.S. Wiggins and A.D. Puckett: Hydrolyzable poly(ester-urethane) networks from L-lysine diisocyanate and D,L-lactide/ϵ-caprolactone homo- and copolyester triols *J. Polym. Sci. A Polym. Chem.* **32**(12), 2363 (1994).

68. Q. Fu, M.N. Rahaman, B.S. Bal, L.F. Bonewald, K. Kuroki and R.F. Brown: Silicate, borosilicate, and borate bioactive glass scaffolds with controllable degradation rate for bone tissue engineering applications. II. In vitro and in vivo biological evaluation *Journal of Biomedical Materials Research Part A.* **95A**(1), 172 (2010).

69. J.R. Jones: Review of bioactive glass: From Hench to hybrids *Acta Biomaterialia.* **9**(1), 4457 (2013).

70. O.G. Cisneros-Pineda, W.H. Kao, M.I. Loria-Bastarrachea, Y. Veranes-Pantoja, J.V. Cauich-Rodriguez and J.M. Cervantes-Uc: Towards optimization of the silanization process of hydroxyapatite for its use in bone cement formulations *Materials Science & Engineering C-Materials for Biological Applications.* **40**, 157 (2014).

CHAPTER IX

EXPERIMENTAL PROTOCOLS

Method base on protocol reported in:
E. Verne, C. Vitale-Brovarone, E. Bui, C. L. Bianchi, A. R. Boccaccini. Surface functionalization of bioactive glasses, *Journal of Biomedical Materials Research Part A*, 90A (4), 981-992 (2009).

Materials and Equipment:

- Glass beakers for sonication (~80 mL)
- Acetone
- DI water
- Sonicator
- Ceramic filler

Procedure:

- Incubated filler (i.e. bioglass) with 95 vol% solution acetone (to water)
    - 6.4 g 45S5 bioactive glass : 75 mL solution
- Sonicate for for 5 min
- Rinse with distilled water, 3 times, each for 5 min in sonicator
- Dry at 100°C for 1 h under vacuum

Notes:

- Takes ~30 min

Method base on protocol reported in:
G. Jiang, G.S. Walker, I.A. Jones and C.D. Rudd: XPS identification of surface-initiated polymerisation during monomer transfer moulding of poly(epsilon-caprolactone)/Bioglass (R) fibre composite *Appl. Surf. Sci.* 252(5), 1854 (2005).

Materials and Equipment:

- Glass beakers for sonication (~80 mL)
- Acetone
- DI water
- Sonicator
- (3-aminopropyl)trimethoxysilane (APTES)
- Ceramic filler
- Large magnetic stir bar
- Parafilm
- Syringe (for extracting APTES)
- Magnetic plate mixer

Procedure:

- Clean ceramic based on previously described procedure
- For every 4 grams of filler:
    - 150 mL of solution (90 vol % ethanol and 10% DI water) in 2 L glass beaker
    - Mix using largest stir bar, speed ~4
    - Add cleaned filler
    - Add 70 µL APTES
- Cover beaker with parafilm
- Allow to react for 5 hours
    - Mix beaker by hand once every hour to turn over filler
- Allow filler to settle, dispose of ethanol solution in waste
- Rinse twice with pure ethanol
- Allow excess ethanol to evaporate in hood for ~ 1 h (otherwise will boil during heat treatment)
- Heat treat at 100°C for 1 h under vacuum

Ratio of solid filler to APTES solution may need to be adapted depending on size, surface area exposed of filler

Notes:

- Takes ~7 h

Method base on protocol reported in:
G. Jiang, G.S. Walker, I.A. Jones and C.D. Rudd: XPS identification of surface-initiated polymerisation during monomer transfer moulding of poly(epsilon-caprolactone)/Bioglass (R) fibre composite *Appl. Surf. Sci.* 252(5), 1854 (2005).

Materials and Equipment:

- ε-caprolactone monomer
- magnesium sulfate
- stannous octoate ($Sn(Oct)_2$) catalyst
- Glass beaker (~200 mL)
- filter paper and glass funnel
- 100 mL glass reactor
- stir rod, plastic mixer, reactor/stir rod holder
- Reaction set up: water pump, reactor mixer, condenser, silicon plug, thermal couple, temperature controller, 16-gauge needle, Argon gas

Procedure:

Glassware preparation:

- The night before reaction: put 100 mL glass reactor, stir rod, plastic mixer, and reactor/stir rod holder in 70°C oven to fully dry
- Glass reactor should have minimal wear and scratches on inside

Material preparation: Ratios from paper

- For every 1 g of filler, 3.679 g e-caprolactone and 0.01306 g $Sn(Oct)_2$ catalyst
    - In 100 mL reactor, usually need ~45 mL of ε-cap to provide enough room for temperature controller to be fully immersed in solution without being obstructed by plastic stirrer
- Dry ε -cap
    - Measure more 'wet' ε-cap than necessary, because ~10g is lost from filtering process
    - Measure ε-cap (rough)
    - Add at least two heaving scoops of magnesium sulfate into beaker
    - Cover with parafilm and allow to sit for >20 mins
    - Filter out magnesium sulfate (takes ~15 mins)

Reactor (dynamic polymerization, for particles):

- In glass reactor (on cork holder) measure add necessary mass of three components (dried ε-cap, $Sn(Oct)_2$, and filler)
- Attach reactor to holder, stir rod etc – be sure to grease joints
- Connect one neck to condenser (connected to connect to silicon gas-flow indicator)

  - Turn on water pump
- Plug one neck with rubber stopper, with thermometer and 16 gauge needle connected to Argon (or Nitrogen) gas tank
  - Allow gas to flow, preventing atmospheric air from entering reaction (presence should be seen by bubbles in silicon gas-flow indicator)
- Use heater connected to temperature controller to heat glass reactor
  - Make sure heater is proper size, not too small/larger
    - Should be snug around reactor, but covering at least 75% of the bulb portion
- Stir at brisk pace
- Reactor for 24 h at 230°F (110°C)
  - MW ~25,000 Da
  - For low MW: 4 h ~7,000 Da

Extracting filler:

- Turn off heater (allow heater to stay under reactor)
  - Important not to allow polymer to cool too quickly and solidify, otherwise much more difficult to get our modified filler
- Fill 50 mL plastic tubes with ~35 mL of chloroform (8 tubes for a 50 mL ε-cap reacted)
- While still being stirred, allow mixture to cool for about 10 min
- Poor small amounts of chloroform into reactor
  - If chloroform boils, allow to cool more
- As soon as chloroform no longer boils when put into reactor, begin taking out polymer solution as fast as possible
  - Continue to add chloroform to make solution less viscous and easier to work with
  - Using a plastic pipette (cut off some of tip to make opening larger)
  - Put polymer/filler mix into 50 mL tubes with chloroform
- Take out small sample for GPC***
- Vortex 50 mL tube for ~1 min to loosen polymer/filler
- Centrifuge tubes at 2000 RPM for 2 min (may need to be faster depending on filler particle size) to collect filler to bottom of tube
- Remove chloroform/polymer solution, leaving filler in tube
- Condense tubes and repeated step of washing with chloroform (vortex, centrifuge)
- Dry filler via vacuum pump/filter
- Dry in oven under vacuum at 40°C for 24 h

Static polymerization (i.e. for disks)

- Night before: dry 'G133' glass vial in 70°C oven
  - Bought at Chem store → fits snugly into heating block
- Ratio of $Sn(Oct)_2$ to ε-cap holds, while amount of solution can be changed depending on material, surface area exposed etc

  - For ½ BG disk (1 cm diameter) that is 2-3 mm thick: 3 mL solution
- Follow procedure to dry ε-cap as above
- Combine ε-cap and $Sn(Oct)_2$, mix with magnetic stir bar vigorously for several minutes
  - Think it is best to make large batch and combine catalyst and monomer first so all static polymerizations, though separate, are most similar
  - Catalyst will not dissolve into e-cap, small dispersed bubbles
- Add filler, and ε-cap/ $Sn(Oct)_2$ to glass vial
- Purge vial with argon
- Allow to react at 110°C (see that thermometer in heating block is at 115)
- 30 h gives ~25,000 Da
- Soak each disk in chloroform (statically) for ~12 h to rid of PCL
- Dry in oven under vacuum at 40°C for 24 h

Method base on protocol reported in:
T. Kokubo and H. Takadama: How useful is SBF in predicting in vivo bone bioactivity? *Biomaterials.* 27(15), 2907 (2006).

Materials and Equipment:

- Simulated body fluid (SBF): method in publication
- DI water
- Glass beaker (2 L) – relatively new and very clean
- Plastic tube (15 mL)
- Material to be incubated/analyzed ideally should be disk form with flat surface

Procedure:

Make simulated body fluid (SBF): ~3 hrs to make

- Follow directions from paper as closely as possible
- Ok to use glass beaker (1.5 – 2 L) as long as new and very clean
- Keep reagents as dry as possible
- Abandon solution if precipitate forms at all
- Good for 30 days

Bioactivity Study Design

- Followed protocol/suggestions from paper
- In 15 mL plastic tube
    - 10 mL SBF
        - Amount of SBF per surface area exposed alters surface reaction rate
    - ½ Bioglass disk (2-3 mm thick, 1 cm diameter)
- Frequency of changing SBF alters surface reaction rate
    - Changed SBF every 3 days
    - Keep solution → can analyze with ICP-MS
- When taking out specimen from SBF, rinse with DI water and try in oven at 40°C

Analysis

- X-ray Diffraction (XRD) – shows crystallinity of HA (presence of HA)
- X-ray photoelectron spectroscopy (XPS)- Presence of HA
- Scanning electron microscopy (SEM) and energy-dispersive X-ray spectroscopy (EDS)
    - DO LAST!
    - Most likely will need to sputter coat gold onto surface and use a lot of conducting carbon tape, so composition of samples will be ruined

Notes: Keep SBF reagents as dry as possible (in desiccator)

Method base on protocol reported in:

Materials and Equipment:

- Material to be analyzed
- XRD machine located on 8th floor of Chemistry building in Lukeheart lab

Procedure:

- Hydroxycarbonate apatite (HCA) will crystallize at later time points (7+ days)
- Do this form of bioactivity analysis first because it is very sensitive to contamination and does not alter specimen

Parameters

- General: step mode, 0.1 step size, 20-55 deg, preset time: 13, total time per scan: 1:17 min
- Publishable: 0.05 step size, preset time: 30, ~7 hrs
- Compare peaks to to PDF 9-432

Materials and Equipment:

- Fabricated composite/material
  - Ideally height=2*diameter
- MTS load cell, located in Biomechanics lab (Jeffry Nyman) in basement of medical center north (MCN)

Procedure:

- Turn on computer (Password: admin)
- Turn on MTS controller (power in back)
- Turn on pump (at the back of the room)
- Locate specimen holders (Silver on top, Black on the bottom)

- To open the program
  - Station manager → Project 1 → 85AT
- Once the program opens:
  - Interlock1 → RESET
  - Station controls → 2nd button (detectors) → Load, lower limit: -10 kN → close and check again
- Activating the hydraulic pump:
  - Check: Exclusive control → HPU Power: click on the 1 line, then 2 lines, finally 3 lines button
- Warming up the equipment:
  - At the left, click on: Function Generator
  - Check that the parameters are: 40mm, 10mm, 2Hz, and control mode is set at 'displacement'
  - Click on the PLAY button and let it run for 3 min
  - Click the STOP button
  - Reset load (in the window: Signal Auto Offset)

- Running an experiment:
  - At the left, click on MPT (4th down on left column) on station manager window
  - Check that the current method is: Guelcher compression
  - If ok, locate sample centered between the two specimen holders
  - Name sample
  - In the Manual Commands Window:
    - Check: "Enable Manual Comand"
    - Use the manual controls to bring the specimen holders together (there are 3 different speeds at which this can be done, start fast and end slow)
    - Preload the sample to 12N (0.012kN)
    - Uncheck "Enable Manual Command"
    - Reset displacement
    - Press PLAY (a curve of force vs. displacement should pop)
    - When the curve changes direction drastically, press STOP
    - Click on the NEW SPECIMEN button (!)
    - Name your next sample
    - Check "Enable Manual Command"
    - Separate the specimen holders and change your sample

- Repeat steps i-x until you've measured all your samples

- When finished:
  - In the manual command window: separate the holders to 40mm
  - HPU power: 3, 2, 1 lines
  - Close program (don't save any changes to the parameters)
- To obtain data:
  - My Computer→ C: → MTS 793 → Projects → Project 1 → MPT → Specimens (and each sample should have a folder here)
  - Save each folder into a USB drive

Method base on protocol reported in:
K.B. Garnier, R. Dumas, C. Rumelhart and M.E. Arlot: Mechanical characterization in shear of human femoral cancellous bone: torsion and shear tests *Medical Engineering & Physics.* 21(9), 641 (1999).

Materials and Equipment:

- Fabricated composite/material needs to be >2 cm (Max=3.2 cm)
    - The longer the better, so more composite is attached to potted PMMA
    - 1.6 g batch size (low porosity, 5%) is about right
- Permanent market
- Technovit 4000 kit
- Potting mold (stand and connected holder)
- Grease
- Numerous green 1 mL and white 3 mL plastic syringes
- 10 mL plastic cups got Technovit mixing
- PBS
- 50 mL centrifuge tubes
- Instron load cell, located in Biomechanics lab (Jeffry Nyman) in basement of medical center north (MCN)

Procedure:

Potting (two composites at a time =~40 min)

- With permanent marker, make marks on composite ~12.7 mm apart
- First pot separate/independent mold
    - Cover inside of circular mold with grease, to prevent material from sticking to mold
    - Using tweezer holder, place composite in tweezer (on one black lines drawn) and set up stand so that composite will go into mold straight and at appropriate level
    - Best to have stand on left side, pointing to the right, and have the screws of the mold facing right as well, away from tweezer stand
    - Practice putting composite into independent mold
        - Best to have (other) black line covered by top of mold
- Technovit 4000:
    - Mix 1.5 mL of large bottle liquid (3 mL syringe) and 0.75 mL small bottle liquid (1 mL syringe) together, with 1 mL syringe
        - Easiest to use medium size plastic cups
    - Add/mix same volume (of total liquid) of powder to reactive mixture liquids
        - On first mixture, combing liquids and then make mark at same height on another cup (same size) to use as a refill cup for powder
        - Does not have to be exact, but close
- Pour Technovit into mold (close to top, leave a little space)
    - Carefully put composite into Technovit

        - Do not raise composite out of Technovit after having been deeper, residue will stay on material and change mechanical properties
    - Make sure composite is perpendicular to mold, by looking at other it from all sides
- Do the same for second composite as first one dries
- Second mold – attached to stand
    - Line inside with grease
    - Screw in first mold, as close to top as possible
        - With black marks facing you, stand/screws should be on right side, able to pour in from left side
    - Make Technovit, and pour into mold
    - Carefully loosen screws attaching first mold to stand
    - Carefully lower first mold, keeping as level as possible, until second black line is covered by Technovit
    - Tighten screws, make sure composite is perpendicular to second mold, by looking at other side, and adjust as necessary
    - Allow to dry (Technovit should lighten up)
- Do the same for second composite as first one dries
- Removing from molds
    - Unscrew (semicircle) halves of molds – take off these halves of molds
    - Loose screws attaching independent mold
    - Carefully remove potted composite from both molds as same time

Mechanical Testing

- Specimen preparation
    - Place alignment marks with permanent marker on composite, and three sides of potted material to make sure composite does not slip within the potted material post torsion
    - Place in PBS (50 mL centrifuge tubes) for 24 h before testing
    - After 24 hours, measure diameter and gap length 3x

- Turn on machine (black button) and then connected computer
- Warm up Instron to low power
    - O : No power, I : Low power, II: High power
- Align head with load cell (using arrows) and secure head and everything tightly
    - Horizontal rotation
- Software: Open *Fast track console*
    - Switch from displacement to rotation
        - Right click on button in top right corner (left of stop)
        - Select user states
        - Recall state → choose appropriate file
    - Calibrate load cell
        - Right click load cell icon in top right corner → Calibrate wizard
            - Auto calibrate → next

        - Type: torque, Nm
        - Span Point: 1.7654 Nm (nonzero: 0)
        - Next → start, uncheck 'lock and save' → Finish
    - "Sensor Properties:" Set limits to protect cell
        - Right click load cell icon → limits
        - Enable upper and lower limits: 1.85 Nm, action: actuator off
- Bring rotation to zero degrees (+/- buttons as well as fine control near power buttons)
- Turn on to high power
- Load specimen
- Software: Open *Wave Maker Editor*
    - Location of saved files
        - Desktop: Instron data → Torsion→ User Name
    - Protocol
        - First block:
            - Shape: hold, duration: 4 sec
        - Second block:
            - Relative ramp
            - End point: 135 deg
            - Rate: 2 deg/sec
        - Max rotation: 130 deg
    - Click Data storage button
        - Finale name and location
        - Click 'Apply to all blocks'
        - Save
    - Hit 'running man'
    - Hit 'play' button (triangle)
        - Open, Yes or ok to rest

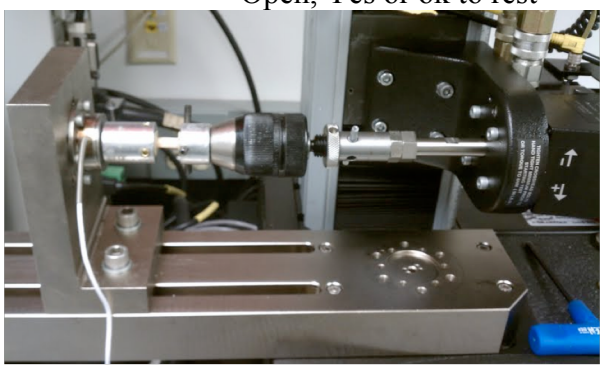

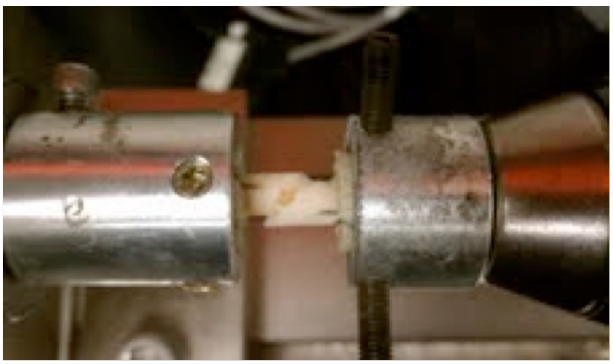

Data Analysis

Shear stress, G calculations are based on equations from Arlot (1999)

Method base on protocol reported in:

ASTM: Designation F2118-10. Standard Test Method for Constant Amplitude of Force Controlled Fatigue Testing of Acrylic Bone Cement Materials *ASTM International.* (2010).

Materials and Equipment:

- Fabricated composite/material
  - Ideally height=2*diameter
- Medical gauze
- Room temperature water
- Water drip system
- MTS load cell, located in Biomechanics lab (Jeffry Nyman) in basement of medical center north (MCN)
- MTS Extensometer (634.31F-24)
- Silicon elastic bands (for attaching extensometer)
- 'Screw rod' platens for fatigue

Procedure:

- Turn on computer
- Log in: (Name: administrator, Password: admin)
- Turn on MTS controller (power in back)
- Turn on pump (at the back of the room)
- Locate specimen holders (two cylinder screws)
  - Attach one to transducer and one to actuator
  - Use bucket with hole in bottom side of 'screw rod' in between rod and transducer to catch water

- To open the program
  - Station manager →Project 1→85AT_Strain
- Once the program opens:
  - Interlock1 → RESET
  - Station controls → 2nd button (detectors) → Load, lower limit: -10 kN → close and check again
- Activating the hydraulic pump:
  - Check: Exclusive control → HPU Power: click on the 1 line, then 2 lines, finally 3 lines button
- Make sure extensometer is plugged in
- Warming up the equipment:
  - At the left, click on: Function Generator
  - Check that the parameters are: 40mm, 10mm, 2Hz, and control mode is set at 'displacement'
  - Click on the PLAY button and let it run for 3 min
  - Click the STOP button
  - Reset load (in the window: Signal Auto Offset)
  -
- Running an experiment:
  - At the left, click on MPT (4th down on left column) on station manager window

- Check that the current method is: 'drew_bonecement_fatigue_ *' (*=appropriate loading for 6.4 mm diam x 12.8 mm h cylindrical specimen)
- Calibrate P, D, I values for each load/specimen group (but not for each specimen)
  - Verify that appropriate P, D, I values are set
- Loosely wrap specimen in soaked medical gauze
  - About 1 cm wide and 6 cm long piece
- Put sample centered between the two specimen holders
- Name sample
- In the Manual Commands Window:
  - Check: "Enable Manual Command"
  - Use the manual controls to bring the specimen holders together (there are 3 different speeds at which this can be done, start fast and end slow)
  - Preload the sample to 12N (0.012kN)
- With 'pin' still in extensometer, attach extensometer via rubber bands
  - First top attachment, so that it fits in the cut notches
  - Then bottom
- Attach tube from water drip system and ensure water is following at steady pace and is completely wedding gauze/specimen
- Remove pin from extensometer
- In the Manual Commands Window:
  - Uncheck "Enable Manual Command"
  - Reset displacement
  - Press PLAY
  - A sinusoidal curve should pop up
  - Make sure 'load command' curve and 'load' curve match up well
    - If they do not, alter calibration parameters (P, D, I)
- When finished:
  - In the manual command window: separate the holders to 40mm
  - HPU power: 3, 2, 1 lines
  - Close program (don't save any changes to the parameters)
- To obtain data:
  - My Computer→ C: → MTS 793 → Projects → Project 1 → MPT → Specimens (and each sample should have a folder here)
  - Save each folder into a USB drive
  -

- Data analysis can be done by hand in Excel, but recommend using a Matlab code

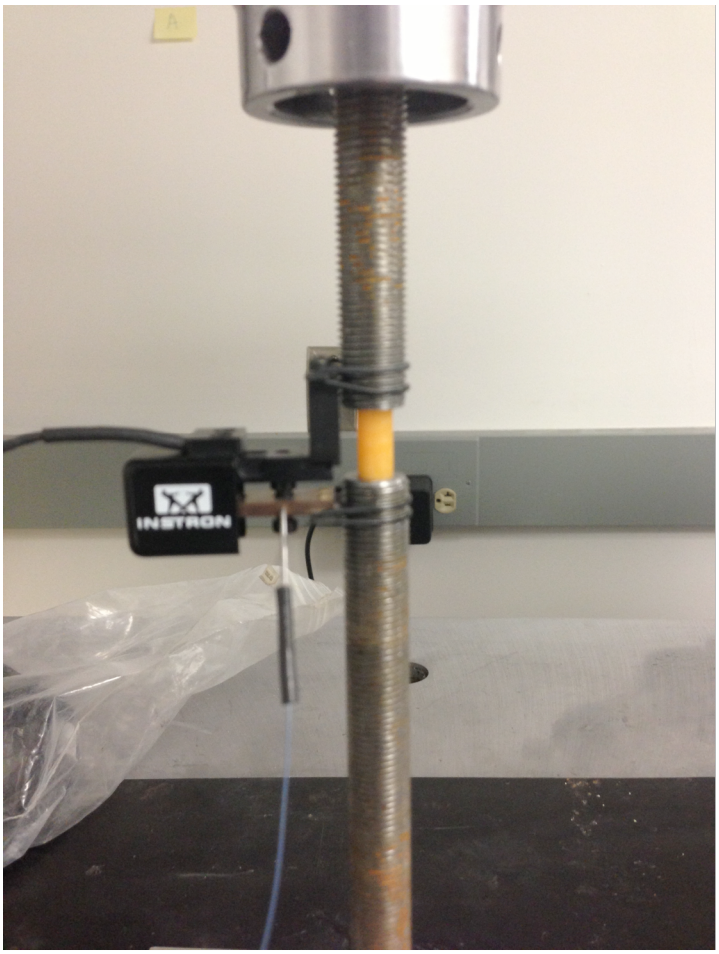
INSTRON